NASA Contractor Report No. 152407

AN INVESTIGATION OF AUTOMATIC GUIDANCE CONCEPTS TO STEER A VTOL AIRCRAFT TO A SMALL AVIATION FACILITY SHIP

J.A. Sorensen, T. Goka,
A.V. Phatak, and S.F. Schmidt

Contract No. NAS2-10288

July 1980

ANALYTICAL MECHANICS ASSOCIATES, INC.

NASA Contractor Report No. 152407

AN INVESTIGATION OF AUTOMATIC GUIDANCE CONCEPTS TO STEER A VTOL AIRCRAFT TO A SMALL AVIATION FACILITY SHIP

J.A. Sorensen, T. Goka,
A.V. Phatak, and S.F. Schmidt

Prepared for:
Ames Research Center
under Contract No. NAS2-10288

July 1980

ANALYTICAL MECHANICS ASSOCIATES, INC. 2483 Old Middlefield Way • Mountain View, California 94043 • (415) 964-1844

FOREWORD

This effort to investigate automatic guidance concepts to steer a VTOL aircraft to a small aviation facility ship was supported under NASA Contract No. NAS2-10288, by Ames Research Center, Moffett Field, California. The project Technical Monitor at Ames Research Center was Clyde H. Paulk, Jr.. Technical discussion and suggestions from Mr. Paulk, Bruce E. Tinling, and Vernon K. Merrick at NASA Ames are gratefully acknowledged. The mathematical models for the RTA aircraft, SRFIMF flight control scheme, and wind-over-deck wake turbulence were provided by NASA Ames.

At AMA, Inc., the project manager was John A. Sorensen. Stanley F. Schmidt served as advisor to the project. Engineering support was provided by Tsuyoshi Goka, Anil V. Phatak, and Antony W. Merz. Project programming support was provided by Marianne N. Kidder, Quyen T.L. Nguyen, Michael Schueller and Paul F. Flanagan.

TABLE OF CONTENTS

LIST OF FIGURES

LIST OF FIGURES (Con't)

LIST OF FIGURES (Con't)

LIST OF FIGURES (Con't)

LIST OF FIGURES (Con't)

LIST OF FIGURES (Con't)

LIST OF TABLES

AN INVESTIGATION OF AUTOMATIC GUIDANCE CONCEPTS TO STEER A VTOL AIRCRAFT TO A SMALL AVIATION FACILITY SHIP

J.A. Sorensen, T. Goka, A.V. Phatak, and S.F. Schmidt

Analytical Mechanics Associates, Inc.
Mountain View, California 94043

SUMMARY

The objectives of this study were to develop a detailed system model of a VTOL aircraft approaching a small aviation facility ship, to use this model to investigate several approach guidance concepts, and to conduct a preliminary analysis of the aircraft-vessel landing guidance requirements. This report presents a summary of the system model and the results of the analytical investigation.

In this report, the various sub-elements and constraints of the flight system are first described including the landing scenario, lift fan aircraft, state rate feedback flight control, MLS-based navigation, Sea State 5 induced ship motion, and wake turbulence due to wind-over-deck effects. These elements are integrated into a systems model with various guidance concepts. Guidance is described in terms of lateral, vertical, and longitudinal axes steering modes and approach and landing phases divided by a nominal hover (or stationkeeping) point defined with respect to the landing pad. The approach guidance methods are evaluated, and the two better steering concepts are studied by both single pass and Monte Carlo statistical simulation runs. The simulation results are used to recommend further cockpit simulator studies. Four different guidance concepts are defined for further analysis for the landing phase of flight.

I

INTRODUCTION

The NAVTOLAND project is the Navy's integrated systems approach to improve the V/STOL aircraft and helicopter operational capabilities at sea and at tactical sites. This improvement consists of upgrading the system from the present capability of 60m (200 ft) ceiling, 0.5 n.mi. visibility, Sea State 3 ship motion limits to zero ceiling, 213m (700 ft) visibility, Sea State 5 ship motion limits. The coordinated development includes

a) aircraft flight control and display systems to provide handling qualities with satisfactory pilot workload,

b) shipboard approach and landing guidance systems and visual aids to effect precision in touchdown, and

c) improved guidance and control techniques for all-weather and rough seas operation with both current and future Navy V/STOL aircraft.

The effort reported in this document is part of the overall NAVTOLAND project objectives. It focuses on the requirements for automatic guidance to steer a VTOL aircraft to a small aviation facility ship.

The project has unusual complexities because of several factors. Among these are:

a) The ship is small (either a Spruance class destroyer or frigate), so that the wave action (up to Sea State 5) causes a larger than typical carrier landing vessel motion during the landing approach.

b) The mission may be sea rescue or some other objective which requires both night and all-weather (down to Cat IIIA) conditions to be within the landing scenario possibility.

c) Because the vessel approach and landing is at the end of the mission, the aircraft will be low on fuel. It is important

that the landing take place in a safe, efficient manner with a high probability of success on the first pass.

These and other factors are described in further detail in this report.

The specific objectives of this project have been the following:

1. To develop a flight system mathematical model and computer simulation that describes the approach and landing scenario in sufficient detail so that various guidance sensitivity studies and error effects can be evaluated. This model has consisted of integrating the results of various previous studies which describe the lift fan VTOL aircraft, the model-following flight control system, an MLS-based navigation system, six-degree-of-freedom vessel motion, and turbulence due to wind-over-deck effects.

2. To use this model (and simpler variations of it) to analyze the types of automatic approach guidance techniques which would be most suitable for achieving landing success on this mission. (Here, approach is defined as being that phase of flight down to some hover point offset from the landing pad.) This objective included defining all the factors and constraints relevant to selecting the approach guidance concept.

3. To outline briefly the similar factors and methodology which should be followed to determine automatic guidance concepts for the landing phase. Landing is defined as going from the hover (or stationkeeping) point down to the landing pad.

4. To define the additional cockpit simulator studies which are required to answer pilot preference (human factor) questions that cannot be answered by mathematical analysis and computer simulation alone.

This undertaking has benefitted greatly from the work of many previous studies and the opinions and suggestions of many researchers. The key sources are referenced throughout this report.

Chapter II describes the many facets and elements of the flight system model. This includes the modes of the approach and landing phases, the elements of the flight system model, and the constraints placed upon the guidance system.

Chapter III presents guidance concepts for lateral, longitudinal, and vertical modes of the approach phase. Then, the results of using a point-mass simulation of the aircraft to narrow down the guidance concepts are described.

Chapter IV outlines a brief, preliminary evaluation which has been made of the landing phase of flight. Here, emphasis is placed on describing what motion prediction and guidance alternatives are potentially possible to facilitate landing the aircraft.

Chapter V presents the results of using the computer simulation, (based on the model described in Chapter II) to evaluate two approach guidance concepts (selected in Chapter III) in more detail. The sensitivity of guidance performance to various navigation and flight control sensor errors, ship motion, and wind-over-deck turbulence is examined. Both single pass and Monte Carlo cases are used to make the evaluations. Statistical evaluation results of an open loop landing guidance concept are also included.

Chapter VI summarizes the conclusions made in this study and outlines a cockpit simulator test program for answering remaining questions.

Appendices A through H are included to give further details to elements of the system model, the mechanization details for the two guidance concepts studied, and organization of the computer program based on these details.

II

SYSTEM MODEL

The key initial step to determining guidance, navigation, or flight control requirements for landing a VTOL aircraft on a small aviation ship under adverse weather conditions is to develop a thorough understanding of the system structure. This understanding comes from formulating a mathematical model of the system including each of its important elements. Those elements which must be considered for analyzing automatic guidance requirements include:

1) The approach geometry and phases of flight the aircraft is expected to go through,
2) Sub-elements of the system and their inter-relationship, and
3) Various types of constraints.

The constraints that are included in the approach guidance problem can be classified as follows:

a) Environment and landing scenario,
b) Navigation and control system factors,
c) Pilot/crew factors,
d) Flight path end conditions, and
e) Guidance command considerations.

This chapter describes each of the flight phases, system elements, and constraints.

Overview

The problems of landing a VTOL aircraft on a relatively small aviation facility ship under adverse weather conditions are, in a word - complex. At this stage of analyzing such a complex system, it is mandatory to make several assumptions concerning the configuration of the system. This is required to reduce the number of options so that meaningful quantitative and qualitative results can be obtained within the available study budget.

Throughout this chapter and the associated appendices, these assumptions are indicated. Thus, the reader should keep in mind that alternative assumptions could lead to different results and conclusions.

The first assumption concerning the landing process is that it consists of two phases separated by a hover point. These phases have the following steps:

Phase 1 Approach to the hover (rendezvous) point near the moving vessel.

a) Cruise and speed reduction,
b) Transition from aerodynamic to powered lift,
c) Capture of approach initial conditions,
d) Constant speed approach,
e) Deceleration (flare), heading alignment, and rendezvous, and
f) Stationkeeping.

Phase 2 Landing (hover to touchdown)

a) Stationkeeping,
b) Letdown (transition from local level to ship-fixed coordinates), and
c) Touchdown (or wave-off/go-around).

An alternate scheme which has been suggested is to eliminate the hover point and to proceed directly to touchdown without a stationkeeping step. However, using a hover point does not appreciably affect the sequence of the previous steps of the approach, so it is included.

This study is mainly directed toward analyzing the automatic guidance requirements for Phase 1. However, both phases must be considered in designing the guidance system because the Phase 2 requirements place constraints (boundary conditions) on the Phase 1 flight paths.

The sub-elements of the flight system and their inter-relationship can be described in terms of the block diagram shown in Fig. 1. This block diagram is based on further assumptions that are discussed shortly. The block diagram forms the basis for constructing a digital simulation of the system and evaluating its performance. Performance evaluation and measure-

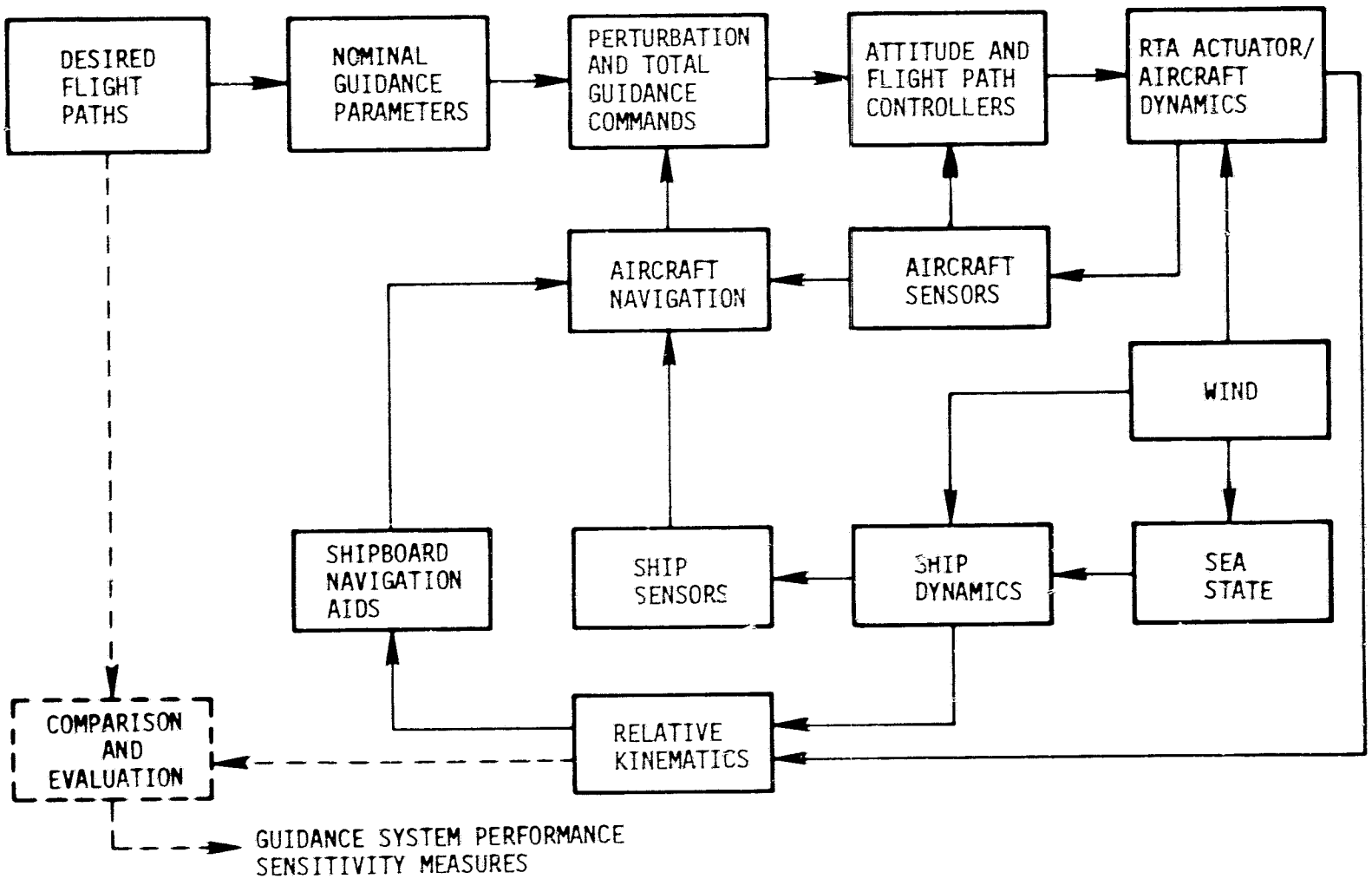

Figure 1. Block Diagram of Flight System Model with Performance Evaluation Additions

ment of its sensitivity to variations in parameters of the model are indicated by dashed lines in Fig. 1. The simulation and performance evaluation of the flight system are discussed in Chapter V.

System Elements

Geometric definitions and the system elements depicted in Fig. 1, except for Desired Flight Paths, Nominal Guidance Parameters, and Pertubation and Total Guidance Commands, are now described qualitatively. The guidance techniques (which include the desired paths and guidance commands) are discussed in Chapters III and IV.

Many of the system element models used in this study have been developed under a series of previous studies by government and industrial researchers. These sub-models have been appropriately modified and integrated to form a suitable working model of the system. In describing the model elements, then, the following descriptions are summaries of source references which are cited. In many cases, these sub-models have been developed by previous integration of other models as can be seen by checking their references. The primary sub-model sources are:

Wind/Sea State/Ship Dynamics - R.L. Fortenbaugh, et al - Vought Corp. [1]
Navigation System and Sensor Models - S.F. Schmidt, et al - AMA, Inc. [2]
Flight Control Scheme - V.K. Merrick, et al - NASA Ames Research Center [3]
RTA Lift Fan Aircraft Dynamics - M.P. Bland, et al - McDonnell Douglas Corp. [4]

These references provide descriptive detail. Technical summaries of each are found in Appendices A-E.

Approach Geometry Definitions Before proceeding with description of the system elements, the reference frames and approach geometry involved in the overall problem are first defined. Figure 2 shows the relationship of the VTOL aircraft to the hover point in the horizontal plane. The hover

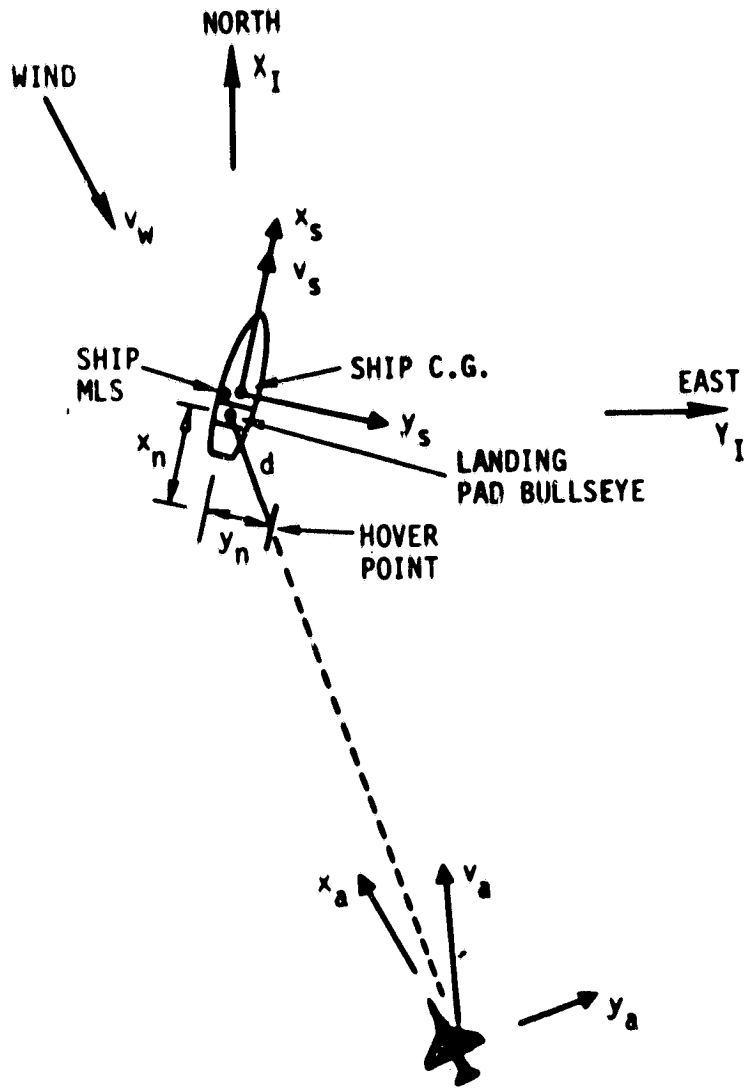

Figure 2. Sketch Showing Relative Locations of Ship c.g., MLS Station, Landing Pad Bullseye, Hover Point, and Aircraft During Approach.

point is defined to be at some average location away from the landing pad bullseye. This is shown as distance d and components (x_h, y_h) in the ship reference frame (X_s, Y_s). Because the ship is "tossed around" by the heavy seas, the hover point is considered to be located at an average position with respect to the bullseye. Thus, the vector d is time varying.

Notice also in Fig. 2 that the bullseye is not located at the ship center of gravity (c.g.). In addition, the aircraft obtains position measurements of its location with respect to the shipboard MLS. The MLS is not located at the bullseye or the c.g. The airborne navigation system must be able to work with all these reference points.

Figure 3 defines several velocity vectors projected into the horizontal plane. Here, the reference direction is along the average heading of the ship centerline X_s. As shown on the left side of Fig. 3, the aircraft longitudinal axis X_a is rotated an angle ψ_B with respect to X_s. The aircraft horizontal component of the airspeed vector V_a has sideslip angle β and is rotated ψ_a with respect to X_s. The wind vector V_w is added to V_a to obtain the aircraft inertial velocity vector V_I. The wind vector is rotated an angle ψ_w with respect to X_s.

The right side of Fig. 3 defines the wind-over-deck vector V_{WOD}. It is obtained by subtracting the ship velocity V_s from V_w, and it describes the wind an observer on the deck of the moving ship would feel. V_{WOD} has heading angle ψ_{WOD} with respect to X_s.

Also defined in this sketch is the velocity of the aircraft relative to the ship V_R. It is obtained by subtracting ship velocity V_s from aircraft inertial velocity V_I. V_R has heading angle ψ_R with respect to X_s. In this study, no ocean current effects are assumed to be present so that the inertial velocity of the ship V_s is also the velocity with respect to the water mass.

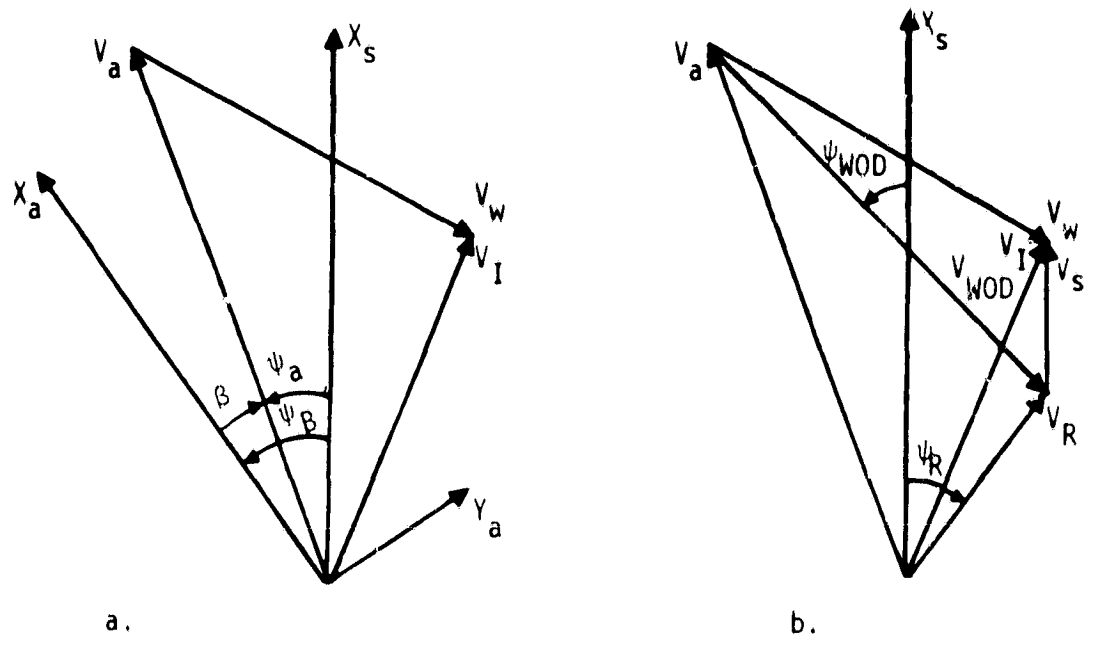

Figure 3. Vector Definitions of Relevant Velocities in Horizontal Plane.

Vessel Geometry It is assumed that a DD963 Spruance class destroyer is the vessel being used. The profile of this vessel is shown in Fig. 4 A detailed schemetic of the landing pad is shown in Fig. 5. The location of a roll-pitch stabilized glideslope indicator also being considered is shown in Fig. 6. It is assumed in this study that the MLS antenna is located at the same point as this glideslope indicator. However, for this study, it is assumed that the MLS transmitter is not attitude stabilized. For computational ease, the geometries of Figs. 5 and 6 are combined to the simplified form shown in Fig. 7. A candidate hover point is shown directly over the landing pad bullseye and on the 3° glideslope beam eminating from the MLS. The vessel geometry depicted in Fig. 7 is used throughout the remainder of this report.

Wind, Sea State, and Ship Dynamics The Navy mission requirements include landing on a ship that is underway and traveling at speeds of up to 30 kts. The requirements also include landing in the presence of rough seas. This roughness is measured by the energy distribution and frequency content of the surface waves, and it is specified in practical terms by sea state. Sea State 5 conditions with wave heights of up to 4 m (12 ft) must be considered.

The ship motion, wind-over-deck (airwake), and sea state models have been unified into a compatible set for thirteen different environmental scenarios by Fortenbaugh [1,5]. These conditions, which relate sea state, ship speed, wind speed, wave height, and five other parameters are presented in Table C.1. Appendices C and D are summaries of the ship motion and environmental wind modeling.

Briefly, the ship motion is modeled in six degrees of freedom - roll, pitch, yaw, surge, sway, and heave. Each degree-of-freedom is modeled as the sum of six sine waves, where the six frequencies, their amplitudes, and their phase angles are chosen to span the wave encounter frequency driving the ship's motion. For each of the thirteen conditions of Table C.1, there is a set of six frequencies, amplitudes, and phase angles for each degree of freedom. The simulation is constructed so that choosing which of the thirteen conditions of Table C.1 to study also selects the

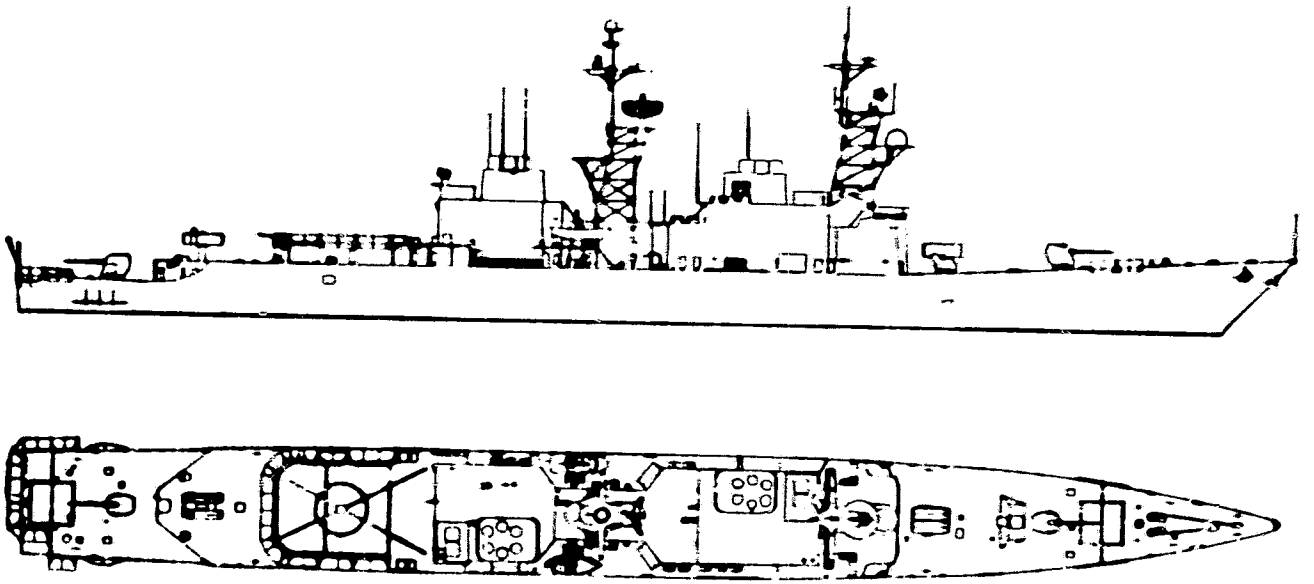

Figure 4. Profile of Spruance Class DD963 Destroyer
(7800 Tons, 563 ft Long, 30 kts)

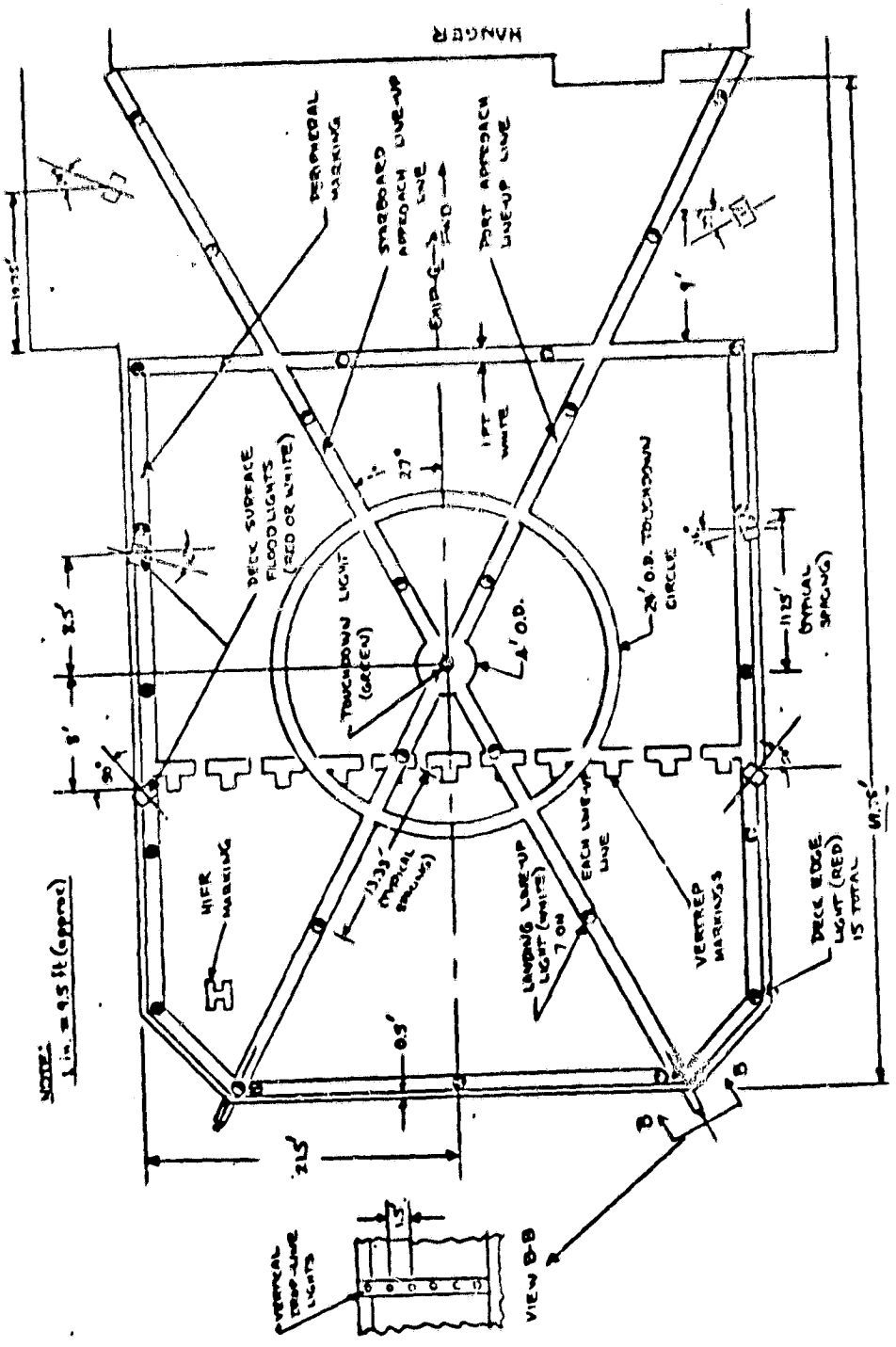

Figure 5. Schematic of DD963 Main Flight Deck Marking and Lighting [1]

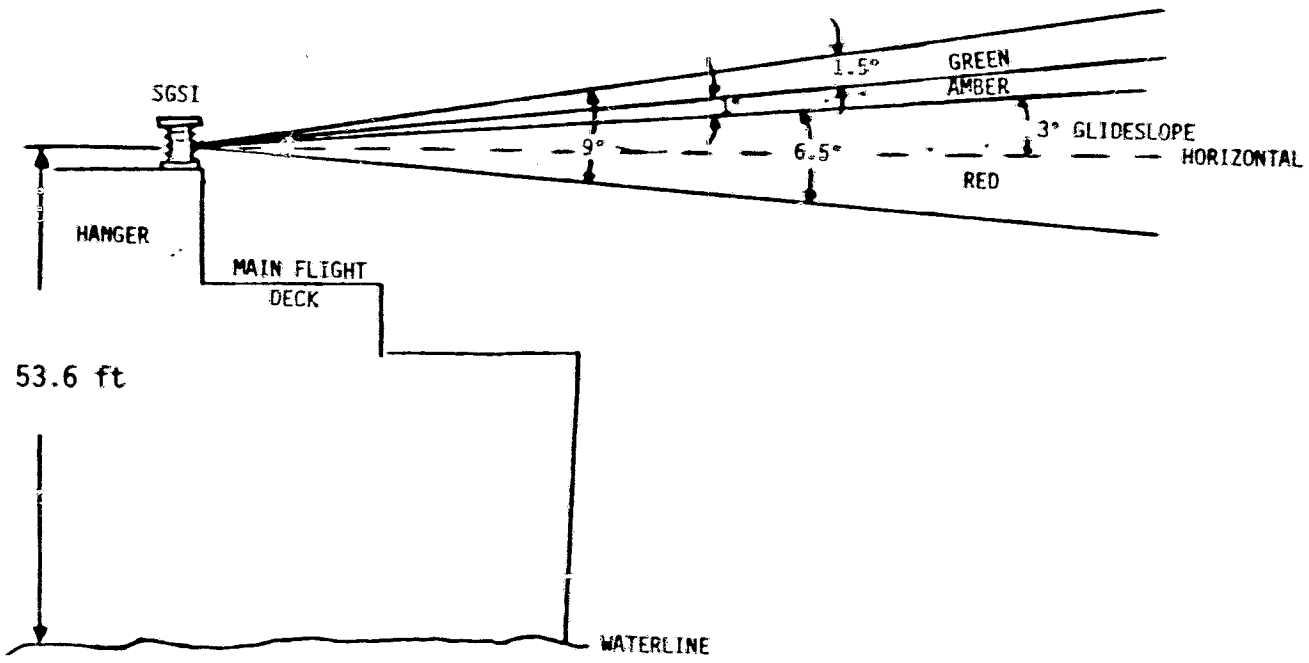

Figure 6. Schematic of Roll-Pitch Stabilized Glideslope Indicator [1]

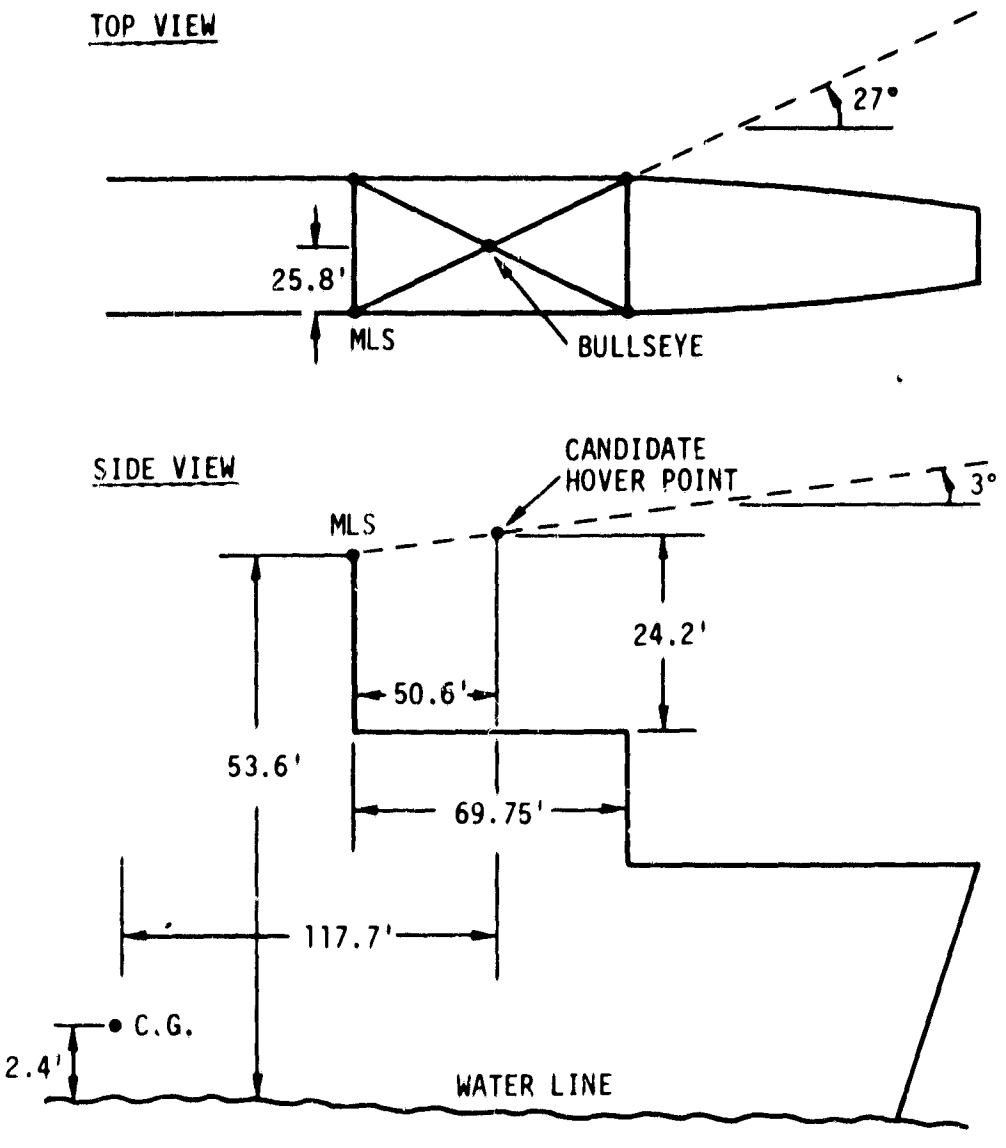

MLS #1	(-67.' , -25.8 ', -51.2')	w.r.t. ship c.g.
Hover Point	(-117.7', 0., -53.33')	w.r.t. ship c.g.
Bullseye	(-117.7', 0., 29.1')	w.r.t. ship c.g.

Figure 7. Standard Ship Geometry for Computation Purposes

appropriate coefficients for the sum-of-sine-waves model. An example of actual Sea State 5 motion for the USS Bowen is shown in Fig. 8. Figure 9 shows 90 sec of simulated Sea State 5 motion using the sum-of-sine-waves mode. Here, the surge, sway, and heave accelerations are in m/s^2, and the roll, pitch, and yaw are in degrees.

The ship motion causes several problems to the approach and landing process. Chief among these are:

1) The aircraft must somehow land on a pad that is moving with six degrees of freedom. This implies that either (a) the aircraft control system must have the authority and bandwidth to bring the aircraft into synchronized motion with the ship, or (b) the guidance system must be able to predict when an acceptable lull exists in the ship motion so that it is safe to land, or (c) the aircraft structure, landing gear, and pilot protection devices must be constructed to withstand the impact between the aircraft and ship at touchdown.

2) A computation sequence must be made, as part of the approach guidance mechanization, which defines where the hover point is. In this study, the hover point is chosen as an average position above the center of the moving landing pad. Thus, the hover point computations must account for the ship's motion.

3) The aircraft determines its position and velocity relative to the moving ship and the hover point by use of an MLS system fixed to the ship deck. It is assumed that the MLS system is not attitude stabilized. Thus, additional computations and sensor measurements are required to compensate the nonsteady MLS navigation signals for the ship motion.

Coupled to the ship's motion are the wind-over-deck effects, as described in Appendix D. The wind-over-deck is a model of the wind turbulence caused by the assumed constant wind (taken from Table C.1) reacting with the ship superstructure. This model, devised by Fortenbaugh, was based on the work reported in Ref. 6. The model includes three orthogonal mean wind terms plus three orthogonal random terms. The

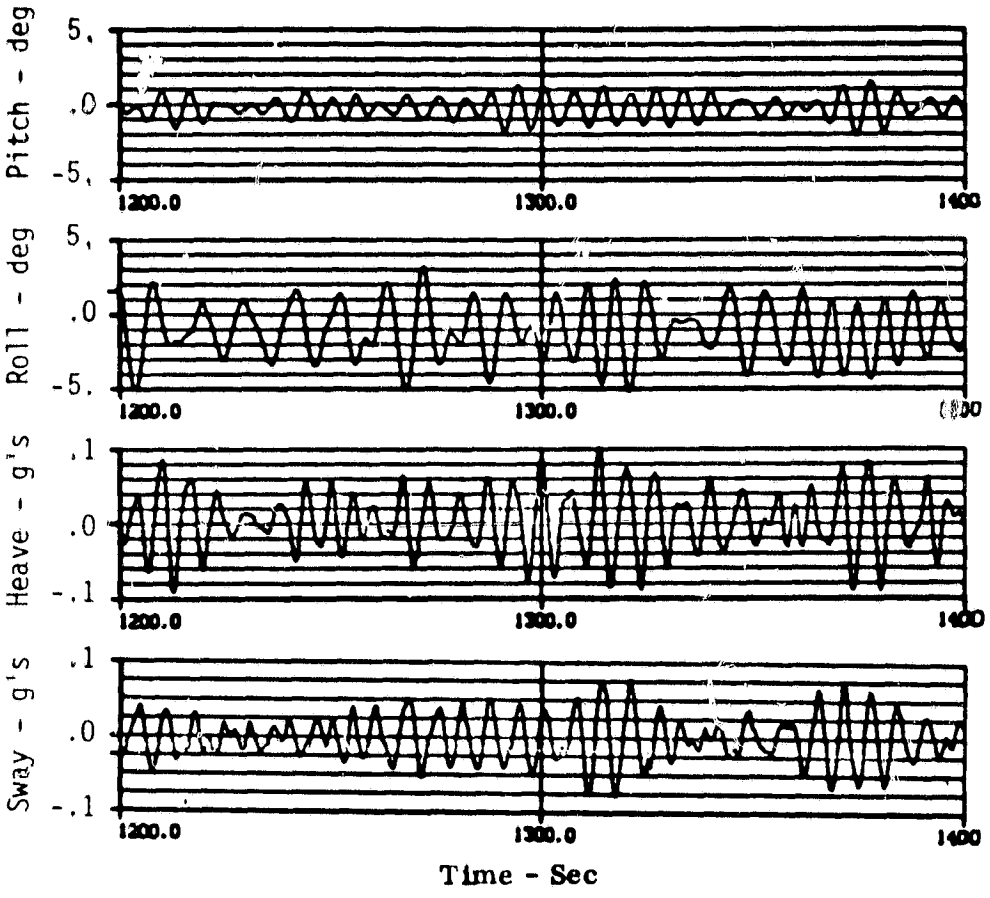

Figure 8. Representative Ship Motion: Pitch and Roll in Degrees; Heave and Sway in g's

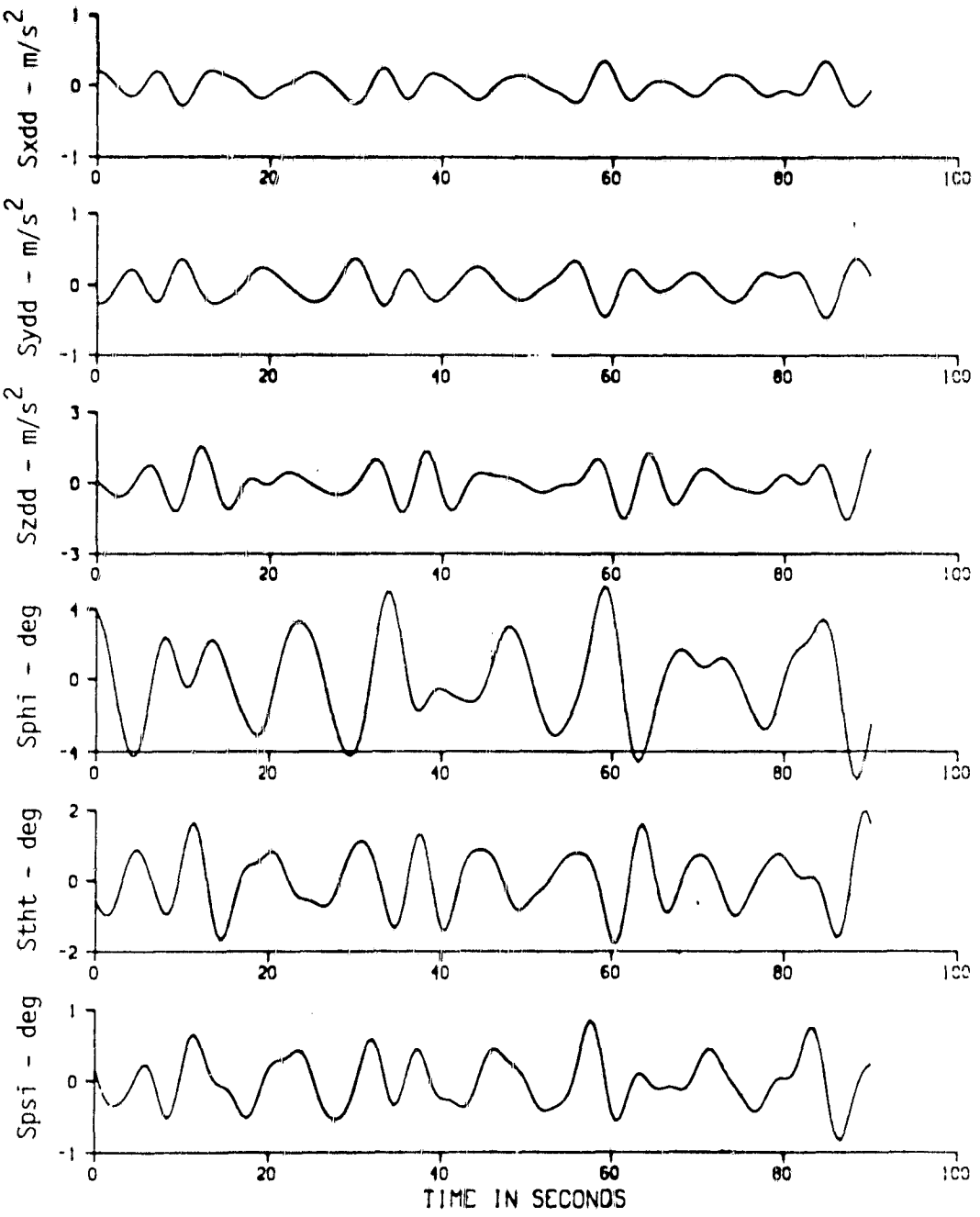

Figure 9. Sum of Sine Waves Model of Ship Motion in Sea State 5

magnitudes of the six terms are dependent upon the geometric position with respect to the ship deck. Thus, the wind model is attached to the ship and moves with the ship motion. Also, the wind turbulence that the aircraft experiences in flying through the wind-over-deck is dependent upon the specific path followed in going to the hover point. Examples of the variation in the three components of wind-over-deck magnitude are shown in Fig. 10. More detail on the geometric variation is presented in Appendix D.

The wind-over-deck turbulence causes variations to both the aerodynamic loads on the aircraft and to the thrust provided by the lift fans. In a study of manual approaches of a VTOL aircraft to a destroyer with a cockpit simulator at NASA Ames Research Center (Autumn, 1979), the wind-over-deck effects proved to cause unacceptable handling qualities [7, 23]. However, in similar tests at Ames with a different aircraft, the wind-over-deck effects were regarded as secondary [8]. At this writing, the reason why different wind-over-deck effects were experienced and their relative significance have not been determined. (As shown later, this may be due to the hover altitude.)

Aircraft Flight Control and Dynamics The aircraft model used in this study is the lift/cruise fan V/STOL research technology aircraft (RTA). This model was developed by McDonnell Douglas [4]. This design is a modified T-39 Sabreliner powered by three turbojet engines which drive three fans. A more complete description is given in Appendix A. The aircraft transitions from aerodynamic control to the powered lift mode below 120 kt. In this study, the approach phase is considered to begin when the aircraft is in the powered lift mode.

It is assumed that the RTA aircraft has a flight control system based on the state rate feedback implicit model following (SRFIMF) control concept of Merrick [3]. A description of this flight control philosophy is given in Appendix B along with block diagrams of the control logic associated with the RTA aircraft. The basic idea of this control is to cancel the aircraft dynamics by introducing an equivalent inverse into the control logic. If this cancellation can be accomplished, then the aircraft can be controlled with some desired response characteristics.

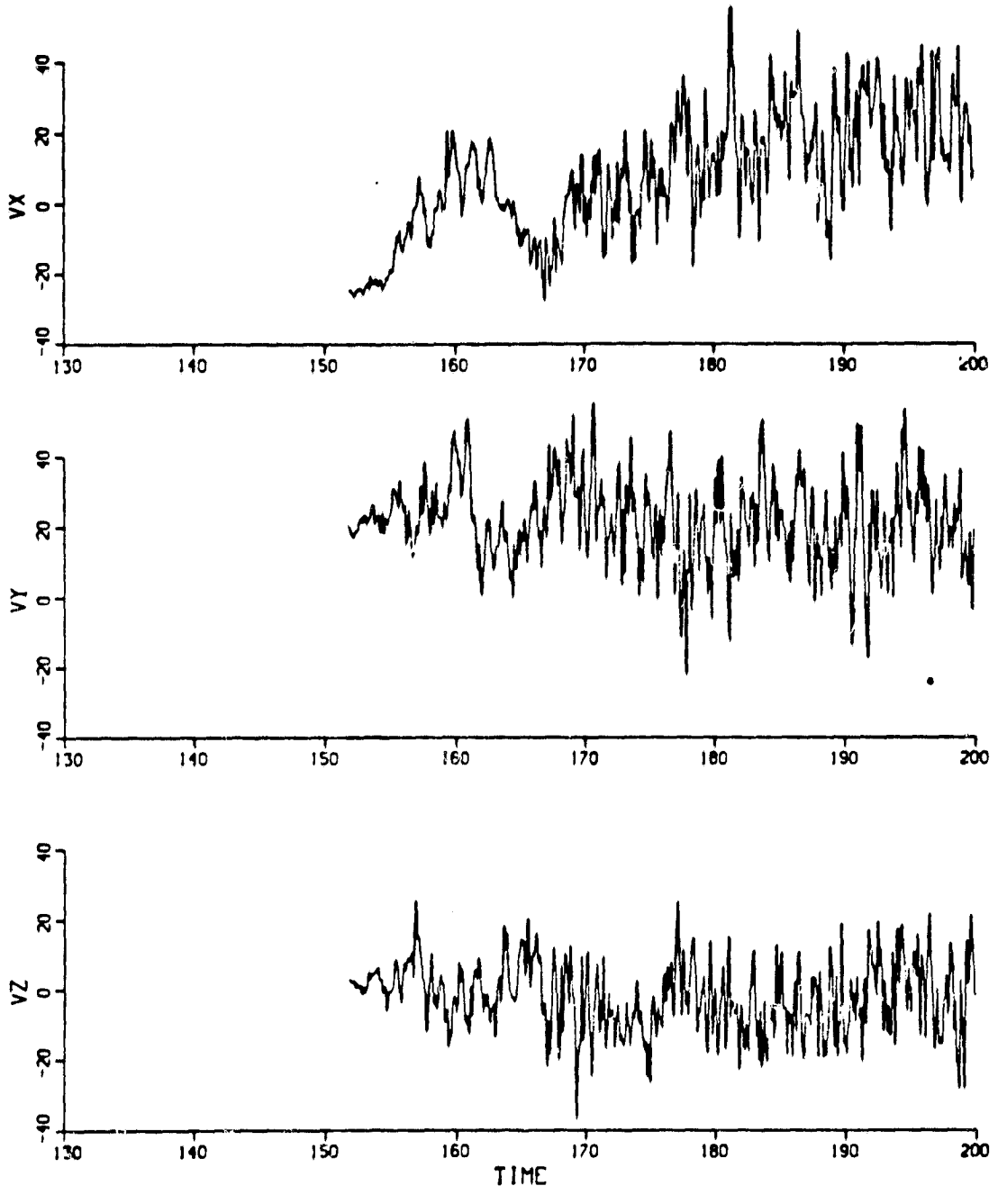

Figure 10. Examples of Three Components of Wind-Over-Deck Turbulence for 25 kt Ship Speed Heading into a 25 kt Wind (in Aircraft Body Axes).

The success of applying this philosophy to the RTA aircraft, under somewhat ideal conditions (perfect sensors), is reported in Ref. 3.

A convenient way of characterizing the dynamics of the RTA aircraft/SRFIMF flight control combination can be obtaining by examining the step response to inputs into the primary control axes. This was done for roll angle and longitudinal, vertical, and lateral speed commands when the aircraft was traveling at 20, 60, and 120 kt in level flight.

Figures 11a-d show the roll response to a $\pm$ 5° command, longitudinal speed to a $\pm$ 1.5 m/s ($\pm$ 5 ft/sec) command, vertical speed to a $\pm$ 1.5 m/s ($\pm$ 5 ft/sec) command, and lateral speed to a $\pm$ 1.5 m/s ($\pm$ ft/sec) command at 20 kt. Figures 12 and 13 show similar responses at 60 and 120 kt. Each of these responses exhibits approximately a 0.7 damping ratio. The reason for lack of symmetry in these responses is under current investigation. The output-to-input transfer function is approximately second order and of the form,

$$\frac{O(s)}{i(s)} = \frac{\omega_n^2}{s^2 + 2\rho\omega_n s + \omega_n^2} \quad .$$

Table 1 shows the corresponding natural frequencies for each axis.

Table 1. Natural Frequencies of Given Step Responses (rad/sec)

Axis/Speed	20 knot	60 knot	120 knot
Roll (ϕ/ϕ^c)	0.29	0.35	0.32
Longitudinal (V_x/V_x^c)	0.19	0.20	0.18
Vertical ($\dot{h}/\dot{h}^c$)	0.19	0.18	0.18
Lateral (V_y/V_y^c)	0.21	N/A	N/A

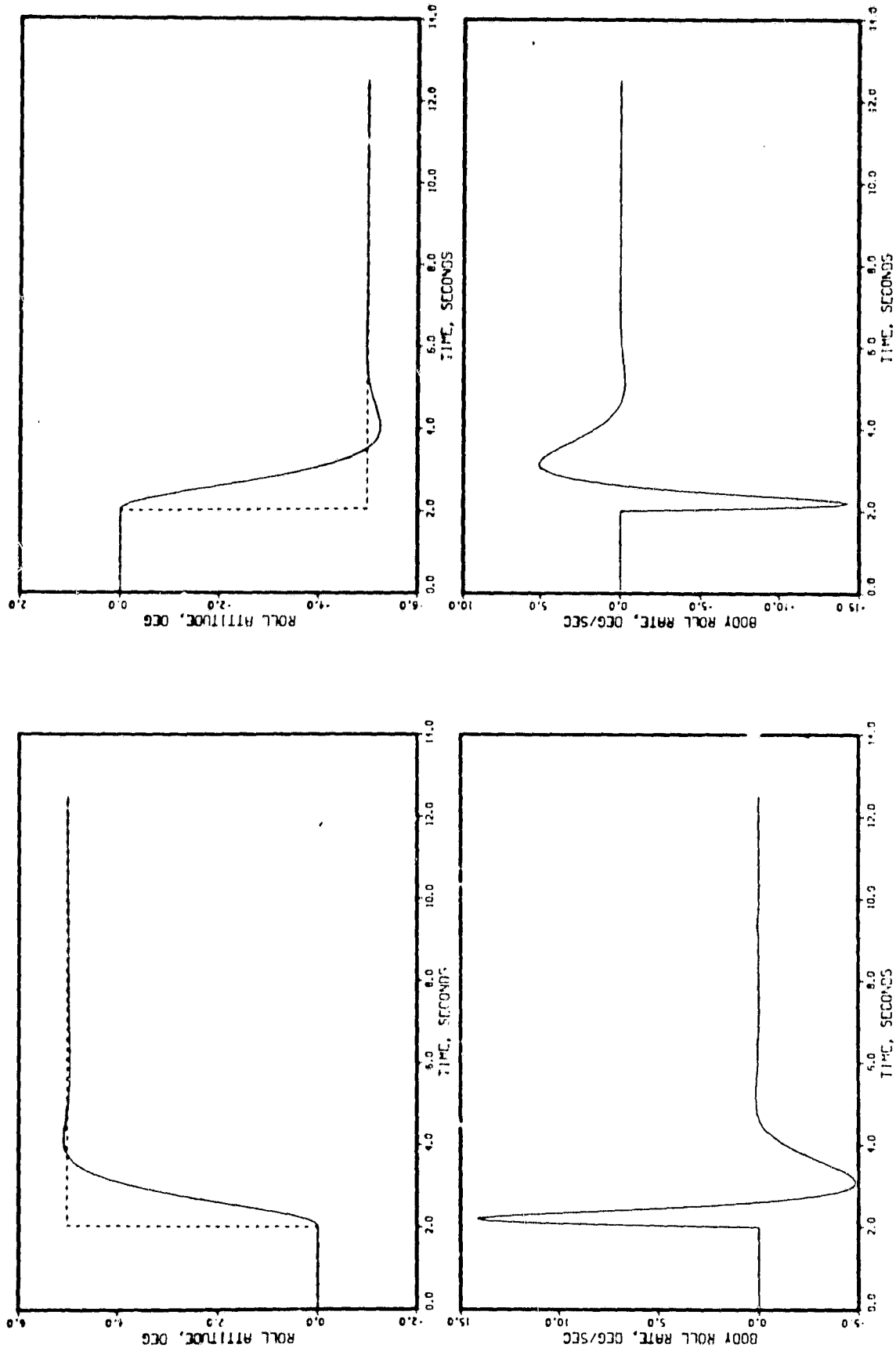

Figure 11a. Roll Responses at 20 knot for ± 5 deg. of Commands

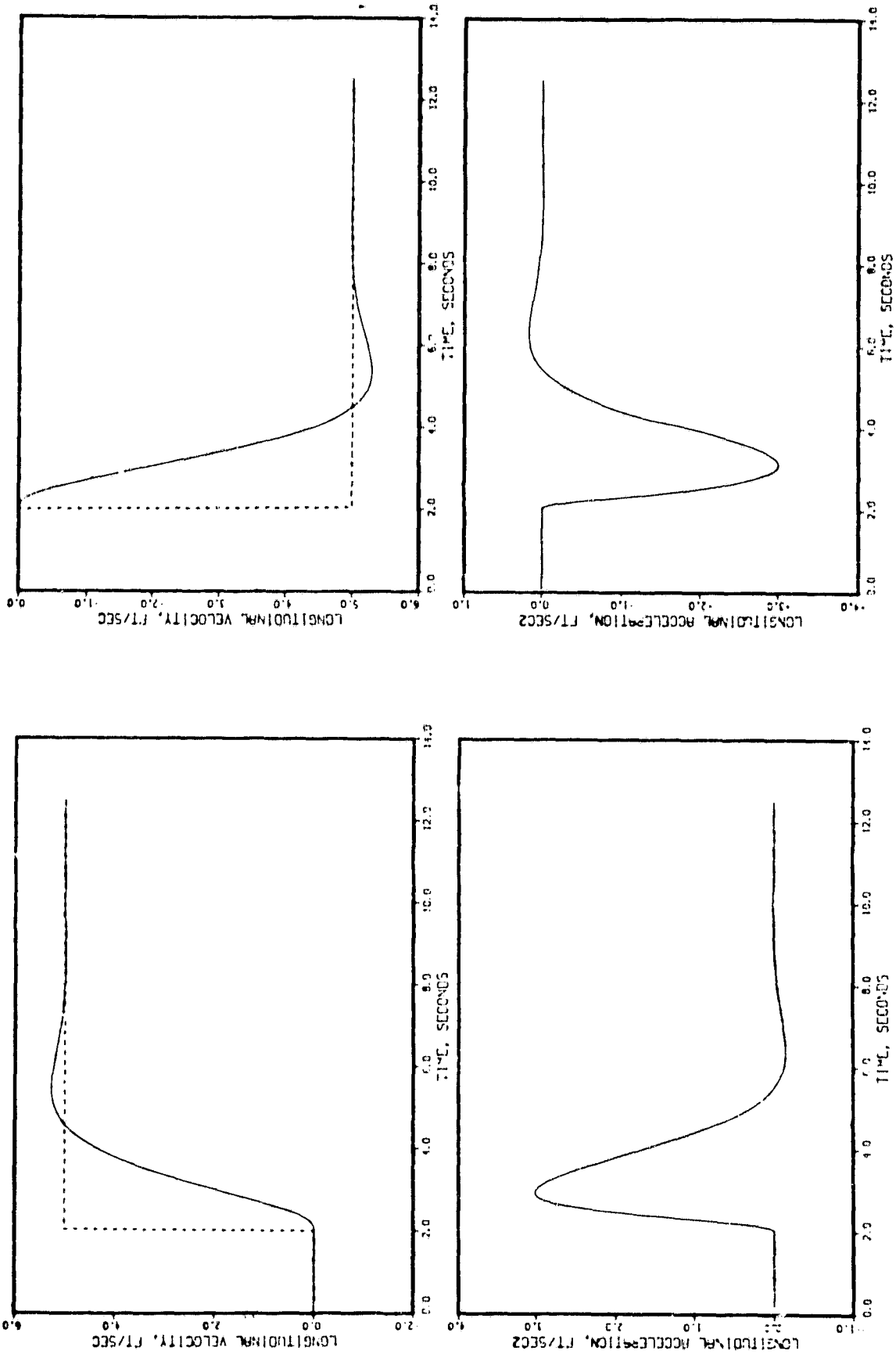

Figure 11b. Longitudinal Velocity Responses at 20 knot for ± 5 ft/sec of Commands about Nominal

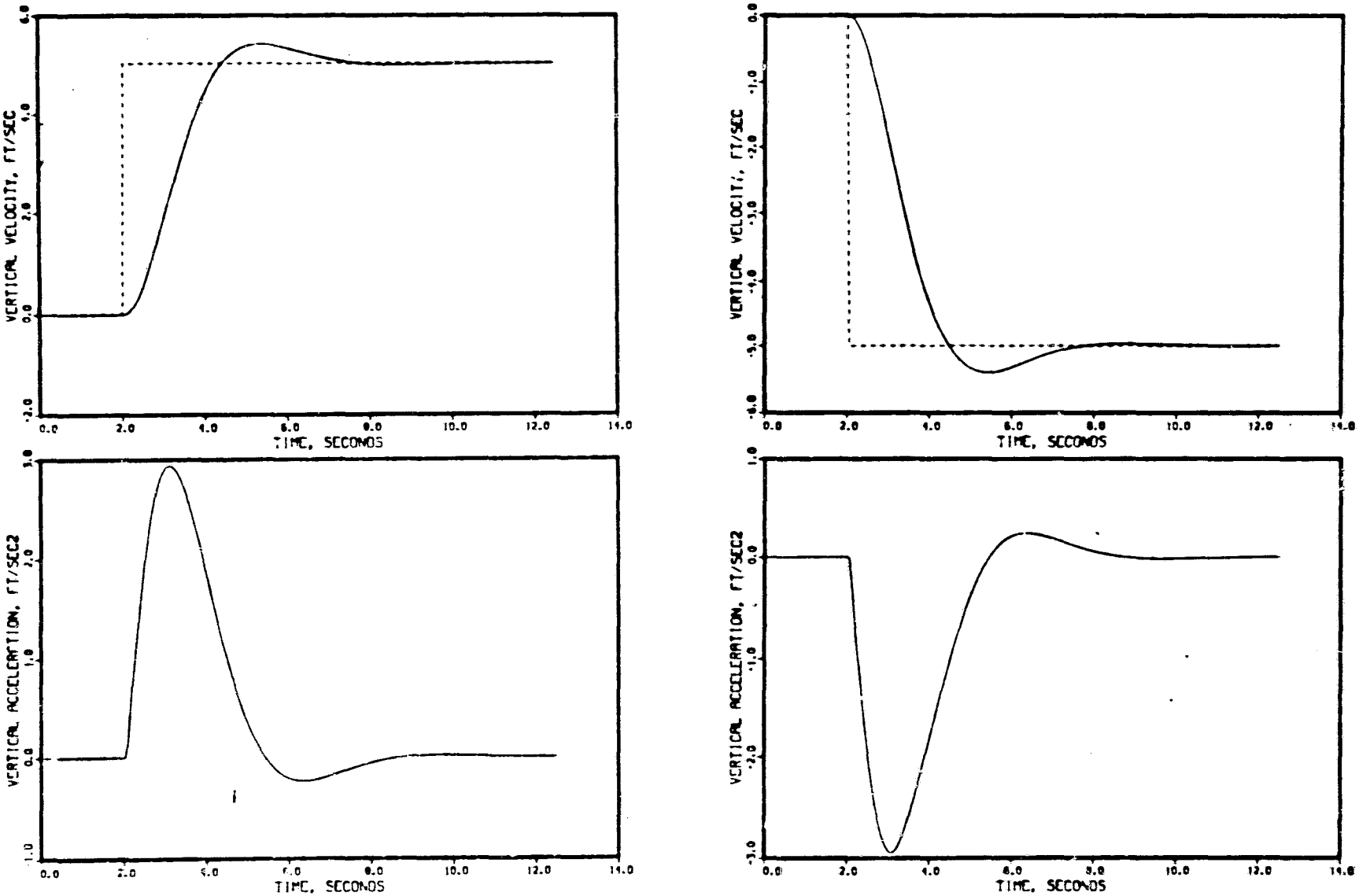

Figure 11c. Vertical Velocity Response at 20 knot for ± 5 ft/sec of Command

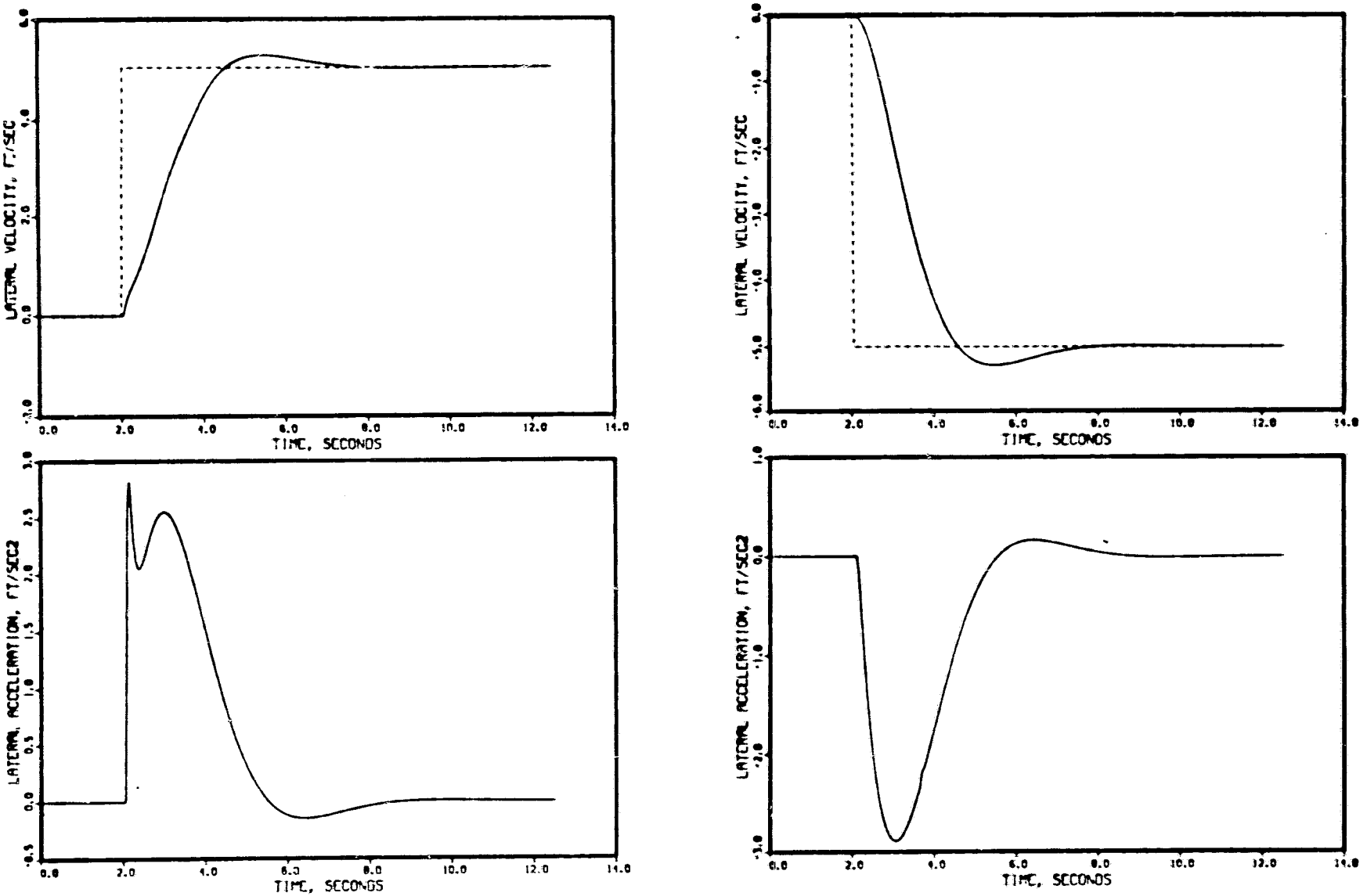

Figure 11d. Lateral Velocity Response at 20 knot for ± 5 ft/sec of Step Commands. (Note the lack of symmetry.)

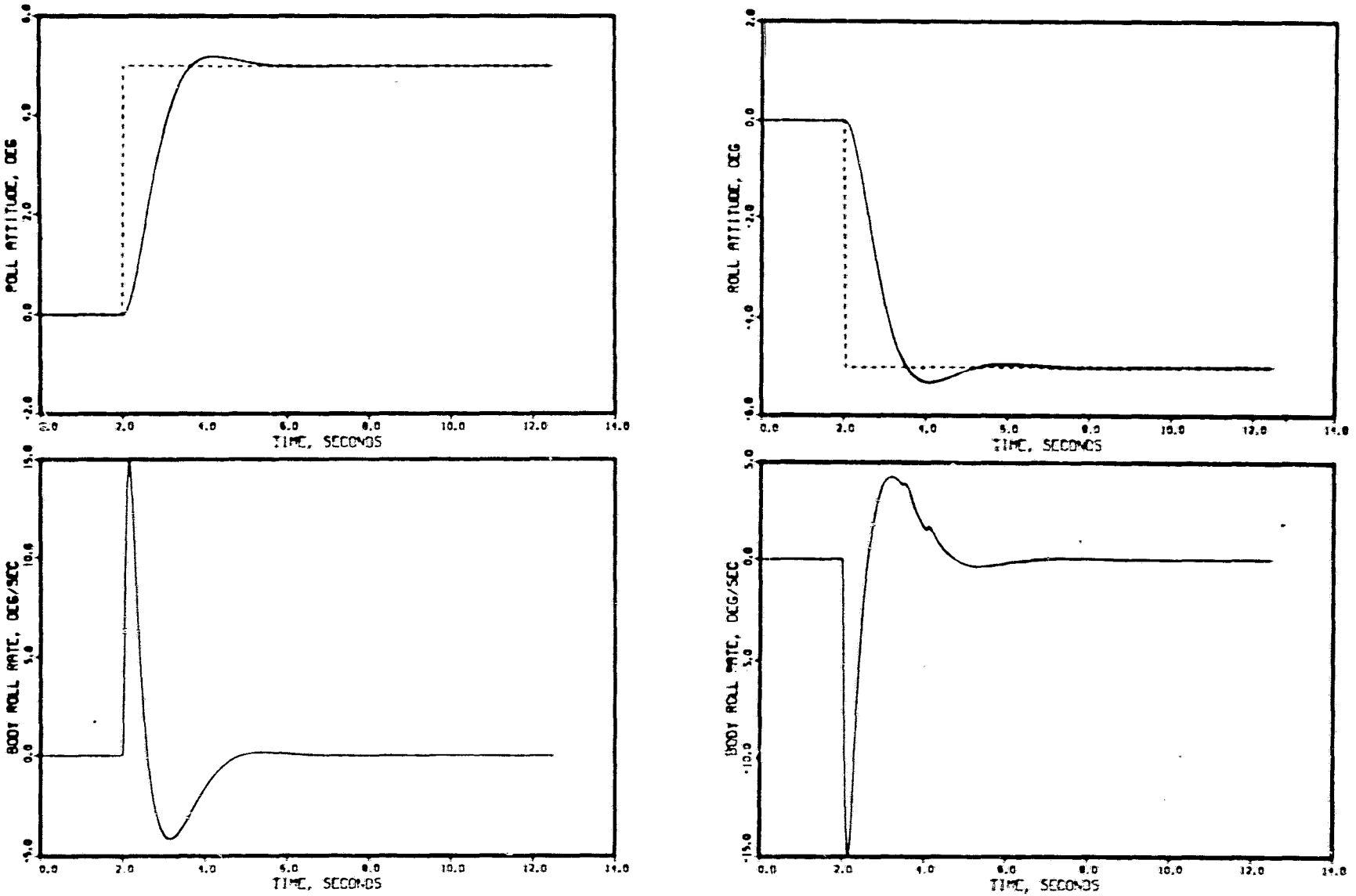

Figure 12a. Roll Response at 60 knot for a ± 5 deg Command

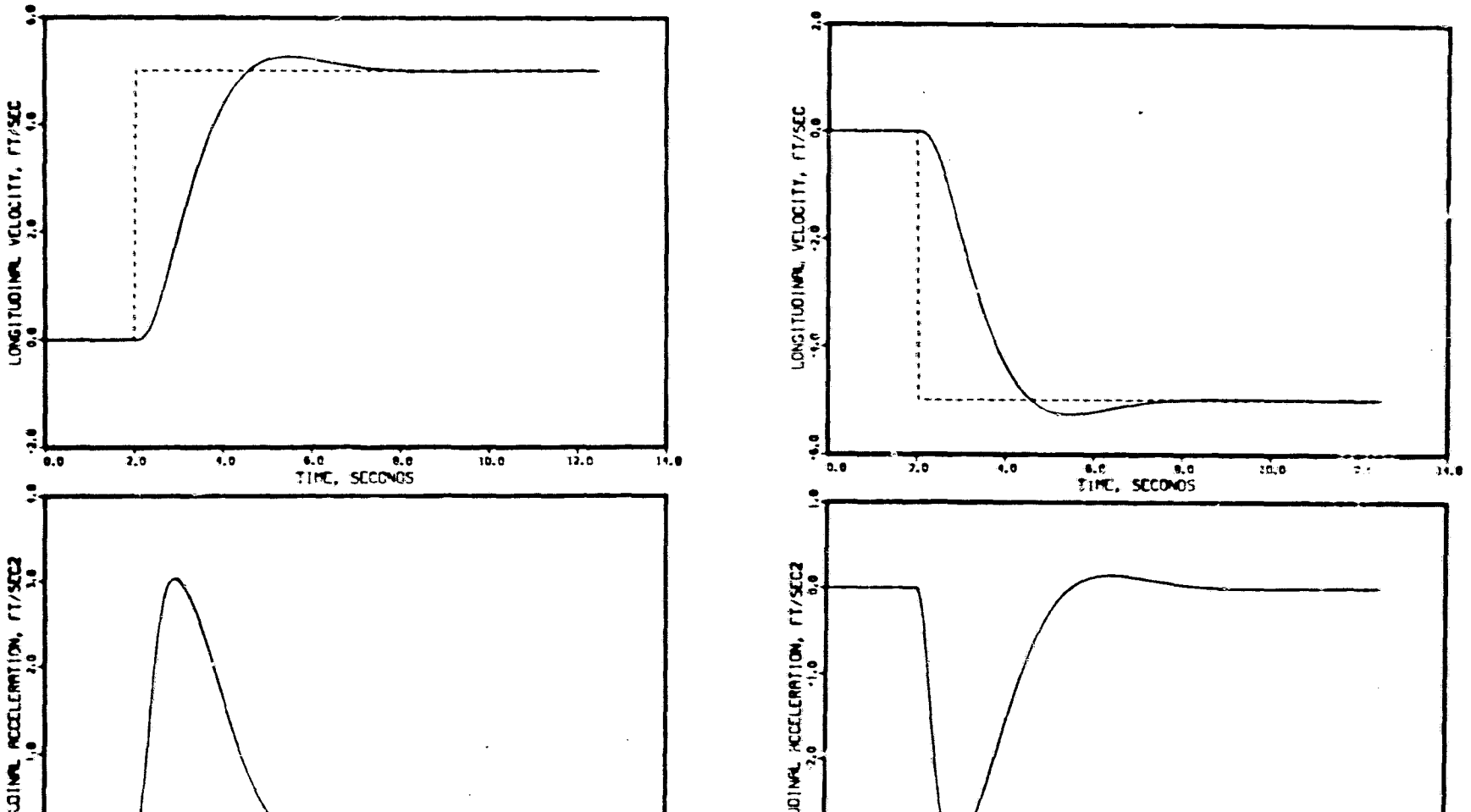

Figure 12b. Longitudinal Velocity Response at 60 knot for ± 5 ft/sec Command about the Nominal

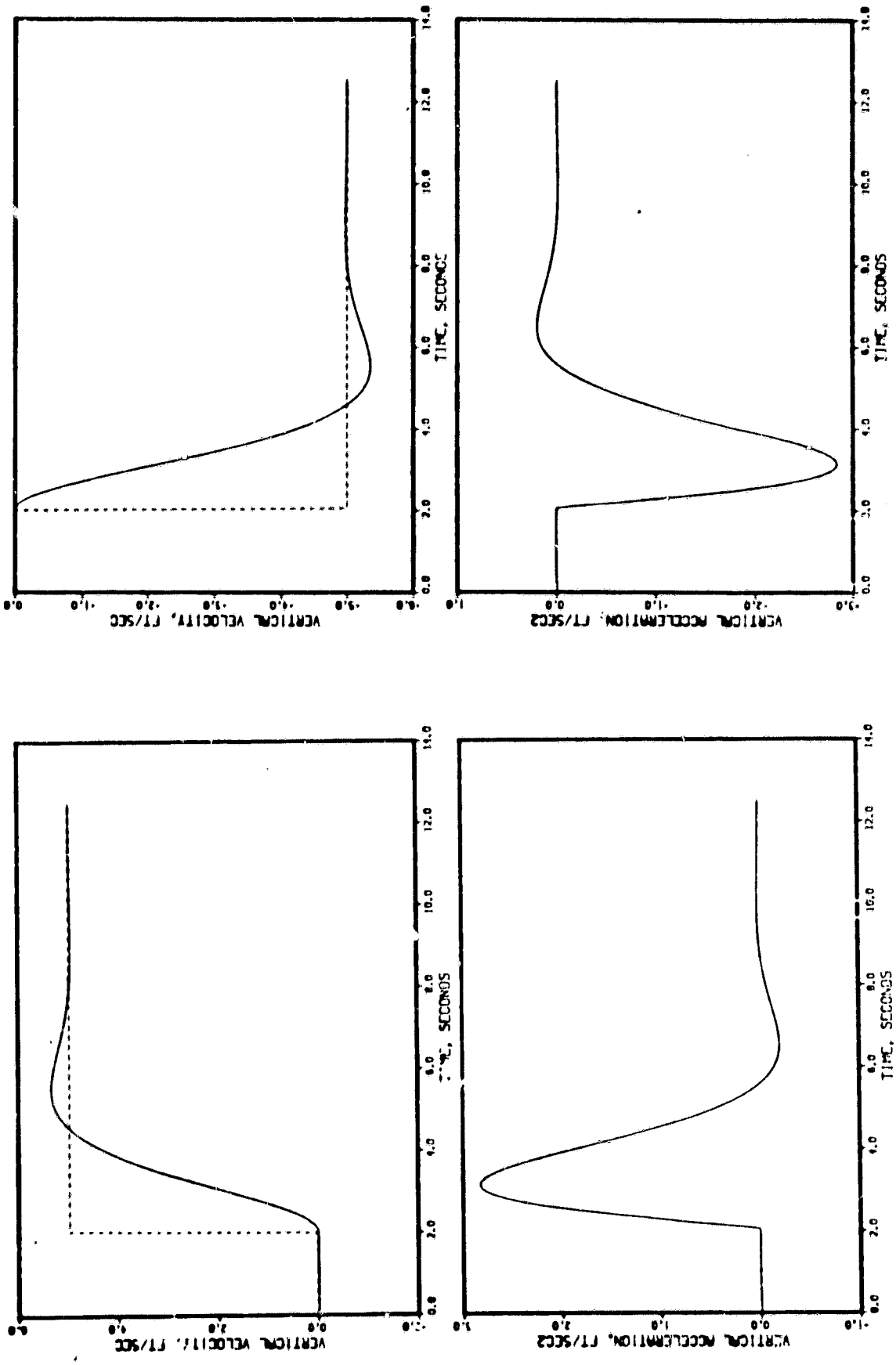

Figure 12c. Vertical Velocity Response at 60 knot for ± 5 ft/sec of Commands

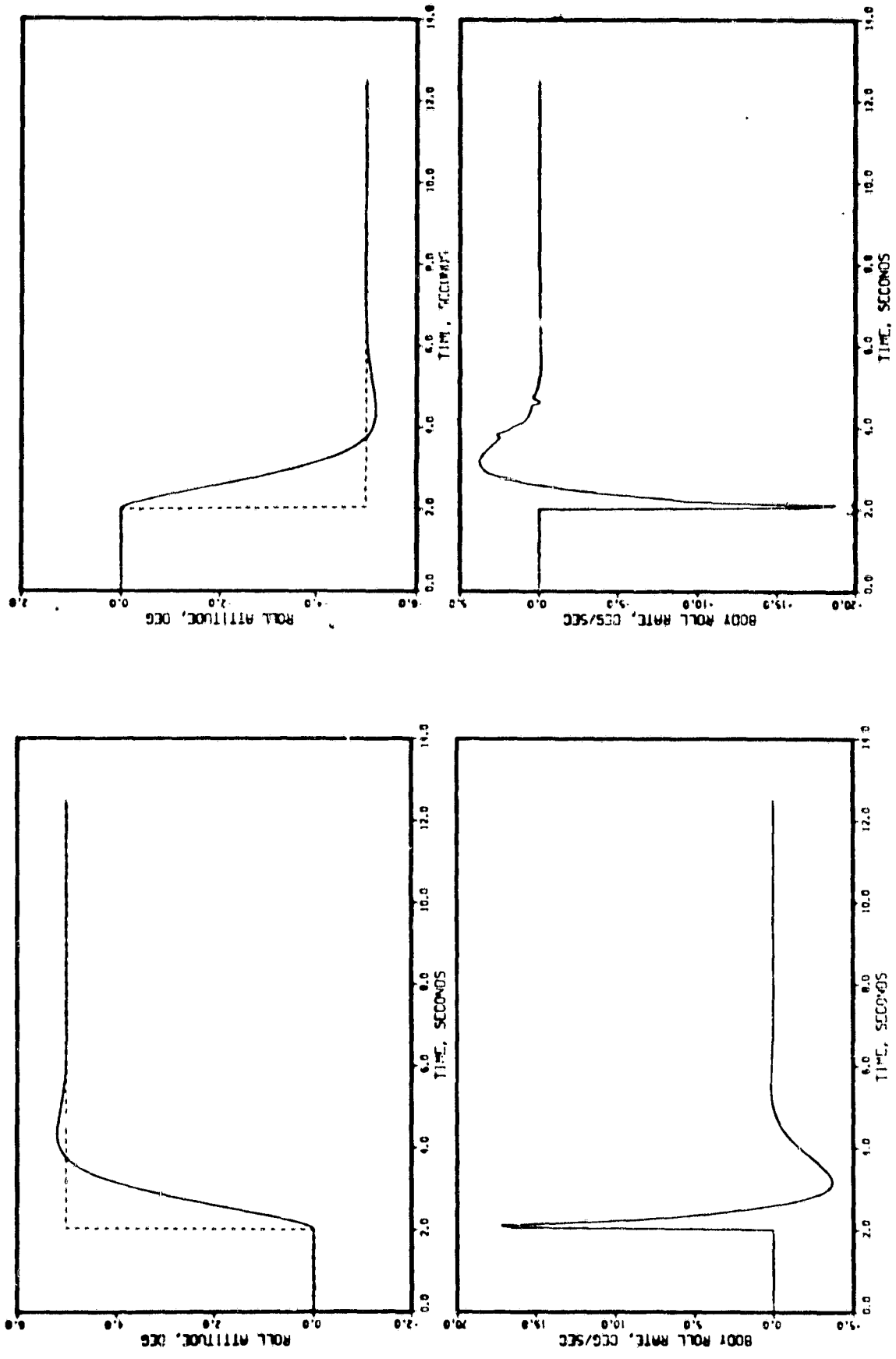

Figure 13a. Roll Response at 120 knot for a ± 5 deg Command

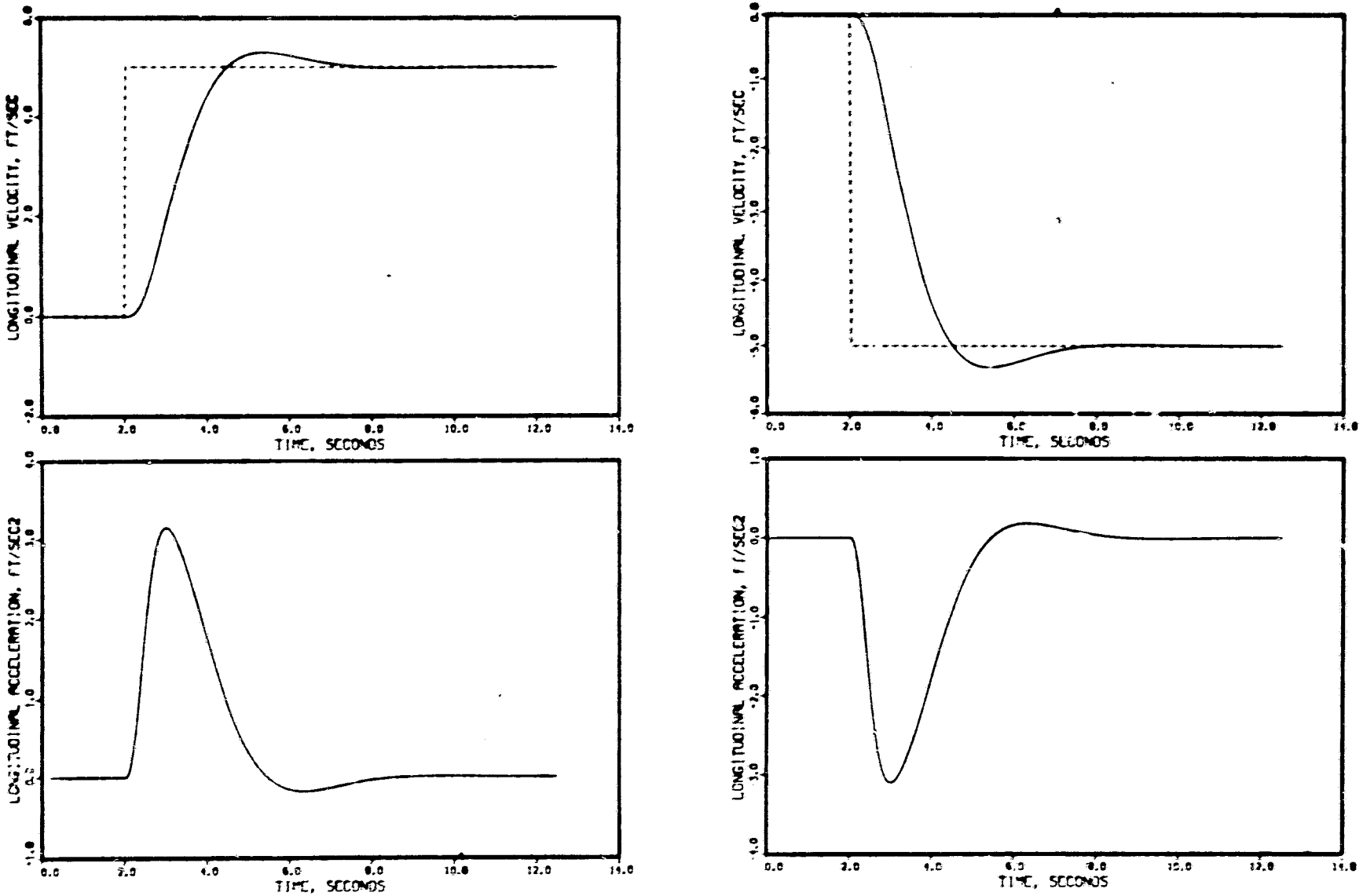

Figure 13b. Longitudinal Velocity Response at 120 knot for a ± 5 ft/sec Command

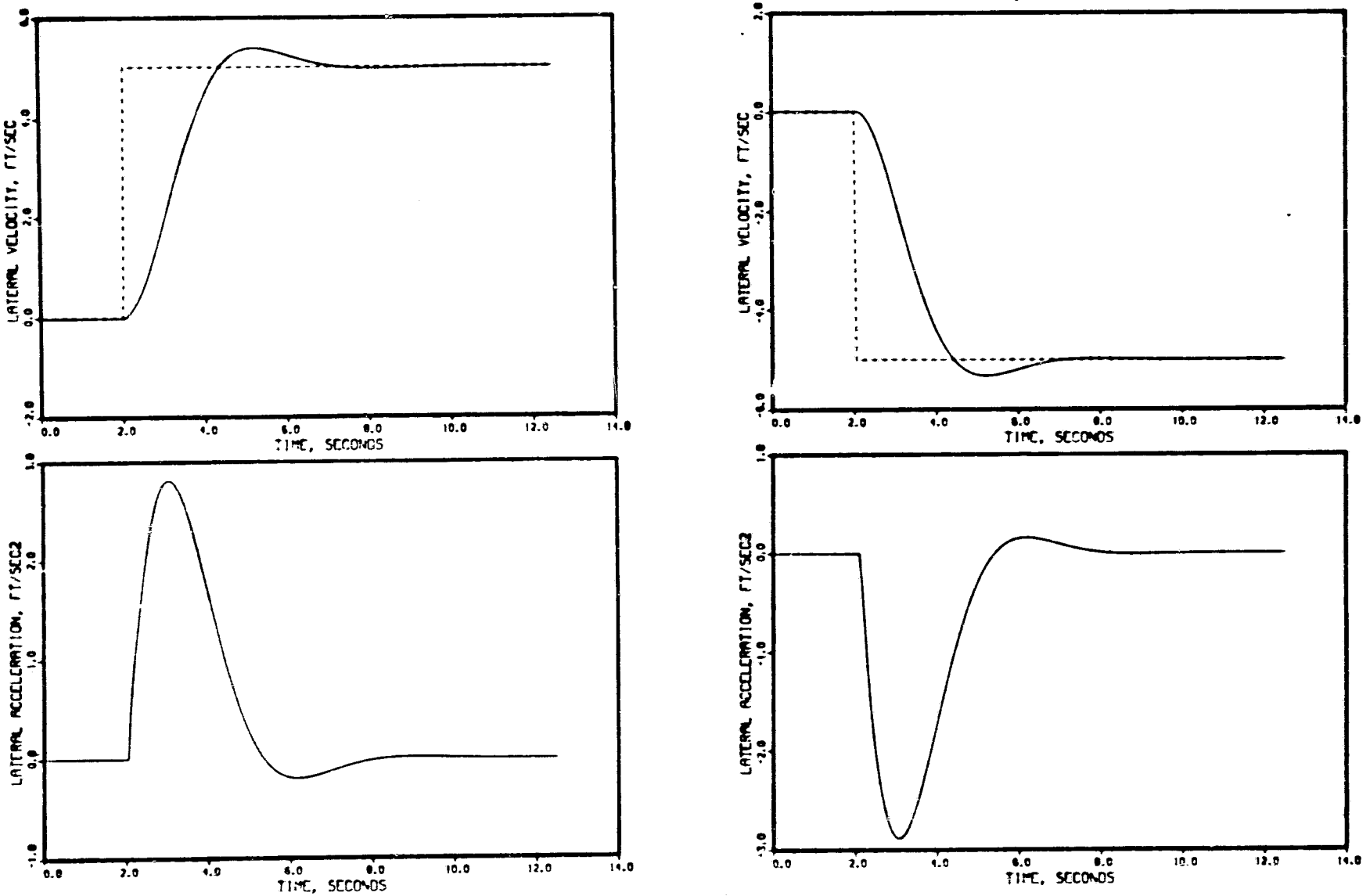

Figure 13c. Vertical Velocity Response at 120 knot for a $\pm$ 5 ft/sec Command

From these results, there emerges two important conclusions: (1) For all practical purposes, the RTA with SRFIMF controller can be considered as a decoupled linear second order system for each axis, and (2) the response of each axis is independent of flight speed. Point (1) implies that simple guidance and navigation analysis can be carried out using the simplified second order dynamics; however, the external disturbances, most dominent of which is the wind-over-deck turbulence effect, cannot be analyzed using the above models because the resulting aerodynamic and engine effects are not included in such simplified models. Point (2) implies that the guidance law design can be simple, since there is no need for decoupling axes nor gain scheduling with respect to the speed.

Another issue which required investigation is the effect of flight control sensor errors to the performance of the RTA/SRFIMF. A discussion of the effects of simulated flight sensor errors on the overall system performance is presented in Chapter V.

From an approach guidance requirements point-of-view, the aircraft and flight control system introduce particular response lags into the overall performance of the system. In addition, the lift fans have deadbands which can produce limit cycles in the guidance response. (These non-linear effects were not investigated in this study). Finally, the dynamic characteristics of the aircraft/flight control system interact with the dynamics of the navigation filters and steering laws; overall guidance performance must take into account possible degradation due to this dynamic coupling.

Navigation The approach and landing navigation system is explained in Appendix E and is based on Refs. 2 and 22. The shipboard segment of this system has an MLS/DME, three-axes body-fixed attitude gyros, and three-axes linear accelerometers. In addition, a shipboard computer is used to estimate an average position of the MLS antenna. This estimate is used to remove the effects of roll and heave on the nominal location of the antenna position. These computations determine a "landing pad deviation vector" which is data-linked to the aircraft. Ship velocity is also data linked to the aircraft.

The aircraft segment of the navigation system includes the MLS/DME receivers, three-axes body-fixed linear accelerometers and attitude gyros, and a navigation computer. The aircraft segment uses the landing pad deviation vector to compensate the MLS-derived range, azimuth, and elevation signals partially for ship motion effects. The airborne navigation computer resolves the MLS/DME measurements, landing pad deviation vector, and aircraft accelerations into a common inertial reference frame. Then, three-axes complementary filters are used to determine estimates of the aircraft position and velocity with respect to the MLS antenna. These state estimates are used by the guidance system for steering to the hover point.

The navigation software has several additional features such as rejecting bad data points, re-initializing after prolonged data loss, and variable filter gains to account for improving position measurement accuracy during approach. Each of these features is discussed in Ref. 2.

From the guidance point-of-view, the aircraft will be steered, based on where the navigation system estimates the aircraft is relative to the desired approach trajectory. Thus, time-varying navigation errors will cause variations in the path followed. Also, limitations in the MLS coverage constrain where the aircraft can be flown.

Sensor Errors Sensors on both the ship and aircraft are used for navigation purposes. In addition, sensors on the aircraft are used for flight control. Outputs from the airborne linear accelerometers, attitude gyros, and MLS are used for both navigation and flight control. The aircraft also uses rate gyros and angular accelerometers to provide appropriate inputs to the SRFIMF controller. Thus, errors in these sensors affect the guidance system's performance because they enter both the navigation and flight control computations. Error models for the various sensors are described in Appendix G.

System Constraints

Earlier in this chapter, we listed five different types of constraints that must be considered with regard to approach and landing of a VTOL air-

craft on a small aviation ship. These constraints are now described in more detail. For completeness, this discussion includes mention of constraints not specific to the RTA aircraft and other elements of our chosen system configuration. Those constraints which are particularly pertinent are identified so that they can be examined in the subsequent study.

Environment and landing scenario constraints As described earlier, the aircraft is required to rendezvous with a moving landing pad. This is because the ship is underway and may be traveling up to 30 kts with respect to the sea. The sea may have currents which add to the ship's inertial speed. In addition, the ship is subject to the effects of winds and wave motion up to Sea State 5 in magnitude.

A high wind environment must also be considered. Wind effects include those due to gusts, shear, and variable direction. In addition, as the aircraft approaches the vessel, it is subject to wind-over-deck turbulence caused by the normal wind going past the ship superstructure.

The aircraft must land in visibility conditions as low as those equivalent to Category IIIA. (zero ceiling; 213 m (700 ft) runway visual range). Thus, the position and velocity error at the hover point must be small enough to allow visual inspection and possible manual letdown to the landing pad. This affects placement of the hover point.

The deck structure itself represents a landing constraint in several ways. The approach path must be designed so that if an aborted landing and go-around are required, there will be no interference from the deck superstructure. The landing pad is of finite dimensions, and this places a constraint on the allowable errors at hover and touchdown. Figure 5 shows the landing pad of the DD-963 Class destroyer. If a latching device is available as part of the system design, more error is allowable in the landing phase. Also, there are ground effects that take place between the aircraft and ship deck. With lift fans or rotors, these can be completely different. Also, the possibility exists that one wing of the aircraft can be experiencing ground effects while the other is over open water. These ground effects are not considered as part of this approach guidance study.

The aircraft structure also must be considered in the landing analysis. First, the structural limits of the landing gear may restrict the closing velocity between the aircraft and deck at touchdown. Because both the ship and aircraft have attitude motion, there is increased possibility of wing damages or tipping at touchdown. Also because of possible surge and sway motion of the pad, the aircraft may experience skidding which could lead to going off the pad. These effects are not important for approach guidance analysis.

Navigation and control related constraints The MLS system is subject to coverage limitations. (For example, it could have a ± 60° azimuth coverage, + 20° elevation coverage, and 15 n.mi range limit.) This system is assumed to not be attitude stabilized, and it signals move with the ship motion. It has normal radio signal-in-space errors. In addition, in rough seas, it is subject to multi-path effects by reflecting off the sea surface.

The presence of coverage limitations would restrict the approach path that could be followed. For example, an approach from the bow of the vessel could not be used. Also, a go-around maneuver could move out of the normal MLS coverage, and would require that the aircraft fly back to behind the vessel before re-establishing the approach.

The characteristics of the navigation signals will affect the position and velocity errors sent to the guidance steering computations. The choice of steering law gains must take into account the navigation error characteristics so that (a) the aircraft response is fast enough to null out perceived errors as the hover point is approached, but (b) the aircraft does not chase high frequency errors.

The aircraft is limited in both response speed and control authority. Thus, the nominal trajectory must be designed to be well within these limits so that a margin is available to be used for perturbation control. During the landing phase, the aircraft control limits govern whether the aircraft can be synchronized with the ship motion or whether the aircraft must be steered to land when the ship state is acceptable for touchdown.

For helicopters, the attitude and translational motion are directly related. This constrains the type of maneuvers that can be made, especially during the landing phase. Also, because the vessel may be traveling at up to 30 kt, the helicopter may have to be in a relative hover condition at a state where it has relatively poor handling qualities. (For the UH-1H helicopter, this occurs around 30 kt.) For this study, the RTA aircraft essentially has decoupled attitude and translational control capabilities during slow speeds because of the SRFIMF flight control system. Thus, some problems which affect helicopter performance do not have to be considered here.

Pilot/human factor constraints It is assumed for this study, that the approach and landing guidance are automatic. In this case, the pilot's roles are (a) to monitor and approach for purposes of assuring that the path followed is reasonably correct, (b) to detect system faults, and (c) to takeover and fly the aircraft manually in case of a detected fault. From a guidance system point-of-view, the approach and landing trajectory then must be designed (a) to allow the pilot to perform the monitoring and fault detection roles with reasonable accuracy, and (b) to ensure pilot ride quality and safety at touchdown.

To obtain specific, quantitative constraints on the guidance system and nominal approach to ensure that the above human factors are met, further study is required using a cockpit simulator. However, we can list general points which should be used for preliminary guidance system design.

First of all, the approach path should offer the pilot a reasonable perspective of the landing pad through the aircraft canopy. If a heads-up display (HUD) is to be used, the landing pad should be located (in an angular sense) so that it falls within the HUD dimensions throughout most of the approach. It is desirable that the landing pad perspective time history be similar to the view of a runway that the pilot has been trained to land on.

The flight trajectory should also provide appropriate motion cues and display information so the pilot can assess the quality of the approach. This is especially true for low visibility approaches.

The approach and landing trajectory must be reasonably smooth, and the sequence of events must be favorable in terms of the monitoring work load. Enough time must be available (that is, the approach speed must be slow enough) to allow the pilot to take over and manually abort the approach in case of a problem.

Finally, the touchdown part of the landing phase must consider the pilot's safety and physical comfort. The aircraft may be designed to take a sharp impact with the deck, but this contact must also consider what impact loads are reasonable for the pilot to experience.

Hover point constraints An important decision in designing the nominal approach trajectory is where to place the hover point. Some items to consider are:

1) From the hover point, the pilot should have some visibility of the landing pad and deck officer, or other landing cues of adequate information, so that he can assess whether the landing phase should take place.

2) There should be adequate maneuver space for a safe letdown from the hover point. That is, there should be adequate airspace between the hover point and the landing pad to allow nulling out aircraft state errors which exist at hover.

3) The hover point should allow complete safety of the aircraft with respect to the ship superstructure. This must be true for both a letdown trajectory and one that would be followed in an aborted letdown.

4) The hover point should be selected so that the aircraft has a favorable position with respect to the ship and the direction of the prevailing wind. This is a consideration of wind-over-deck effects. Perhaps the hover point could be adjusted based on the prevailing wind conditions.

The hover point location will, in turn, specify how accurate the state of the aircraft must be at this point to allow a safe letdown-phase.

This places constraints on (a) the accuracy of the navigation system at this point, and (b) the ability of the aircraft flight controller to cancel the effects of wind disturbances so that the aircraft can be adequately held in the stationkeeping condition.

Guidance command considerations In addition to the above, there are two other constraints regarding the guidance system. First the guidance software should be relatively simple. It must be placed within the limitations of the airborne computer where navigation, flight control, display generation, and other avionics functions are probably present.

Second, the approach trajectory must take into account (a) that the aircraft has limited fuel, (b) that most of the fuel may be gone near the end of a mission, and (c) that the fuel burn rate is probably high when using the lift fans. It is advisable to design an approach trajectory that is both safe and fuel efficient.

Each of the above constraints was considered when evaluating possible approach guidance concepts, as discussed in Chapter III.

III

APPROACH GUIDANCE TECHNIQUES

The purpose of the approach guidance system is to steer the aircraft to approach the ship along some desirable flight path. The definition of this path (approach trajectory) includes the specification of relative velocity and acceleration limits at each point. The desired path may be either pre-determined so that it is always the same, or it may be computed in real time.

In Fig. 1, the guidance technique is contained in three blocks:

1. Desired Flight Paths - This block is not part of the mechanized guidance equations. However, it contains a physical description of the guidance concept or of the path relative to the ship that the aircraft is to be steered to follow. From it, the nominal guidance technique is derived. Also, the resulting ideal path that the aircraft is expected to follow can be computed in this block. This is compared with the actual path to compute the aircraft guidance errors as functions of time and range-to-go.

2. Nominal Guidance Parameters - This block represents actual mechanized software which is used to compute parameters for following the desired path. If the desired path is pre-determined (e.g., constant bearing lateral approach), the parameters which describe this path are contained in this block. If the desired path is computed in real time, (e.g., pursuit lateral approach), the equations and parameters which are required for this computation are included. The outputs of this block are the nominal path guidance parameters for translational control of the aircraft.

3. Perturbation and Total Guidance Commands - This block mechanizes the guidance commands in the form of a translational guidance law. This guidance law nulls out perceived path errors by comparing the desired aircraft state with that measured by the navigation system. The guidance law issues simultaneous commands for removing the path perturbation and following the desired path.

In choosing possible guidance concepts to consider, the various constraints described in Chapter II were taken into account. Actually, there are numerous paths that join some arbitiary starting point to the chosen hover point near the ship's landing pad. The system constraints were used to eliminate many of these. Then, digital simulation of the aircraft being steered by each of the remaining concepts was used to reduce the choices further.

The digital simulation first used to examine the guidance concepts was based on a simplified system model which emphasized the guidance aspects of the problem. The assumptions used in constructing this program included the following:

1. The aircraft was treated as a point mass with three degrees of translational freedom. Guidance commands were converted directly to inertial accelerations in a North-East-Down reference frame. No flight control or aircraft response lags were assumed.

2. The aircraft was assumed to follow coordinated turns. Thus, the bank angle (ϕ) was computed from the commanded lateral acceleration. The pitch angle (θ) was assumed to equal the flight path angle (γ). The aircraft yaw angle (ψ) was set equal to the heading of the aircraft velocity.

3. Perfect navigation was assumed. Also, no ship motion, other than constant velocity, was assumed.

4. Although the wind-over-deck was computed, it was assumed to have no effect on the aircraft dynamics.

To simulate the path that the aircraft would follow under each guidance scheme required mechanizing the associated guidance law. In this way, we were able to evaluate the relative complexity required for digital on-board mechanization of a given concept. Various guidance laws that were mechanized are presented in Appendix F.

The output of the point mass simulation included the following:

1. The horizontal and vertical paths (x vs y; z vs range) that the aircraft would follow to reach the hover point.
2. The idealized attitude angles (ϕ,θ,ψ) that the aircraft would have in following a given translational path with some commanded acceleration/deceleration schedule.
3. The look angles (azimuth and declination as measured with respect to the aircraft body axes) to the landing pad that the pilot would perceive visually as the aircraft would automatically follow a given trajectory. These angles included those to the bullseye plus the perspective of the landing pad out of the cockpit window.
4. The approximate wind-over-deck turbulence components that the aircraft would encounter during the final portion of the approach path.

Examples of this output are presented and discussed shortly.

Guidance Concepts Considered

The approach guidance commands were decoupled into lateral, vertical, and longitudinal components. In this study, four lateral, five vertical, and two longitudinal steering concepts were examined. The equations required to mechanize these concepts are presented in Appendix F. The concepts were:

Lateral

1. Pursuit - Here, the horizontal component of the aircraft inertial velocity is directed to point at the hover point. (Eq. F.3).
2. Constant bearing - The horizontal component of the aircraft velocity relative to the ship is directed to lie in a vertical plane with constant bearing relative to the ship heading. This plane contains the hover point. The constant bearing angle is fixed and is predetermined. (Eq. F.12 - F.14).
3. Zero bearing rate (Variable bearing angle) - The horizontal component of the aircraft velocity relative to the ship is directed to point at the hover point. This nominally results in a constant bearing approach. However, the bearing angle is dependent on the initial position and velocity of the aircraft. Perturbations cause the aircraft to obtain new bearing angle approaches. (Eq. F.11).
4. Constant heading - The aircraft is steered to follow a constant inertial heading to intercept the ship. The heading angle is chosen at the beginning of approach so that by following a fixed longitudinal deceleration schedule, intercept will occur when the aircraft speed is equivalent to the ship speed. (Eq. F.4 - F.6).

Vertical

1. Pursuit - The vertical component of the aircraft inertial velocity is directed to point at the hover point. (Eq. F.3).
2. Constant elevation angle (relative glideslope) - The aircraft is steered either to stay at a constant altitude or to follow a fixed constant elevation angle relative to the plane containing the deck of the ship. (Eq. F.12 - F.14).
3. Zero elevation rate (variable elevation angle) - The vertical component of the aircraft velocity relative to the ship is set so that a constant elevation angle is maintained relative to the hover point. The elevation angle is dependent on the initial position and velocity of the aircraft. (Eq. F.11).

4. Constant inertial glideslope - The aircraft is steered to follow a constant inertial glideslope to intercept the ship or to intercept the altitude of the hover point. The glideslope may be either predetermined (fixed constant) or it may be computed on line. (Eq. F.4 - F.6).

5. Constant sink rate - The vertical component of the aircraft inertial velocity is set at a constant value until the altitude of the hover point is reached. At that altitude, sink rate is set to zero. (Eq. F.16).

Longitudinal

1. Constant speed/constant deceleration - Here, the aircraft maintains constant closing speed until a fixed, predetermined range from the ship is reached. Then, the aircraft decelerates at a constant rate to reach the flare point (a small distance from the hover point) at a fixed closing speed relative to the hover point. A deceleration proportional to the closing speed then brings the aircraft speed to match the ship speed.

2. Step guidance - This is a combination of constant longitudinal deceleration followed by constant speed at a fixed altitude alternating with constant elevation angle/constant speed until a lower fixed altitude is reached. As many segments as desired can be used.

Point Mass Simulation Results

The point mass aircraft simulation was set up to simulate flight to the nominal hover point shown in Fig. 7. The hover point was selected to be 7.4m (24.2 ft) directly above the landing pad bullseye. This places the hover point on the line with 27° azimuth and 3° elevation from the assumed location of the MLS antenna. The ship was assumed to have a velocity vector of 20 kts heading due North. The aircraft was initially located near a 35° azimuth line at an initial range of about 5 n.mi. Initial altitude was 426.7m (1400 ft) above the hover point.

Figure 14 shows the horizontal path followed by the aircraft relative to the ship for the last 2 n.mi. Each of the four lateral guidance concepts causes a different approach path to be followed. The aircraft begins with a velocity of 120 kt relative to the ship. At about 1 n.mi. range, the aircraft nominally decelerates at 0.1g (3.22 ft.sec^2) until 30 ft behind the hover point. Then, the linear flare law is used to drive the aircraft velocity to match that of the ship. The constant deceleration causes the constant heading final approach to be normal to the x (North) axis in Fig. 14. Because the ship is moving ahead, the pursuit guidance causes the final approach to be along the x axis.

Figure 15 illustrates the vertical paths followed (altitude vs. range) for the various vertical guidance concepts. The constant elevation angle concept has two paths shown - one for a constant 3° elevation angle and one for alternating between altitude hold and a constant 6° elevation angle. The latter vertical approach is associated with the longitudinal vertical step guidance illustrated in Fig. 16. Note in Fig. 15 that the constant sink rate of 4.5 m/s (15 ft/s) causes the aircraft to reach the hover altitude when range is still 2286 m (7500 ft). This is before deceleration has begun. The sink rate can be regulated so that the hover altitude is reached at an arbitrary range-to-go.

Figures 17-22 show the following combinations of lateral and vertical guidance concepts on the movement of the bullseye look angles in the cockpit window:

Fig. 17: Constant 27° and constant 3° elevation angle;
Fig. 18: Lateral pursuit and constant (15 f/s) sink rate;
Fig. 19: Zero bearing rate and zero elevation rate;
Fig. 20: Constant heading and constant 3° inertial glide slope;
Fig. 21: Constant 27° bearing and constant (15 f/s) sink rate;
Fig. 22: Constant 27° bearing, step vertical/longitudinal guidance.

Azimuth and elevation are measured with respect to the longitudinal axis of the aircraft which is assumed to be the same axis the pilot's eyes would see if he looked straight ahead. Also shown in Figs. 17-22 are the

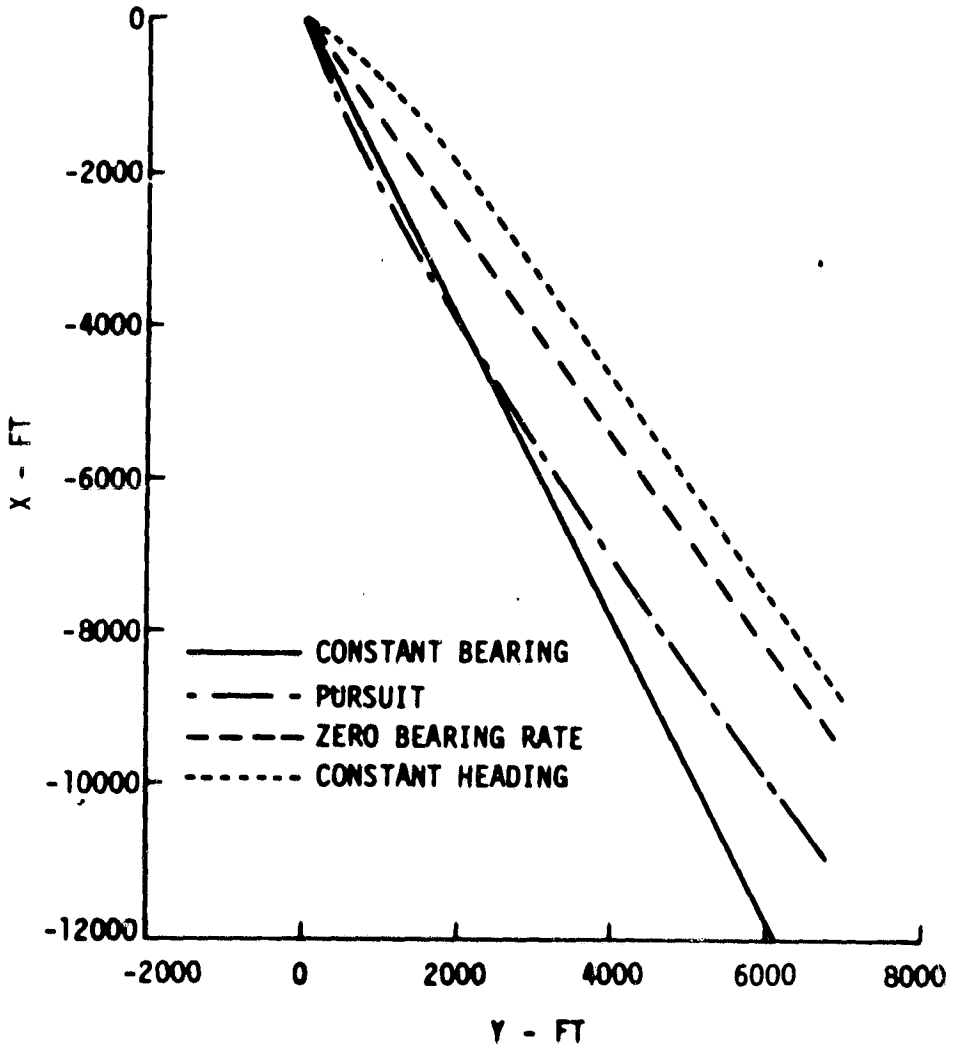

Figure 14. Lateral Steering Options Shown in the Horizontal Plane

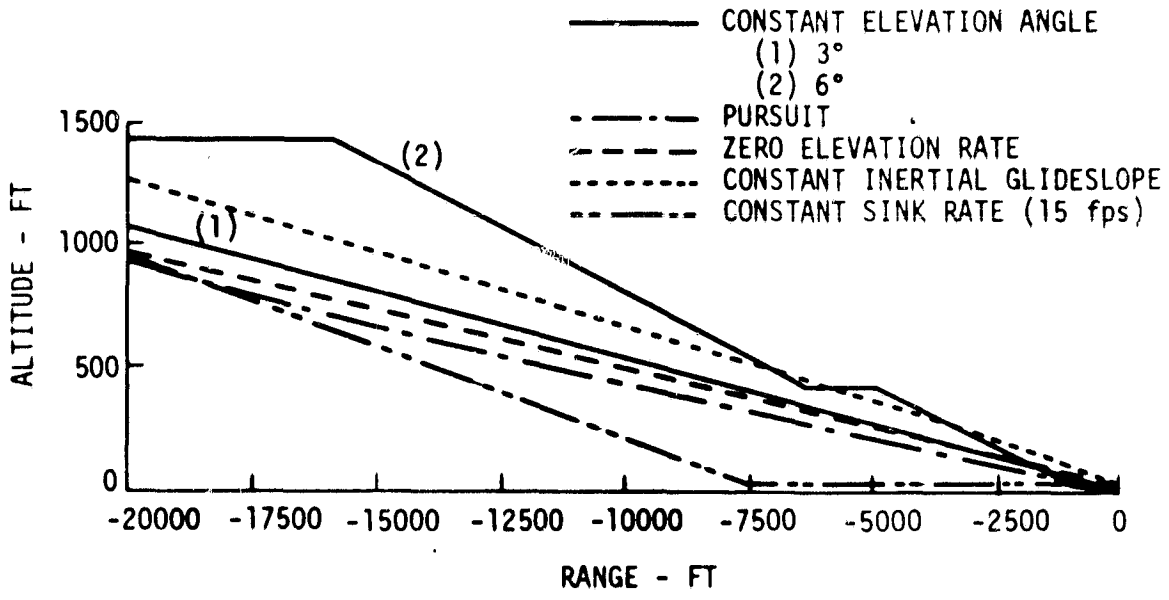

Figure 15. Vertical Steering Options Shown in the Vertical Plane

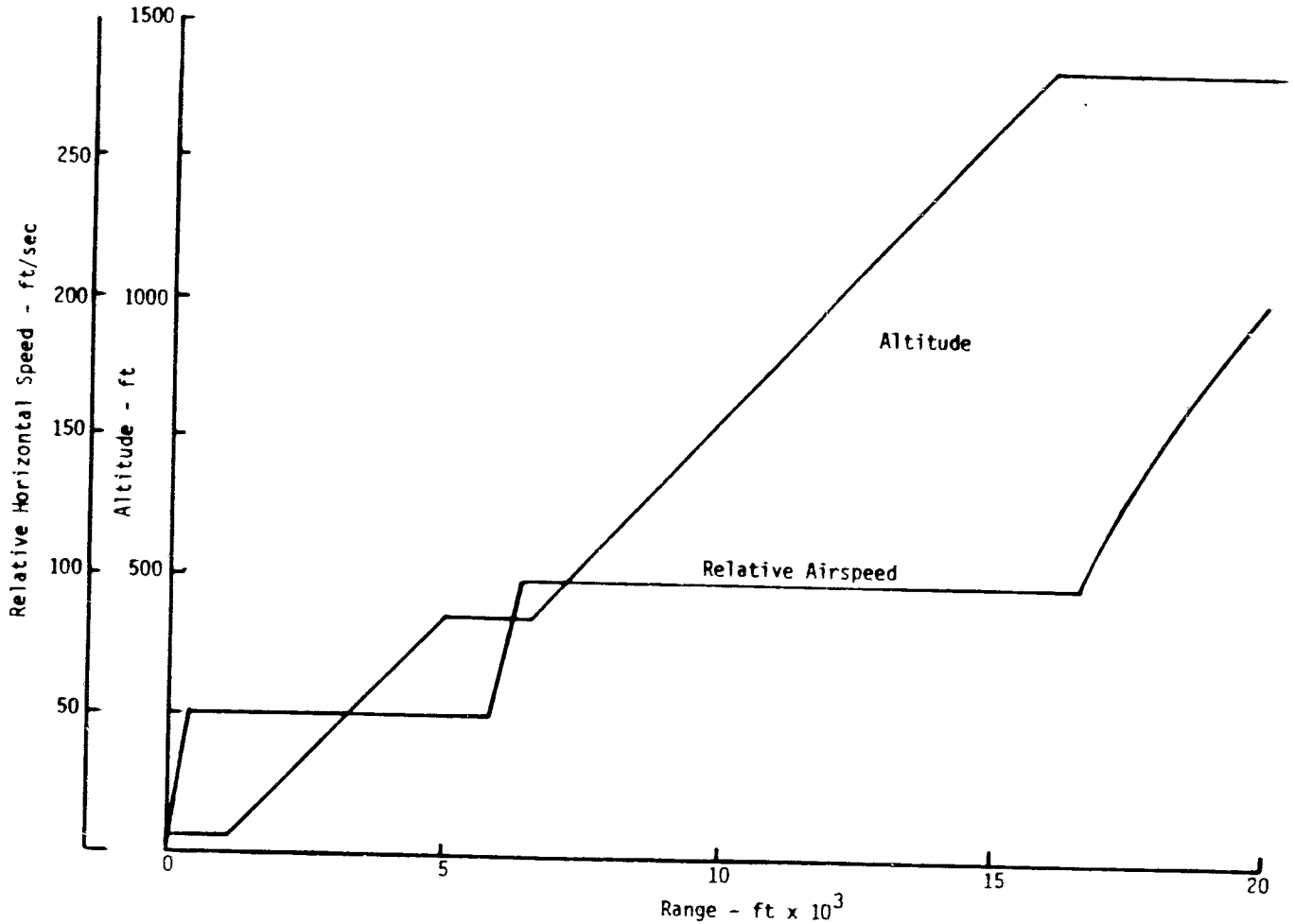

Figure 16. Typical Longitudinal - Vertical Step Guidance

perspective views of the landing pad at ranges-to-go of 600, 300, 150, 60, and 30m (2000, 1000, 500, 200, and 100 ft). These represent idealized views that the pilot would have. No account is taken of the blocked view which would occur because of the fuselage walls and canopy structure. (This geometry was not available for the conceptual design of the RTA aircraft.)

Figures 17-22 do give an idea of how the landing pad perspective would move in time and what the pilot would tend to see. Note in Fig. 17 that for constant bearing lateral steering, the 27° marking on the landing pad tends to be parallel to the pilot's vertical axis. Note in Fig. 18 that for lateral pursuit, the bullseye tends to be very close to the zero azimuth. Both of these locations and perspectives have advantages from a visual cue point of view.

Figure 20 shows that for a constant heading approach, the bullseye tends to move out the side of the canopy. Movement would continue to a 90° azimuth if a switch to zero bearing rate were not made.

Figure 22 illustrates that constant relative speed keeps the bullseye on a vertical line in the cockpit window. (2000, 1000, 500 ft points). Constant deceleration causes the bullseye to move to the left (200, 100 ft points).

The approaches shown in Figs. 14-22 did not take into account the region of the predominant wind-over-deck turbulence. That is, for a wind-over-deck angle ψ_{WOD} of -30° (see Fig. 3b), these approaches fly through the region where the turbulence amplitudes are high. This could have been avoided by approaching the vessel from the port side. This was not done because the wind-over-deck effects on the guidance errors could not be assessed by using the point mass model. Wind-over-deck effects are discussed further in Chapter V.

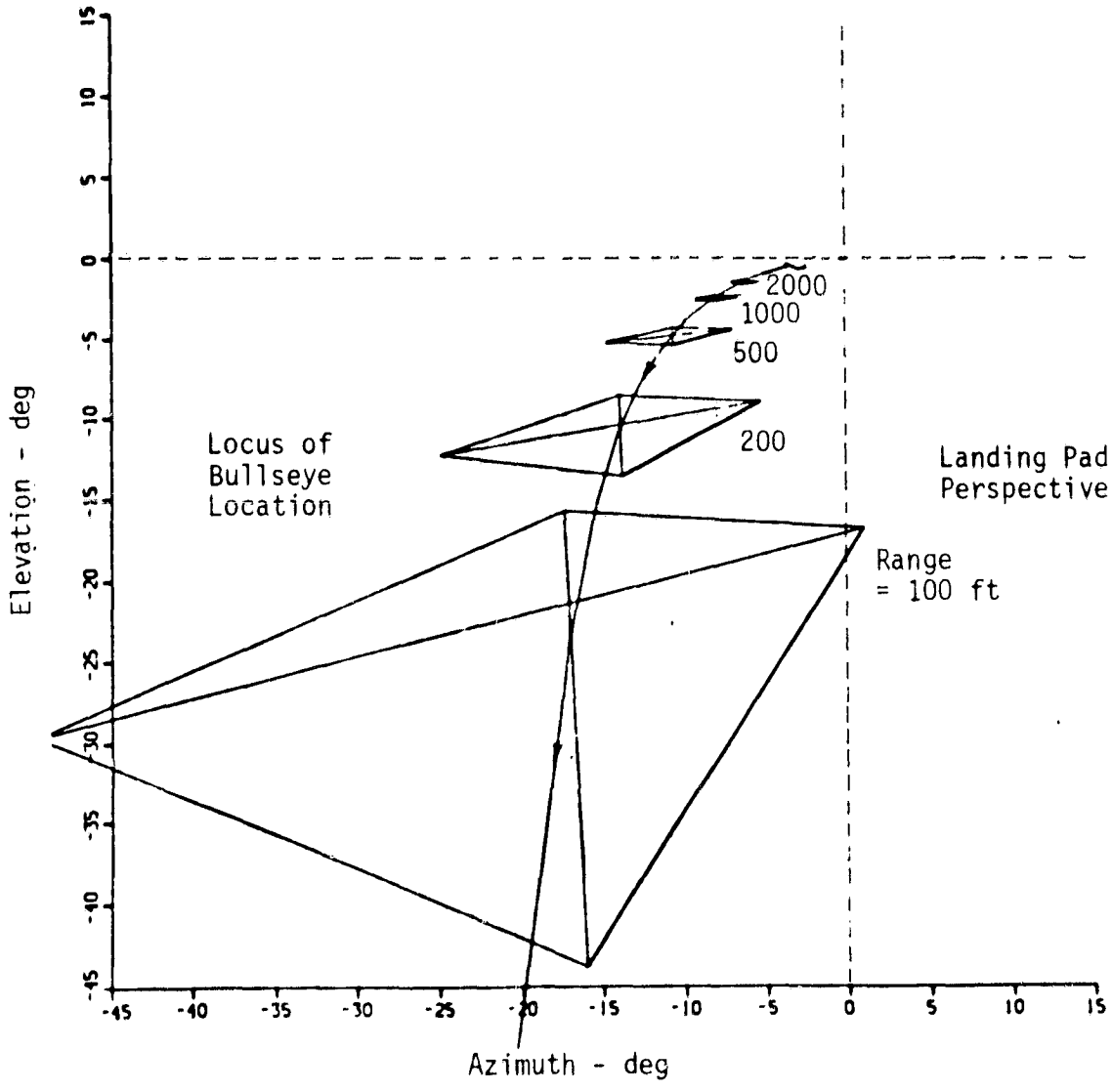

Figure 17. Constant Bearing and Elevation Angle Approach

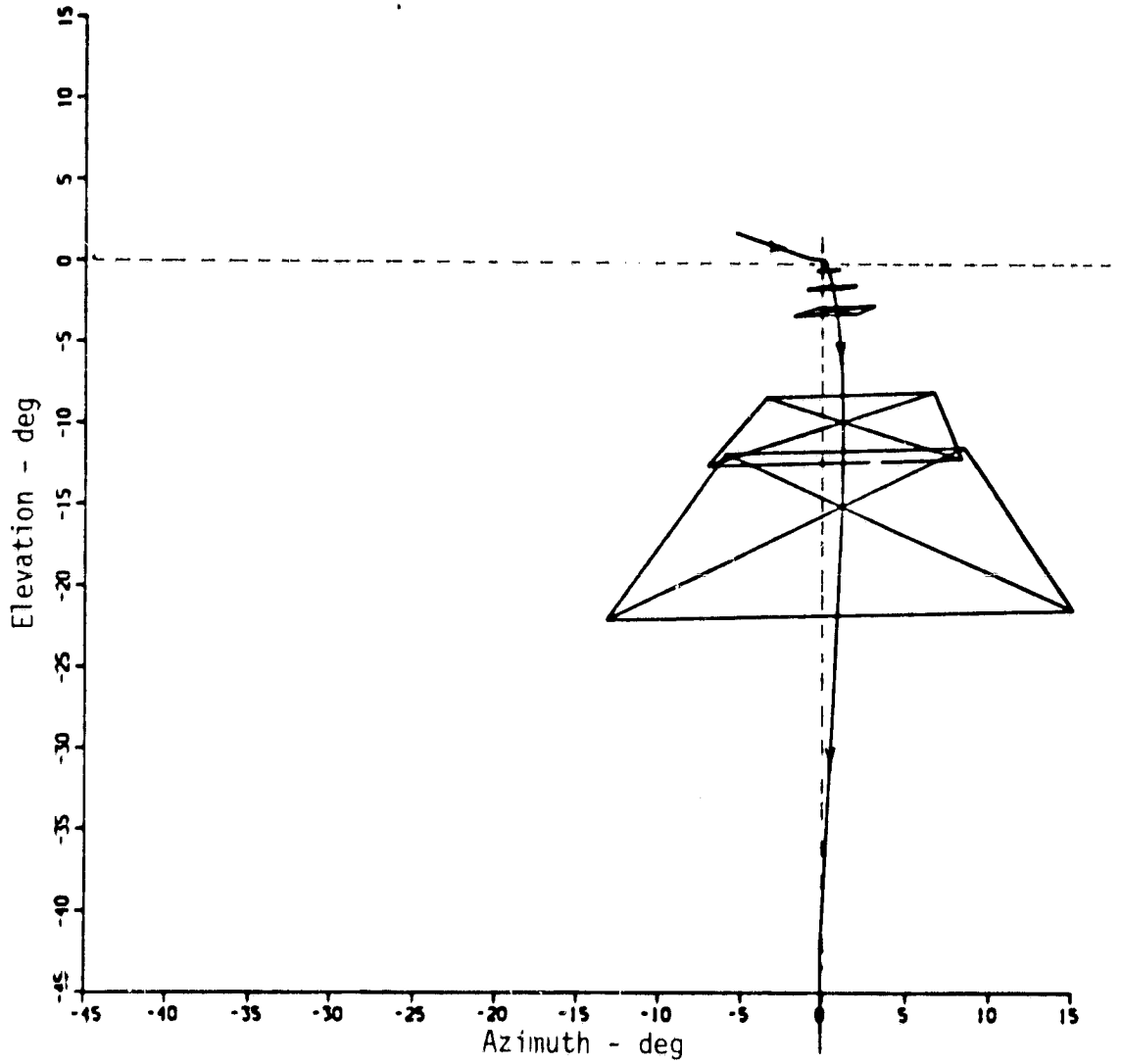

Figure 18. Lateral Pursuit and Constant Sink Rate Approach

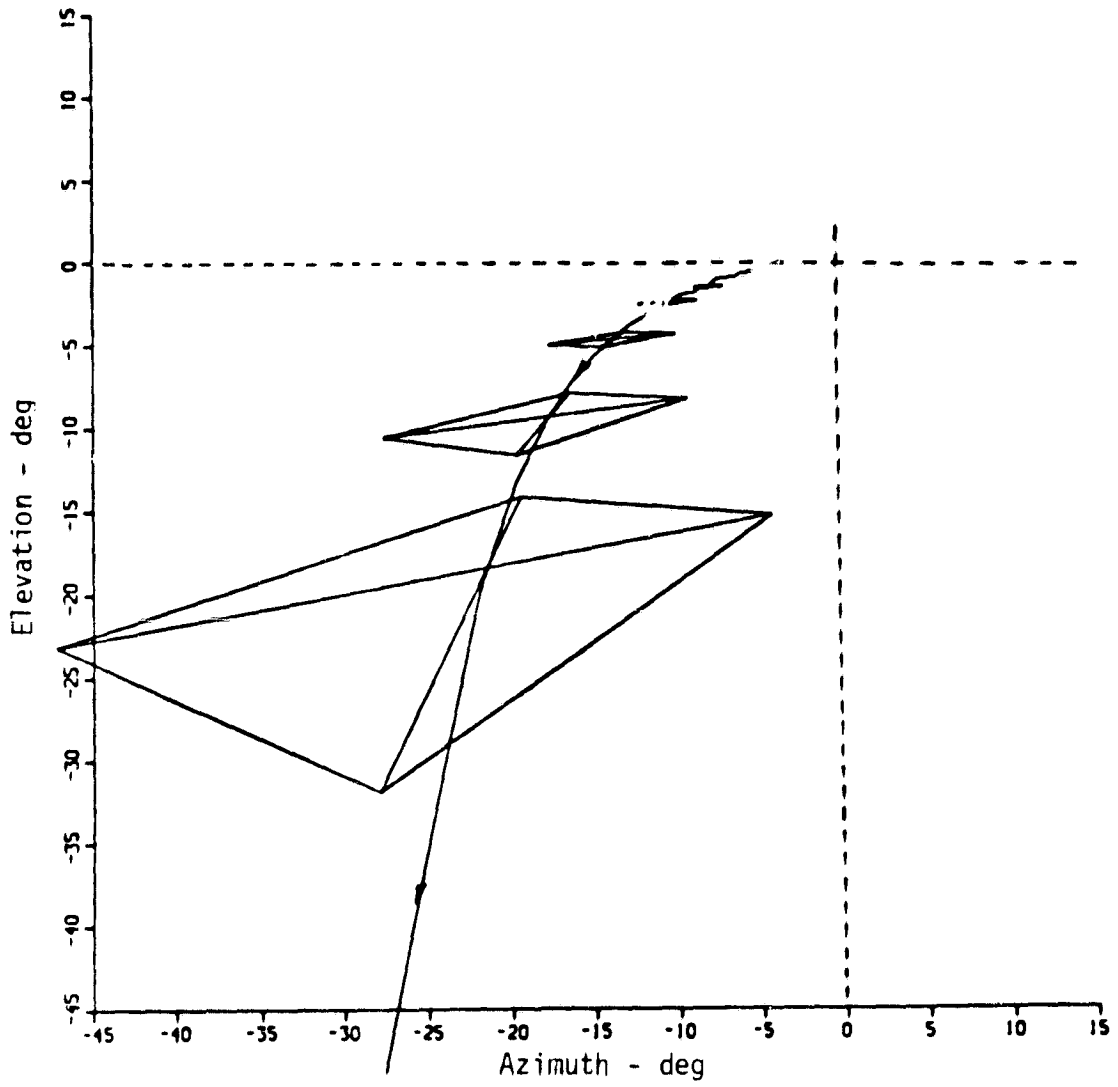

Figure 19. Zero Bearing Rate and Zero Elevation Rate

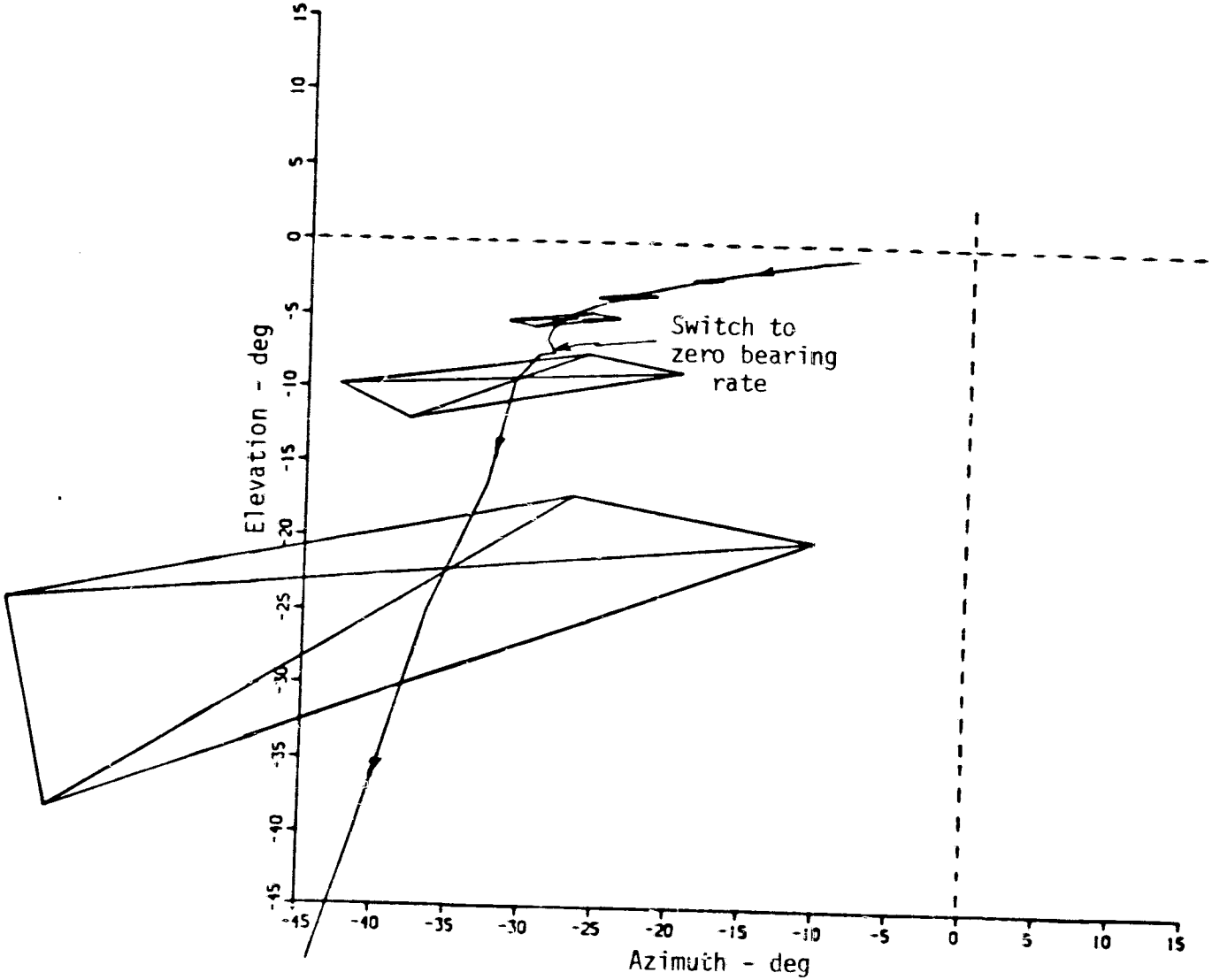

Figure 20. Constant Heading and Inertial Glideslope Approach (Transitions to Zero Elevation/Bearing Rate)

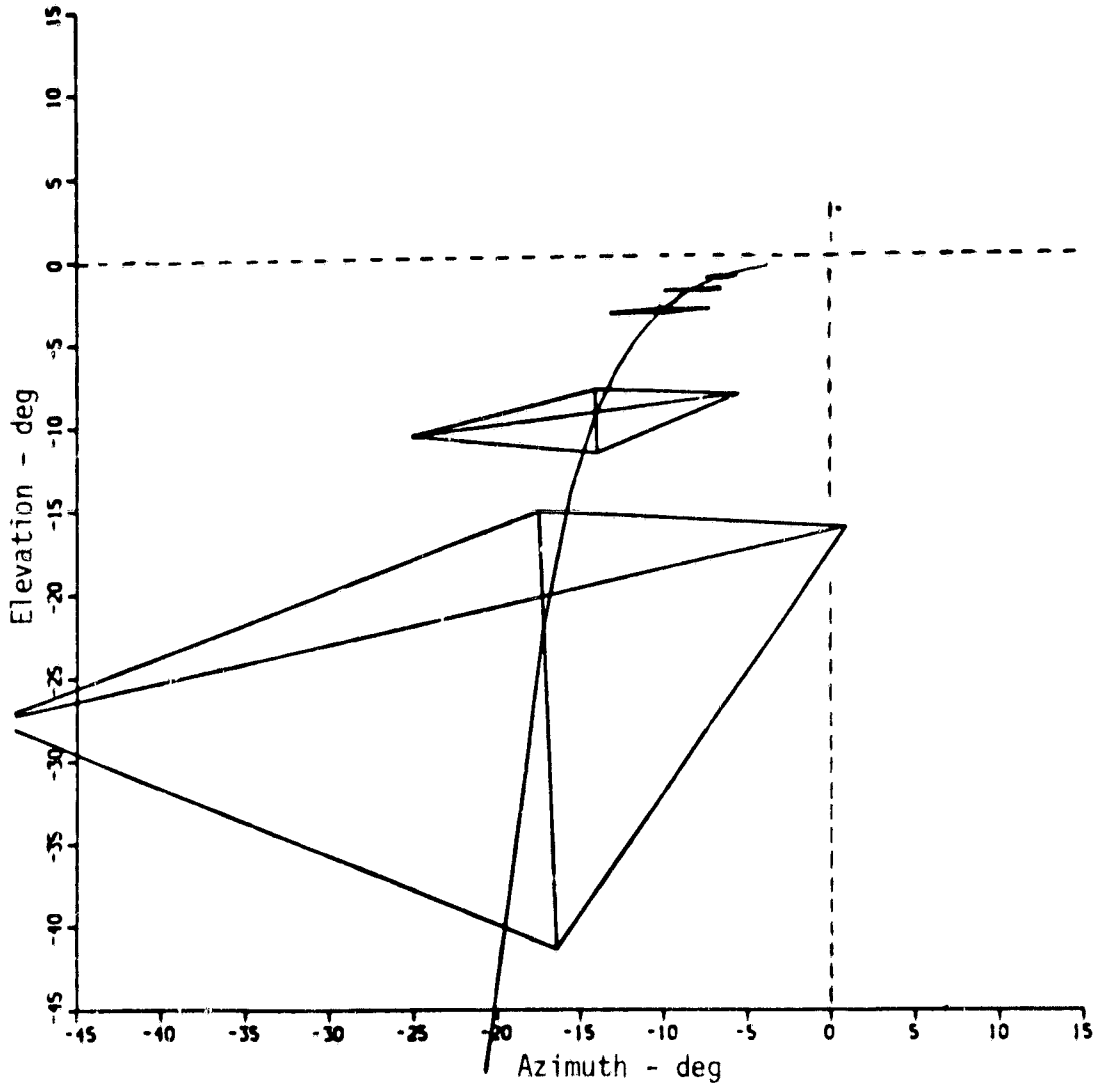

Figure 21. Constant Bearing/Constant Sink Rate Approach

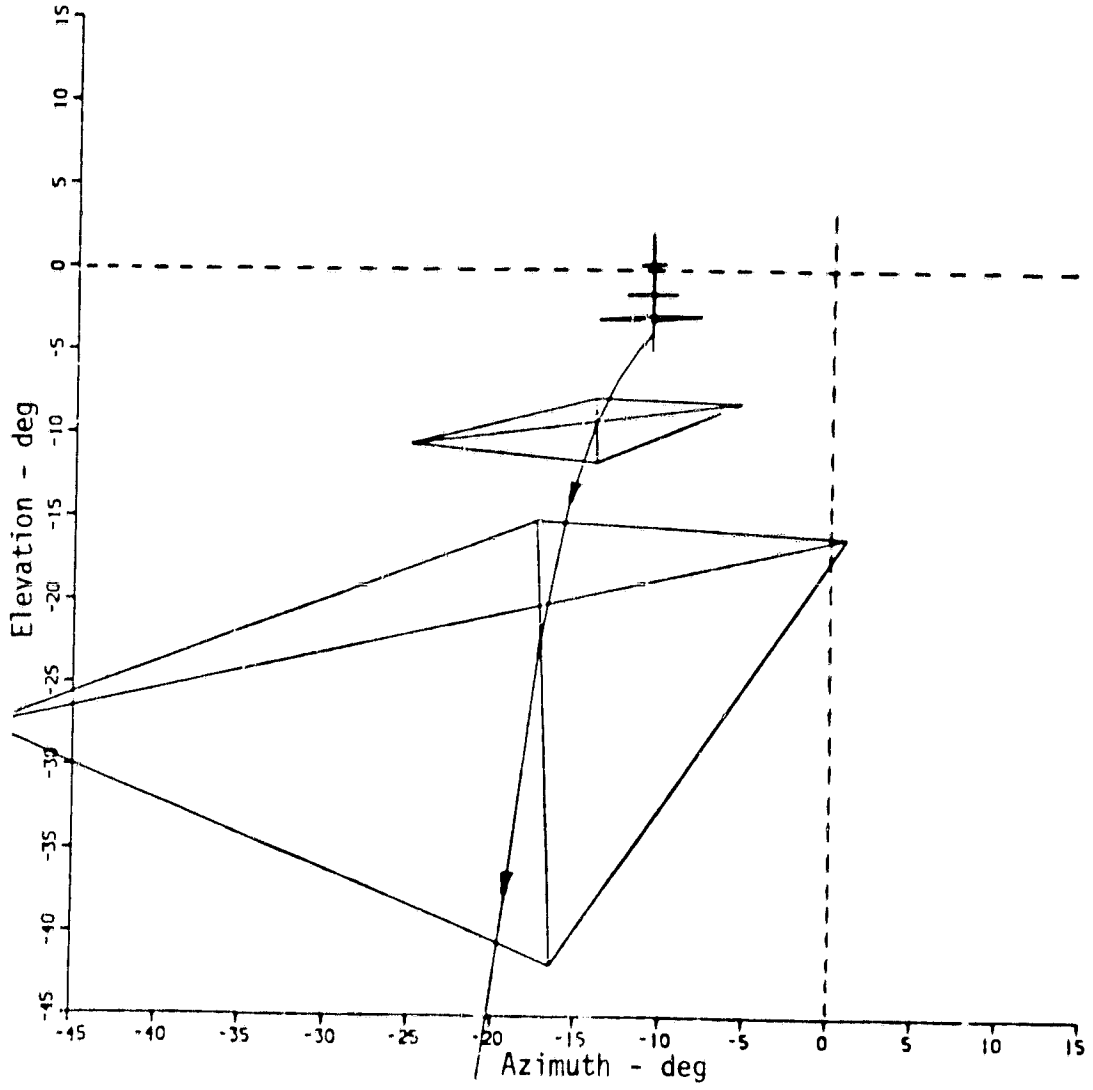

Figure 22. Constant Bearing/Step Vertical-Longitudinal Guidance Approach

Approach Guidance Critique

The guidance concepts can be mixed in several combinations when one considers that four lateral, five vertical, and two longitudinal methods are available. In addition, lateral guidance, for example, can begin with one type of steering and then transition to another. Thus, there are many possibilities to consider.

The purpose here is to review a number of these possibilities and to reduce them to two choices so that a more detailed, but managable set can be examined further. In this regard, five combinations of lateral and vertical guidance are reviewed based on the results of the point mass simulation and the software mechanization requirements presented in Appendix F. The longitudinal guidance concepts are reviewed separately.

Lateral/Vertical

1. Constant bearing/constant elevation (measured in ship MLS axes)

   Possible advantages The landing pad lights are nominally aligned for a 27° bearing approach. The 27° constant bearing approach then provides improved visual cues for night landing or in time of limited visibility flight. Furthermore, if a visual glideslope indicator such as shown in Fig. 6 is used, the constant 3° elevation angle approach would have the same advantage in the vertical plane.

   The guidance software for steering to a constant bearing and constant elevation is easy to mechanize. A vertical plane can be defined containing the 27° bearing line, and lateral position and speed errors can be computed based on the aircraft's position with respect to this plane. Likewise, a plane containing the 3° elevation line can be used to compute vertical errors.

   Using standard bearing and elevation angles ensures that the final approach is always standard. That is, the final portion of the automatic approach will always be the same, regardless of the aircraft initial position when beginning the approach. Thus, the pilot would have a single standard approach to learn.

The constant bearing angle concept is flexible in that any angle can be used. Thus, for example, a 0° rear approach could be mechanized using this concept.

The 27° lateral approach allows deck overflights which avoid the superstructure in case of an overflight. This provides a safety convenience to the pilot in that relative forward motion of the aircraft can always be maintained.

Using constant bearing/constant elevation angle guidance provides a means of position control all the way to the hover point. Some of the other guidance concepts do not provide a definition of position error at hover, and thus a transition to position control must be made.

Possible disadvantages As seen in Fig. 17, for constant 27° bearing guidance with a decelerating relative velocity, the hover point and landing pad move out the left side of the canopy. (This is actually an aircraft crab angle relative to the landing pad). This may be a disadvantage for providing visual cues and for implementation on a heads-up display (HUD). This type of question would have to be answered by use of cockpit simulator experiments.

Another disadvantage of fixed bearing/fixed elevation angle approaches is that they may not be convenient for the particular initial position of the aircraft relative to the vessel. If the aircraft begins on the port side of the vessel, it must fly to the 27° bearing plane on the starboard side before continuing toward the vessel. This can prolong the landing time.

A third possible disadvantage of this type of approach is during the presence of gusts and steady cross winds. The gusts drive the aircraft off the 27° path, and control effort would be required to return to this path. Steady cross winds would introduce an additional crab angle requirement to hold the aircraft on this path.

2. Lateral and vertical pursuit

Possible advantages The pursuit guidance directs the aircraft inertial velocity vector to always point toward the hover point. This velocity orientation causes the aircraft velocity vector to become aligned with the ship velocity. Ship velocity alignment produces a rear approach that is similar to a standard runway approach. The rear approach may be preferable to the side approach from a pilot acceptance point-of-view.

The pursuit guidance is adaptable to any starting position of the aircraft. Steering is always toward the single hover point.

As seen in Fig. 18, the landing pad bullseye (or the hover point) is always near the center of the forward cockpit window. This would be advantageous for HUD mechanization, and it may be superior from a pilot's viewpoint.

Possible disadvantages As seen in Appendix F, mechanizing the pursuit guidance requires knowing the ship velocity (heading and speed). Thus, these are two extra pieces of information that must be transmitted from the ship to the aircraft. (The MLS-based navigation system provides aircraft velocity relative to the ship. For constant bearing guidance, this is all that is required).

Pursuit guidance does not allow deck overflight in case of an aborted approach. A solution is to place the hover point off the side of the ship. This is a loss of flexibility, however.

Pursuit errors are not defined near the hover point. Thus, this guidance must transition to a different position error nulling guidance for hover point control.

The pursuit guidance system does not allow use of visual landing lights as the constant bearing/elevation guidance does.

3. Zero bearing rate/zero elevation rate

Possible advantages This is an easy type of guidance to mechanize The MLS azimuth and elevation angles initially measured are

held. If wind or other perturbations cause the aircraft to deviate off, the new angles are held instead. Thus, this type of guidance is very adaptable to any initial condition.

Possible disadvantages This type of guidance usually provides a non-standard approach. Neither a fixed bearing angle nor a rear approach (as with pursuit guidance) is provided. Thus, the pilot perspective will always be different.

Again, as with constant 27° bearing guidance, the landing pad perspective may move out of the field that is visible from the cockpit window.

Because of the variation that is possible in the approach direction, the ability to overfly the deck and avoid the superstructure may not be present.

4. Constant Inertial Heading and Guidance (Intercept Guidance)

Possible advantages This type of guidance provides the most direct path from the starting initial relative position of the aircraft to the hover point. It is the most natural type of guidance to use at large ranges.

Once the heading and glideslope are set, this type of guidance produces the least attitude motion of the aircraft. Thus, during the approach, the aircraft would move most like a land-based approach to a fixed runway.

Possible disadvantages The equations to mechanize this type of guidance are the most complex. Anticipation of the ship's future position is required, and changes in either deceleration rate or intercept point have to be made continually.

This type of guidance requires greater lateral MLS coverage from the vessel because the final approach is from 90° with respect to the vessel velocity vector. Also this non-standard lateral and vertical approach causes the landing pad to deviate the most with respect to the cockpit window centerline.

The constant heading angle causes the aircraft velocity vector to cross the ship vector. Guidance redefinition is required to align these vectors.

5. Constant Sink Rate Vertical Guidance

Possible advantages This type of guidance is easy to mechanize. The altitude is commanded either to be constant or to change at a fixed rate. This may alleviate some of the precision required on the elevation measurement from the MLS.

If the final hover altitude is reached before the hover point range is reached, the final portion of the approach is at constant altitude. This provides a low final approach that keeps the landing pad bullseye high in the cockpit window.

Possible disadvantages With constant sink rate vertical guidance, there is no constant elevation angle cue from the ship. Also the range-to-go at bottom of descent will vary depending on relative speed of the aircraft and the range when the descent begins.

Longitudinal

1. Longitudinal Guidance - Constant Speed Followed by Constant Deceleration

Possible advantages This type of guidance is simple to mechanize. It has only one change in mode, and it requires only a measure of range-to-go. Also, because deceleration is all at the end, it is an efficient type of approach from a time and fuel usage point-of-view.

Possible disadvantages All the forward relative speed of the aircraft is killed off at the end of the approach. The pilot may prefer that the speed be changed in small steps as approach continues.

2. Step Vertical/Longitudinal Guidance (Alternates Constant Deceleration at Constant Altitude with Constant Glideslope/ Constant Speed Descent)

Possible advantages The pilot may prefer to have deceleration occur during level flight and have constant speed during descent. Also, this guidance allows the approach to continue at slower speeds. It reduces the deceleration period required during the final approach.

Possible disadvantages This type of guidance is more difficult to mechanize from an automatic point-of-view. The alternating altitude hold and vertical descent phases must be solved before approach occurs.

The landing pad and bullseye will have a varying view angle (elevation) as the descent segments are traversed. This would not provide a convenient visual landing cue sequence.

Finally, this type of longitudinal approach takes longer to reach the hover point and therefore requires a greater expenditure of fuel than the constant deceleration guidance.

Choices for Detailed Simulation Study Some of the questions raised above about the advantages and disadvantages of particular approach guidance concepts cannot be answered without further, more detailed digital simulation and cockpit simulator studies. However, based on the above arguments, the choices were narrowed to two sets of combinations. These are, for lateral and vertical guidance:

1. Constant bearing and constant elevation angle; and
2. Lateral pursuit combined with constant vertical sink rate.

Vertical pursuit could also be used, but the above combinations produce choices with distinct, alternate characters. The constant bearing/constant elevation angle has been studied the most. It is known to work well but it has some noted disadvantages. The pursuit guidance removes some of these disadvantages but has disadvantages of its own. Constant vertical sink rate combined with altitude hold provides a distinct alternative to constant elevation descent control.

For longitudinal guidance, the constant speed/constant deceleration concept was selected. The second alternative did not seem to have sufficient advantages to warrant its further study from an automatic implementation point-of-view. For manual approach control, it would always be available anyway. Pilot opinion can perhaps shed some further light on this decision.

IV

LANDING GUIDANCE

This section considers the problem of bringing the VTOL aircraft from the stationkeeping (or hover) point to a touchdown at the center (bullseye) of the ship's landing pad. A sketch illustrating the relative geometry of the terminal shipboard landing scenario is given in Fig. 23. Both the aircraft and the ship landing pad motions are defined with respect to a ship-fixed local level reference frame (X_s, Y_s, Z_s) centered at the average position of the bullseye and with the X_s-axis aligned with the ship longitudinal axis. The stationkeeping point (x_h, y_h, z_h) represents the position of the aircraft at the end of the approach phase and prior to the initiation of the landing maneuver. The landing pad is far from being stationary. In fact, it is being continually disturbed because of ship pitch, roll and heave motions in response to heavy seas and adverse weather conditions.

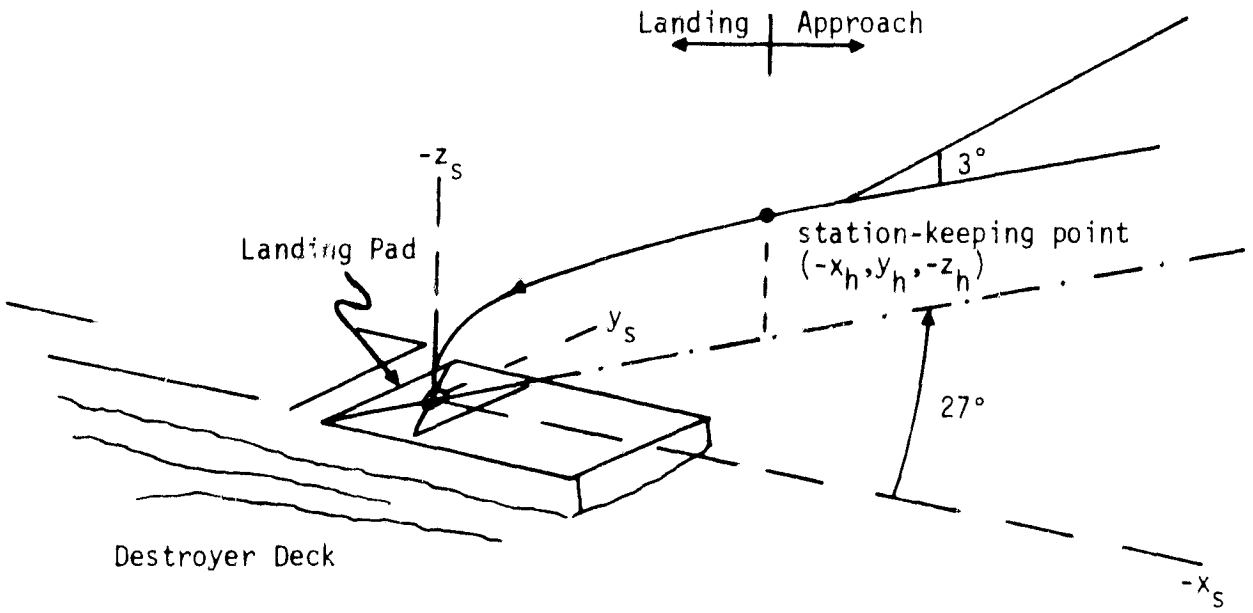

Figure 23. Shipboard Landing Scenario

The objective of the landing guidance system is to maneuver the aircraft from the hover point to touchdown on-board the ship's landing pad in a safe and efficient manner. As a minimum, the aircraft should be able to land on the deck without damaging its landing gear or skidding off the deck. This requirement imposes a minimal constraint on the relative position $(x_{a/s}, y_{a/s}, z_{a/s})$, translational velocity $(\dot{x}_{a/s}, \dot{y}_{a/s}, \dot{z}_{a/s})$, attitude $(\psi_{a/s}, \theta_{a/s}, \phi_{a/s})$, and angular velocity $(p_{a/s}, q_{a/s}, r_{a/s})$ vectors of the aircraft with respect to the landing pad at touchdown.

Thus, the landing control task under ideal conditions consists of maneuvering the aircraft from the hover point to a touchdown such that the relative errors in position, velocity, orientation and angular velocity of the aircraft with respect to the landing pad are approximately zero. However, this assumes that an ideal aircraft is present with unlimited control authority and speed of response (bandwidth) in all six degrees of freedom. Additional operational constraints on the landing pad position and orientation at touchdown must be imposed because of aircraft limitations, human factors requirements and environmental and safety considerations.

Operational Constraints

In order to achieve a safe landing on-board the ship, the aircraft must be able to follow the ship motions in the six degrees of freedom prior to touchdown. However, under most realistic operational conditions, the principal problem lies in following or matching the deck motions in the vertical (Z_s), pitch (θ_s), and roll (ϕ_s) degrees of freedom. Deck motions in the remaining degrees of freedom - namely surge (X_s), sway (Y_s) and yaw (ψ_s) are relatively easy to follow within the capabilities of existing aircraft flight control system characteristics and limitations.

The control system characteristics of the lift-fan VTOL aircraft considered in this study must be understood before proceeding with the design of a letdown guidance law. Step response data for the roll and vertical (SRFIMF) control system are presented in Figs. 24 and 25, respectively.

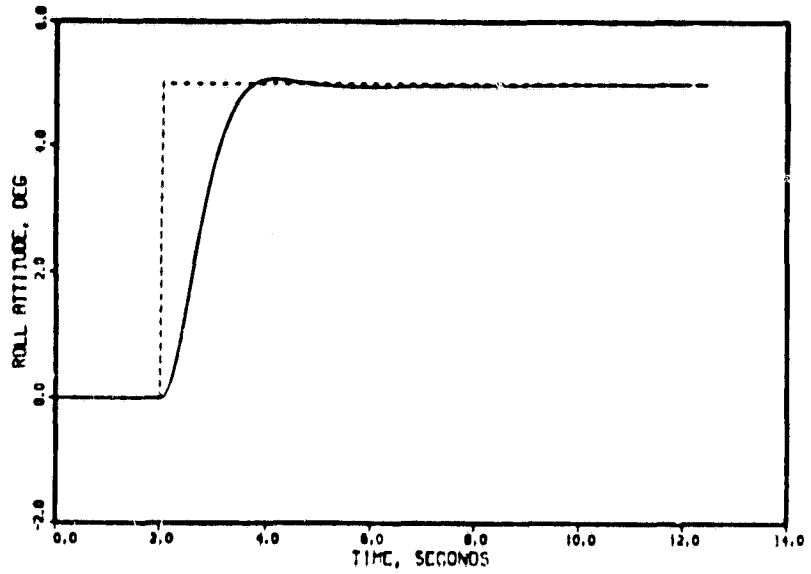

Figure 24. Step Response of Aircraft Roll Control System. (at 20 Knots)

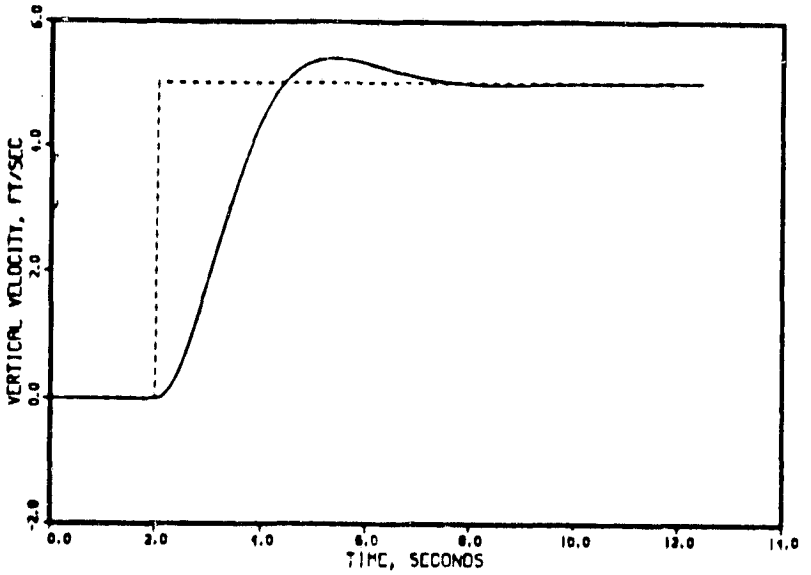

Figure 25. Step Response of Vertical Velocity Control System. (at 20 Knots)

The roll system transfer function (ϕ/ϕ_c) is approximately second order with unity gain, damping $\zeta \cong 1.0$ and natural frequency $\omega_n \cong 1.0$ rad/s (or 0.16 Hz). The vertical system ($\dot{h}/\dot{h}_c$) is also second order with unity gain, damping $\zeta \cong 0.7$ and natural frequency $\omega_n \cong 0.82$ rad/s (or 0.13 Hz). Thus, it takes approximately 2-4 seconds for either system to follow a step change in commanded position or attitude. Additional velocity and acceleration constraints on the actuator servos further limit the dynamic range and speed of response of these control systems.

The vertical and lateral impact velocity limits and skid characteristics of the landing gear must be considered in defining acceptable touchdown dispersions in relative vertical velocity, lateral velocity, and roll attitude.

The shipboard landing of VTOL aircraft constitutes an exceptionally demanding task which must be performed under hostile environmental conditions. Additional constraints on the ship's attitude (pitch and roll) may be necessary from an operational safety viewpoint. The severity of these constraints would depend upon the level of sophistication employed in securing the landing gear following touchdown. Clearly, the absence of any specific clamping or clasping mechanism would necessitate the deck being relatively level at touchdown. Additional requirements on the deck heave position at touchdown may also be imposed to account for the aircraft vertical control system's bandwidth limitations.

As a result of the above factors, the following constraints on acceptable landing pad motion at touchdown may be necessary:

1) The pad vertical position with respect to its average value shall be greater than zero.

2) The vertical velocity of the pad shall be positive (moving upward) but shall be less than some prescribed value (e.g., 0.6 m/s).

3) The pitch and roll attitudes of the pad shall be less than some prescribed value (e.g., 3°), and

4) The pitch and roll angular velocities of the pad shall be less than some prescribed value (e.g., 0.3°/sec).

The constraints listed above represent one plausible set and provide an example for elucidating the basic concept.

Landing Controller Design

The basic objective of landing guidance is to bring the aircraft to a gentle touchdown, under varying environmental conditions, while staying within its control system limitations. The principal problem here lies in the vertical control of the aircraft. Therefore, the following discussion on shipboard landing is limited to the design of letdown guidance and vertical control system design.

Two types of vertical letdown guidance laws with no future ship motion prediction may be formulated:

1) Designs based upon present and past information alone that are independent of future deck motion forecasting, and

2) Designs based on availability of future deck motion forecasts.

In the absence of ship motion forecasting, there are two design options available. Figure 26 illustrates the design where the guidance law is basically open loop and commands the aircraft to follow a prescribed rate of descent or vertical velocity $\dot{z}_{Ac}$ to touchdown. The relative velocity at impact is given by $|\dot{z}_{Ac} - \dot{z}_s(t_f)|$ where t_f is the touchdown time. The maximum impact velocity would depend upon the maximum upward deck heave velocity $|\dot{z}_s|_{max}$ and the maximum downward aircraft guidance velocity error. This open loop guidance law would be acceptable for sea states where $(|\dot{z}_{Ac}| + |\dot{z}_s|_{max}) \leq \dot{z}_{Rmax}$. Here, $\dot{z}_{Rmax}$ is the maximum allowable relative impact velocity at touchdown. For high sea states, $|\dot{z}_s|_{max}$ may be greater than $\dot{z}_{Rmax}$ thereby rendering this control law unacceptable. This type of open loop landing guidance was investigated in this study, and Monte Carlo results of typical landing dispersions in vertical impact velocity and horizontal position errors are presented in Chapter V.

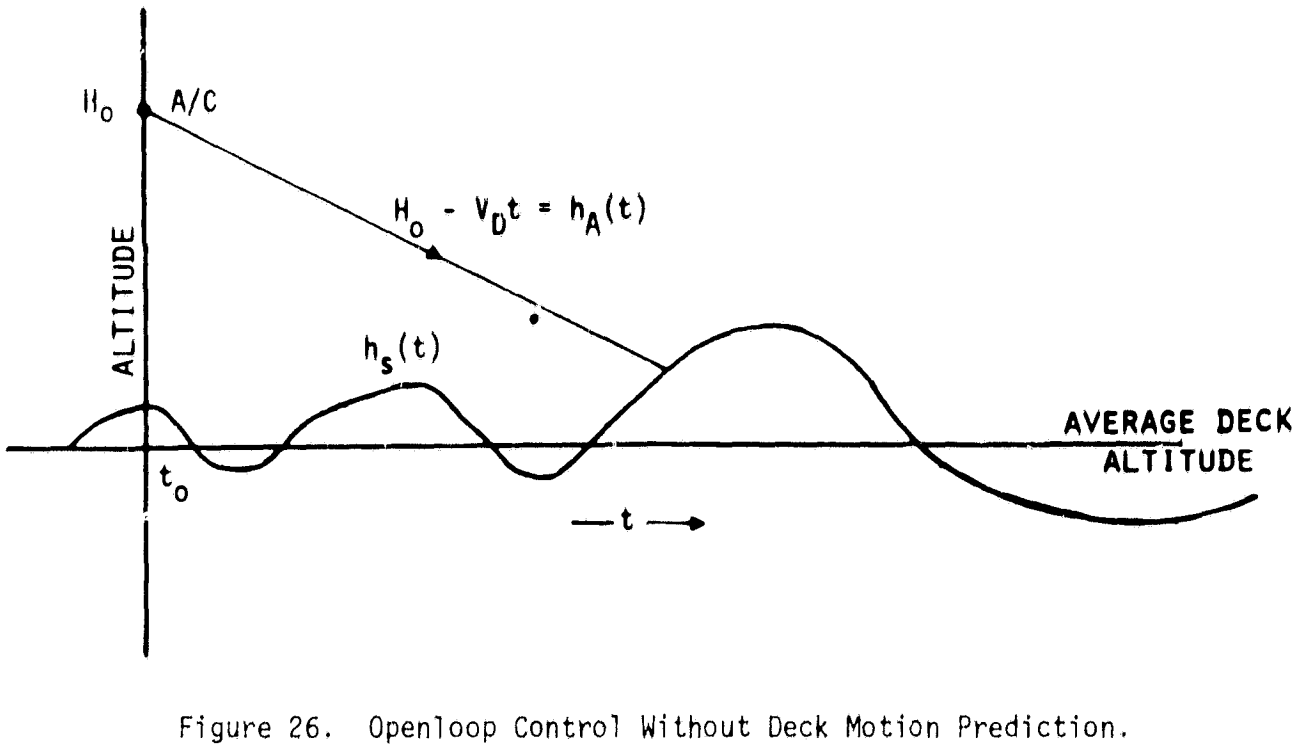

Figure 26. Openloop Control Without Deck Motion Prediction.

The open loop control law of Fig. 26 does not allow the aircraft to respond to measured altitude and sink rate with respect to the deck. An approach to reducing relative impact velocity at touchdown is to superimpose a feedback controller on the nominal open loop control so as to attempt to follow or track the instantaneous deck vertical motion in time. This leads to a closed loop feedback controller design as shown in Fig. 27. Typical response of this design is illustrated in Fig. 28. The total control command $\dot{h}_{CT}$ is the sum of the nominal open loop feed-forward command $\dot{h}_{CNom}$ and a closed loop control $\dot{h}_{Cf}$. Thus,

$$\dot{h}_{CT} = \dot{h}_{CNom} + \dot{h}_{Cf} , \tag{1}$$

where $\dot{h}_{CNom}$ corresponds to a nominal sink rate, of say 1 m/s, that would be used in the absence of any deck motion. The term $\dot{h}_{Cf}$ is the feedback control required in an attempt to follow the vertical deck motions. The design of the feedback controller may be carried out using classical and/or modern control theory methods depending upon the nature and quality of the a priori information (i.e. mathematical models for the aircraft, deck motion dynamics and external disturbances).

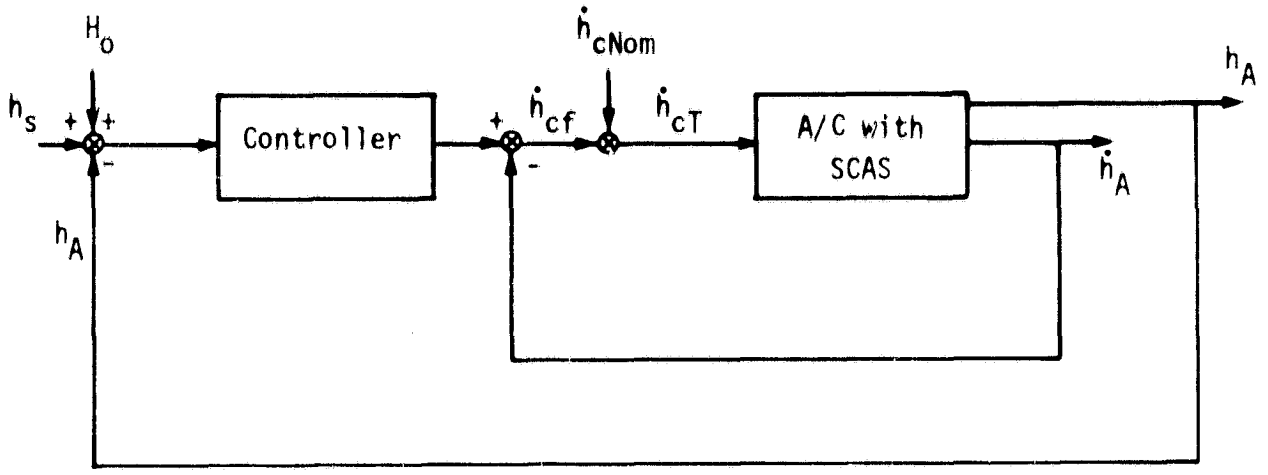

Figure 27. Feedback Control Law Without Deck Motion Prediction.

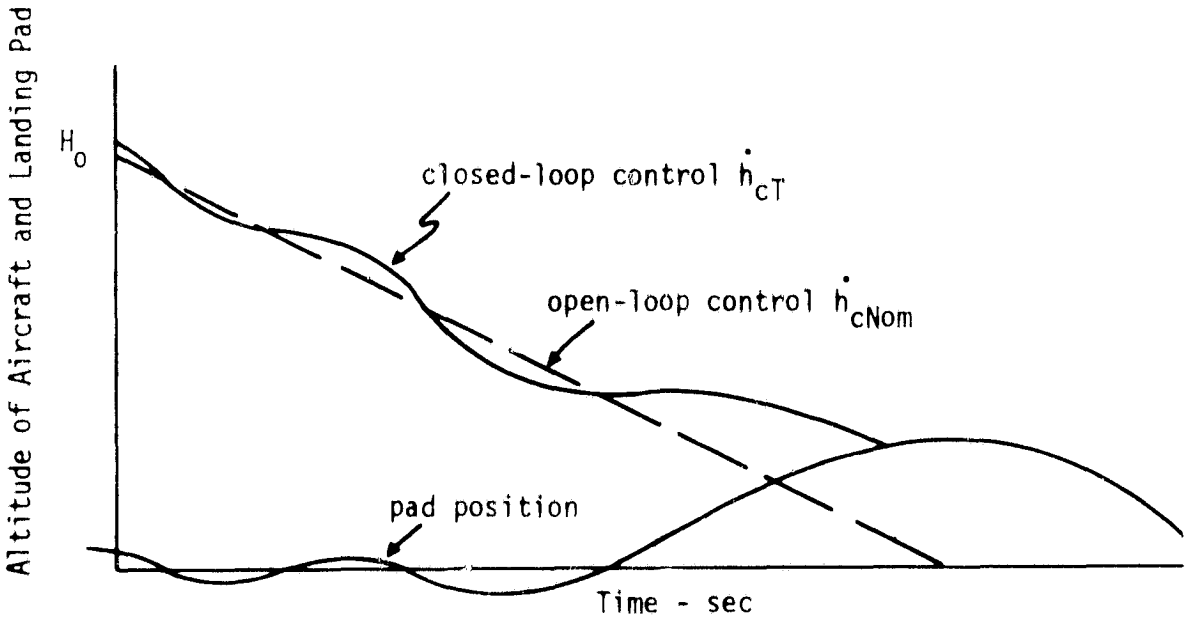

Figure 28. Closed-Loop Control Without Deck Motion Prediction.

The closed loop letdown law of Fig. 27 can be successfully used only if the aircraft can follow the deck heave motions with reasonable fidelity. This would require the aircraft vertical control axis to have a sufficiently high bandwidth (at least 3 times the highest significant frequency in the deck vertical motions), servo actuator velocity, and acceleration authority limits to allow successful implementation. However, for the lift-fan VTOL aircraft, the vertical system has a bandwidth of 0.82 rad/s, which is within the frequency spectrum of the deck heave motions (0.3 - 2 rad/s). Hence, this aircraft would not be capable of following any but the lower frequency components of deck heave motion. Furthermore, maximum vertical velocity and acceleration may be as high as 10 - 15 ft/s and 0.05 - 0.1 g in magnitude, respectively. This requires aircraft control authority limits of comparable value or greater. Existing VTOL aircraft do not have large values for control authority, and would, at best be marginally acceptable. Even if such a high authority aircraft were available, the resulting implementation may be unacceptable to the pilots from ride and handling quality considerations, in addition to being very fuel inefficient.

An alternative approach is to use some kind of ship motion forecasting algorithm to predict future deck motion time histories. Ship motion prediction algorithms can be based on modeling the motion in terms of a Gauss-Markov process in state space [9] or autoregressive, moving average (ARMA) formulations [10]. Standard Kalman filtering or time series analysis prediction methods can be used to forecast future statistics (mean and covariance) of the key variables. The subject of forecasting techniques is an area of on-going research. [2,21] However, this subject is beyond the scope of this present effort and therefore is not discussed further at this point.

Nevertheless, letdown guidance laws can be investigated by assuming that ship motion forecasts (mean and covariance) are available. Again, two types of vertical lewdown guidance laws may be formulated:

1. A nominal open loop control law to bring the aircraft from the stationkeeping point, at time t, to touchdown at some acceptable predicted deck position at future time $t + t_f$.

2. A nominal open loop law plus some perturbation closed loop law which removes effects due to gusts and errors in the ship motion prediction as the touchdown point is reached.

The design of these nominal and perturbation controllers could be carried out using modern control methods or by using an intuitive ad-hoc technique.

Finally, ship motion forecasting is not a deterministic process and is subject to error even under ideal conditions. Consequently some mechanism must be provided to carry out the following higher level supervisory functions:

1. Determine at prescribed intervals the "acceptability" of forecasted deck positions for successful landing - time, state , and confidence limits,
2. Choose a predicted touchdown point or landing window for initiation of landing,
3. Implement the control law for landing at the predicted touchdown point,
4. Continue updating the location of the landing window at prescribed intervals,
5. Decide if the nominal control law needs to be recomputed and implement the decision, and
6. Abort the letdown if the confidence in the forecasted time histories degrades substantially or if a landing window is suddenly disqualified.

The specific criteria for acceptability of a forecasted deck position for landing would depend upon the stipulated touchdown constraints discussed earlier and on the aircraft control system limitations.

Study Requirements

The above discussion indicates the complexity of the problems associated with the final phase of shipboard landing of VTOL aircraft. A fundamental conclusion of this investigation is that the various components of the system (namely, the aircraft characteristics, the ship motion prediction algorithms, and operational factors) are closely connected and must be considered together in designing suitable letdown guidance laws.

A combined analytical and computer simulation investigation of alternate letdown guidance schemes is recommended. A combination of a tracking or feedback controller with a nominal open-loop control law based on ship motion forecasts may prove to be the best compromise. The feedback controller may be able to follow the lower frequency components of deck motion thereby requiring a shorter forecasting interval for successful landing.

The following overall approach to the problem is recommended:

1. The shipboard landing problem must be approached in an integrated way. Landing controller design is effected by aircraft control system and structural characteristics as well as ship motion prediction capabilities. The two aspects are intimately related and should not be artifically separated during the design stages.
2. An evaluation of both model-based and multivariate time series analysis methods of forecasting is recommended. Such an evaluation should provide the theoretical limits on prediction accuracy versus lead time of forecasts for the two approaches.
3. Optimum forecasts (mean and covariance) may be used to compute the probability of the ship motion satisfying the touchdown constraints and hence the relative frequency of landing opportunities.

4. Conversely, definition of landing pad opportunities, constraints at touchdown and the desired frequency of landing may be used to determine the requirements on prediction accuracy of the ship motion forecasts.

5. The results may be used to establish the inverse relationship between the tightness of the landing pad constraints at touchdown and the required level of prediction accuracy.

6. The results of such a study can be used towards the design of a safe and efficient landing controller design.

7. Finally, a computer simulation investigation should prove extremely useful in evaluating alternate control laws and system performance under perfect a priori assumptions about models for ship motion, aircraft dynamics and environmental disturbances. Results of such a study would show the relationship of touchdown dispersions to forecasting accuracy and aircraft control system characteristics.

V

ANALYSIS AND SIMULATION RESULTS

This chapter presents the simulation results of the combined system model used to study the chosen two types of approach guidance described in Chapter III. For added interest, a simple open-loop letdown guidance procedure was added to the simulation so that landing position dispersions could be related to those at the hover point. An overview of the simulation study is first given, followed by a discussion of single pass and Monte Carlo results.

Overview

Each of the system elements discussed was put into a digital program MAALS resident at NASA/Ames Research Center. The program is organized in modular form as depicted by the system block diagram of Fig. 1. The program contains convenient input and output subroutines which facilitate parameter changes and plotting of results. It is made to accomodate both a single pass simulation and multiple (Monte Carlo) passes with mean and variance computation.

Appendix H gives the MAALS program macro flow charts and explains each of the modules. Appendix F presents details of the guidance law and logic developed for the approach guidance study.

Figure 29 shows the nominal approach path that was used in this study to establish standard initial conditions. In the simulation scenario, the RTA aircraft is initially positioned at 4 km (10,065 ft) with a 27° bearing with respect to the ship at an altitude of 137 m (450 ft) above the ship c.g. (400 feet above the average landing pad). The ship is underway at a speed of 20 kt with Sea State 5 conditions. The aircraft ground speed is 120 kt resulting in a 100 kt relative speed. The speed range below 120 kt corresponds to the powered lift flight regime for the aircraft. For both the constant bearing (27°) and elevation (3°) and the

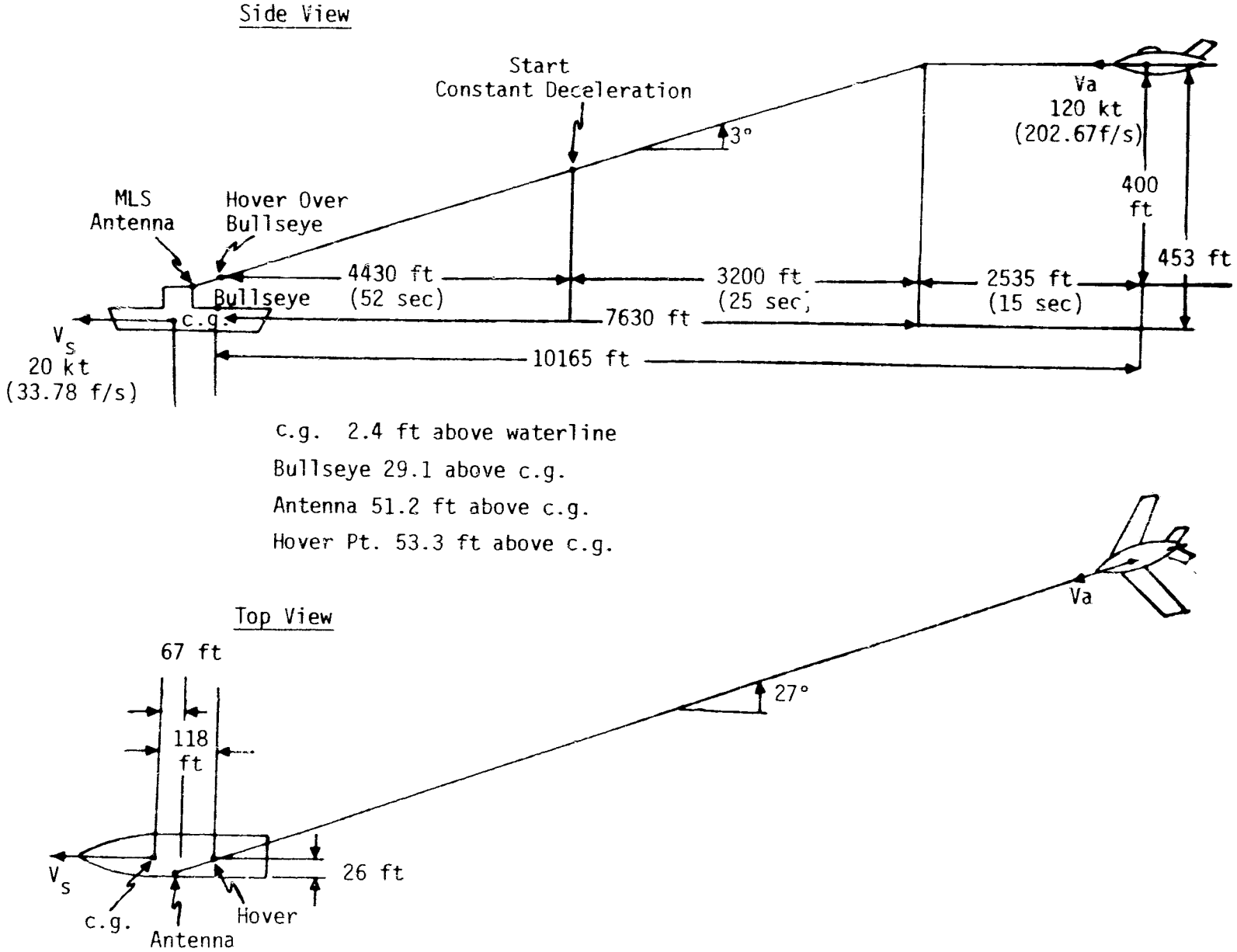

Figure 29. Candidate Nominal Approach Path.

pursuit guidance modes, it takes approximately 115 seconds of flight time before touchdown. Initially, the aircraft is flown with altitude hold, ground speed hold, and wings level modes of guidance until the navigation filter is initialized (5 seconds). Immediately, the 27° reference bearing and 3° reference elevation are captured and tracked. At 40 seconds, the longitudinal deceleration maneuver at 0.1 g is initiated. At 80 seconds, the final approach mode for the lateral axis is initiated. Several simultaneous maneuvers are commanded:

1. the aircraft heading is aligned to the ship heading,
2. the reference bearing is slewed to zero,
3. roll-to-level is commanded, and
4. the lateral velocity command mode is activated.

At approximately 85 seconds, flare maneuvers for the longitudinal and vertical axes are initiated to bring the aircraft smoothly to the hover point (station keeping state). At 110 seconds, the letdown maneuver of 3 ft/sec is initiated strictly on an open loop basis. The aircraft touches down 7 seconds later. The wake turbulence caused by the wind-over-deck becomes effective approximately 60 seconds into the flight. For the pursuit and constant sink rate, the guidance scenario remains essentially the same except that the sink rate command of nominally 10 ft/sec is initiated at 30 seconds.

Nominal Case

Figures 30 through 37 show the constant bearing (27 deg) and elevation (3 deg) and the pursuit and constant sink rate (10 ft/sec) guidance cases side by side. The cases correspond to (a) no MLS errors, (b) no aircraft or ship sensor errors, (c) no wind, and (d) no ship motion.

Figure 30 shows the (x,y) and (range, altitude (z)) plots with respect to the ship axes. The (x,y) plots show the difference in the lateral trajectories. The constant bearing approach shows the straight line with the bearing angle of 27 deg; it shows an initial transient due to the reference capture maneuver and also a small transient at the end due to the guidance mode switching. The (x,y) plot for the pursuit guidance shows the typical "chase" trajectory exemplified by the aircraft coming in from the ship's stern. The pursuit trajectory overshoots the ship's extended centerline which is caused by the guidance gain "mismatch". More results showing the effect of pursuit guidance gain changes are presented later. Never the less, both of these guidance methods successfully bring the aircraft to the landing pad.

The range/altitude plots show a marked difference in the vertical trajectory profiles. The constant elevation (left) plot shows that the altitude holds smoothly until it transitions to the elevation reference mode. It has a final vertical flare for stationkeeping. The trajectory is approximately a straight line of 3 deg with respect to the ship. The plot on the right shows the altitude hold transitioning to the constant sink rate (10 ft/sec) and flaring to the stationkeeping point. The trajectory is concave down with respect to the ship axes, even though the altitude plot with respect to time is linear. The concaveness is the result of the longitudinal deceleration maneuver. Again the corresponding guidance laws bring the aircraft to the landing pad as is expected.

Figure 31 shows the time plots of along-track, cross-track and altitude above the stationkeeping point. The along-track plots show a similar characteristic, because the longitudinal guidance law is the same. They show the straight line followed by a parabola caused by a constant deceleration.

The next plots show the cross-track components. For the constant bearing guidance, the heading hold mode is followed by the reference capture and track. At 70 sec, the aircraft transitions to the final mode.

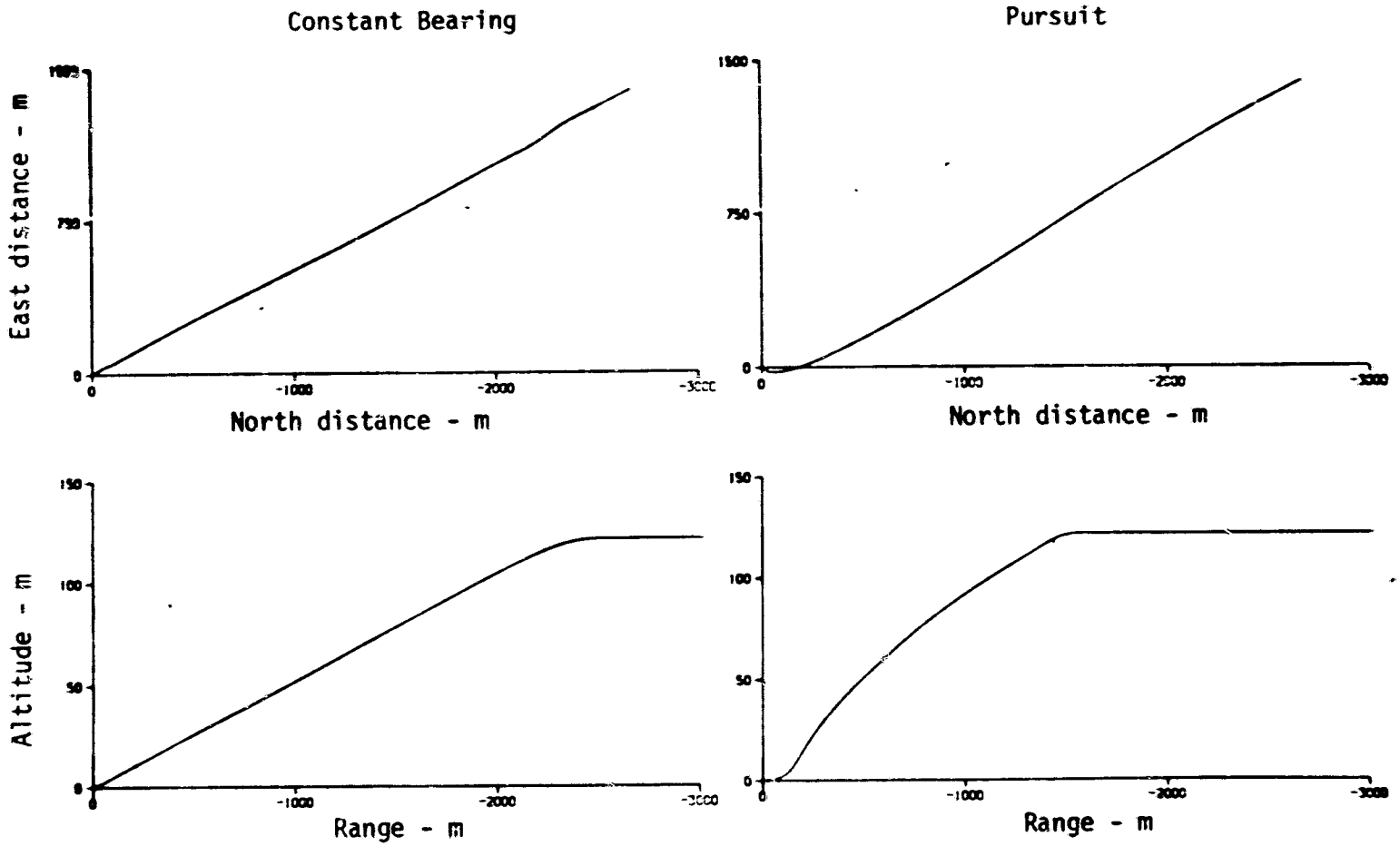

Figure 30. Y vs X and Z vs Range Plots for Nominal Constant Bearing and Pursuit Cases

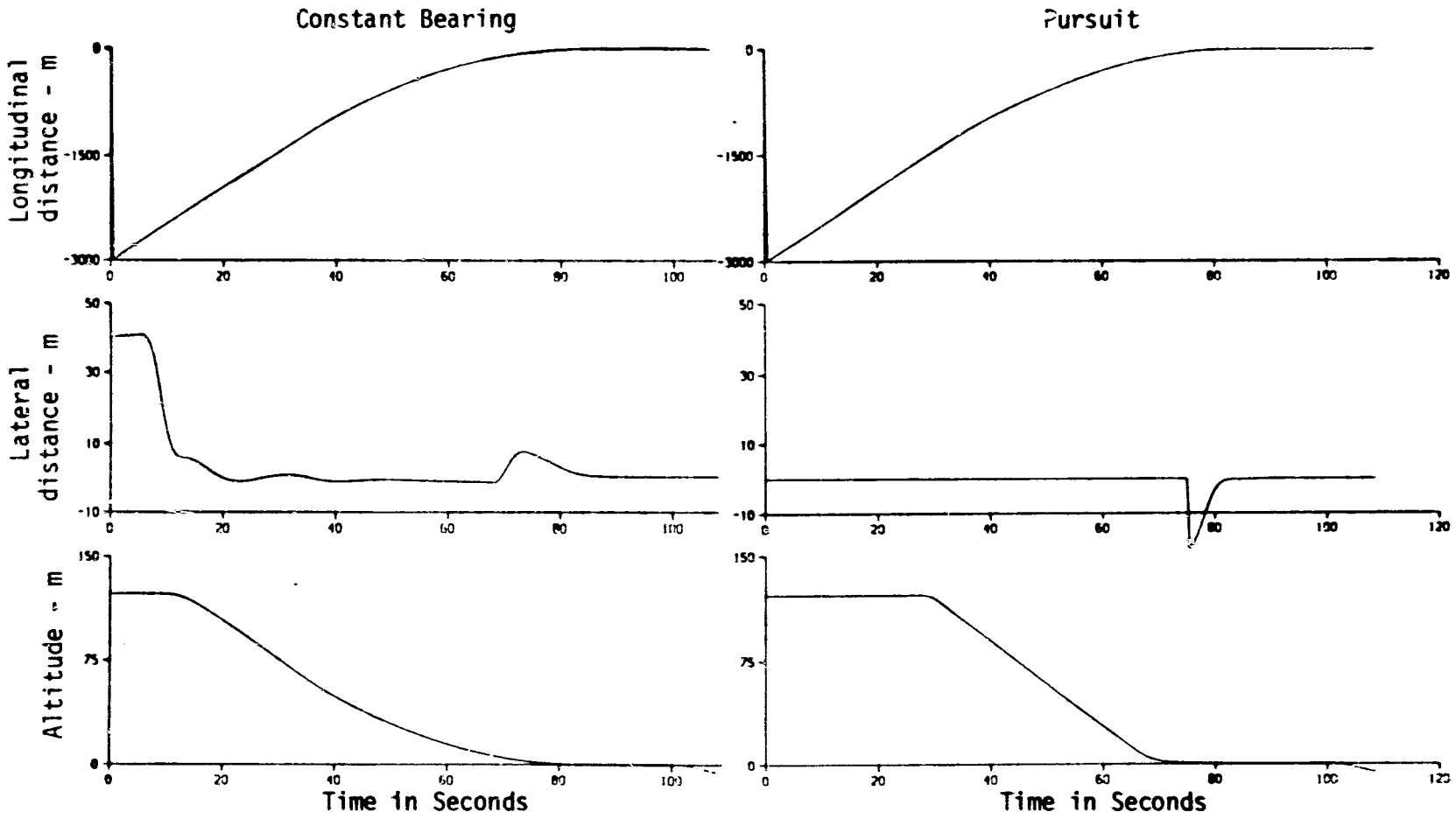

Figure 31. Time Plots of Position for the Nominal Cases.

Note the cross-track error transient induced by the heading alignment maneuver. For the pursuit mode, the cross-track error is not defined (this is indicated as a zero value until the final mode switching). At 75 sec, the final lateral mode is initiated. (The switching is incorporated in order to have better control of lateral position during the hover.) The effect of the pursuit overshoot (see Fig. 30) is apparent at this point.

The bottom plots show altitude vs time. The constant elevation guidance shows a concave up characteristic caused by longitudinal deceleration. It is noted that for the constant sink rate guidance the aircraft spends more time in the altitude hold mode; this is because the vertical velocity for this mode is independent of the longitudinal velocity.

Figure 32 shows the time plot of along-track, cross-track and vertical velocities for the nominal cases. The along-track velocity plots are almost identical including the final flare maneuver. The next plot shows the "cross-track" components. In the left plot, two transient activities are prominent; the first one is caused by the bearing reference capture mode. The second transient, occuring at 70 sec, is caused by switching to the final mode. The plot on the right shows the cross-track velocity for the pursuit guidance. Initially, the guidance law attempts to orient itself to the pursuit trajectory by banking to the left. Because of a low guidance gain, the pursuit trajectory overshoots and starts correcting back to the desired trajectory. The correcting process lasts until mode switching. (The effect of guidance gain variations for the pursuit trajectory is shown later.)

The bottom plots shows the vertical velocities. The left plot shows the constant elevation guidance. After the altitude hold mode, the 3 deg reference is captured and tracked by holding the steady sink rate of 2.8 m/sec; as the longitudinal speed slows due to the deceleration, the sink rate becomes smaller, and it terminates with the flare and hover maneuvers. The let-down sink rate of 1 m/sec is apparent at the end of the hover. The plot on the right shows the constant sink rate case.

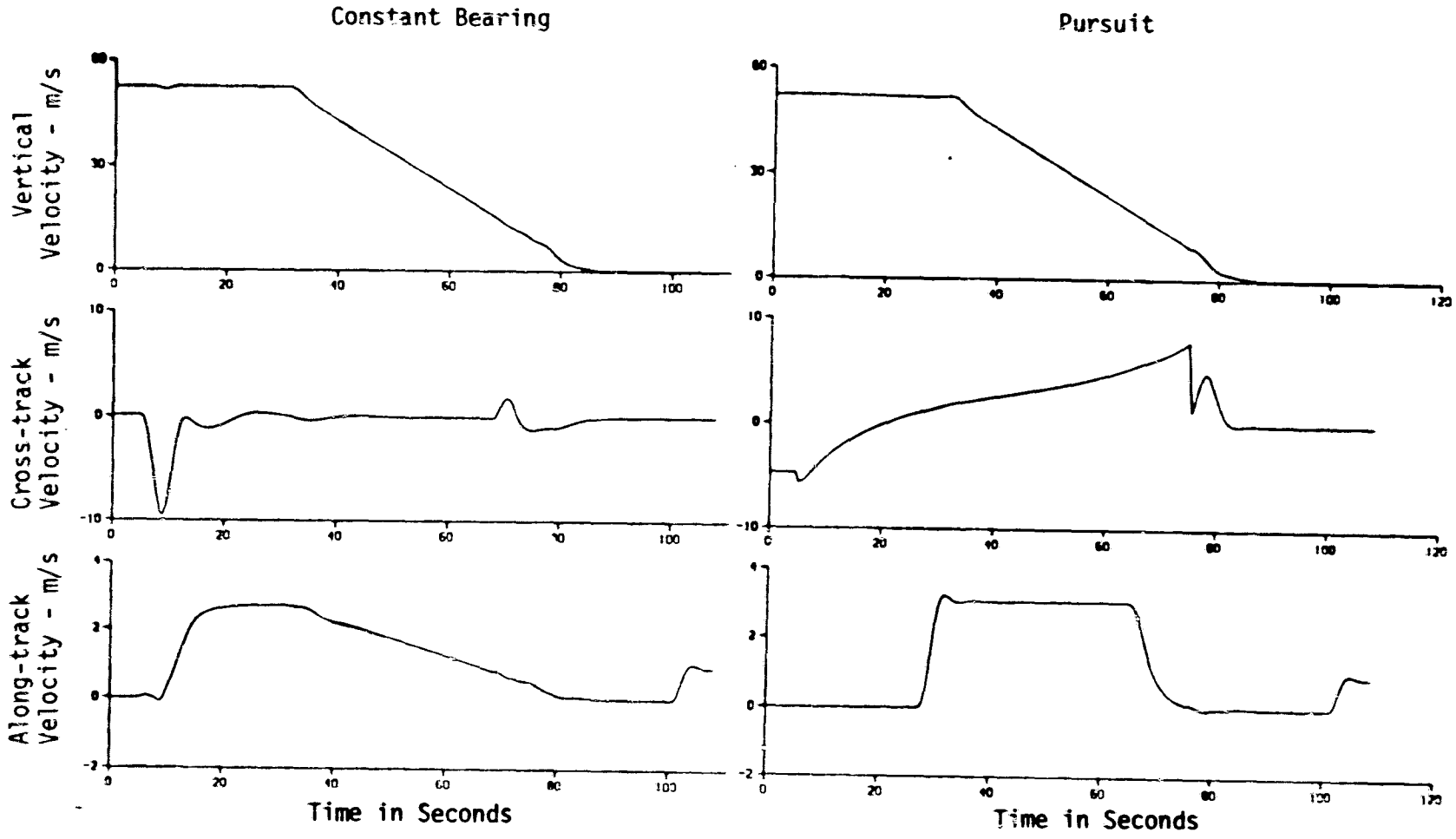

Figure 32. Time Plots of Velocity for the Nominal Cases.

After the altitude hold mode, a 3 m/sec (10 ft/sec) sink rate is commanded and held. The exponential flare is commanded at the proper time which brings the vertical speed to zero smoothly for stationkeeping. The guidance law becomes identical after that time.

Figure 34 shows the total position errors from the guidance reference. The top plot shows the actual along-track position. The middle plots show the cross-track errors. These are identical to those of Fig. 31. The bottom plots show the vertical errors. On the left, the 3 deg/sec capture maneuver is apparent. After 35 sec, this plot shows a small hang-off error which is caused by the cross-feed of the longitudinal deceleration. On the right, the vertical error is indicated to be zero until 65 sec. This is due to the fact that for the constant sink rate mode, vertical error is not defined. The exponential flare maneuver is apparent followed by hover and let-down after 65 sec.

Figure 35 shows the corresponding velocity errors. The top plots show the longitudinal velocity errors. Note, the error transient at 35 sec is due to deceleration maneuver initiation. Also, the transients due to the lateral final mode switching are apparent for both cases. The next plots show the cross-track velocity errors, which are identical to those of Fig. 32. The bottom plots show the vertical velocity errors from the references. The left side shows the transient due to the glideslope capture. This proves essentially that the glideslope track mode combined with the constant deceleration longitudinal mode provides continuous guidance. The plot on the right shows two transients; one is at the initiation of the constant sink-rate maneuver, and the other is for the exponential flare. The transient shapes are different, because the former uses the guidance law with the velocity feedback only, and the latter uses position and velocity feedback.

Figure 36 shows the aircraft attitude angles, angle-of-attack and sideslip angle. The top plots show the roll angle. For the constant bearing mode, there is a roll excursion of $\pm$ 20 deg for the capture maneuver (guidance gains are four times larger). The roll angle steadies out to a

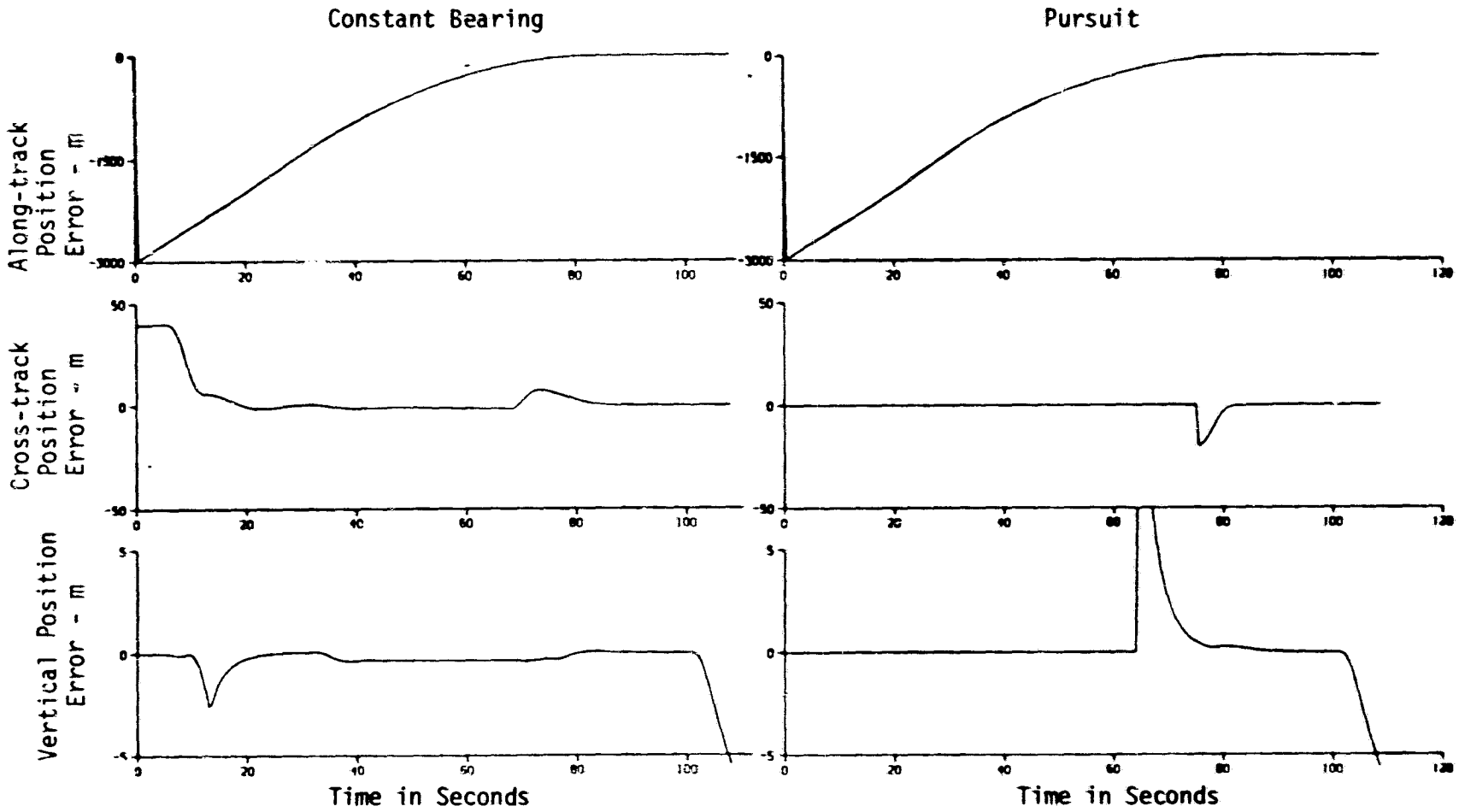

Figure 34. Total Errors wrt the Guidance Reference for the Nominal Cases.

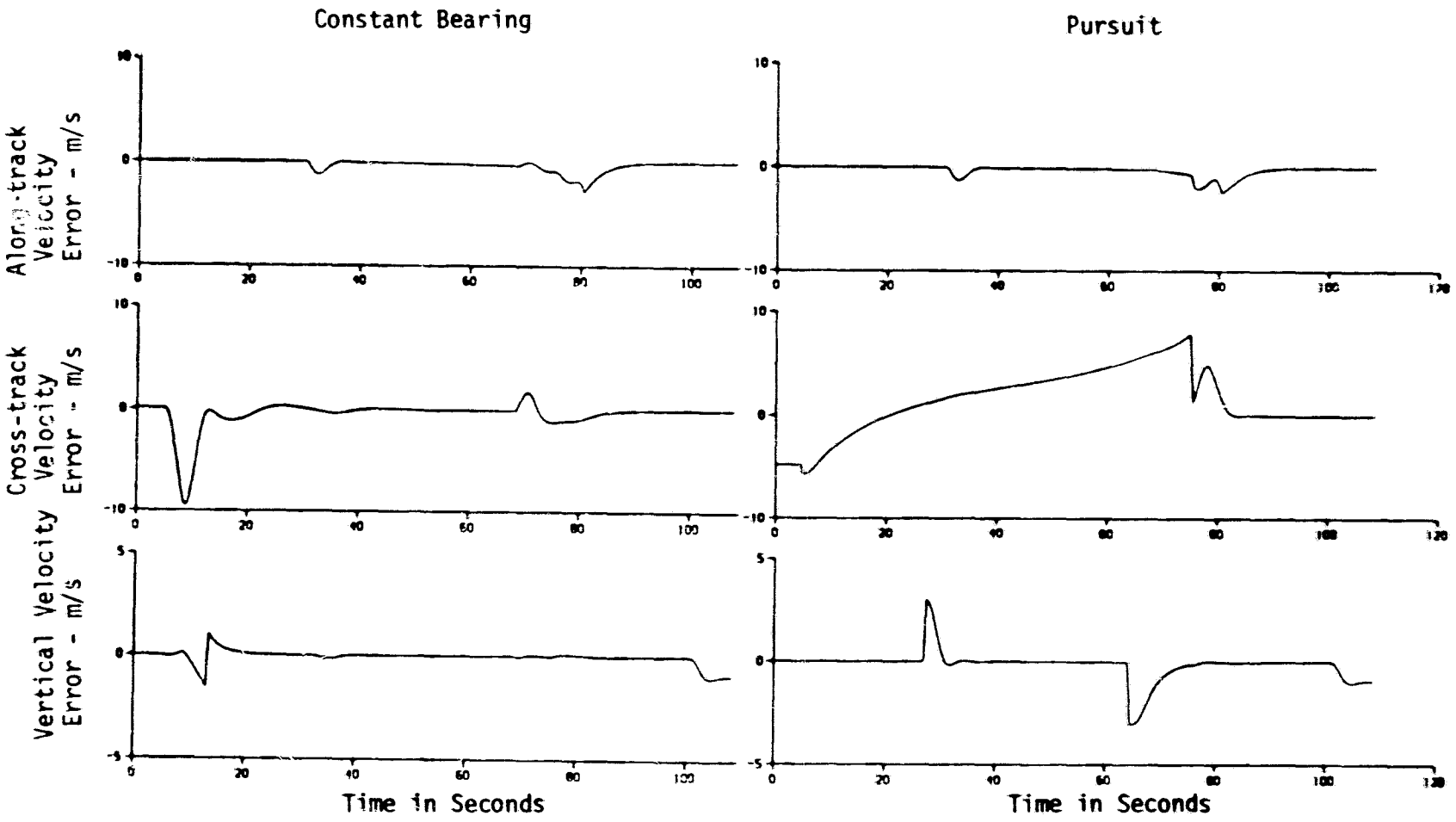

Figure 35. Total Velocity Errors wrt the Guidance Reference for the Nominal Cases.

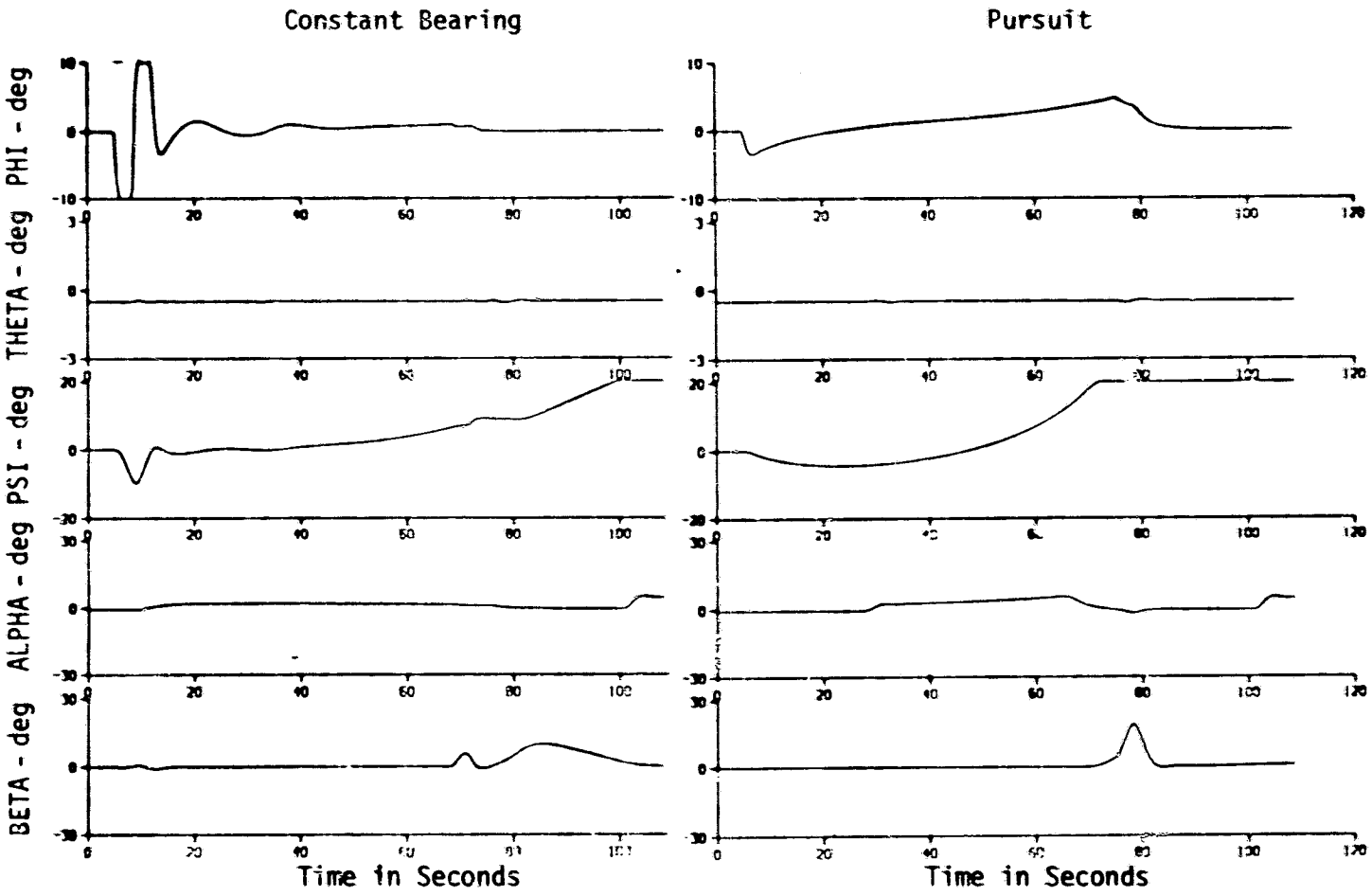

Figure 36. Aircraft Attitude, Angle-of-Attack and Sideslipe Angles for the Nominal Cases.

small value as the reference is tracked. It developes a small offset value due to the longitudinal deceleration and then goes to zero as roll-to-zero is commanded during the hover and let down period. The plot on the right shows the roll attitude for the pursuit guidance. The roll and heading angles reflect the characteristics of the pursuit guidance, viz., it requires a constantly changing cross-track velocity.

The next plot shows the pitch attitude which is held constant throughout the flight. (It is not used to control guidance deviations specifically.) A very small effect of the vertical cross feed can be seen.

The next plots show the heading angle. The left plot shows the transient due to the roll maneuver for capture. The aircraft holds a steady heading until longitudinal deceleration begins. As the lateral mode switches, the result of the heading alignment maneuver is apparent as it terminates at the ship heading of 23 deg. The right plot shows the resulting heading due to pursuit. Because of the initial relative heading between the aircraft and the ship, the aircraft heading initially swings to align itself and overshoots. It then starts correcting itself in chasing the ship heading. At the terminal stage, the aircraft heading overshoots the ship heading by five degree, but the alignment mode brings it back smoothly.

The angle-of-attack shown in the next plots exemplifies the inertial flight path angles for the nominal case, because pitch angles are constant and there is no wind. Notice the angle-of-attack during the letdown; even through the aircraft is stationary with respect to the ship, it is non-zero due to the inertial flight path angle caused by the sink rate of 1 m/sec (3 ft/sec) and the ship velocity of 10 m/sec (20 knot). The sideslip angles β, shown in the bottom two plots show the results of the coordinated turn prior to the final lateral mode (the yaw axis is "slaved" to the roll axis). The sideslip transients during the final mode show the effect of actively controlling the heading angle.

Figure 37 shows the time plots of the various aircraft control actuator input signals as well as the fan RPM. The first plots show the nozzle angle input. Combined with the throttle actuator signal (third plot), they control

C-2

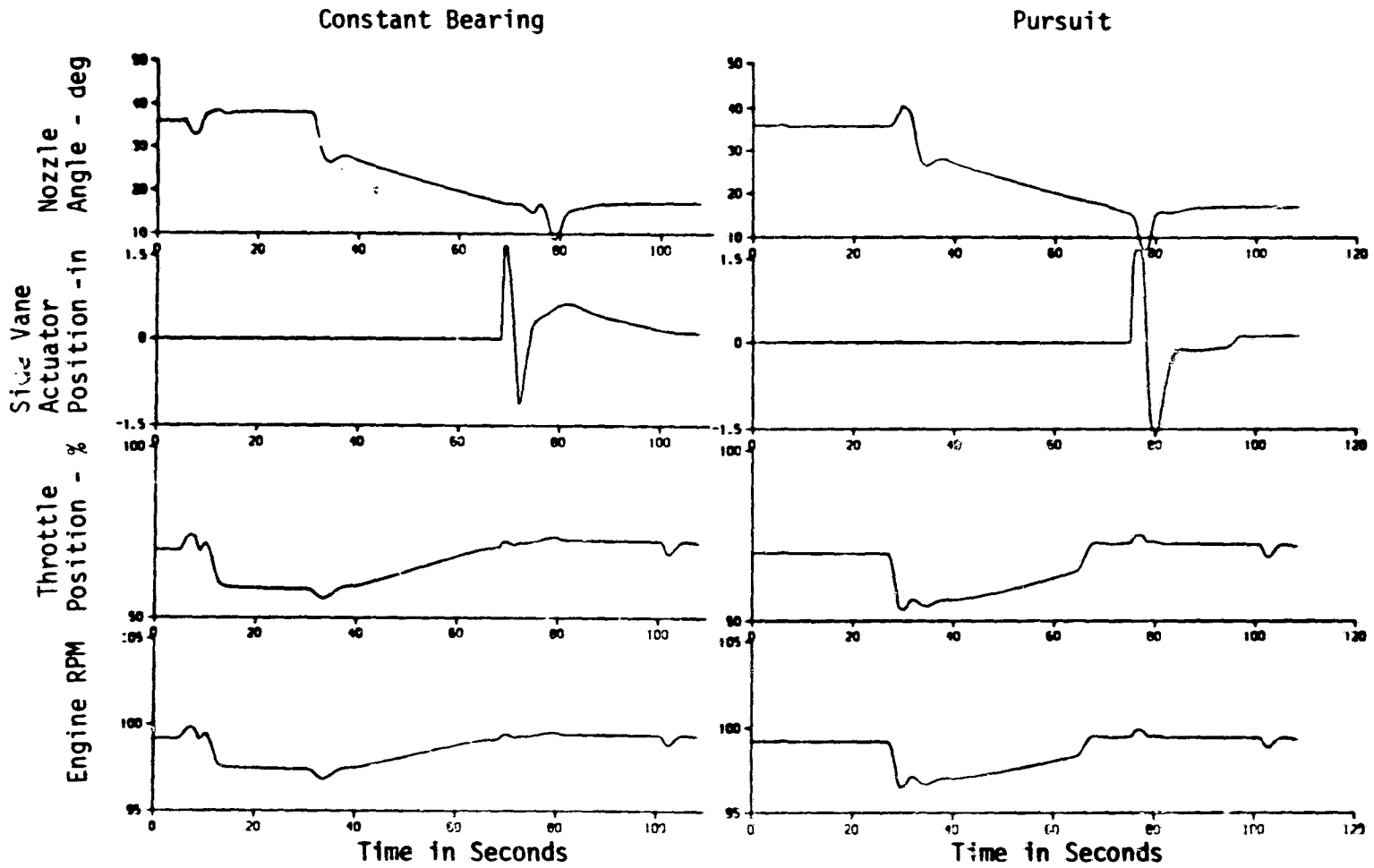

Figure 37. RTA Control Actuator Input Signals for the Nominal Cases.

the longitudinal and vertical thrust vector components in unison. Therefore, the differences in both of these plots are caused by the difference in vertical guidance. For example, the effects of the longer altitude hold mode for the constant sink rate guidance can be seen. The second plot show the side vane actuator signals which becomes active during the final mode to control the side velocity. Therefore, these reflect the cross track error during the lateral final mode. The bottom plots show the fan RPM which provides the thrust for the direct powered lift flight regime. It is seen that the engine and fan dynamics are evidently very fast, because the RPM plots look almost identical to the throttle actuator input signals.

Gain Effects for Pursuit Guidance

It was noted previously that the pursuit guidance performance is related to the guidance gains. The applicable guidance law is given by

$$\phi^c = \tan^{-1} \frac{k\, V_y^c}{g}$$

where

ϕ^c = roll command,

V_y^c = lateral velocity command,

g = gravitational constant (32.2 ft/sec), and

k = guidance law gain.

In order to test the sensitivity of the guidance gain to the performance, simulation runs were obtained with three different gains: $k = -0.8$, -0.4 and -0.1.

Figure 38 shows the flight path results plotted for the three cases. The top plot shows the horizontal trajectories with respect to the ship body axes. The second plot shows the cross-track errors after 70 second

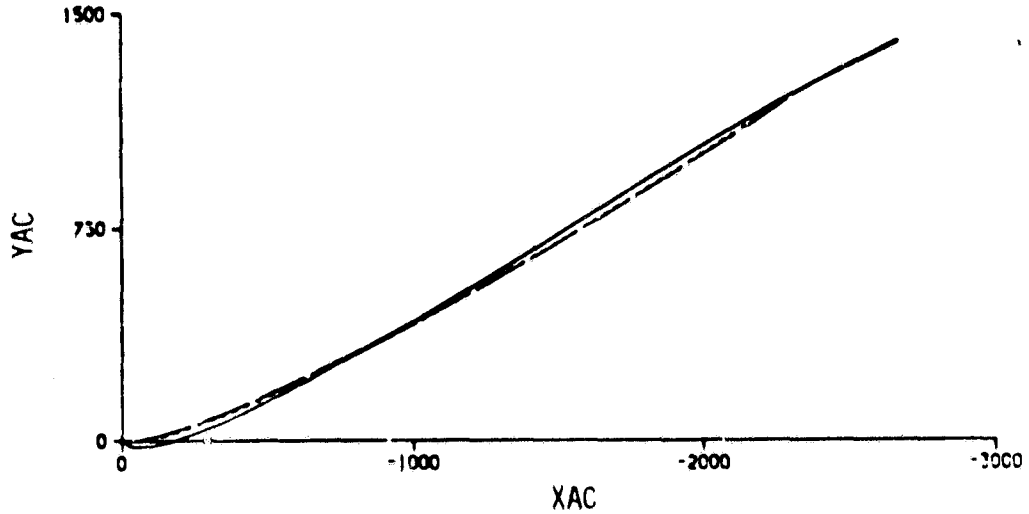

a). Horizontal position (x vs y)

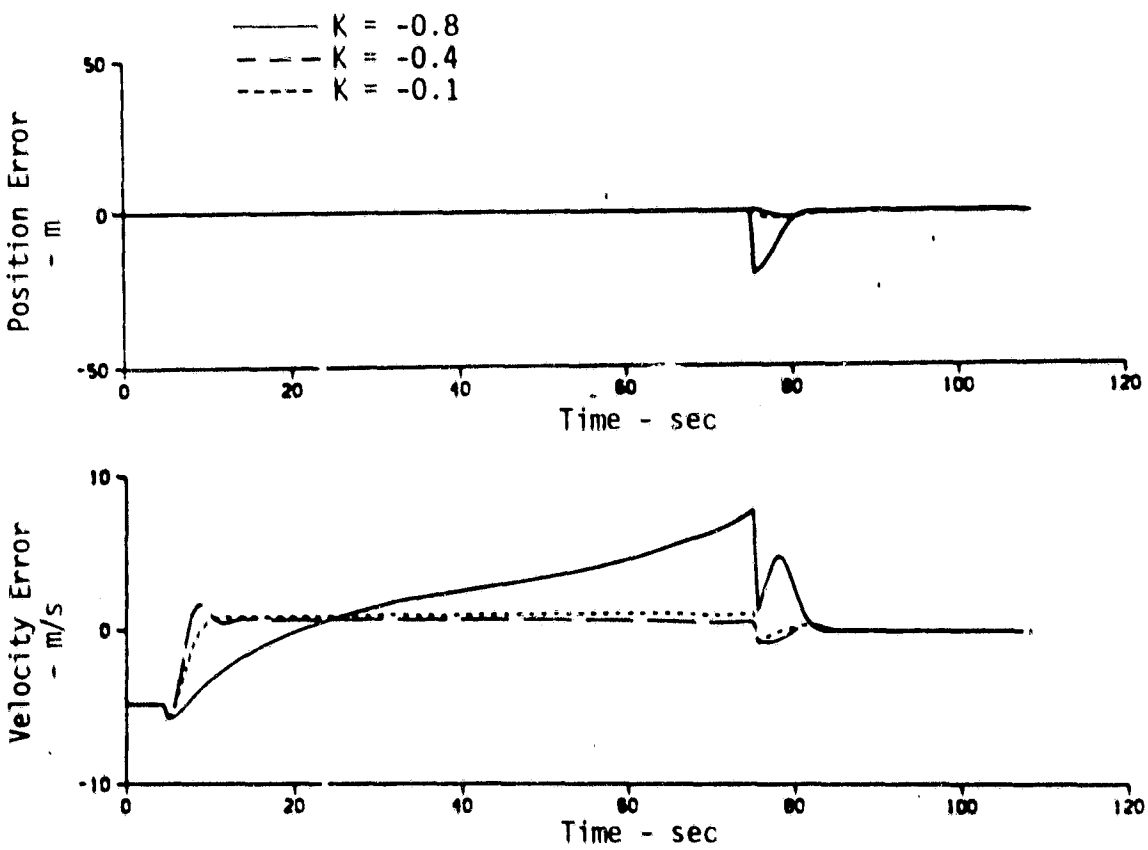

b). Cross-track position and velocity errors

Figure 38. Feedback Gain Effects for the Lateral Pursuit Guidance.

(zero value prior to it indicates that the error is not defined). This shows the performance of the different gains at the terminal condition. The bottom plot shows the lateral velocities until 70 seconds. After 70 sec, these errors are nulled. These plots show that a high gain tends to over compensate for the "ideal" pursuit trajectory at the initial time by aligning the aircraft heading to that of the ship too quickly; the aircraft thus puts itself into an overshoot situation. The low gain law tends to hesitate and let the kinematics align the velocity vectors. This phenonomenon is evidenced by the tendency of pursuit guidance to undershoot the target ship.

To say that low gains are better because the transient induced by the cross-track errors at the onset of mode switching are smaller is not entirely correct. It is true for this particular set of initial states; however, for a different set of initial conditions, the conclusion may be different. Further resolution must come from more extensive simulation study.

Error Sensitivity Analysis of the SRFIMF Flight Controller

The SRFIMF flight contoller was designed from the deterministic input/output point of view using classical design techniques. See Appendix B for a more detailed account. It was never tested nor analyzed as to its sensitivities to the errors in the feedback signals which exist inherently in the aircraft body sensors. A simple and heuristic arguement has been given for this type of flight controller's applicability.

Flights were simulated with two different sets of sensor error magnitudes with the guidance laws using error free positions and velocities. (i.e., for this test, it was assumed that navigation was perfect, and the only errors were due to flight control instrumentation.) Therefore, in these cases, the differences in total errors from the nominal case were induced solely by the sensor errors in the flight controller feedback loop. Table 2 summarizes the magnitudes of the sensor errors used in the experiments. [2,19]

Table 2. Aircraft Body Sensor Error Characteristics

Type	High Frequency	High Frequency (bias)
Standard Inertial Platform Model		
Attitude	0.1° (1σ; 10 sec)	0.1°
Attitude Rate	0.5°/sec(1σ; 10 sec)	0.5°/s
Attitude Accel.	0.1°/sec^2(1σ; 10 sec)	0.1°/s^2
Linear Accel.	0.1 ft/sec(1σ; 10 sec)	0.1 ft/sec^2
Strap-down Model		
Attitude	1°(1σ; 10 sec)	0.5°
Attitude Rate	0.5°/s(1σ; 10 sec)	0.5°/s
Attitude Accel.	1°/s^2(1σ; 10 sec)	1°/s^2
Linear Accel.	0.5 ft/sec^2(1σ; 10 sec)	0.5 ft/sec^2

Figures 39 and 40 show the total position and velocity errors with respect to the guidance references for the corresponding sensor error characteristics given in Table 2, along with the nominal case.

In Figure 39, the second plot shows the cross-track errors. The deviations from the nominal case are small except immediately after the reference capture. The bottom plot shows the vertical position errors. The nominal and the platform error cases are almost identical except for a small stand-off error. The strap-down case shows approximately 1 meter of stand-off error. Also, note the presence of a medium frequency excursion in the latter case. The hang-off error is thought to be caused by the interaction of the steady state value of the integral compensator with respect to the vertical acceleration bias.

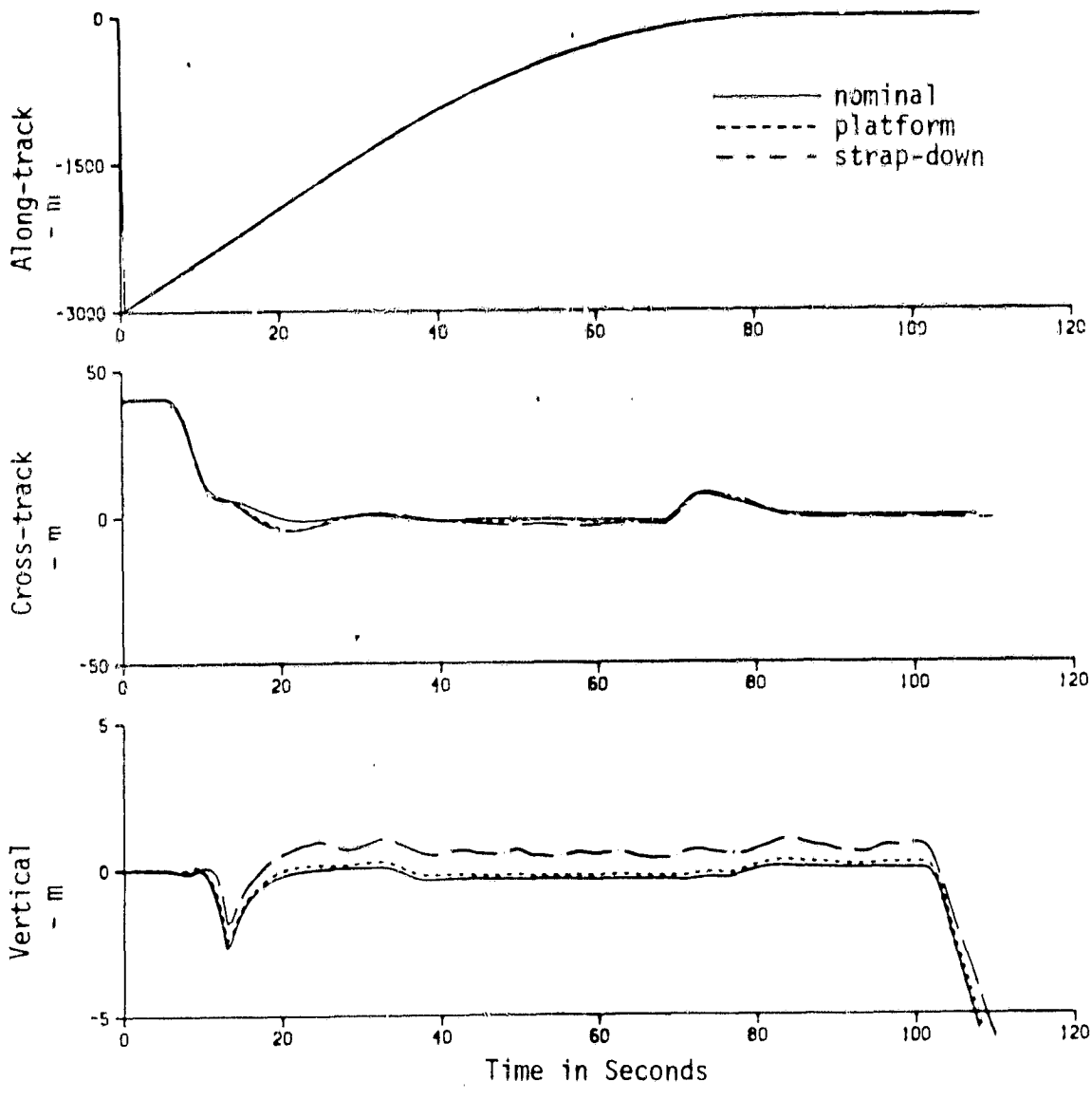

Figure 39. Total Position Errors Due to Errors in Flight Controller Feedback Loop.

In Figure 40, the top plot shows the along-track velocity errors. The second plot shows the cross-track velocity errors, and the bottom, the vertical velocity errors. The deviations are very small for all axes. The strap-down case tends to introduce a small medium frequency excursion caused by the pitch activities due to the pitch attitude feedback loop in the flight controller.

In conclusion, the sensor errors in the flight controller feedback loop do not materially degrade the guidance performance by itself. The controller remains stable in the presence of the sensor errors. Other errors such as guidance errors and linear velocity errors due to navigation have a much larger impact on the total position errors. The study of the guidance errors caused by the feedback sensor errors was not carried out in detail, because the filter is not optimized for the degraded strap-down body sensor error characteristics. Also, the SRFIMF controller used in this study was based on perfect knowledge of the aircraft dynamics. It is not known what the effect aircraft modeling errors would have on this performance.

Figures 41 and 42 show the navigation position and velocity errors that result due to the sensor error magnitudes shown in Table 2. As can be seen, these errors are adequately small near the ship (after 70 sec).

Single Pass Studies

In order to obtain the sensitivities of the total system performance with respect to the system components, single pass simulated flights were performed with various system configurations. As expected, the ship motion and the wind-over-deck turbulence had the most dominant effect in terms of aircraft accelerations and actuator responses.

For brevity, two cases among many that were actually made are shown and discussed here. The cases are the constant bearing/elevation guidance and the pursuit/constant sink rate guidance under the same environmental, sensor error and navaid error characteristics. Table 3 shows the summary of simulated error characteristics used. The ship was subjected to the Sea State 5 condition shown in Figure 43. Figure 44 shows the corresponding estimates of the "landing pad deviation vector" and its rate. Wind-over-deck turbulance was caused by a mean wind of 20 knots and a relative direction of 30 deg with respect to the ship heading.

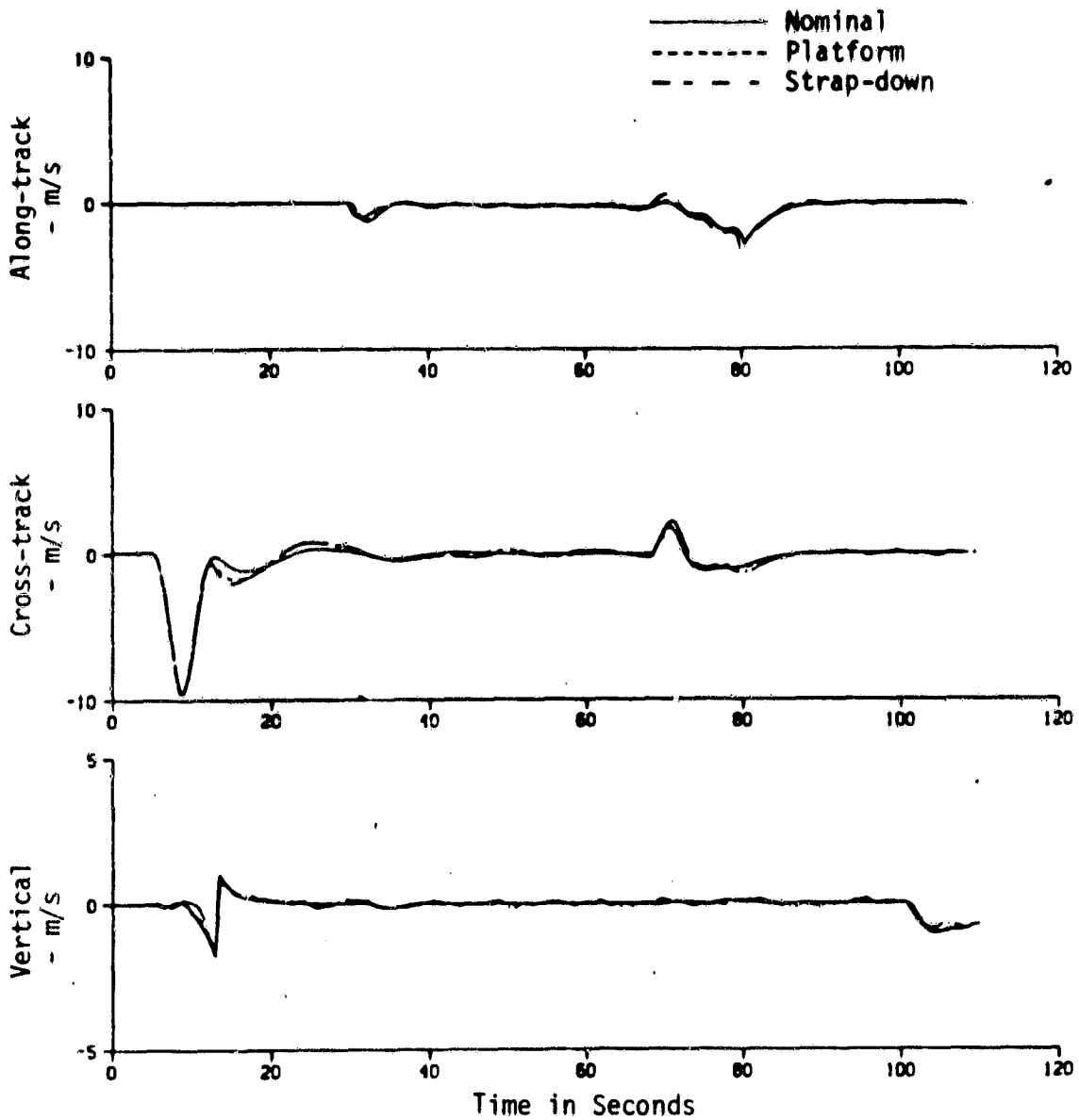

Figure 40. Total Velocity Errors Due to Errors in Flight Controller Feedback Loop.

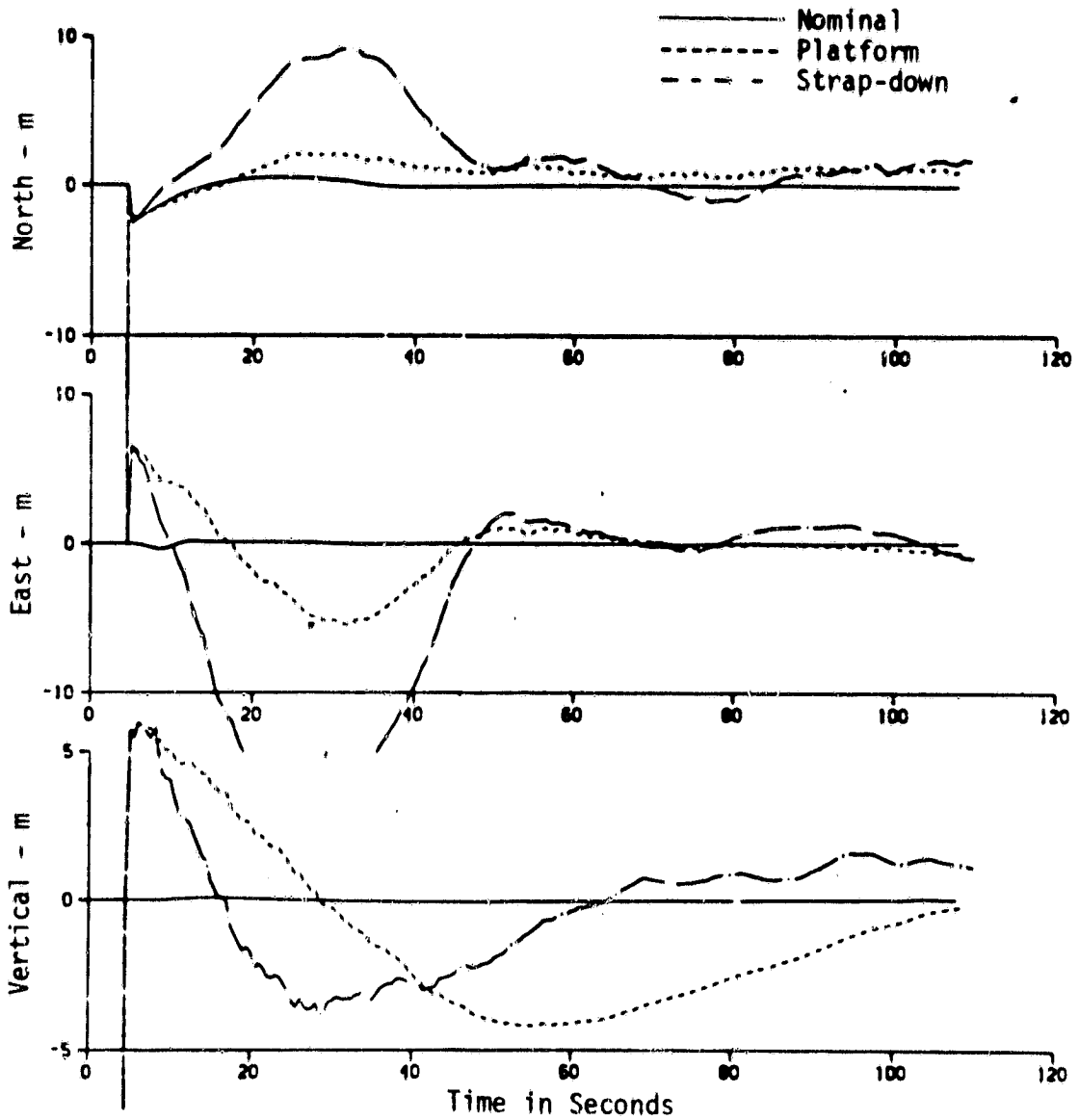

Figure 41. Navigation Position Errors

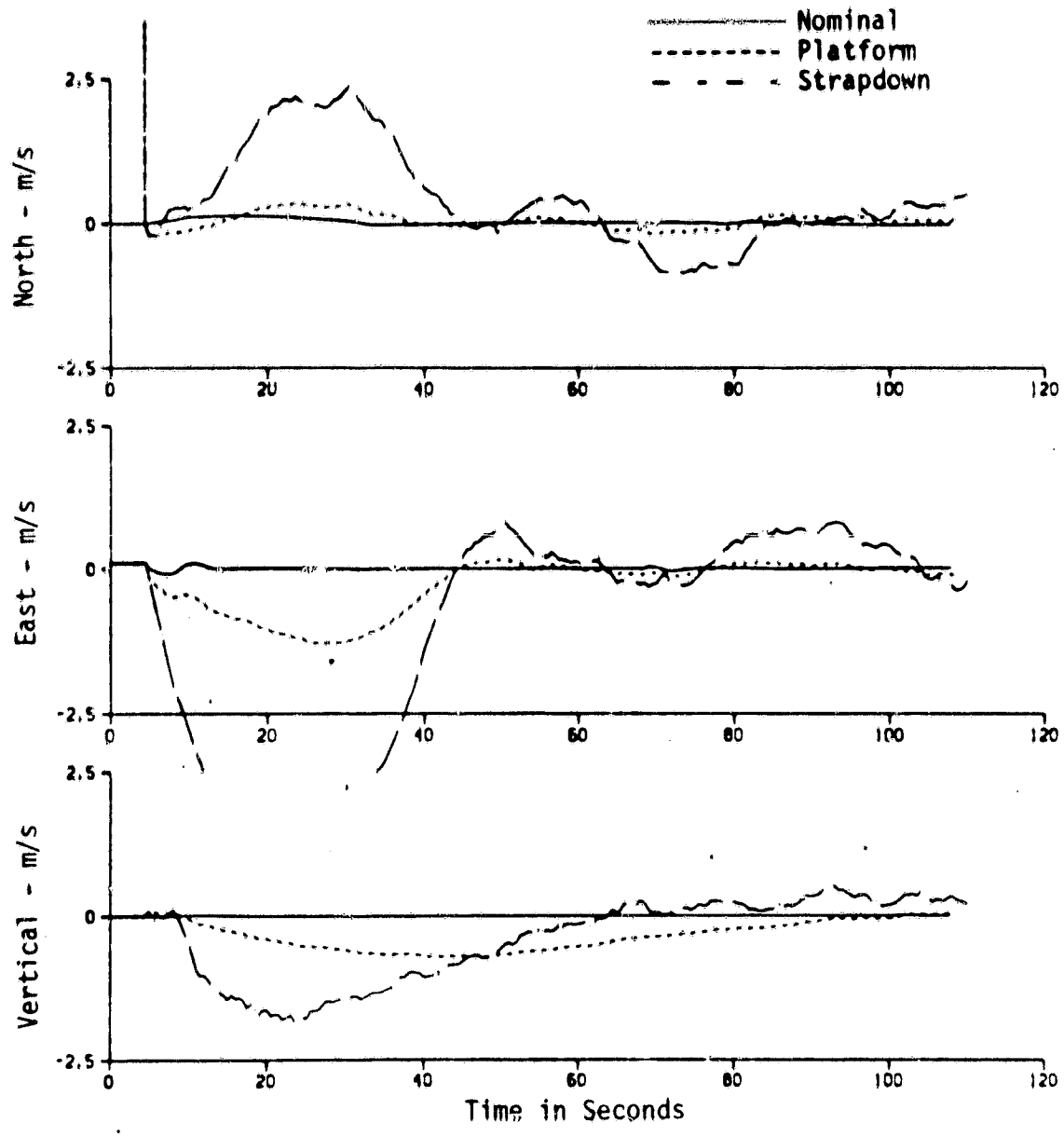

Figure 42. Navigation Velocity Errors.

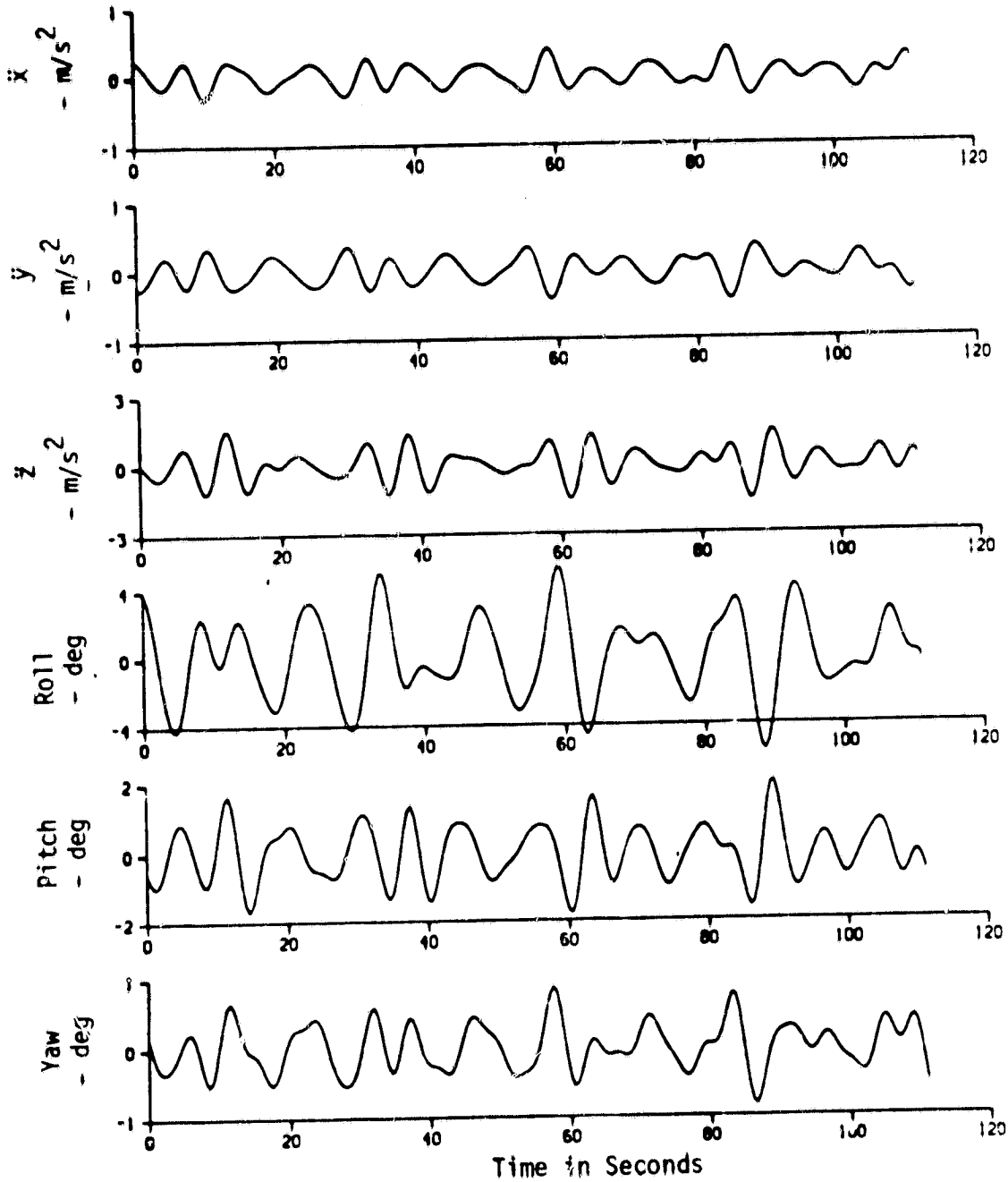

Figure 43. Example Ship Motion at Sea State 5.

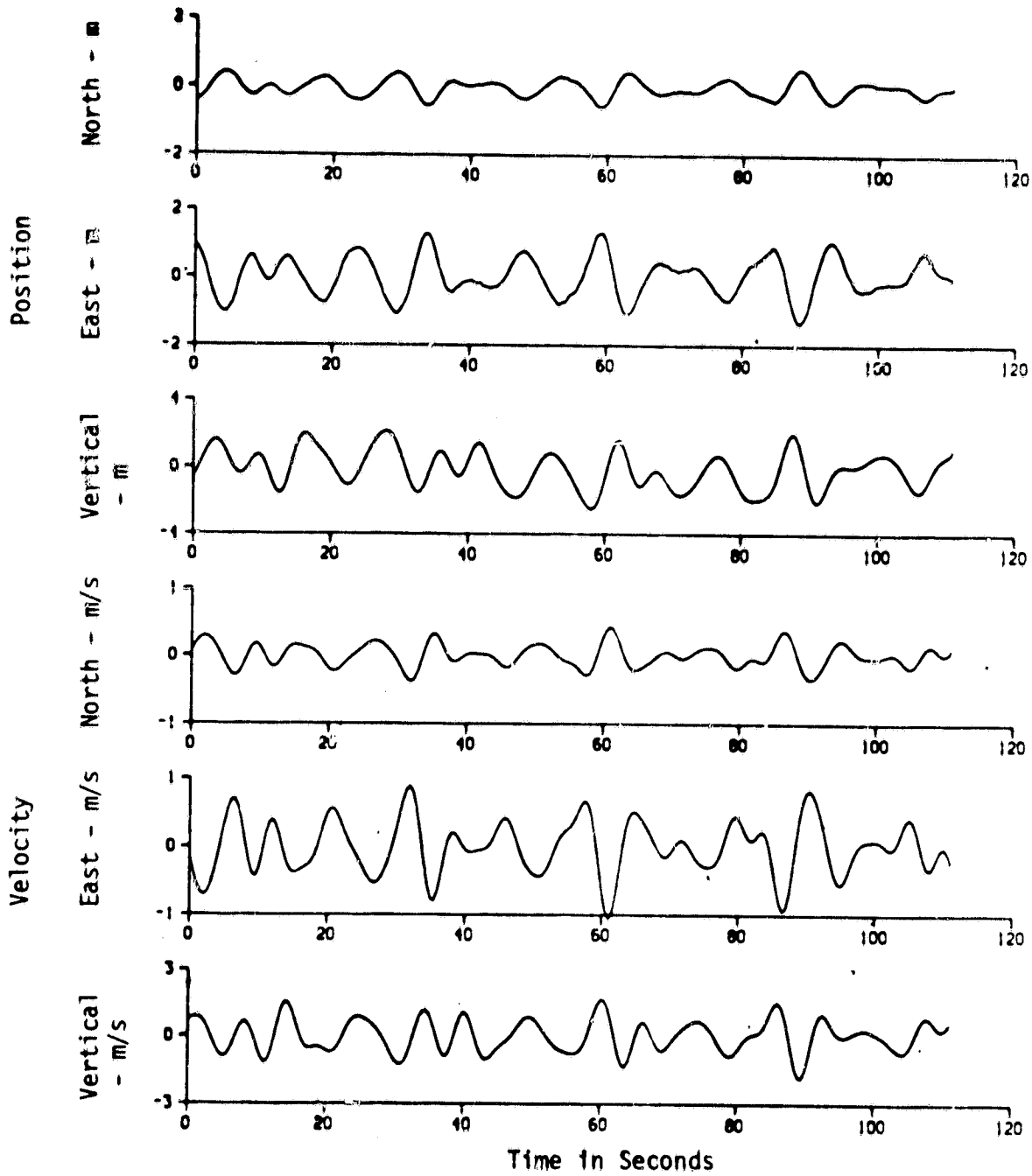

Figure 44. Estimated Landing Pad Deviation Vector.

Table 3. Summary of Simulated Error Models

(Standard Deviations Listed)

Type	High Frequency	Bias
Ship Sensors		
. Attitude - deg	0.1	0.1
. Acceleration - ft/s^2	0.1	0.1
. Ship Speed - kt	0.0	1
MLS		
. DME - ft	3	3
. Azimuth - deg	0.1	0.1
. Elevation - deg	0.1	0.1
Aircraft Sensors		
. Attitude Angle - deg	0.1	0.1
. Attitude Rate - deg	0.5	0.5
. Angular Acceleration - deg/s^2	0.1	0.1
. Translational Acceleration - ft/s^2	0.1	0.1

Figures 45 and 46 show the plots of navigation position and velocity errors respectively for the pursuit case. The navigation errors are not sensitive to the guidance concepts, and they seem to be almost identical. Errors prior to 40 sec are caused by MLS biases and the fact that the navigation filter has not reached the steady state operating condition. Medium frequency errors in x and y (along-track and cross-track) are caused by the ship's pitch and roll excursions. It is seen that the roll influence on the y error is more prominent than that of pitch on x. The same comment applies to the x and y velocity errors. The lack of a similar error in the z-axis is due to the fact that the vertical position of the MLS antenna with respect to the ship c.g. is well compensated by the landing pad deviation vector estimation. It is seen that navigation errors in the immediate vicinity of the ship are typically less than 2 meters in position and 1 m/sec in velocity.

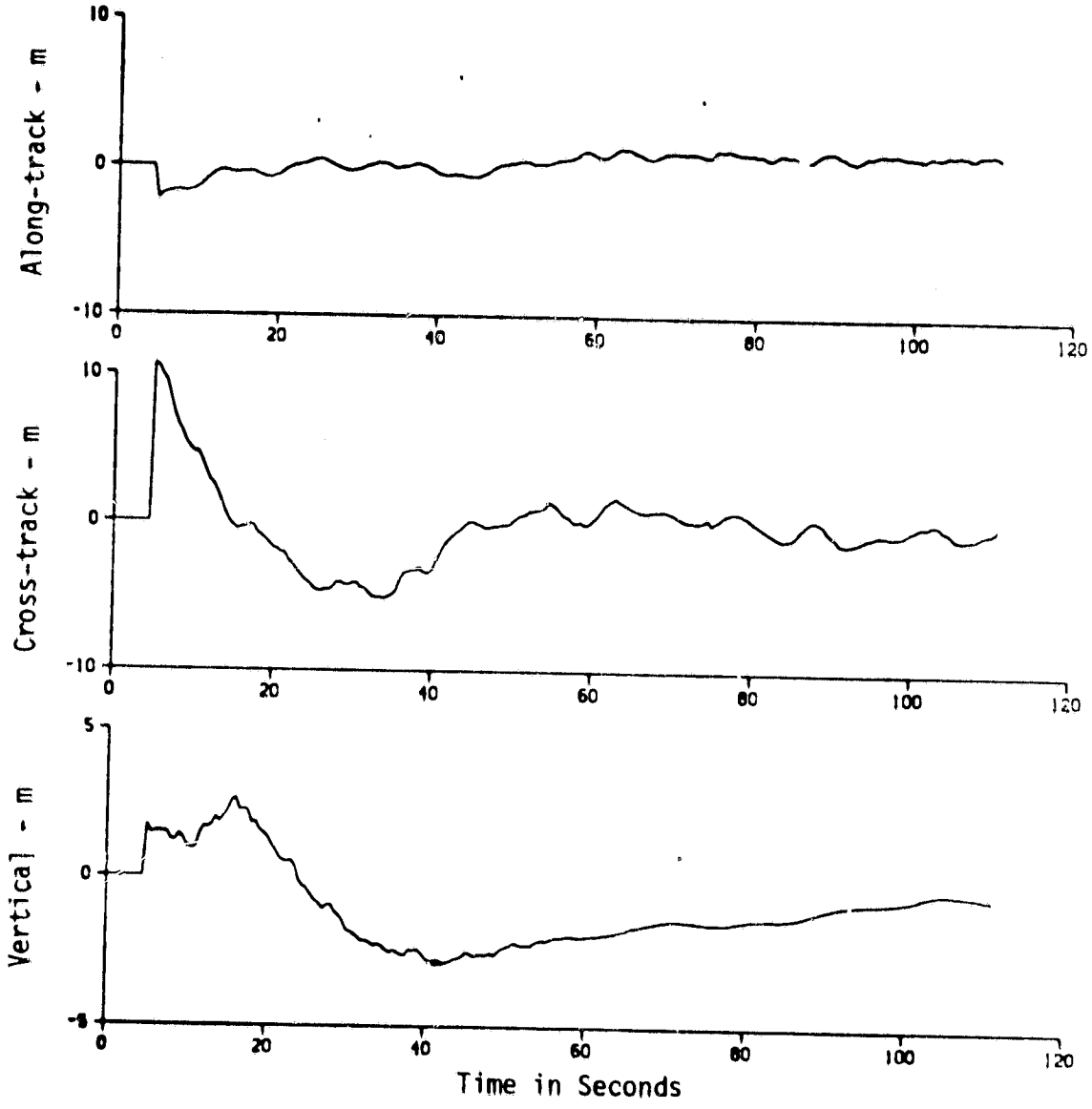

Figure 45. Navigation Position Errors for Pursuit Guidance.

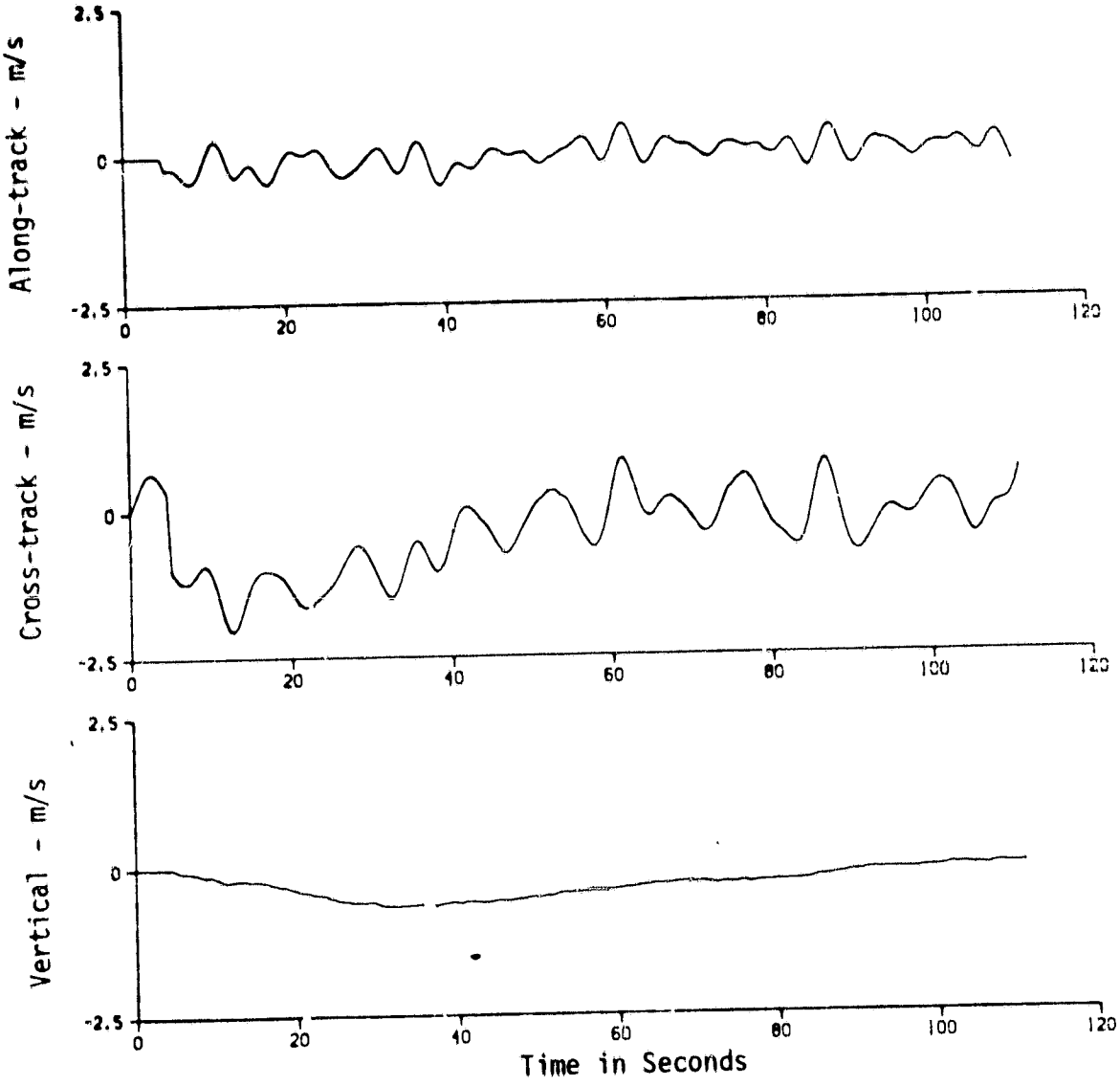

Figure 46. Navigation Velocity Errors for Pursuit Guidance.

Figures 47 through 53 show the time plots of various quantities of interest for the single pass runs. The plots on the left correspond to the constant bearing/elevation guidance; the plots on the right correspond to the pursuit/constant sink rate guidance.

Figures 47 and 48 show the total position and velocity errors with respect to the guidance references. The top plots of Figures 47 are the actual along track positions; they look almost identical because the longitudinal guidance laws are the same. The next plots show the cross track errors. The left plot shows the effects of the ship rolling motion, wind-over-deck turbulence and the mode switching. The lateral error during the hover period is within 3 meters. The plot on the right is zero until 75 seconds (the cross track error is not defined prior to that time). Then, the cross track error is shown during the final mode. Both plots exhibit the same characteristic low frequency excursion due mainly to the ship roll. The bottom plots show the vertical errors. The transient due to turbulence which occurs at 75 sec is apparent on the left plot. For the constant elevation case, the vertical error is within 5 m. During hover, it is less than 1 m.

Figure 48 shows the velocity error plots. The top plots show the along-track velocity errors which are similar except that the constant bearing approach shows a little more turbulence effect. Except for the flare maneuver (at approximately 80 sec), errors are small (within 1 m/sec).

The next plots show the cross-track velocity errors. The constant bearing case has a large error due to the capture maneuver followed by a medium frequency excursion. This is the result of trying to track and regulate lateral position which is constant (due to ship motion). The same error characteristics appear during the final mode. The advantage of the pursuit guidance (combined with a relatively low guidance gain) is apparent on the right plot. During the pursuit trajectory, the velocity error does not show the same characteristics as in the constant bearing track. This is because the guidance does not try to control position error by compensating for the ship roll motion that is in effect. During the final mode (after 75 sec), the error characteristics are the same.

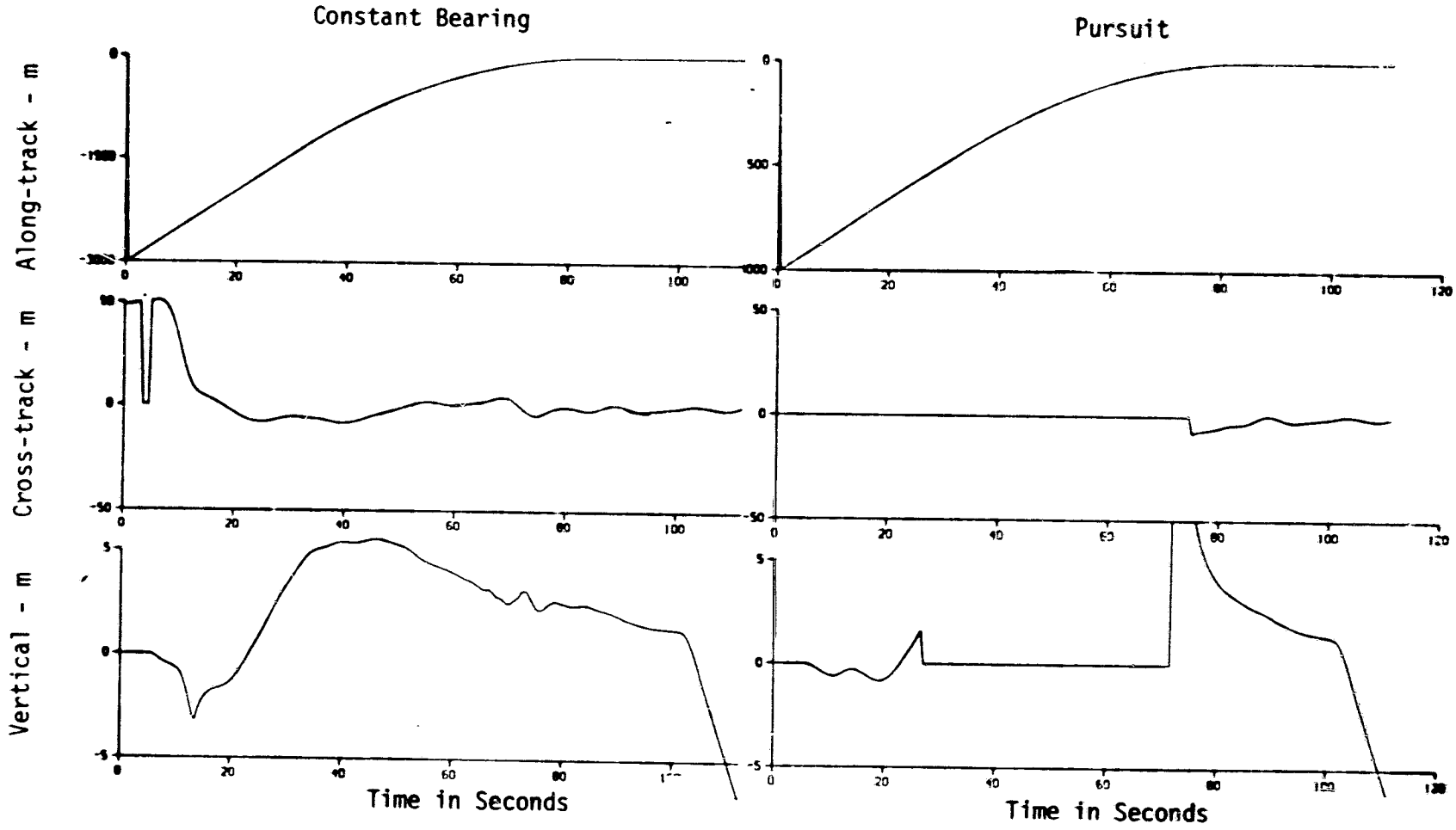

Figure 47. Total Guidance Position Errors

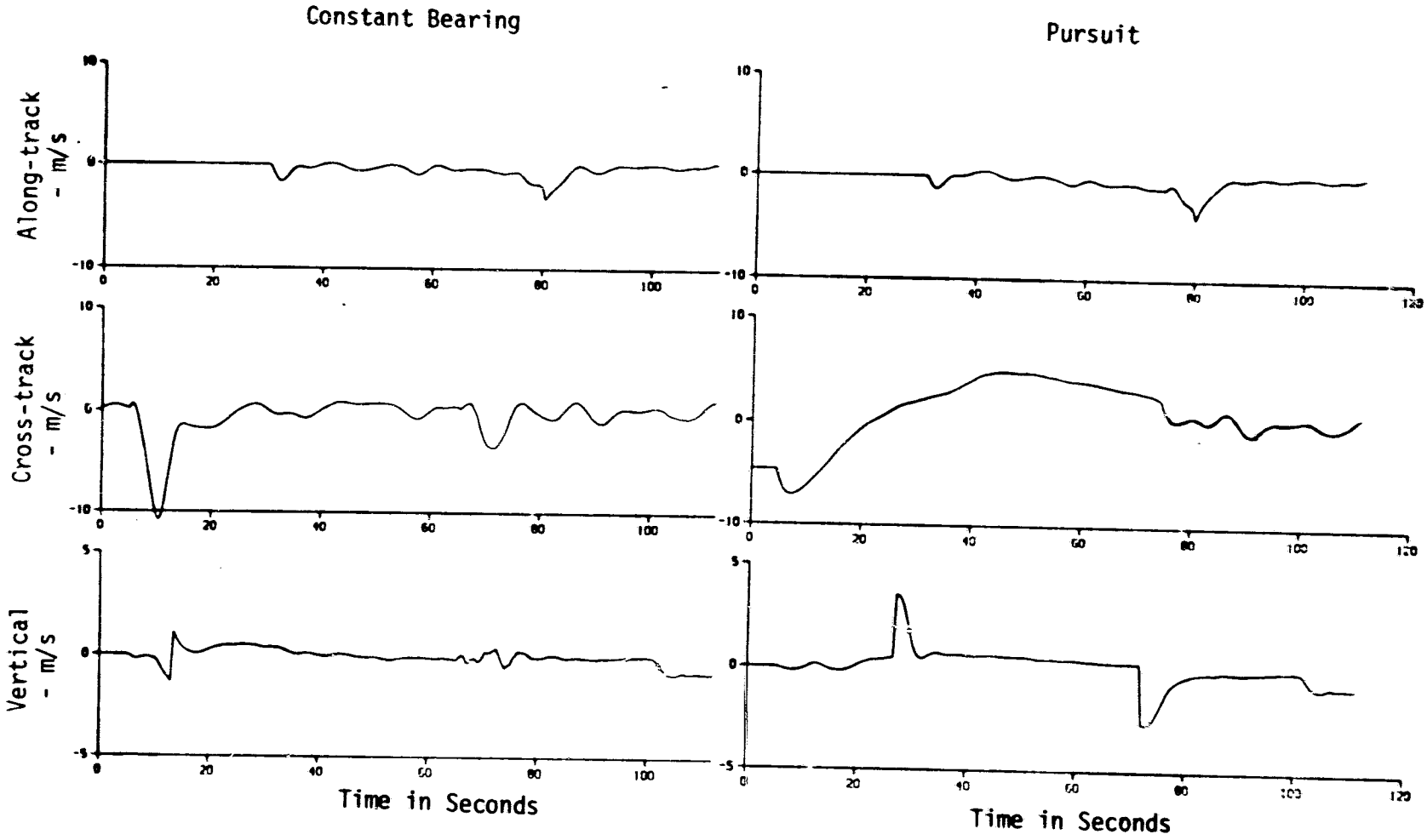

Figure 48. Total Guidance Velocity Errors

The bottom plots show the vertical velocity errors. The same comments regarding the type of guidance used apply to the vertical axis. Controlling the vertical position induces a vertical velocity error. The guidance law forces the aircraft to follow the ship motion within the system bandwidth. The constant sink rate guidance does not show much error, because it only corrects sink rate independent of ship motion. The turbulence effect on the constant elevation guidance is apparent at 70 sec. As can be seen later, the constant bearing guidance trajectory passes through the severest portion of the wind-over-deck turbulence profile for this mean wind heading relative to the ship heading.

Figures 49 and 50 show the time plots of total aircraft position and velocity with respect to the references.

Figure 51 shows the time plots of wind and aircraft acceleration. (This and the next two figures are plotted every 50 msec rather than 0.5 sec in order to indicate the details.) The top three plots show the north-east-down components; the bottom three show the aircraft body accelerations. The constant bearing guidance experiences the severest turbulence. For example, the equivalent vertical wind shear at 70 sec is calculated to be 3 m/sec/sec (23 knot of wind change over 7 sec time period). The time period of 65 to 75 sec exhibits the worst wind variation of peak-to-peak value of $\pm$ 7 m/sec; afterwards, this subsides to $\pm$ 3 m/sec. The acceleration plots essentially reflect the prevalent wind condition. The vertical acceleration, for example, shows the peak-to-peak value of $\pm$ 1.5 m/sec. The vertical axis seems to be most sensitive to the WOD turbulence. This high acceleration rate would seem to be quite disturbing to the pilot.

On the other hand, the wind and acceleration experienced by the pursuit trajectory is very much milder; it completely avoids the worst wind profile location relative to the ship. However, the wind and the resultant aircraft accelerations after 90 sec are the same.

It is false to conclude that the pursuit guidance is better suited for the approach since its trajectory avoids the severe wind-over-deck turbulence. If the wind heading is along the ship longitudinal axis, then the complete opposite result is true.

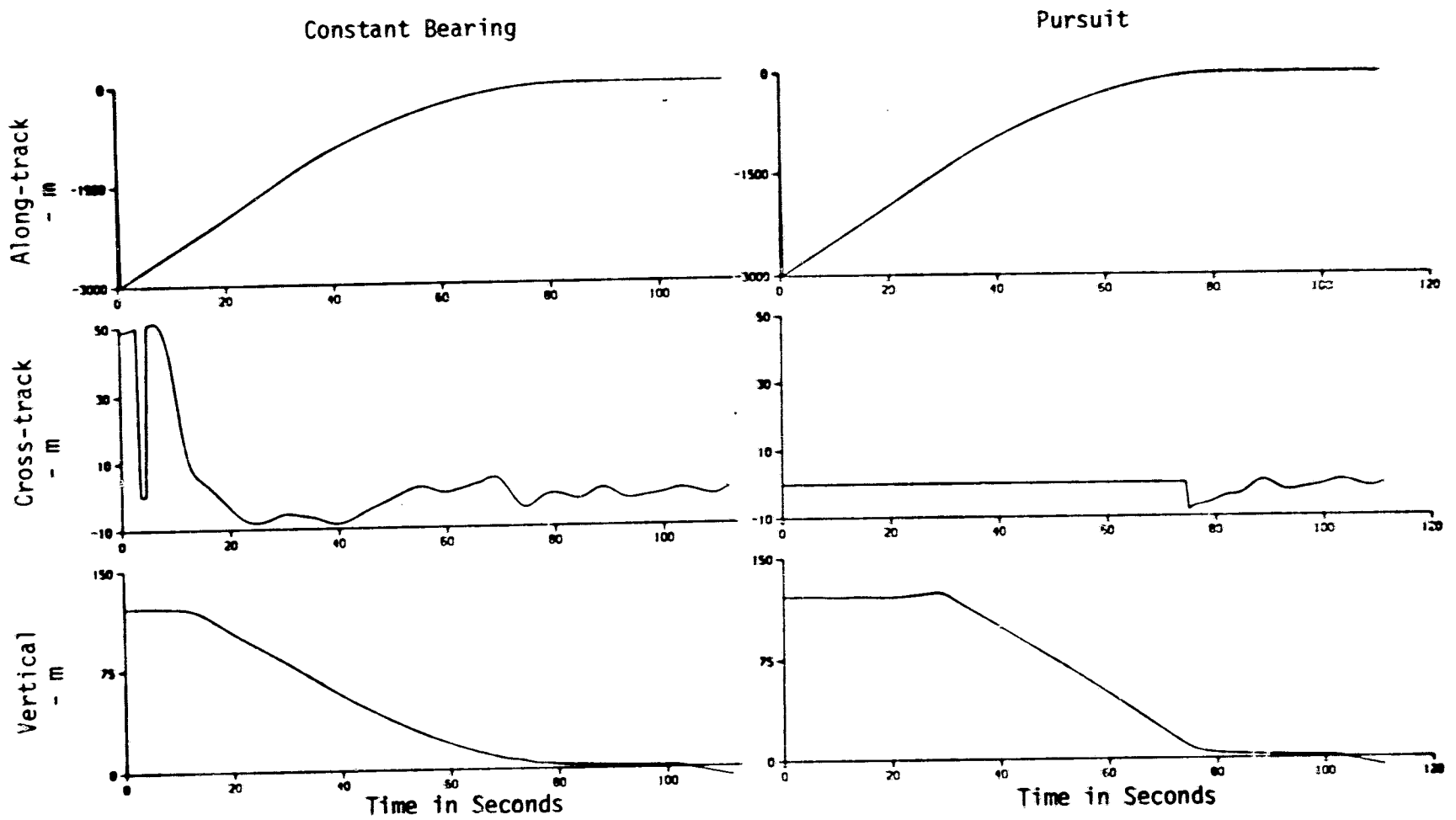

Figure 49. Aircraft Position with Respect to the Reference.

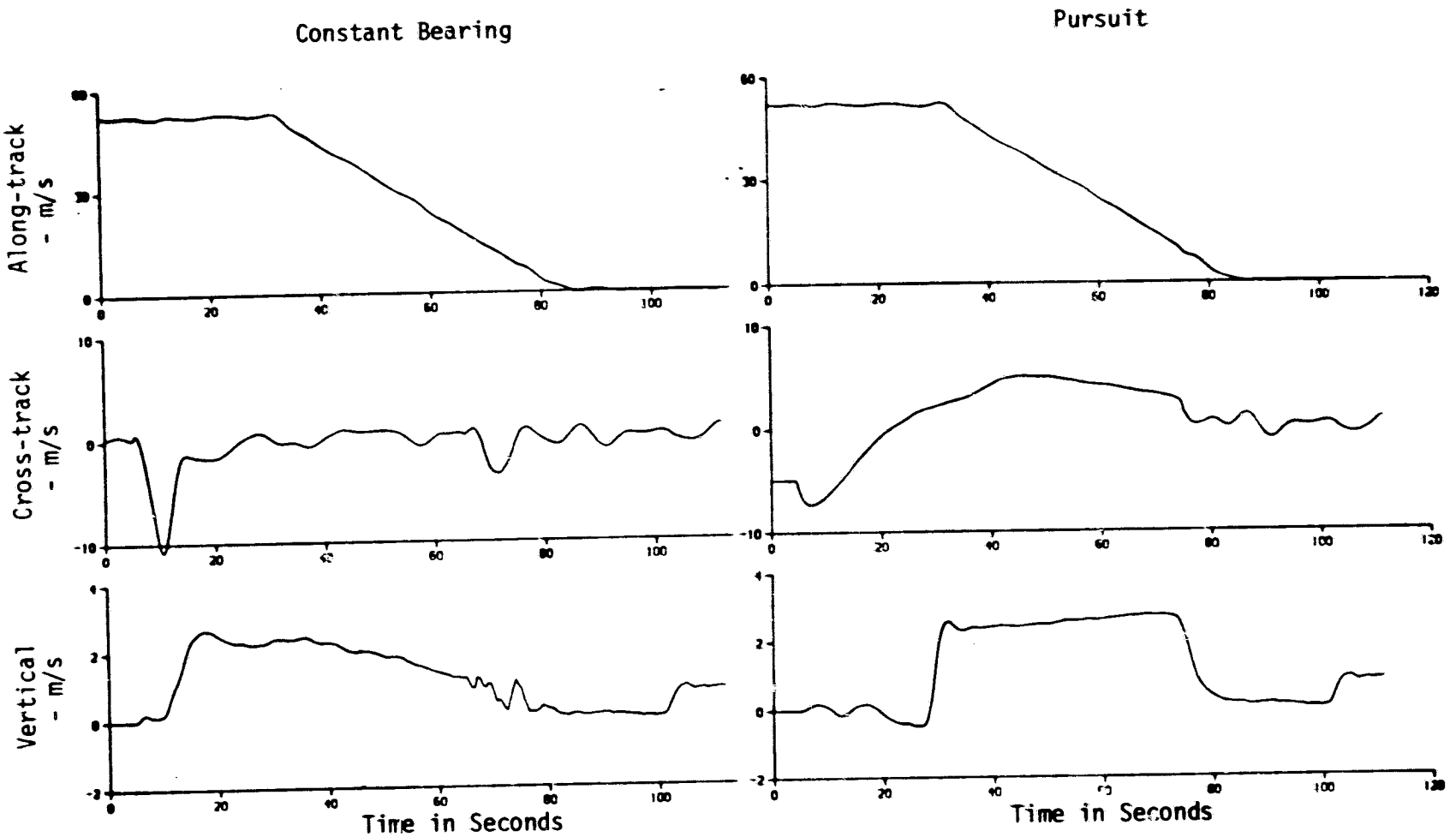

Figure 50. Aircraft Velocity with Respect to the Reference.

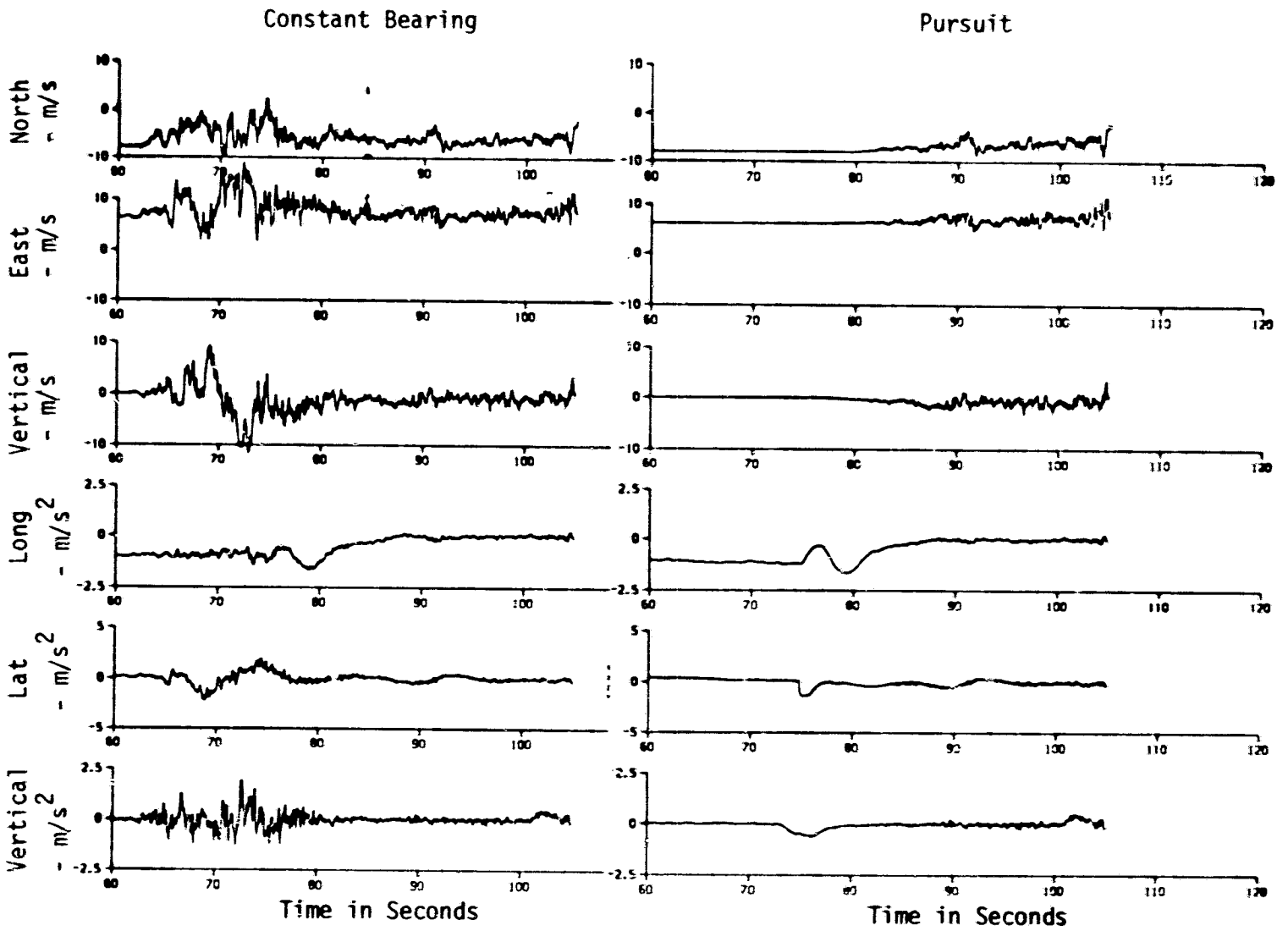

Figure 51. Wind-Over-Deck Turbulence and Body Accelerations.

Figure 52 shows the aircraft attitude angles ϕ,θ,ψ, angle-of-attack α, and side slip angle β for the two approaches. The roll and yaw attitudes are fairly smooth and quiet. The pitch attitude shows a little faster frequency activity mostly caused by the vertical turbulence or cross-coupling from the vertical or longitudinal axes. The yaw attitude on the left plot shows the effect of the heading alignment maneuver of 32 deg. The large high frequency excursions in the angles α and β are directly caused by the WOD turbulence.

The results shown in these plots seem somewhat unexpected considering the given turbulence; the attitude angles ϕ, θ and ψ do not show much effect from the wind. This can be explained by the fact that in this simulation the turbulence adds only to the (translational) forces but not to the (rotational) moments. The WOD turbulence effects on the aircraft rotational aerodynamics are not known or modeled at this time. There may be other effects missing such as the engine fan inlet dynamics due to wind variations. It is recommended that an investigation be conducted to provide information so that the wind-over-deck turbulence can be more accurately modeled.

Figure 53 shows the translational control actuator signals and fan rpm for the same two approaches. Compared to the nominal cases shown in Fig. 37, these signals show considerable control activity. In a sense, these plots indicate the soundness of the design philosophy behind the SRFIMF controller. The controller is generating the actuator signals to overcome the WOD turbulence so that the kinematic states are "wind proofed". Therefore, the controller seems to be suitable to the aircraft with the difficult mission requirements such as described above.

As has been shown, one of the dominating factors contributing to the difficulty of landing a VTOL aircraft onto a small landing pad is the WOD turbulence. Constant bearing approaches are vulnerable to the wind from the opposite side; the pursuit approach is vulnerable to the head wind. One way to avoid most of the severe turbulence is to fly higher. An experiment was performed for the constant bearing/elevation approach where the hover altitude was set to 30 m (100 ft) above ship c.g. instead of 15 m (50 ft).

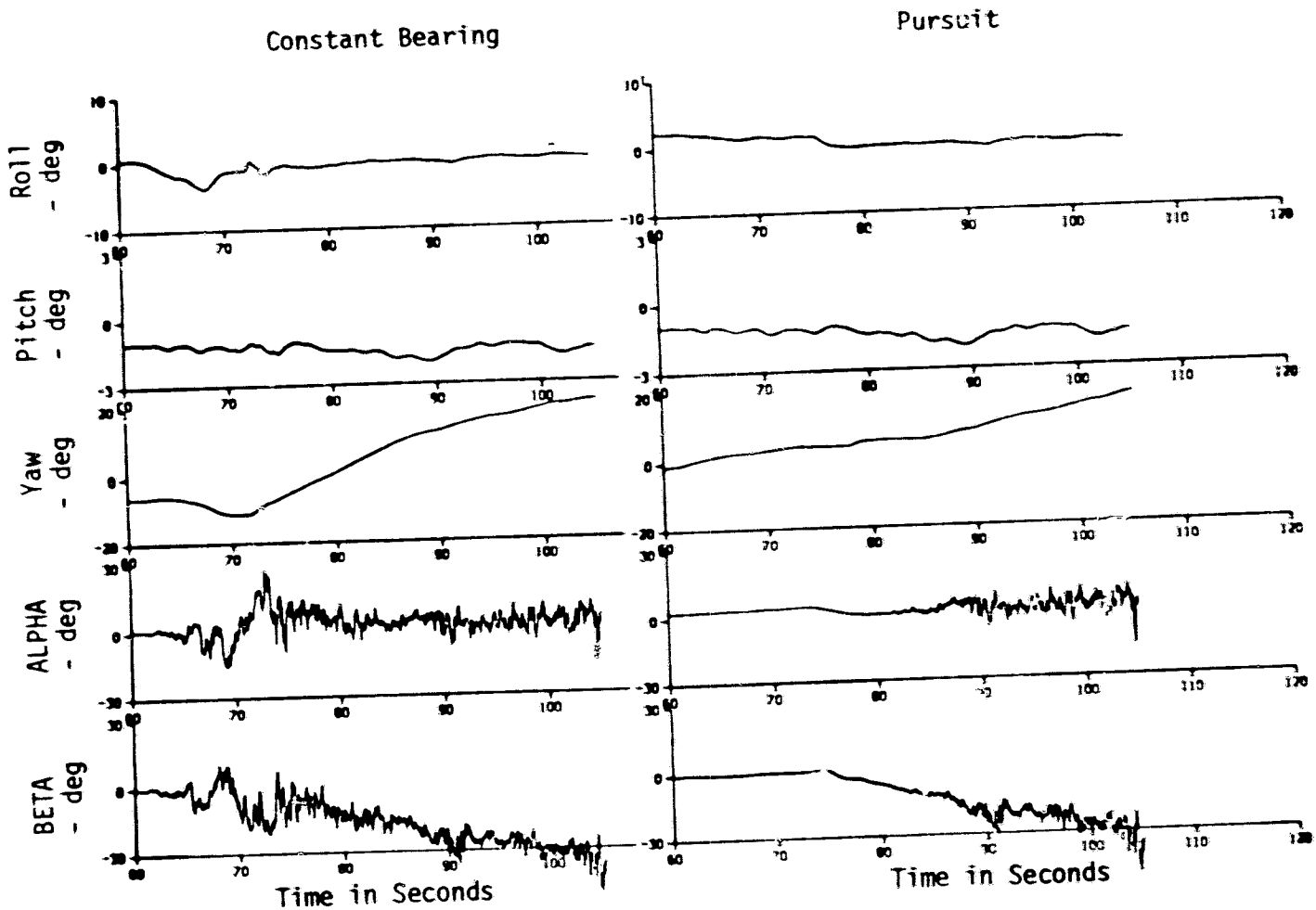

Figure 52. Aircraft Attitude, Angle-of-Attack and Sideslip Angle.

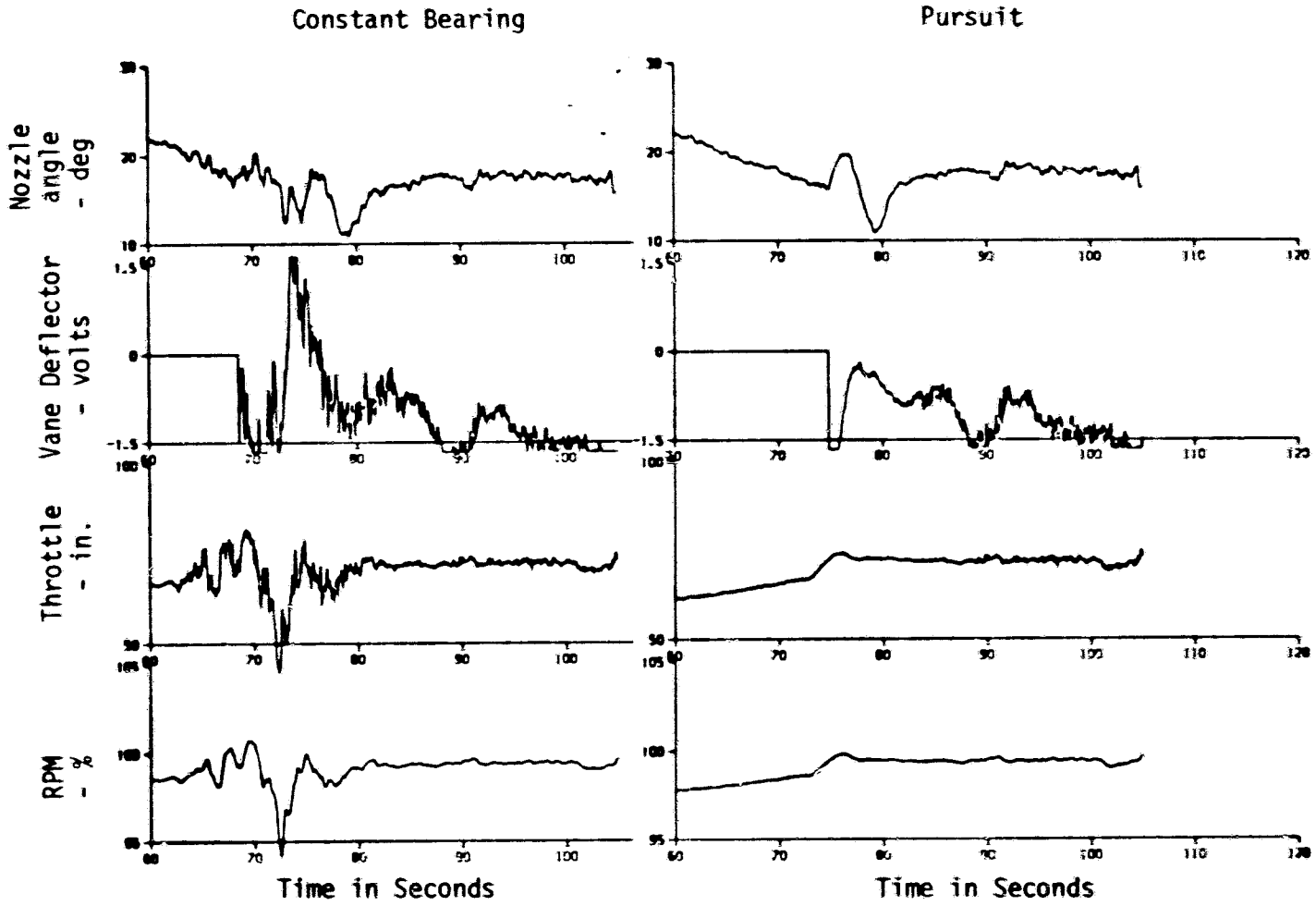

Figure 53. Aircraft Actuator Commands and Fan RPM.

Figures 54 through 56 show time plots of the pertinent variables. Figure 54 shows the WOD turbulence (NED) components and body accelerations. Comparison of Fig. 54 with Fig. 51 reveals that the peak-to-peak values of the turbulence during the worst period is reduced by half. The corresponding accelerations are also 50% smaller.

The angles, α and β, in Fig. 55 show the reduced peak-to-peak excursion due directly to the reduction of WOD turbulence. The aircraft actuator commands shown in the next figure have far less activity. This will undoubtedly reduce wear to the aircraft mechanical and electrical actuator components. It also would provide a smoother ride to the pilot.

The higher hover altitude approach seems to help avoid the severe WOD turbulence. However, it also poses certain operational problems:

1. the MLS azimuth and elevation coverage may need to be expanded (for the above example, the largest elevation angle was 40 deg),
2. the approach geometry may not be compatible to the landing aid lighting system, and
3. the letdown period is longer which requires a longer letdown relative motion prediction period.

Monte Carlo Studies

Discussion Single pass cases are very useful when analyzing and expanding peculiar phenomenon associated with the sequential events along the flight trajectory. However, in order to evaluate the expected performance of a given system, a statistical methodology becomes mandatory. Two popular methods frequently used are (i) linearized analysis by the use of standard linear covariance propagation, and (ii) nonlinear analysis by using the Monte Carlo method. The former was used for example by the Vought Corp. in their study of the similar problem [20]. Some of the drawbacks of the covariance propagation method are that (a) a linearized system model must be obtained, (b) the nominal states and controls must be known, and (c) the state dimension cannot be too large. As a result of these drawbacks, the problem formulation may become unduly and unrealistically

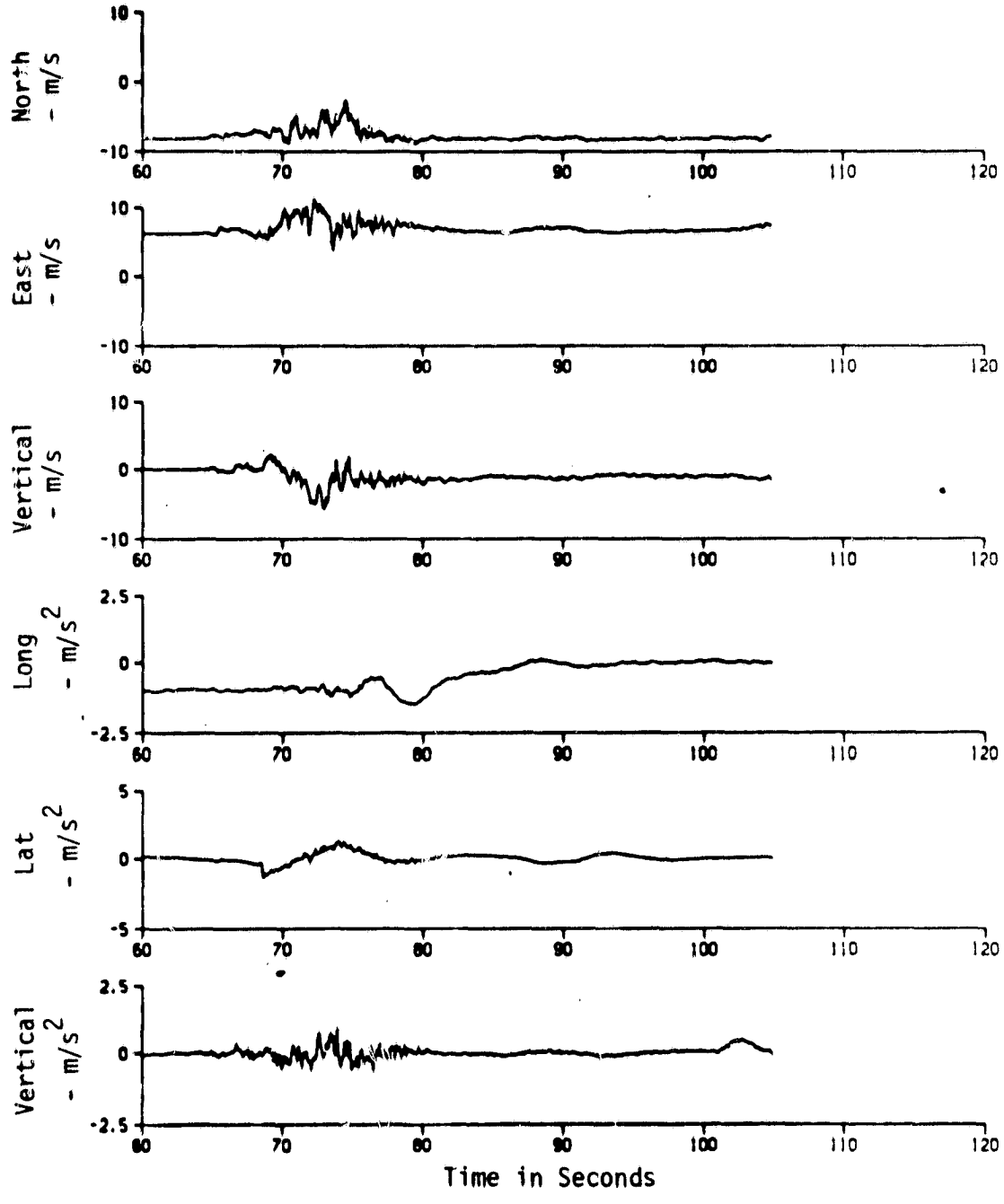

Figure 54. WOD Turbulence and Body Acceleration Components for 100 ft Hover Altitude.

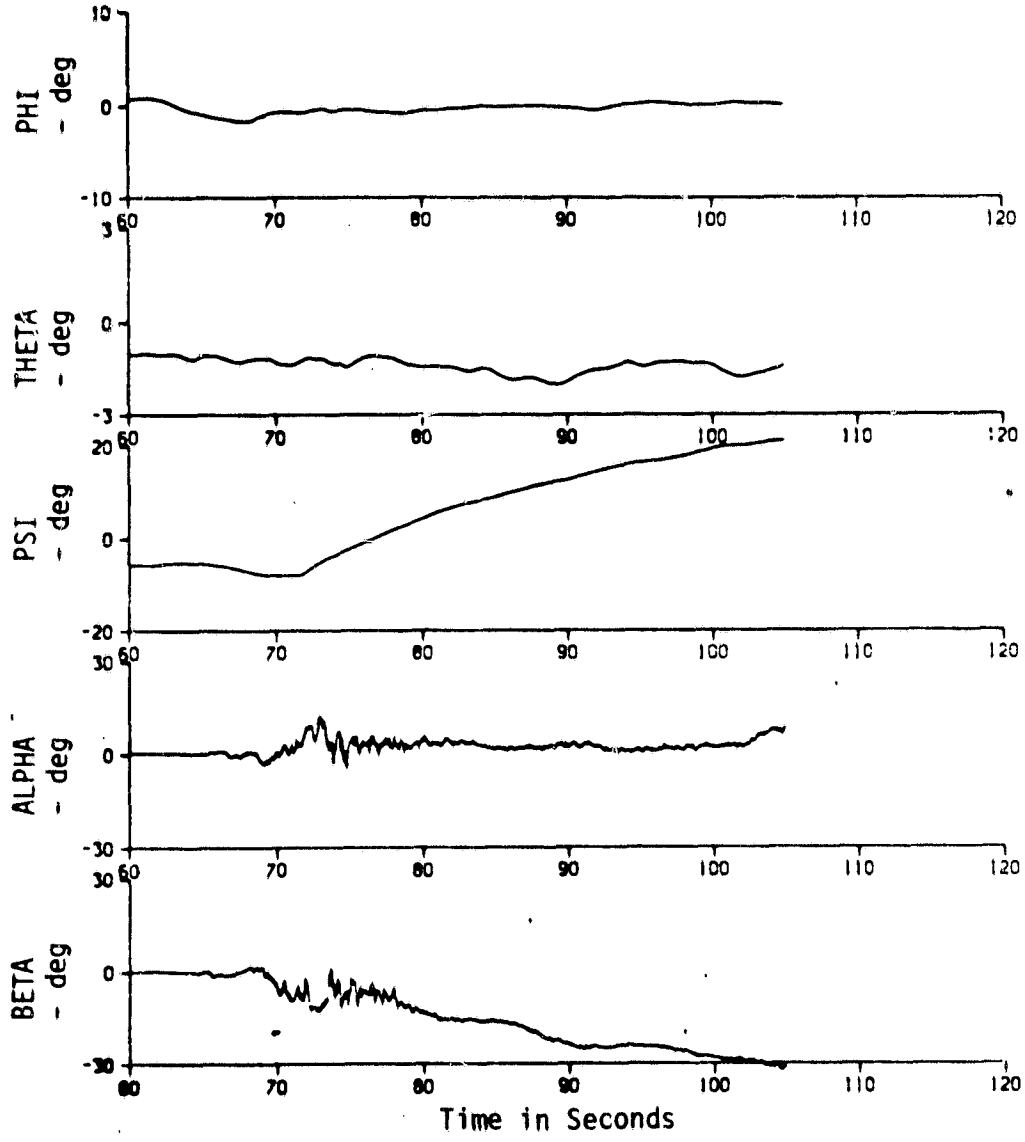

Figure 55. Aircraft Attitude, Angle-of-Attack and Sideslip Angles for 100 ft Hover Altitude.

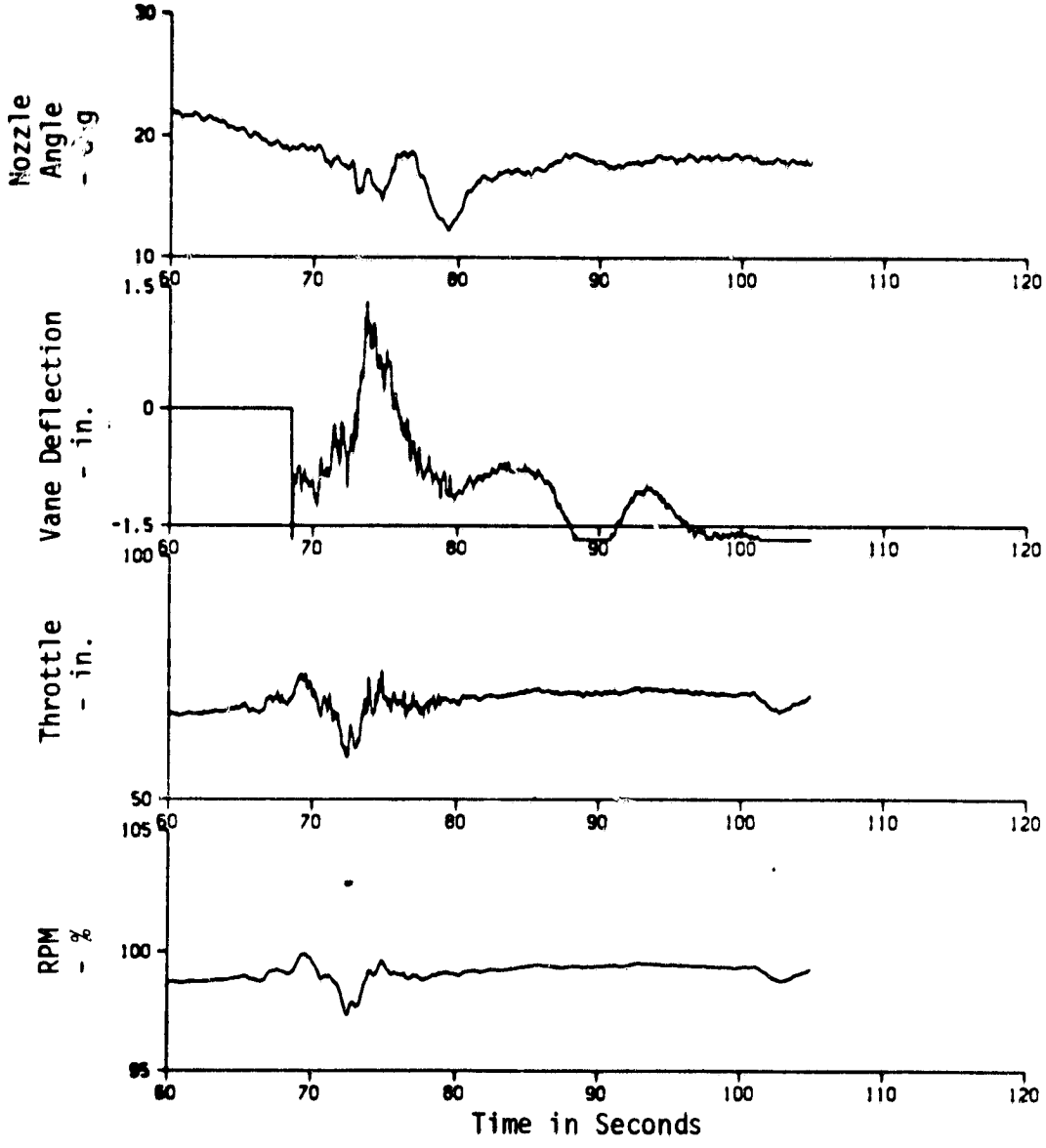

Figure 56. Aircraft Actuator Commands and Fan RPM for 100 ft Hover Altitude.

simplified to the point that some of the important details may be lost.

The Monte Carlo method is opposite in philosophy. The purpose is to make the simulation model as realistic and detailed as possible and then perform as many statistical experiments (with repeated runs) as is required. Some drawbacks of this approach are (a) such a detailed model may not be available, and (b) computational cost in terms of computer time may become prohibitive. As a result, sufficient statistics may not be obtained to draw meaningful conclusions.

In this study effort, the Monte Carlo method was used. The two approaches discussed in the previous section were chosen for the Monte Carlo runs. Initially, each case had fifteen passes. Time statistics (mean and standard deviation along the time axis) were computed and plotted of the navigation and guidance errors. In addition, four event points were chosen along the flight profile, and at each point, the mean, standard deviation and correlation coefficients were computed. These four event points are:

(i) at the end of the constant elevation or the constant sink rate track mode,

(ii) at the end of the vertical flare maneuver,

(iii) at the end of hover, and

(iv) at touchdown.

The points are flight critical (high work load), and they are connected by difficult maneuvers. For example, point (i) constitutes the initial state for the flare maneuver, so the success or the failure of the maneuver depends on the initial state being within a certain envelope. This implies that if the error at point (i) is too large and outside the acceptable bound, then the vertical flare maneuver should not be initiated; the approach should be aborted. In other words, the guidance performance at these points would be the key decision factor as to whether to go on to the next step. This notion is equivalent to the error criteria at the decision height for the CAT III landing approach. If the lateral error is greater than 22.5 m (75 ft) and the vertical error is greater than 6 m(20 ft) at the 15 m (50 ft)

decision height, the landing must be aborted. A statistical analysis based on a detailed simulation such as the one developed here yields this type of information.

In addition to the Monte Carlo simulation consisting of fifteen passes, cases with thirty and forty-five passes were obtained in order to determine the convergence sensitivities of various statistical parameters. This adds credibility to the statistical inferences drawn from the simulation consisting of the relatively small sample sizes.

Results Figures 57 and 58 show the time plots of navigation error statistics in term of mean plus or minus one standard deviation ($\pm$ 1σ). The results were obtained for the constant bearing case; however, the pursuit case results do not differ much. The top plot of Fig. 57 shows the along-track error. The initial transient in the mean error is due to the filter dynamics and the attitude bias error. The standard deviation of approximately 1 m is caused by the MLS/DME random noise directly. The second plot shows the cross-track error. The mean value represents mostly the MLS/azimuth bias and the standard deviation caused by the azimuth noise. The bottom plot shows the vertical error. The mean and standard deviation are caused by the MLS/elevation bias and noise. The cross-track and vertical errors show the range effects. During hover, the x, y and z errors are less than 0.5 m (1σ)

Figure 58 shows the velocity errors. The mean errors are typically small for all axes. The standard deviations at steady state are also small, being less than 0.5 m/sec. The initial transient in the standard deviations in y and z are caused by the filter gains being raised for the convergence mode. The standard deviations during the hover were 0.22, 0.66 and 0.11 m/sec, respectively. Larger values for the cross track error were apparently caused by the ship rolling motion. At any rate, the resulting navigation errors for the given sensors and navaids seem reasonably small so that no landing problems would occur because of them.

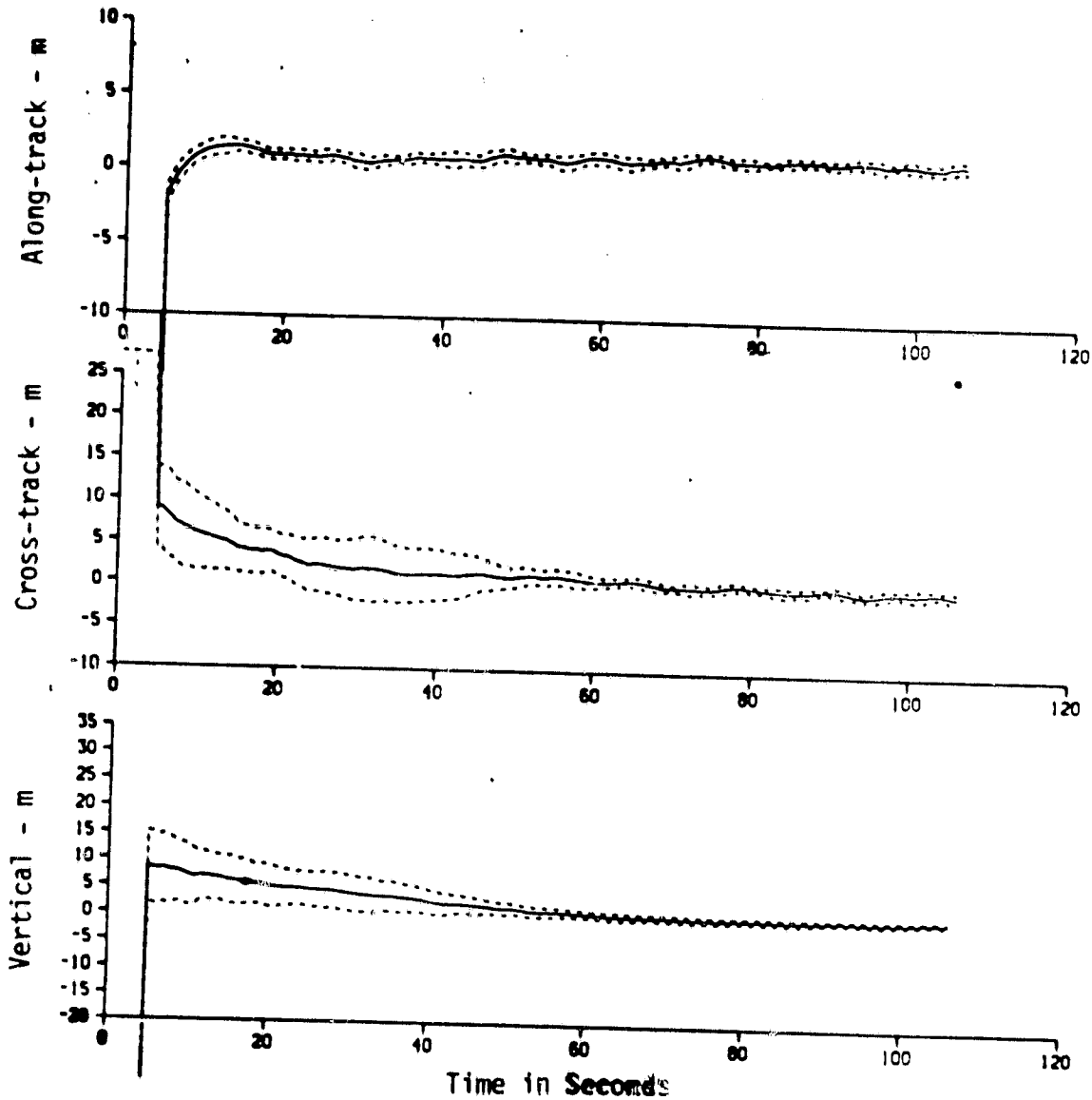

Figure 57. Navigation Position Errors (Mean ± One Standard Deviation).

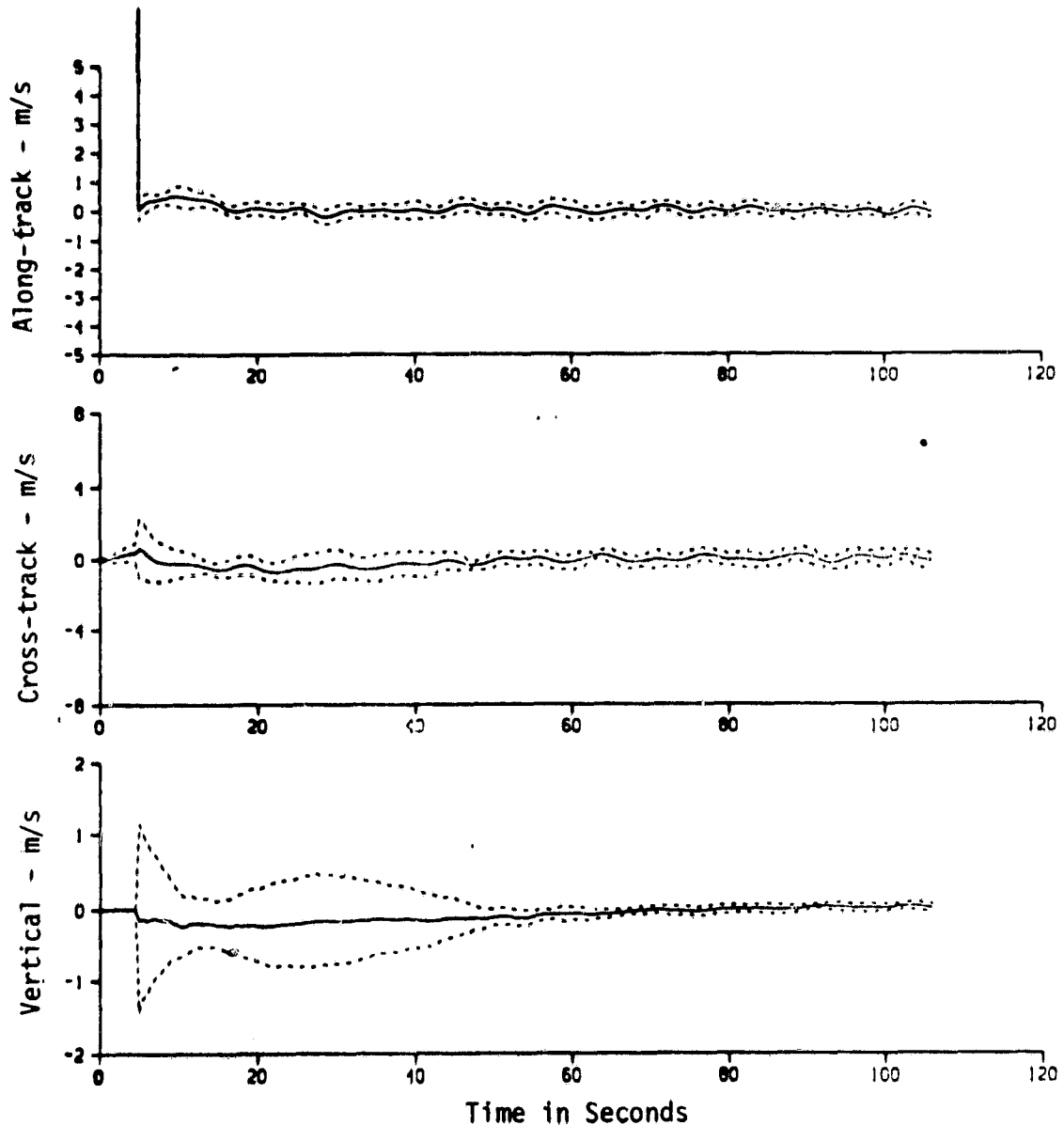

Figure 58. Navigation Velocity Errors with (Mean ± One Standard Deviation)

Figures 59 and 60 show the time plots of statistics of the constant bearing/elevation guidance errors. The top plot of Fig. 59 shows the actual along-track position. On this plot, scale details are lost. The standard deviation during hover is less than 0.5 m. The second plot shows the cross-track error. The mean value essentially reflects various transients such as the bearing reference capture and final mode switching. The standard deviation is caused by the navigation noise. This becomes apparent by comparing the corresponding navigation error plots. The bottom plot shows the vertical error statistics. The mean error represents the maneuver transients. The standard deviation is caused by the navigation error as well as variability of the constant elevation capture maneuver. During hover, the standard deviations are less than 0.5 m for the long-track and vertical components and less than 1 m for the cross-track position. The somewhat larger error in cross-track is due to ship roll. Considering how large the WOD turbulence is, it is surprising that the turbulence does not have much effect on the position errors. This is due to the fast response time of the SRFIMF controller.

The top plot of Fig. 60 shows the along-track velocity errors. The error during the ground speed track mode is negligible. The mean error excursion is caused by the longitudinal maneuver. The standard deviation is caused by the navigation error. It is noted that the maneuver transient also contributes to the speed error. The second plot shows the cross-track velocity error. Again, the same comments apply. The bottom plot shows the vertical velocity error. The elevation reference capture maneuver effects are apparent. The WOD turbulence effect can be seen at 70 sec; however, its magnitude is small. During the hover mode, velocity errors are typically less than 0.3 m/sec in along-track and vertical and 0.7 m/sec for cross-track.

Tables 4 and 5 summarize the statistics at various flight critical points. Figure 61 shows the various 1σ error rectangles. The touch-down footprints in x and y were 0.46 ± 0.74 and 0.01 ± 1.1 meters respectively. Compared to the landing pad dimension of $\pm$ 11 m for x and $\pm$ 8 m for y, the performance of the open loop letdown strategy is credible (the letdown maneuver affects mainly the vertical impact velocity and the relative attitudes of the aircraft with respect to the ship.) The vertical impact velocity had a statistical value of -1.17 ± 0.6 (0.17 min, 2.16 max) m/sec.

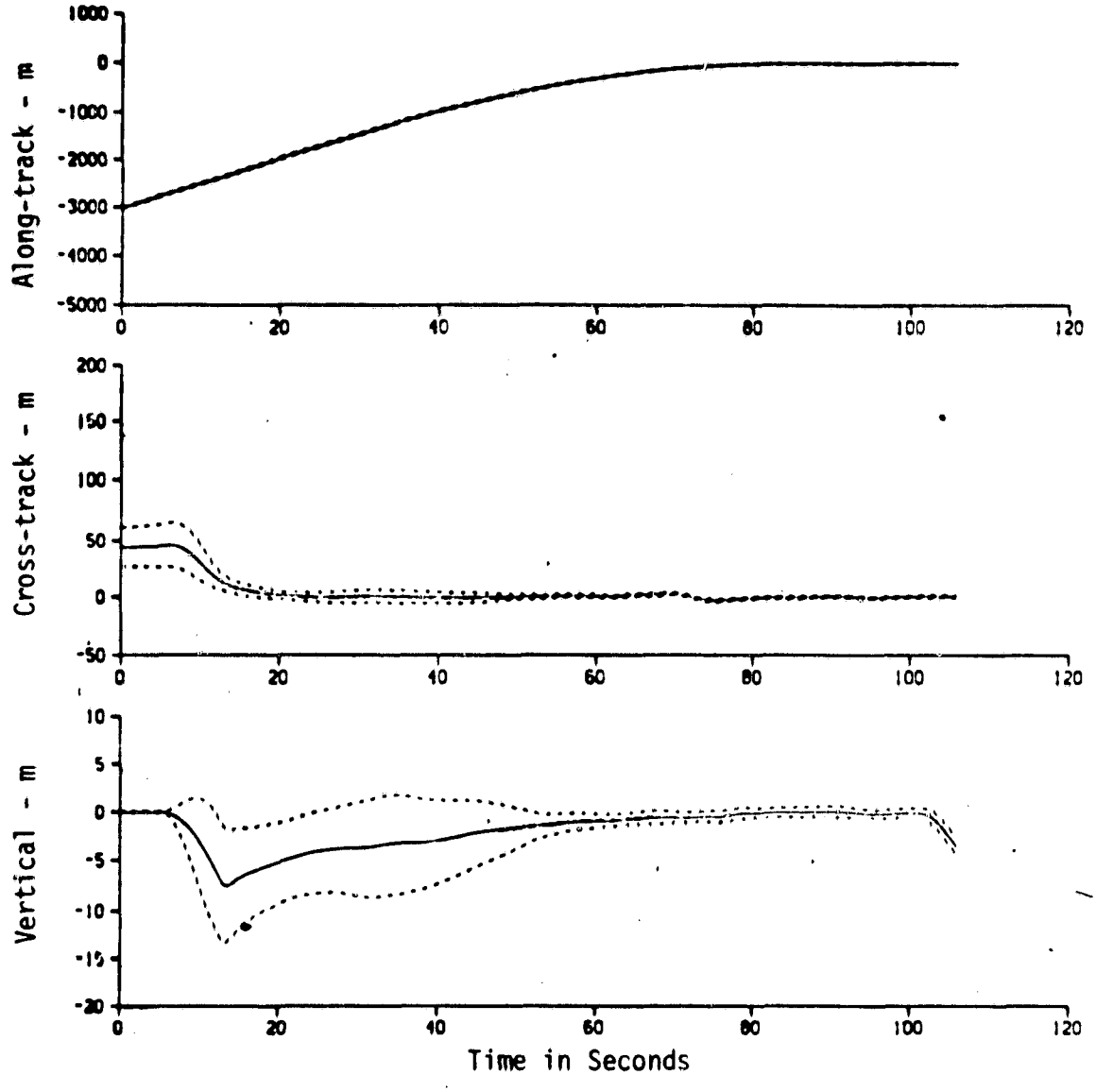

Figure 59. Guidance Position Errors with (Mean ± One Standard Deviation.)

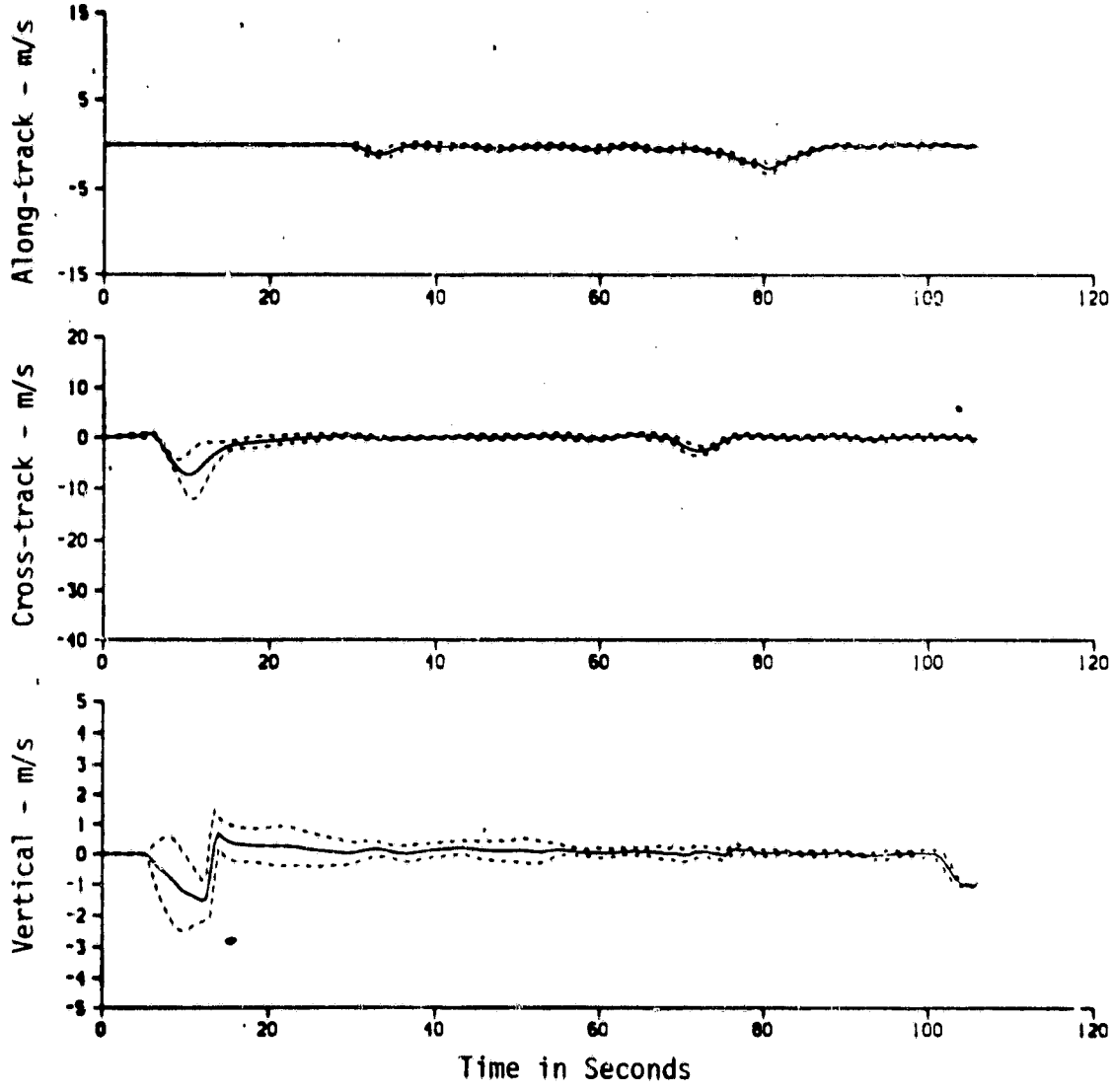

Figure 60. Guidance Velocity Errors with (Mean ± One Standard Deviation.)

Table 4. Navigation and Guidance Error Statistics for 15 Monte Carlo Passes

(m and m/sec)

At the transition from glideslope or sink rate track to flare

	x	y	z	$\dot{x}$	$\dot{y}$	$\dot{z}$	ρ_{xy}	ρ_{xz}	ρ_{yz}
NAVIGATION ERRORS	1.17 .38	0.0 .52	.10 .57	.07 .25	-.05 .45	-.01 .06	-.220	-.308	-.243
GUIDANCE ERRORS	-69.2 20.3	-1.54 2.46	-.26 .49	.60 .44	1.99 .82	0.0 .18	-	-	.01

At the transition from flare to hover

	x	y	z	$\dot{x}$	$\dot{y}$	$\dot{z}$	ρ_{zy}	ρ_{xz}	ρ_{yz}
NAVIGATION ERRORS	.89 .34	.40 .53	.05 .47	.01 .20	.18 .43	-.01 .05	-.372	.612	-.291
GUIDANCE ERRORS	-31.3 14.1	-2.40 1.65	-.29 .63	-1.39 .57	.06 .79	.03 .17	-	-	.253

At the transition from hover to letdown

	x	y	z	$\dot{x}$	$\dot{y}$	$\dot{z}$	ρ_{zy}	ρ_{xz}	ρ_{yz}
NAVIGATION ERRORS	.80 .31	-.20 .58	-.06 .41	-.10 .17	-.03 .44	.03 .05	-.797	.244	-.443
GUIDANCE ERRORS	.82 .59	.22 1.19	-.03 .51	-.01 .24	.02 .56	.01 .12	-	-	.619

At touchdown

	x	y	z	$\dot{x}$	$\dot{y}$	$\dot{z}$	ρ_{zy}	ρ_{xz}	ρ_{yz}
NAVIGATION ERRORS	1.0 .29	-.31 .41	-.02 .53	.04 .15	-.13 .37	0.0 .05	-.422	-.188	0.005
FOOT PRINT AND IMPACT VELOCITY	0.46 0.74	0.01 1.1	-	-	-	1.17 0.6	0.307	-	-

Table 5. Navigation and Guidance 1 σ Error Ellipses for 15 Monte Carlo Passes (m and deg)

At the transition from flare to hover

	PRINCIPLE AXIS	MINOR AXIS	ROTATION ANGLE
NAVIGATION	0.70	0.24	-56.24
GUIDANCE	0.56	1.01	83.63

At the transition from hover to letdown

	PRINCIPLE AXIS	MINOR AXIS	ROTATION ANGLE
NAVIGATION	0.70	0.21	-64.31
GUIDANCE	0.33	0.48	73.50

At touchdown

	PRINCIPLE AXIS	MINOR AXIS	ROTATION ANGLE
NAVIGATION	0.25	0.41	-25.03
GUIDANCE	0.68	1.14	18.52

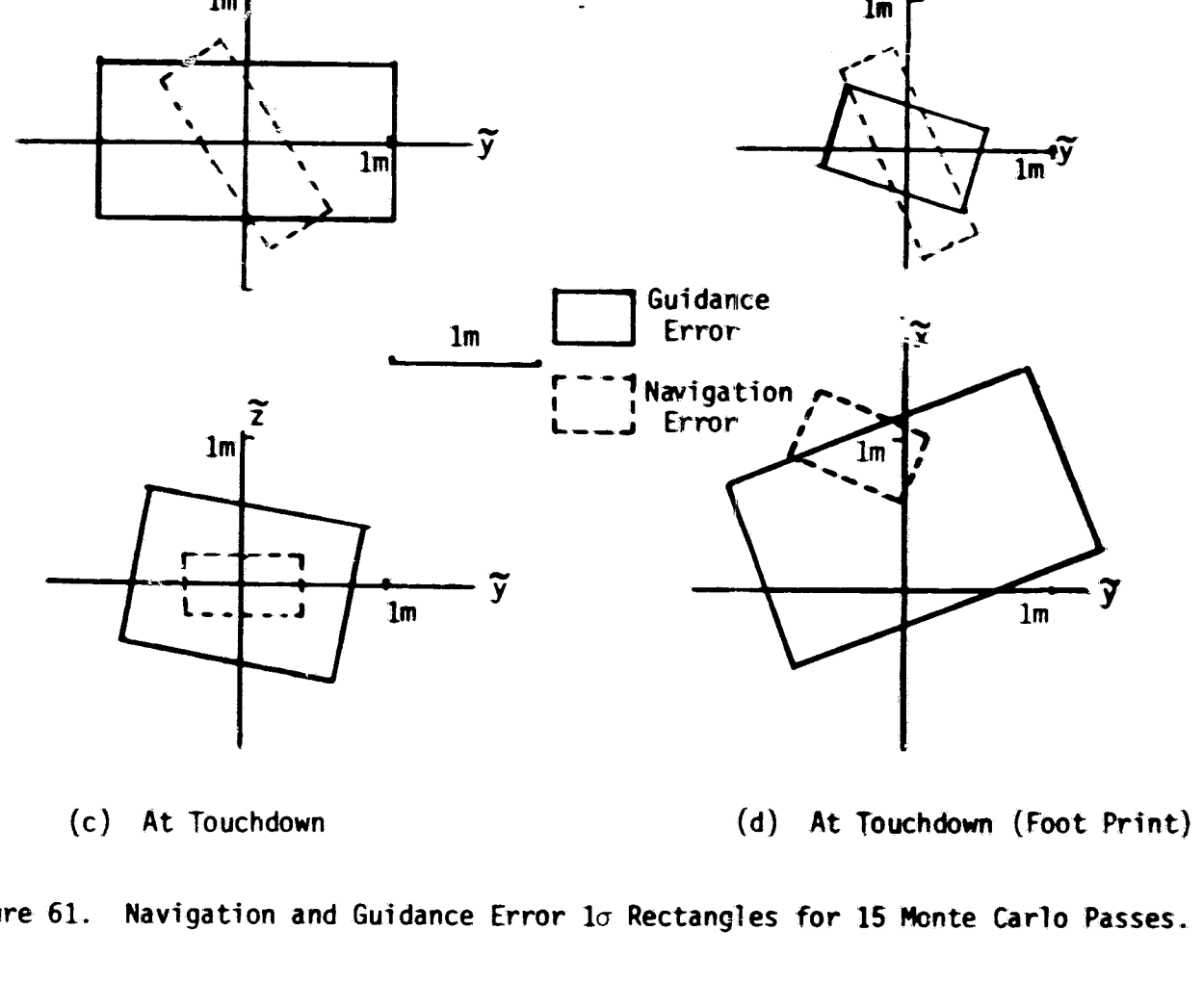

Figure 61. Navigation and Guidance Error 1σ Rectangles for 15 Monte Carlo Passes.

Figures 62 and 63 show the time plots of statistics for the pursuit/constant sink rates guidance errors. The top plot of Figure 62 shows the along-track position. The next plot shows the cross-track error. The error is not defined until 75 sec. After that, the error is with respect to the ship longitudinal axis. A transient due to the final mode switching is apparent. The bottom plot shows the vertical error. The error at the beginning of the flight (until 30 sec) is caused by the navigation error and the constant sink rate maneuver. The error after 75 sec is caused by the vertical flare maneuver. This part of the error shows one of the disadvantages of taking the time statistics, i.e., taking the statistical data at the same time point. The vertical flare maneuver is initiated by the appropriate state variables and not by time. It is suprising that the flare initiation spans some 15 sec. This phenomenon is believed to be caused by the constant sink rate initiation logic. Nevertheless, the flare maneuver is successful in that the position error mean and standard deviation are brought to small values.

Figure 63 shows the pursuit guidance velocity errors. The top plot shows the along-track velocity error which looks almost identical to the constant bearing case. The next plot shows the cross-track velocity. One of the advantages of the pursuit guidance is apparent, viz., there is no violent transition due to the bearing reference capture. The standard deviation seems to be a little larger then the constant bearing guidance. This may be due to the lower guidance gain. After the final mode transition, the error characteristics are similar to the previous case. The bottom plot shows the vertical velocity error. The same comments apply as in the vertical position error.

Tables 6 and 7 summarize the statistics at various flight critical points for pursuit guidance. Figures 64 shows the various 1σ error rectangles. During the hover mode, the position errors were 0.5 m along-track and vertical, and 1 m for cross-track. The velocity errors were less than 0.25 m/sec and 0.7 m/sec respectively for these directions. The touchdown footprint (1σ values) was within 1 m for x and y, and the vertical impact velocity had a statistical value of 1.31 ± 0.55 (0.33 min, 2.21 max) m/sec.

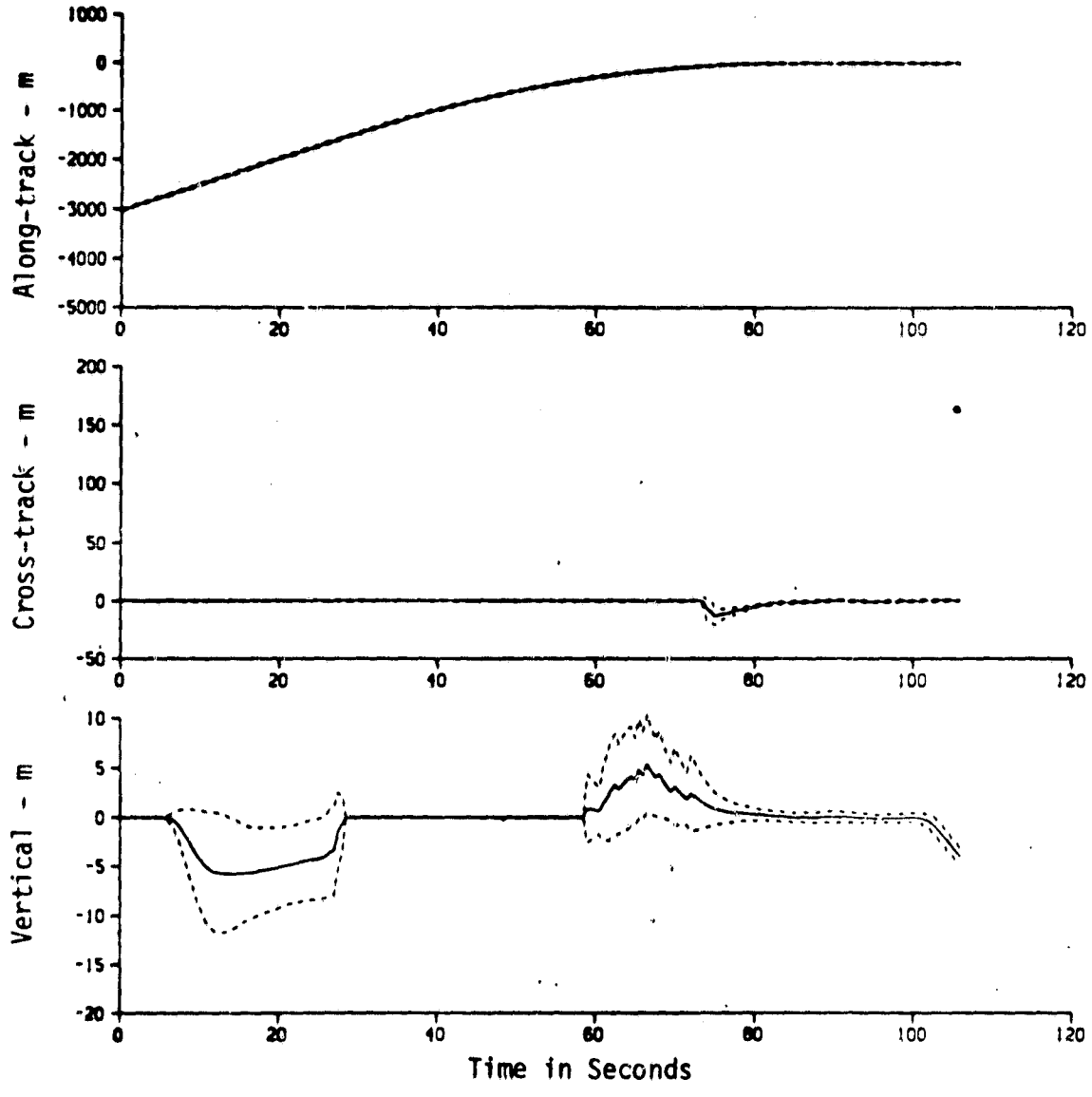

Figure 62. Guidance Position Errors (Mean ± One Standard Deviation)

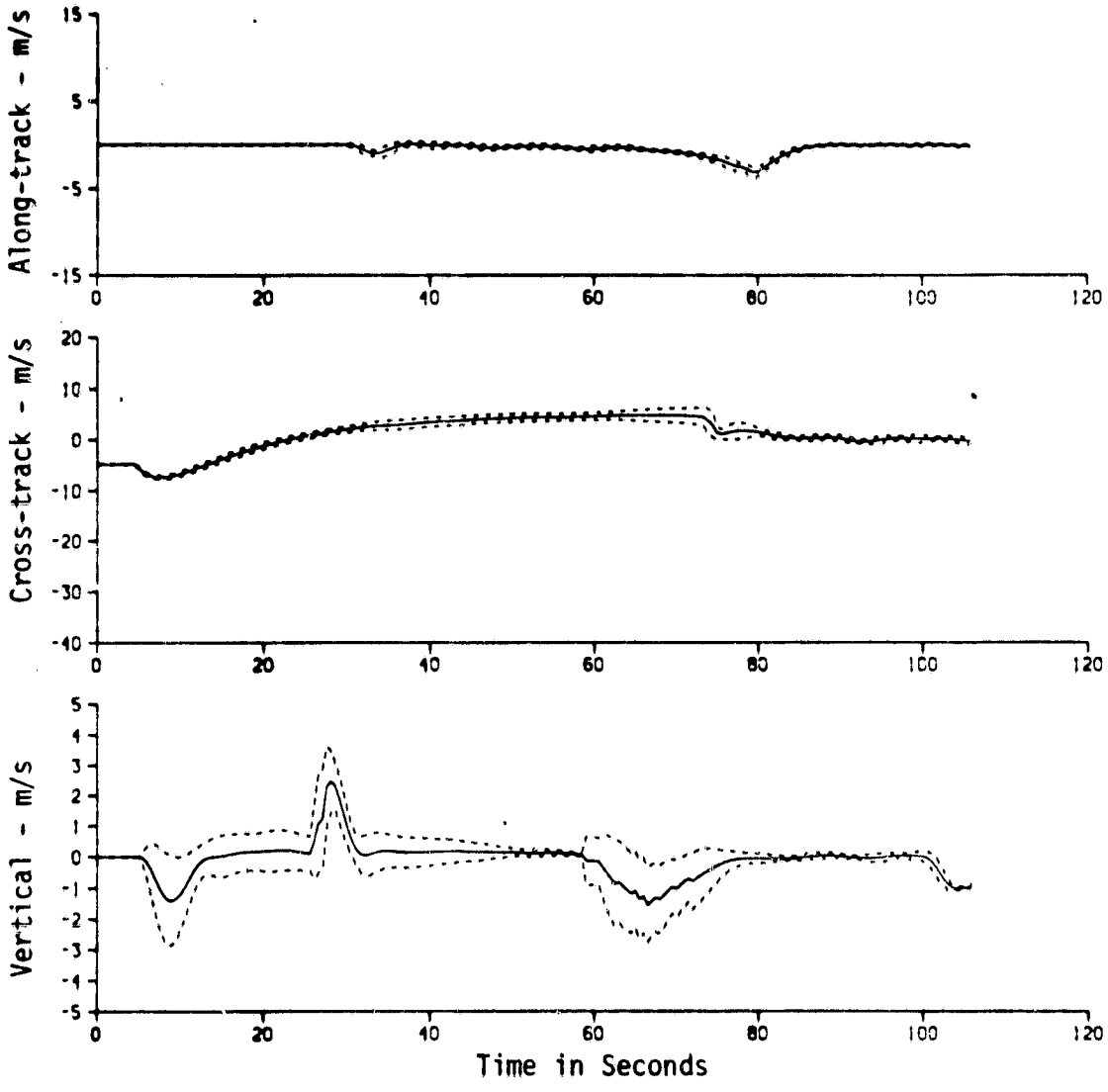

Figure 63. Guidance Velocity Errors (Mean ± One Standard Deviation).

Table 6. Navigation and Guidance Error Statistics for

15 Monte Carlo Passes

(m and m/sec)

At the transition from glideslope or sink rate track to flare

	x	y	z	$\dot{x}$	$\dot{y}$	$\dot{z}$	ρ_{xy}	ρ_{xz}	ρ_{yz}
NAVIGATION ERRORS	1.04 .27	1.03 .45	.48 .62	.03 .17	-.07 .34	-.06 .07	-.33	.5	-.37
GUIDANCE ERRORS	-205.3 87.2	-	-	-.48 .34	4.56 .91	.05 .09	-	-	N/A

At the transition from flare to hover

	x	y	z	$\dot{x}$	$\dot{y}$	$\dot{z}$	ρ_{zy}	ρ_{xz}	ρ_{yz}
NAVIGATION ERRORS	1.06 .31	.77 .51	.2 .58	.08 .19	-.03 .48	0.06 .06	.47	-.31	.06
GUIDANCE ERRORS	-133.7 54.9	-1.14 4.40	4.68 -.52	-.65 .51	4.28 1.30	-1.69 .15	-	-	-.07

At the transition from hover to letdown

	x	y	z	$\dot{x}$	$\dot{y}$	$\dot{z}$	ρ_{zy}	ρ_{xz}	ρ_{yz}
NAVIGATION ERRORS	.8 .34	-.22 .51	.04 .43	-.09 .14	-.03 .48	.02 .05	-.81	.34	-.5
GUIDANCE ERRORS	.72 .47	.04 1.03	-.02 .49	-.02 .22	.03 .66	0.0 .11	-	-	.54

At touchdown

	x	y	z	$\dot{x}$	$\dot{y}$	$\dot{z}$	ρ_{zy}	ρ_{xz}	ρ_{yz}
NAVIGATION ERRORS	1.01 .29	-.24 .41	-.05 .5	.08 .17	-.07 .31	.01 .05	-.18	-.09	-.11
FOOT PRINT AND IMPACT VELOCITY	0.53 0.47	0.14 1.04	-	-	-	1.31 0.55	-0.02		

Table 7. Navigation and Guidance 1 σ Error Ellipses for 15 Monte Carlo Passes.

(m and deg)

At the transition from flare to hover

	PRINCIPLE AXIS	MINOR AXIS	ROTATION ANGLE
NAVIGATION	0.4817	0.2939	12.084
GUIDANCE	0.5271	2.3025	-89.537

At the transition from hover to letdown

	PRINCIPLE AXIS	MINOR AXIS	ROTATION ANGLE
NAVIGATION	1.5004	0.1907	-54.667
GUIDANCE	0.3391	0.4208	73.521

At touchdown

	PRINCIPLE AXIS	MINOR AXIS	ROTATION ANGLE
NAVIGATION	0.27	0.42	-13.5
GUIDANCE	0.47	1.04	0.0

Figure 65 through 68 show the navigation and guidance error statistics plots for a Monte Carlo run consisting of 30 samples. Here, constant bearing/elevation angle guidance is used. Tables 8 and 9 summarize the statistics at the prescribed points, and Fig. 69 shows the various 1σ error rectangles.

Figures 70 through 73 show the navigation and constant bearing guidance error statistics plots for a Monte Carlo run consisting of 45 samples. Tables 10 and 11 summarize the statistics at prescribed points, and Fig. 74 shows the various 1σ error rectangles.

The time plots do not show any marked difference. However, the 1σ error rectangles show differences in size and orientations. This can be verified from the tabulated data also. This probably means that the correlation coefficient are not easily identified especially when the random variables are practically independent. Rectangle sizes are similar for 30 and 45 samples.

Conclusions

As can be seen from this chapter, the fast-time simulation developed from the system model described in Chapters II, III, and the appendices can be used to produce many interesting and quantitatively informative performance results. In this chapter, we examined both the constant bearing/glideslope and pursuit/constant sink rate guidance techniques. Also examined were (a) the effects of sensor errors on navigation, guidance and SRFIMF flight control performance, (b) the effects of changing pursuit guidance constants, (c) the comparison of both guidance techniques with respect to the wind-over-deck wake turbulence, and (d) the improvement in turbulence reduction created by having a higher hover altitude. In addition, navigation and guidance errors statistics were computed using the Monte Carlo option for the constant bearing guidance concept with 15, 30, and 45 passes.

The conclusions were as follows:

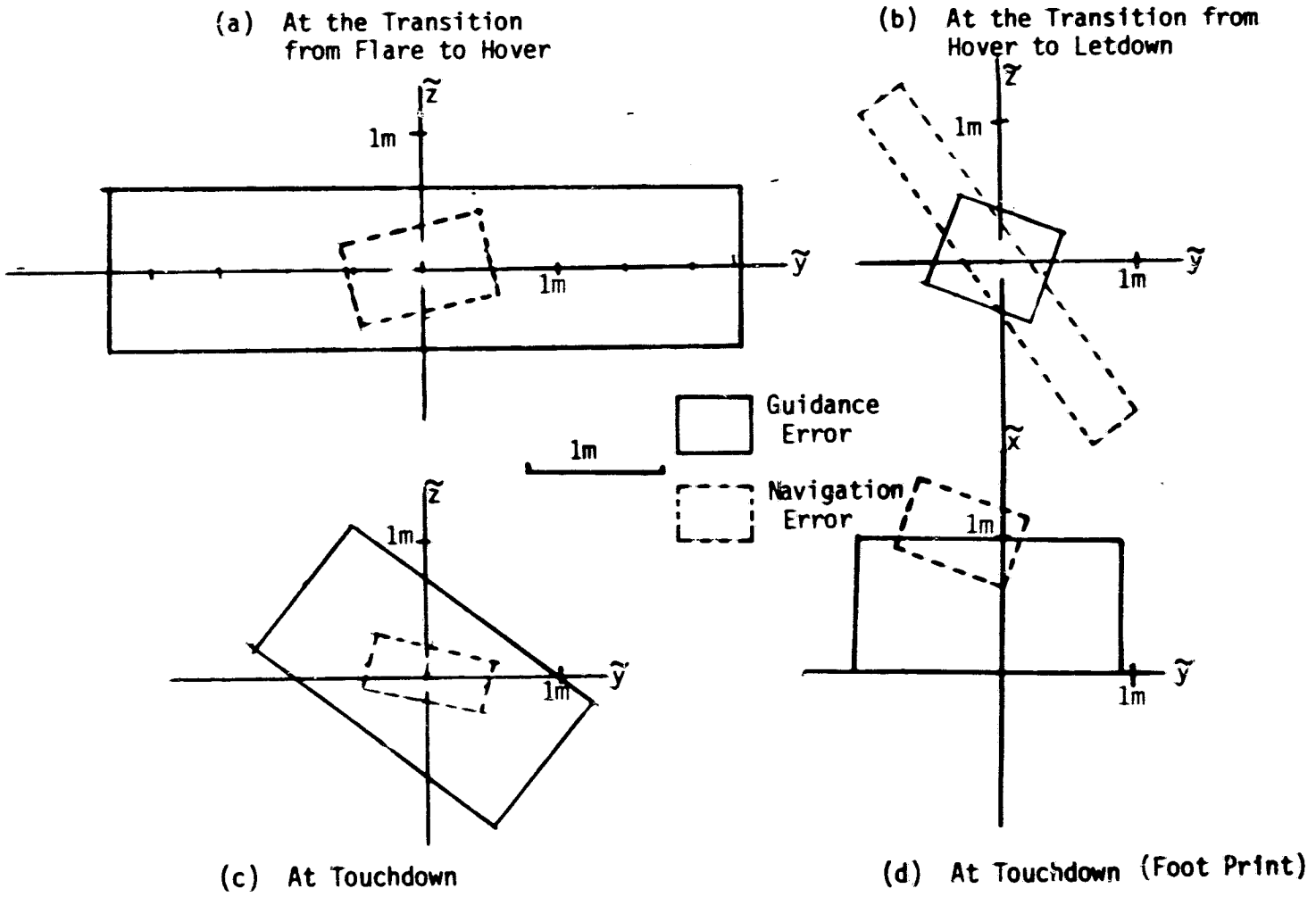

Figure 64. Navigation and Guidance Error 1σ Rectangles for 15 Monte Carlo Passes.

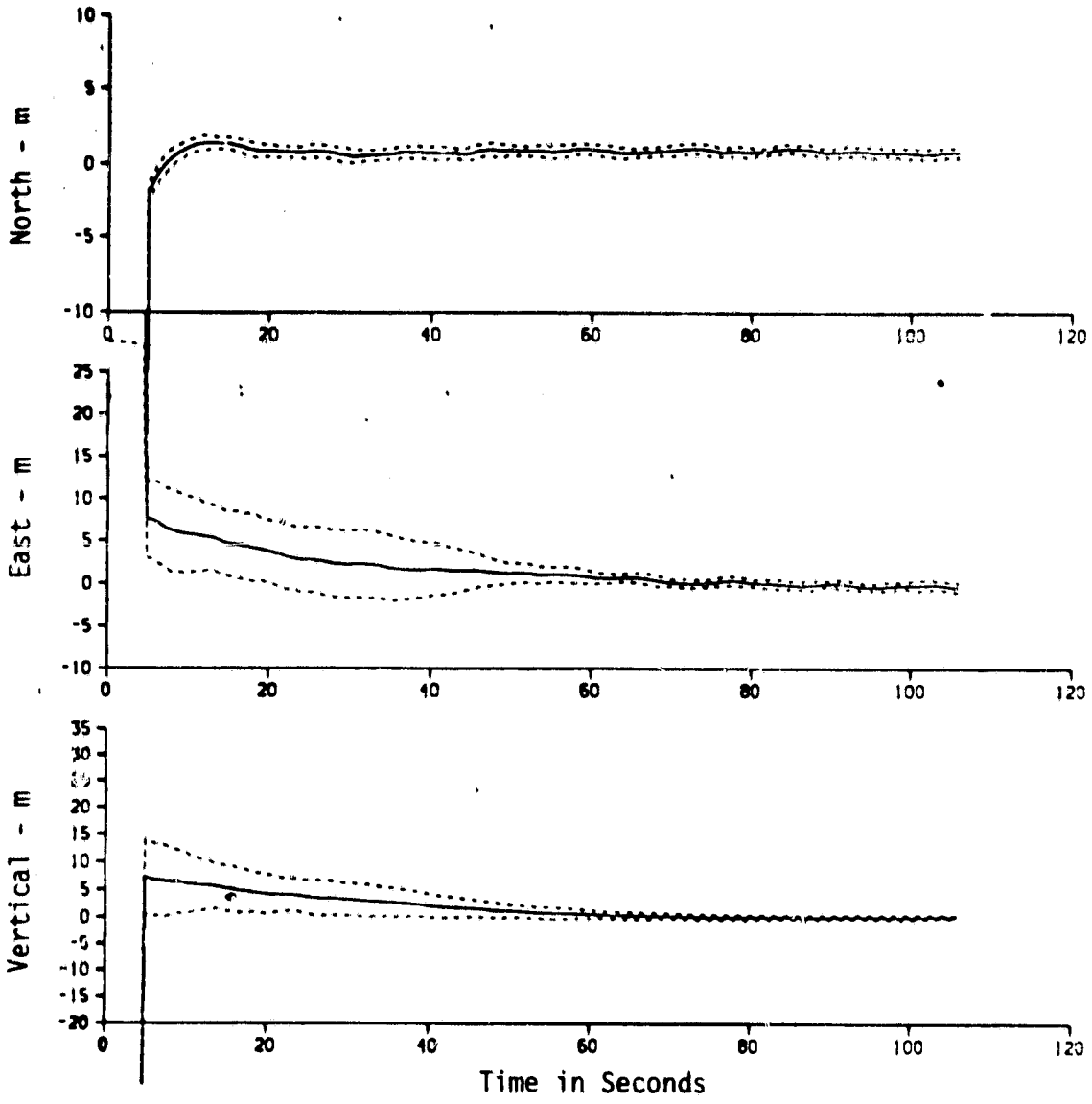

Figure 65. Navigation Position Error Statistics for 30 Samples.

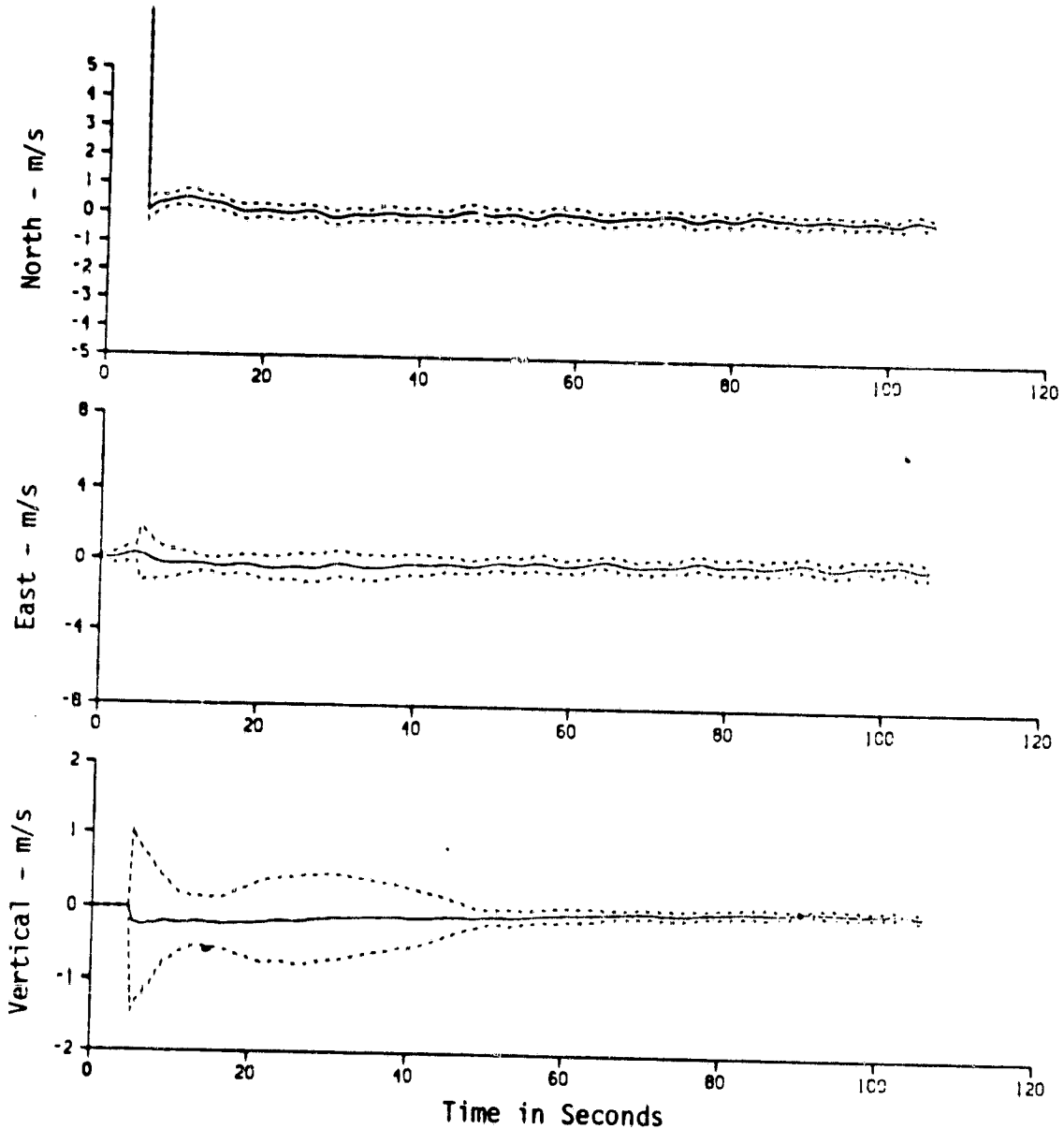

Figure 66. Navigation Velocity Error Statistics for 30 Samples.

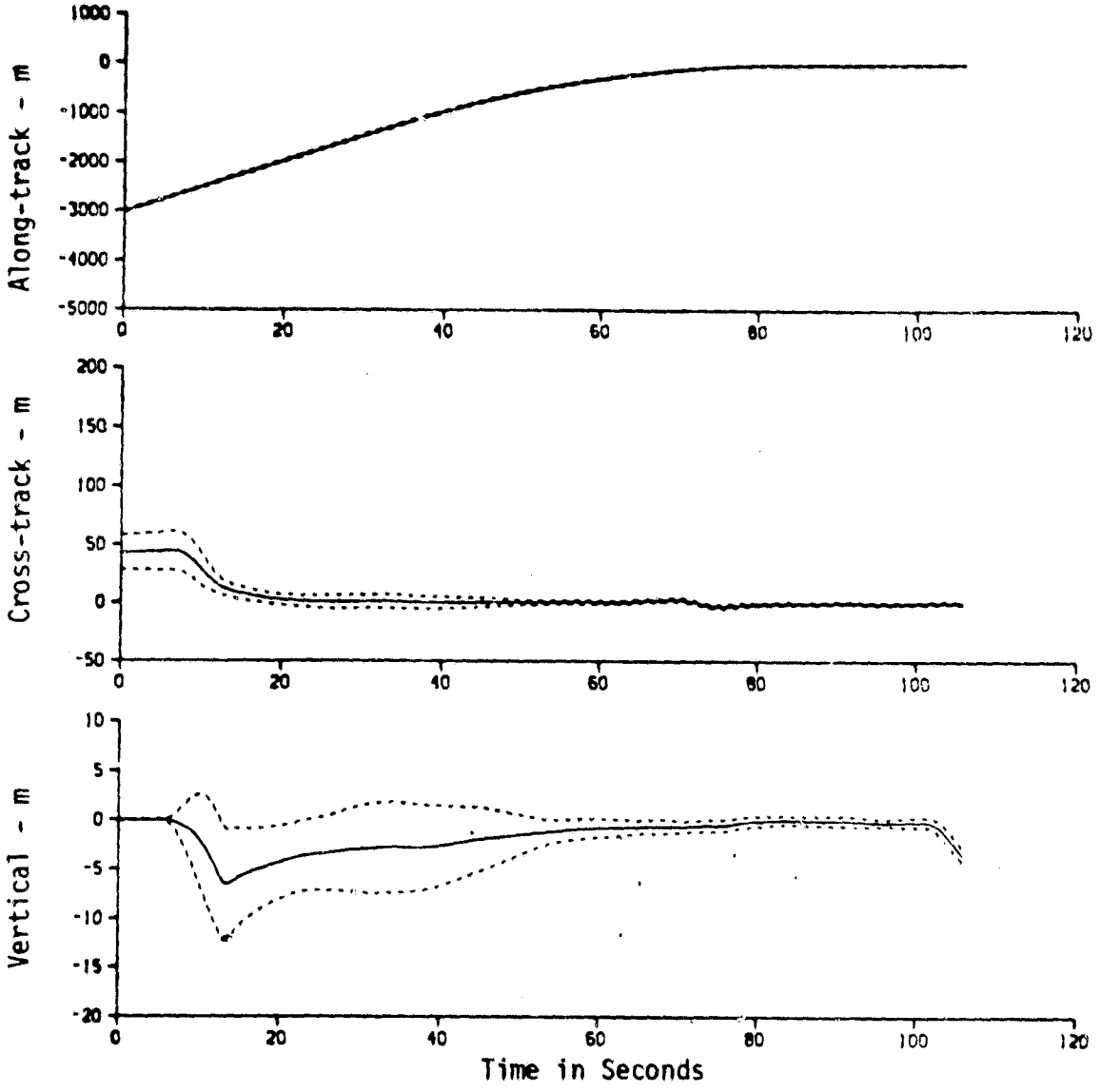

Figure 67. Guidance Position Errors for 30 Samples.

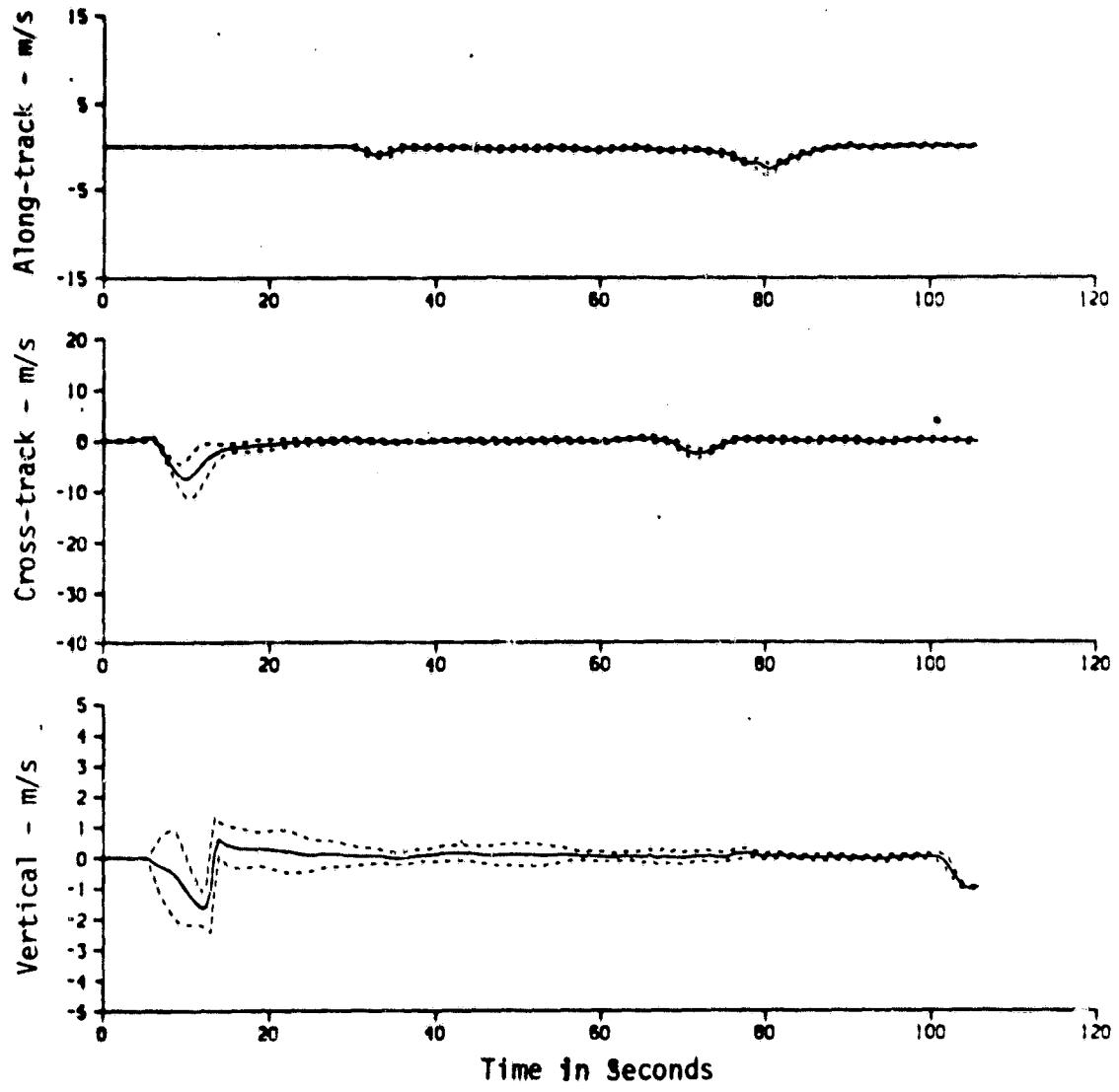

Figure 68. Guidance Velocity Errors for 30 Samples.

Table 8. Navigation and Guidance Error Statistics for 30 Monte Carlo Samples

(m and m/sec)

At the transition from glideslope or sink rate track to flare

	x	y	z	$\dot{x}$	$\dot{y}$	$\dot{z}$	ρ_{xy}	ρ_{xz}	ρ_{yz}
NAVIGATION ERRORS	1.06 .34	.08 .48	.16 .49	.09 .23	-.09 .35	.01 .06	-.24	-.30	-.07
GUIDANCE ERRORS	-73.4 22.9	-.55 2.82	-.35 .53	-.61 .36	-1.69 1.09	-.01 1.70	-	-	-.26

At the transition from flare to hover

	x	y	z	$\dot{x}$	$\dot{y}$	$\dot{z}$	ρ_{zy}	ρ_{xz}	ρ_{yz}
NAVIGATION ERRORS	.92 .33	.23 .54	.04 .48	-.02 .23	.13 .40	-.02 .05	-.4	.31	.07
GUIDANCE ERRORS	-34.3 15.9	-2.2 1.48	-.45 .60	-1.24 .68	-.23 1.08	.02 .16	-	-	-.12

At the transition from hover to letdown

	x	y	z	$\dot{x}$	$\dot{y}$	$\dot{z}$	ρ_{zy}	ρ_{xz}	ρ_{yz}
NAVIGATION ERRORS	.82 .30	-.16 .55	.11 .39	-.06 .16	.03 .43	.02 .04	-.69	.43	-.42
GUIDANCE ERRORS	.76 .66	.15 1.09	-.14 .46	.02 .22	.09 .57	.01 .10	-	-	.57

At touchdown

	x	y	z	$\dot{x}$	$\dot{y}$	$\dot{z}$	ρ_{zy}	ρ_{xz}	ρ_{yz}
NAVIGATION ERRORS	.98 .31	-.25 .38	-.06 .46	.06 .17	-.09 .36	-.02 .04	-.3	-.19	-.02
FOOT PRINT AND IMPACT VELOCITY	0.46 0.47	0.26 0.79	-	-	-	1.31 0.5	-0.163	-	-

Table 9. Navigation and Guidance 1 σ Error Ellipses for 30 Monte Carlo Samples (m and deg)

At the transition from flare to hover

	PRINCIPLE AXIS	MINOR AXIS	ROTATION ANGLE
NAVIGATION	0.4561	0.2587	74.603
GUIDANCE	0.6237	0.8782	-86.814

At the transition from hover to letdown

	PRINCIPLE AXIS	MINOR AXIS	ROTATION ANGLE
NAVIGATION	0.6229	0.1925	-65.099
GUIDANCE	0.3185	0.4150	74.728

At touchdown

	PRINCIPLE AXIS	MINOR AXIS	ROTATION ANGLE
NAVIGATION	0.31	0.40	-26.2
GUIDANCE	0.46	0.8	- 8.36

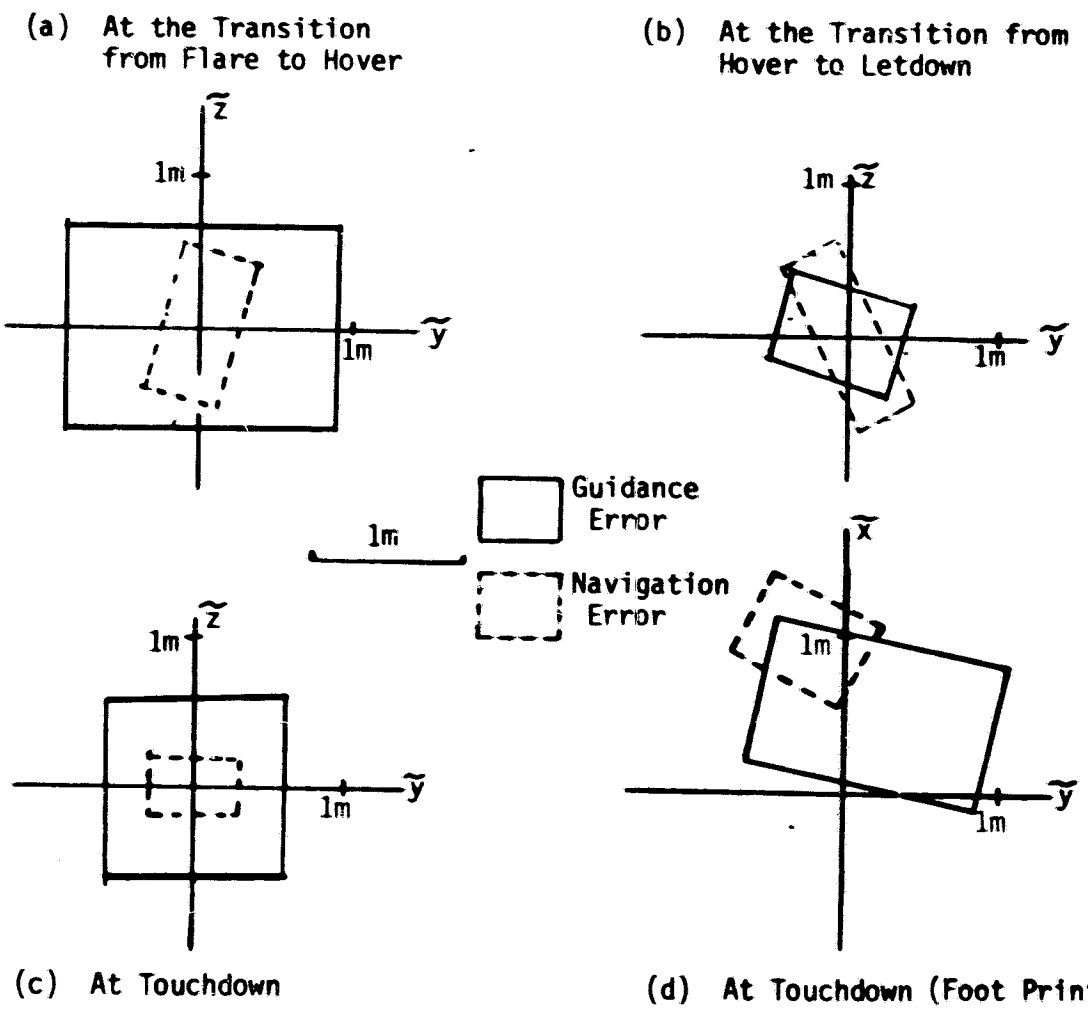

Figure 69. Navigation and Guidance Error 1σ Rectangles for 30 Monte Carlo Passes.

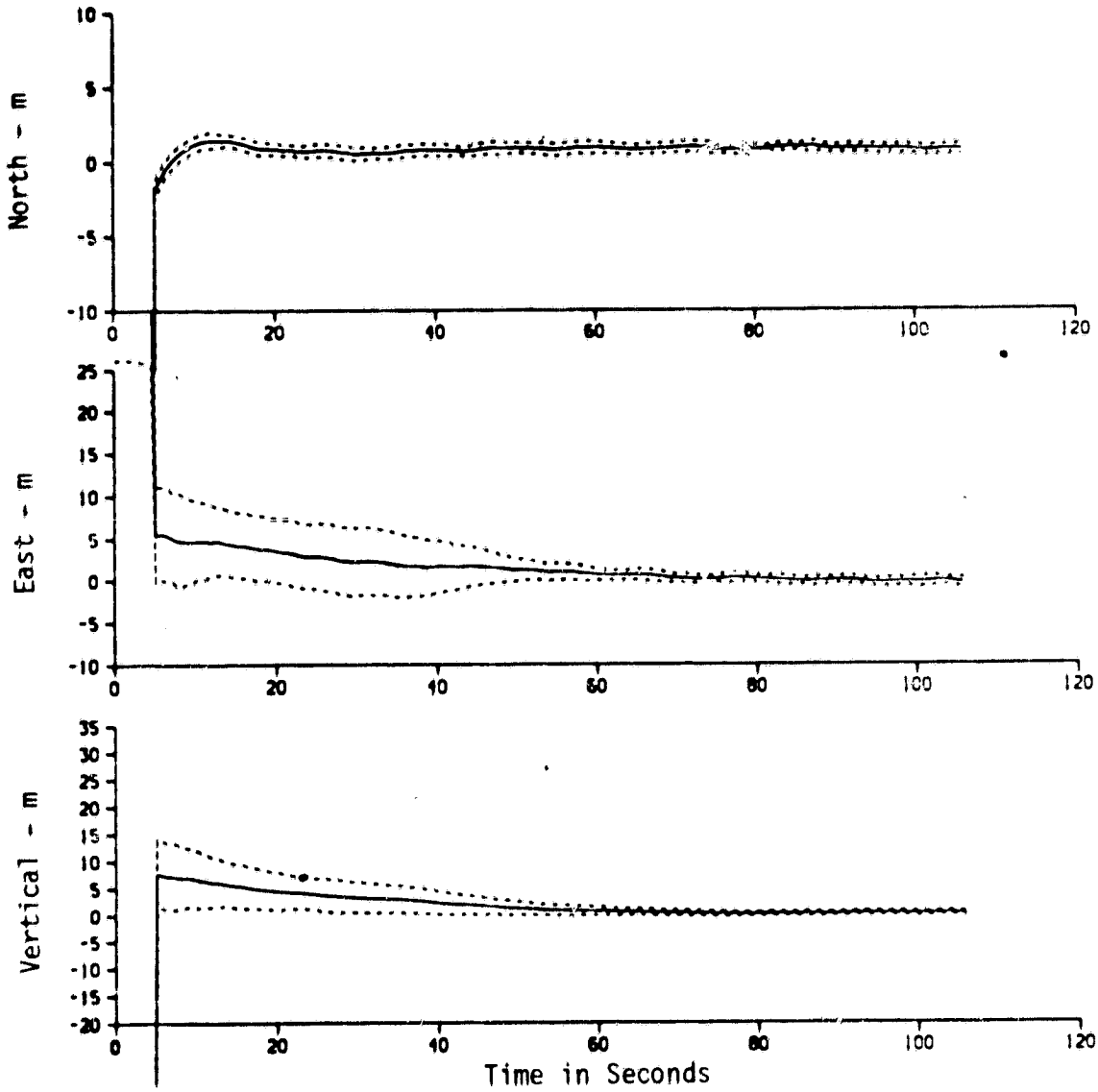

Figure 70. Navigation Position Error Statistics for 45 Samples

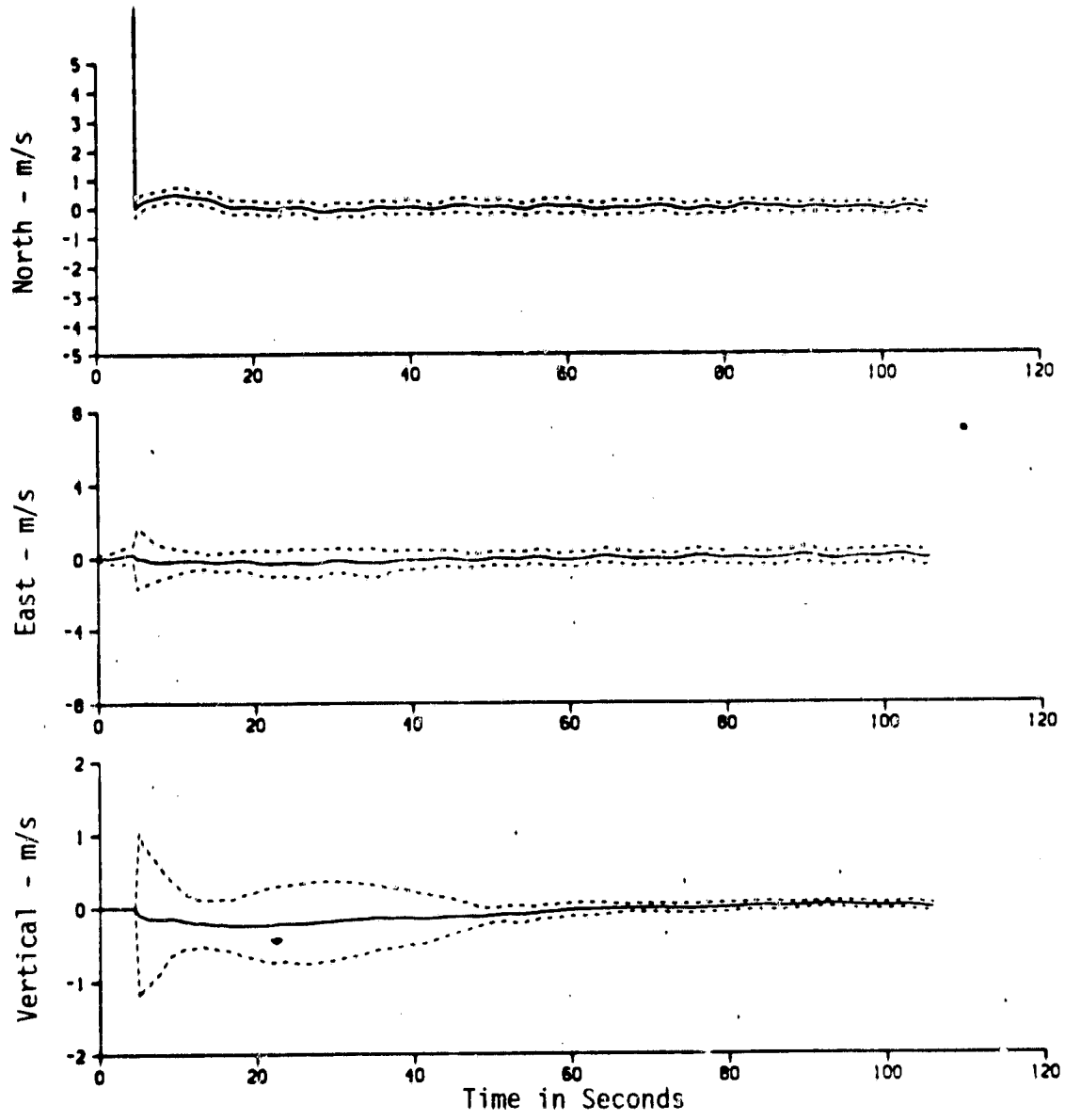

Figure 71. Navigation Velocity Errors Statistics for 45 Samples

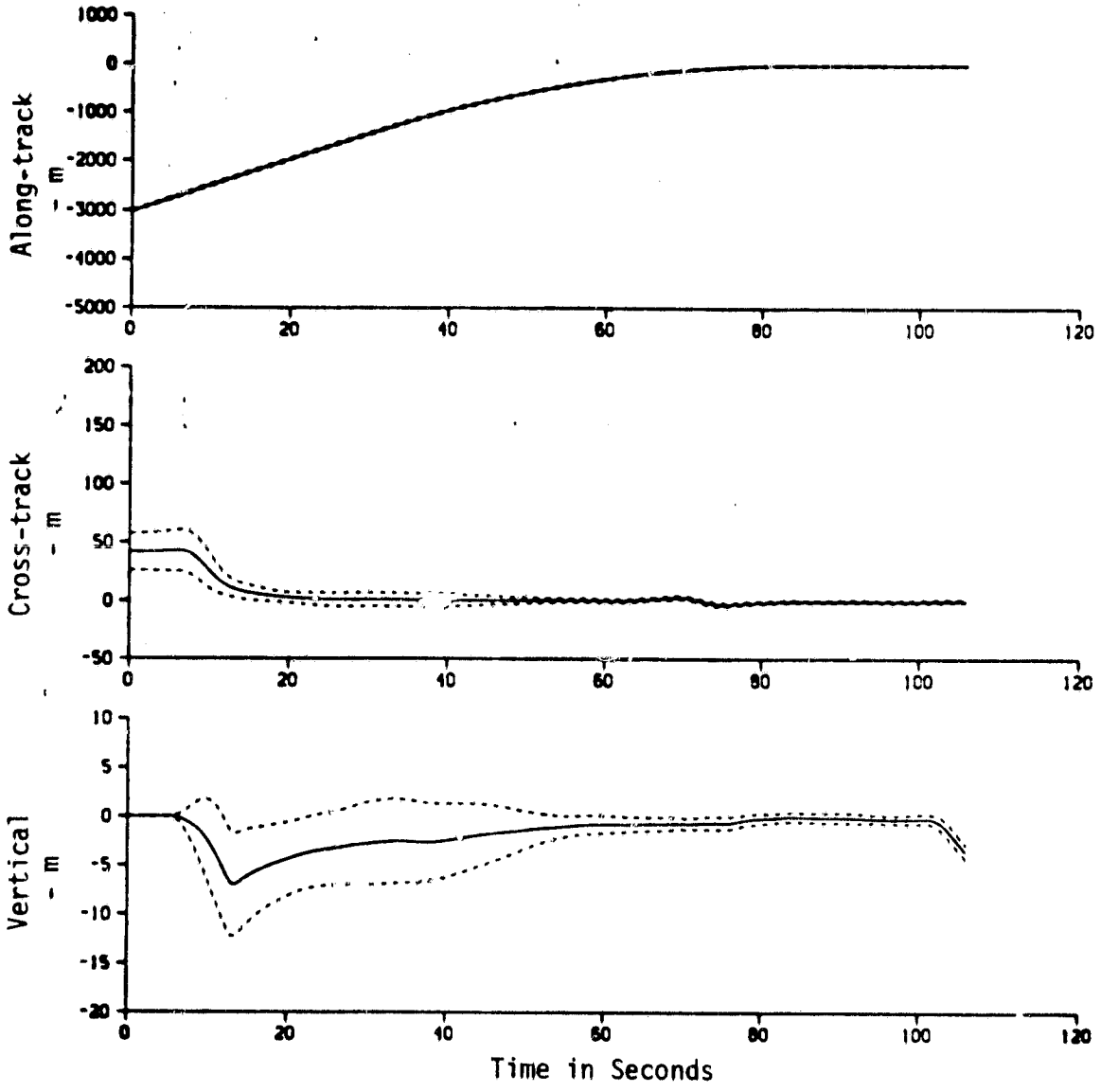

Figure 72. Guidance Position Error Statistics for 45 Samples.

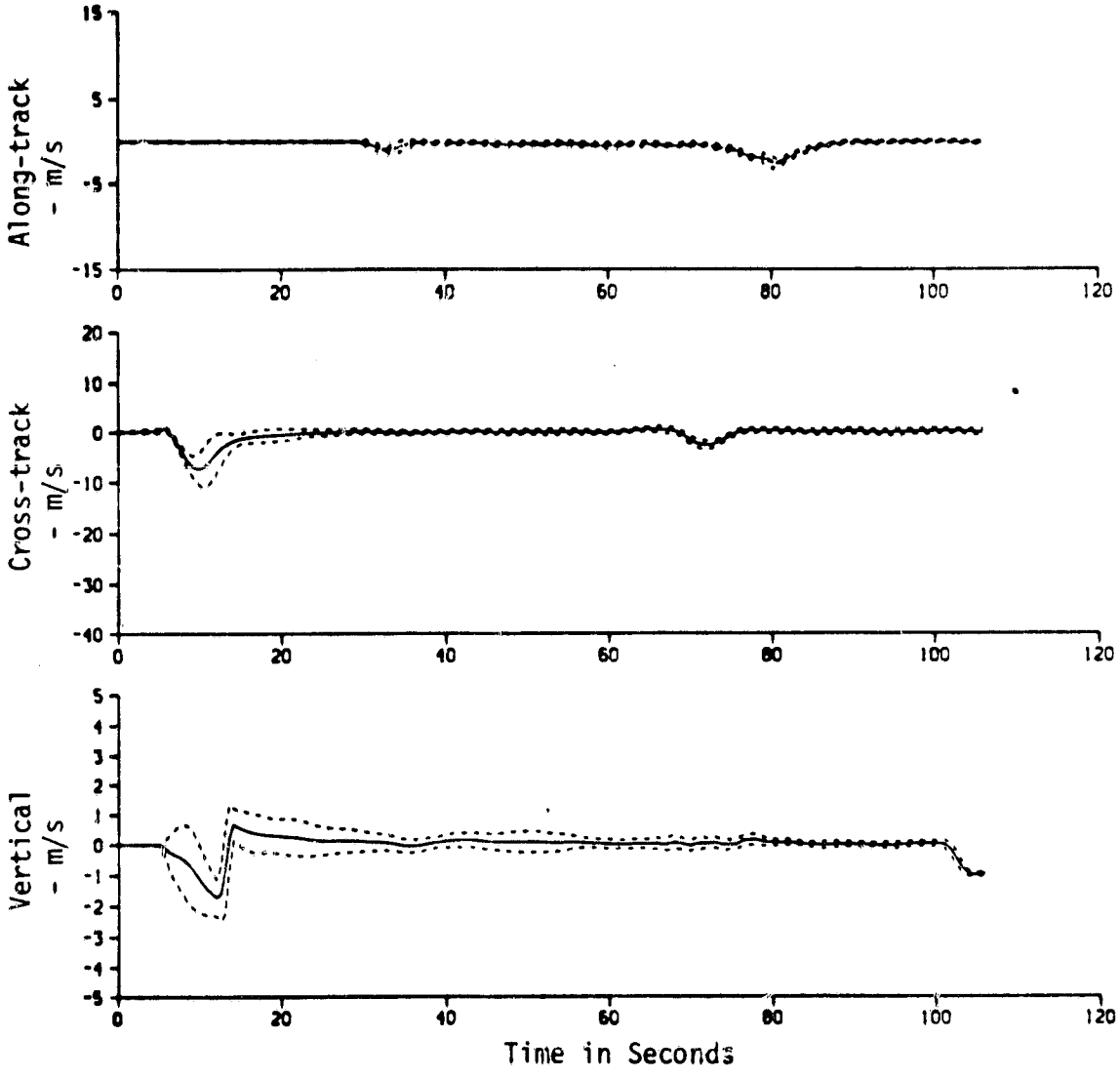

Figure 73. Guidance Velocity Error Statistics for 45 Samples.

Table 10. Navigation and Guidance Error Statistics for 45 Monte Carlo Passes (m and m/sec)

At the transition from glideslope or sink rate track to flare

	x	y	z	$\dot{x}$	$\dot{y}$	$\dot{z}$	ρ_{xy}	ρ_{xz}	ρ_{yz}
NAVIGATION ERRORS	1.03 .34	.11 .49	.23 .48	.07 .25	-.08 .37	-.01 .06	-.35	-.33	-.03
GUIDANCE ERRORS	-76.9 23.9	.01 3.02	-.46 .58	-.54 .38	-1.7 1.04	-.04 .16	-	-	-.39

At the transition from flare to hover

	x	y	z	$\dot{x}$	$\dot{y}$	$\dot{z}$	ρ_{zy}	ρ_{xz}	ρ_{yz}
NAVIGATION ERRORS	.90 .37	.20 .51	.12 .48	.01 .22	.07 .43	-.02 .06	-.32	.33	-.08
GUIDANCE ERRORS	-36.8 16.8	-2.36 1.36	-.59 .62	-1.23 .69	-.49 1.2	.02 .17	-	-	-.03

At the transition from hover to letdown

	x	y	z	$\dot{x}$	$\dot{y}$	$\dot{z}$	ρ_{zy}	ρ_{xz}	ρ_{yz}
NAVIGATION ERRORS	.87 .29	-.25 .58	.16 .41	-.04 .17	.02 .41	.01 .05	-.56	-	-.36
GUIDANCE ERRORS	.90 .64	-.04 1.3	-.20 .48	.01 .20	.01 .55	.01 .10	-	-	.56

At touchdown

	x	y	z	$\dot{x}$	$\dot{y}$	$\dot{z}$	ρ_{zy}	ρ_{xz}	ρ_{yz}
NAVIGATION ERRORS	.93 .34	-.22 .42	-.04 .51	.05 .16	-.05 .36	-.02 .05	-.4	-.32	.197
FOOT PRINT AND IMPACT VELOCITY	0.42 0.5	0.28 0.94	-	-	-	1.24 0.5	-0.312	-	-

Table 11. Navigation and Guidance 1 σ Error Ellipses for 45 Monte Carlo Passes (m and deg)

At the transition from flare to hover

	PRINCIPLE AXIS	MINOR AXIS	ROTATION ANGLE
NAVIGATION	0.523	0.2440	-66.259
GUIDANCE	0.6292	0.8454	-89.044

At the transition from hover to letdown

	PRINCIPLE AXIS	MINOR AXIS	ROTATION ANGLE
NAVIGATION	0.5939	0.2232	-67.297
GUIDANCE	0.3401	0.5161	77.120

At touchdown

	PRINCIPLE AXIS	MINOR AXIS	ROTATION ANGLE
NAVIGATION	0.285	0.463	-31.0
GUIDANCE	0.475	0.873	-24.84

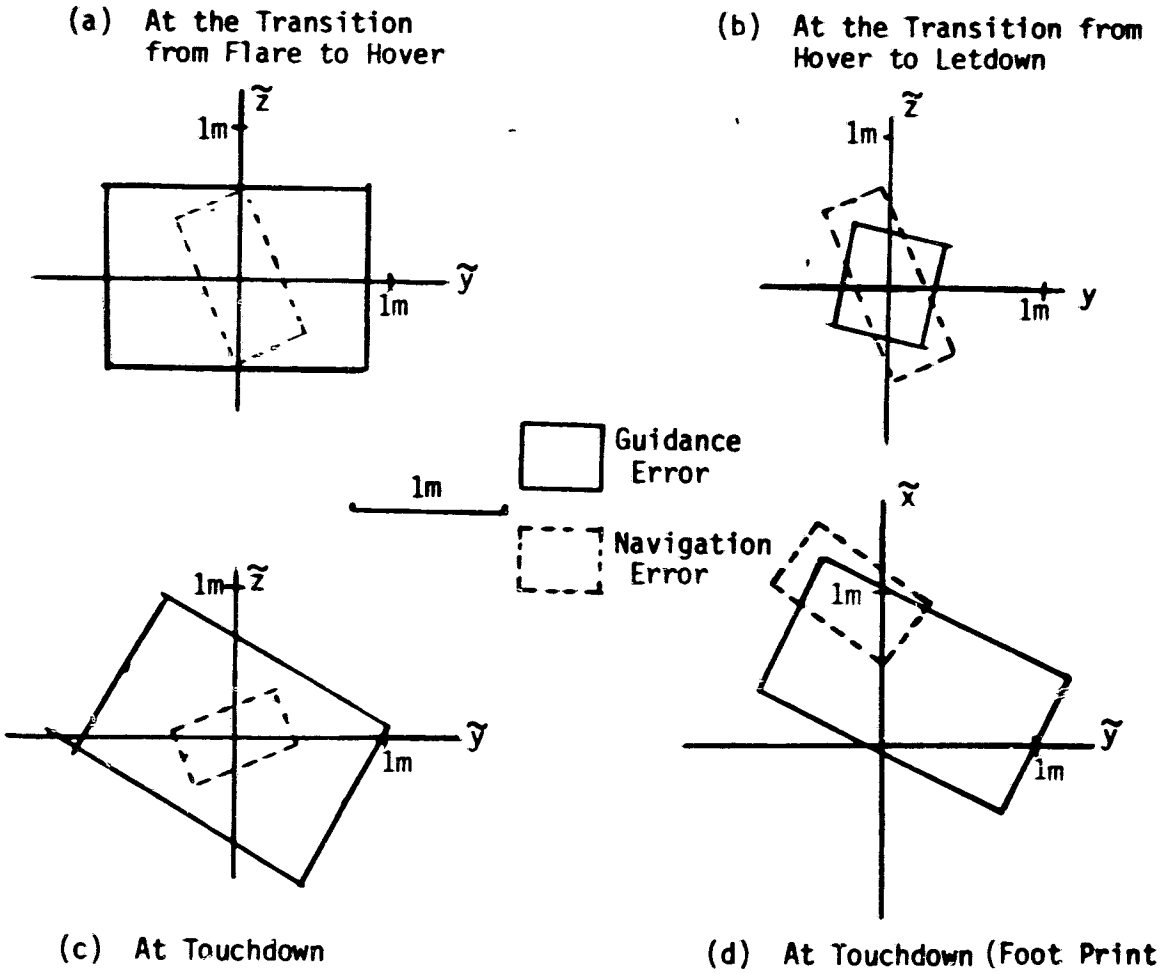

Figure 74. Navigation and Guidance Error 1σ Rectangles for 45 Monte Carlo Passes.

a). The SRFIMF flight controller does an excellent job of cancelling the effects of turbulence with the price of high control activity. There still remains fairly high aircraft accelerations ($\pm$ 1 m/s^2 vertical). However, these accelerations might be even higher without this controller. Even so, the accelerations would prove uncomfortable to the pilot. The SRFIMF controller performance also is quite robust with respect to errors in the inputs from typical strapdown sensors. The effects of aircraft dynamics modeling errors were not investigated.

b). The pursuit guidance avoids the turbulence region that the constant bearing approach encounters for a wind-over-deck angle ψ_{WOD} or 30°. The opposite would be true for a head-on wind. Raising the hover altitude 15 m reduced the turbulence effects 50%.

c). Both guidance concepts do an excellent job of bringing the aircraft to within acceptable error envelopes at hover and touchdown. Standard deviations at hover were less than $\pm$ 1 m. This was true for the 15, 30, and 45 pass cases. The number of passes primarily altered the correlation coefficient, although 30 passes reduced the dispersions somewhat. Touchdown dispersions of $\pm$ 2 m were primarily due to ship motion following the open-loop letdown maneuver.

d). These studies did not point out any significant differences in performance which could be obtained from the two types of guidance. Pilot visibility and other consideration will have to be used to select the desired concept. This information requires cockpit simulation.

e). Because wind-over-deck turbulence can have a significant effect on control activity and accelerations experienced by the pilot, it is important that this phenomena be carefully examined and modeled. This is an important area of investigation for future research.

VI

CONCLUSIONS AND RECOMMENDATIONS

Conclusions

Approach Guidance Two types of approach guidance for bringing a VTOL aircraft to a small aviation facility ship have been selected and analyzed. The two types of approach guidance are divided into lateral, vertical, and longitudinal axes modes with multiple phases for each axis. These types of guidance are:

Lateral axis: constant bearing and pursuit
Vertical axis: constant elevation angle and constant sink rate
Longitudinal axis: constant speed followed by constant deceleration.

The arguments for these choices are presented in Chapter III. Further description of these guidance concepts, their phases, and their mechanization requirements are presented in Appendix F.

The advantages and disadvantages of constant bearing/constant elevation angle approach guidance are:

1. This type of approach can take advantage of vessel landing lights to indicate being on the constant bearing or constant elevation lines eminating from the vessel. This also can include constant azimuth and elevation signals eminating from the ship-board MLS system.
2. Using a standard bearing and elevation angle ensures that the final approach is standard, and the pilot need only be familiar with this single approach.
3. The constant bearing angle can be flexible. For example, a 0° stern approach could be mechanized.
4. A 27° lateral approach (which is the current bearing defined by deck lights) allows deck overflights to miss the deck superstructure in case of an aborted approach.

5. The constant bearing/elevation line provides a means of position control all the way to hover.

6. A possible disadvantage is that a constant 27° bearing angle combined with decelerating longitudinal speed causes the visual perspective of the landing pad, as seen from the cockpit, to move out the left side of the canopy. This required crab angle would be a disadvantage to the pilot for heads-up display mechanization and obtaining visual approach cues.

7. Another disadvantage is that restricting the aircraft to a constant approach line may not be efficient for particular initial positions of the aircraft away from this line.

8. Finally, this guidance law requires control activity to maintain the aircraft on the 27 path in the presence of gusts and an additional crab angle to compensate for crosswinds.

The advantages and disadvantages of lateral pursuit/constant sink rate approach guidance are:

1. Lateral pursuit causes the aircraft velocity vector to point toward the hover point and eventually to be aligned with the ship velocity. This produces a rear approach similar to a standard runway approach but starting from any initial position.

2. For pursuit guidance, the hover point and landing pad bullseye are always near the centerline of the forward cockpit window. This is advantageous for HUD mechanization and obtaining pilot visual cues.

3. Constant sink rate guidance is easy to mechanize, and it alleviates the need for precise elevation measurements from the MLS if precise altitude could be obtained from other sources.

4. Constant sink rate guidance keeps the landing pad bullseye high in the cockpit window near the end of the approach.

5. A disadvantage of pursuit guidance is that the ship velocity must be transmitted to the aircraft for mechanization.

6. Pursuit guidance does not allow deck overflight in case of an aborted approach because the final longitudinal path is in conflict with the ship superstructure.

7. Pursuit guidance does not have a lateral error defined at the hover point. Thus, a different position error nulling guidance law (such as constant bearing) must be used in the hover point vicinity.

8. Disadvantages of constant sink rate guidance are that there is no constant elevation angle cue from the ship, and the bottom of descent will vary with ship speed and the range to the ship where the constant sink rate command begins.

These two guidance concepts were further evaluated and compared using a detailed simulation with MLS-based navigation, state rate feedback implicit model following (SRFIMF) flight control, a model of the research technology lift fan VTOL aircraft (RTA), a model of the vessel motion in Sea State 5, and a model of the wind-over-deck wake turbulence. From this simulation, it was concluded that both guidance concepts do excellant jobs of bringing the aircraft to within acceptable error envelopes at the hover point. Standard deviations of position error at hover were less than $\pm$ 1 m when standard navigation and flight control instrumentation (with nominal error magnitudes) were used. These studies did not point out any significant differences in performance which could be obtained from the two types of guidance. Further evaluation will require cockpit simulator studies with test pilot opinions being obtained.

Landing Guidance Four different letdown guidance approaches can be used to land the VTOL aircraft on the ship landing pad:

1. Guidance based on the present state of the aircraft relative to the ship.

   a). Letdown with an open-loop guidance law. Here, no attempt is made to null out relative state errors because of, for example, excessive relative touchdown velocity.

b). Nominal open-loop guidance with closed loop perturbation guidance. Here, an attempt is made to null out perturbations in the relative letdown motion due to vessel motion and aircraft perturbations due to wind effects.

2. Guidance based on future prediction (forecasting) of vessel deck motion. This requires that algorithms be developed for motion prediction based on past and current measurements. These measurements include ship-board attitude, attitude rate, and translational acceleration.

   a). Letdown with open-loop guidance. Here, an acceptable landing envelope is defined. Whenever the future presence of such an envelope is forecast, the letdown guidance is initiated so that touchdown occurs during the time the landing pad is within that envelope.

   b) Closed-loop preturbation guidance and continuous landing pad state forecasting so that the relative touchdown state can be updated and adjusted during the letdown phase.

Chapter V presented preliminary statistical results of the landing dispersions resulting from using open-loop letdown with no motion prediction. A more complete study approach is to devise each of the four schemes and then to evaluate them through simulation as has been done for the approach phase of the flight. The limits on touchdown dispersion and landing gear constraints should be factored into this analysis. Results would include the recommended landing guidance scheme, a specification of implementation requirements, and recommendations for further research.

Recommendations

There are three specific areas of further research that this study points to. These are: (a) piloted simulation evaluation of approach guidance, (b) analysis of landing guidance requirements, and (c) more detailed investigation of the wind-over-deck wake turbulence model.

Piloted Simulation In deciding between the two types of automatic approach guidance - constant bearing/elevation and lateral pursuit/constant sink rate, several advantages can be found for both on analytical bases.

However, these points are not sufficient by themselves to make a final selection. Issues have been raised concerning which concept would be favored from a pilot monitoring point-of-view. The constant bearing approach is favorable to the pilot for deck light and MLS signal reasons. The lateral pursuit approach appears to be favored from the HUD mechanization and cockpit window perspective point-of-view. (Although a zero degree constant bearing approach would have the same advantage.)

It is recommended that a piloted cockpit simulation study be made which can be used to resolve these questions. This study should be in sufficient detail so that a clear choice of approach technique can be made. This means that the cockpit should have a layout similar to what would be envisioned for the RTA or other advanced aircraft cockpit. This possibly includes a HUD mechanization. It also would have visual perspective limitations and realism so that the pilot could evaluate the optical cues that each approach provides.

At least three pilots should be used in this experiment. They should have small aviation facility ship landing experience. They should also have sufficient training with the guidance concepts so that they can realistically monitor the automatic approaches and takeover control in case of a severe guidance error.

A fixed base simulation would be sufficient because the primary motive of these experiments would be to obtain pilot evaluation of visual cues. Five passes should be made with each guidance concept and each plot, and random error sequences should be used. This would require a total of thirty passes on the simulation. Questionaires should be developed to obtain pilot opinion of each guidance concept.

Landing Guidance Analysis The landing guidance study requirements are described in Chapter IV. An analysis of vessel motion prediction schemes should be made based on models of ship motion and assumptions of various shipboard sensors being available. This analysis would determine how well ship motion forecasting could be done and if it could be used as part of the letdown guidance scheme.

A second analysis should be made of the four automatic landing guidance schemes outlined in Chapter IV. Two are with and two are without future ship motion forecasting. This analysis would include a computer simulation so that landing dispersions could be computed as functions of sea state, hover point initial conditions, and instrumentation accuracy. The output of this study will be a recommended landing guidance scheme to complement the approach guidance results of this study.

Wind-over-deck Modeling The chief disturbance to the aircraft during the final portion of the approach phase appeared to be due to the wind-over-deck wake turbulence. There has been differences in opinion and simulation results among the researchers involved in examining the effects of the wind-over-deck. The existing model was based on limited data taken from finite points in a one-fiftieth scale wind tunnel. Because this turbulence can have significant importance on approach and landing performance, it is recommended that a new wind-over-deck wake turbulence model be developed. This would include rotational disturbances and effects on the engine inlets that do not exist in the current model. Then, care must be used in creating new and modified simulations so that the model is used correctly.

Other Research Areas This study used specific models of the RTA aircraft and SRFIMF flight control. The SRFIMF control needs to be examined in much further detail to evaluate effects of aircraft model uncertainty and other sensor error magnitudes. This can be done with the current system model and simulation developed for the current study.

It would be useful to examine the approach and landing requirements with additional flight control concepts and additional VTOL aircraft and helicopters. In particular, if an existing flight system (such as the Harrier or SH-53 helicopter) were used for the analysis, then the possibility exists of continuing the research through flight test. It is recommended that future guidance requirements research include both existing and potential future aircraft (such as the RTA lift fan model).

APPENDIX A

The Lift/Cruise Fan V/STOL Research Technology Aircraft (RTA)

The simulated aircraft used in this study (Figure A.1) is the Lift/Cruise Fan V/STOL Research Technology Aircraft (RTA) which is a conceptual modification of a McDonnell Douglas T-39 Sabreliner. Table A.1 presents physical dimensions of this aircraft. The aircraft is powered by three turbojet engines which drive three fans. One of the fans is located in the forward fuselage and is used only during powered-lift flight. During the aerodynamic portion of flight the forward fan, called the lift fan, is shut down and its air duct is closed to reduce aerodynamic drag. The other two fans, called the lift/cruise fans, are installed at the wing roots and are used during powered-lift and aerodynamic flight. Their exhaust nozzles can be deflected such that their thrust can be vectored at any angle between horizontally or vertically. In addition, all three fans possess the capability to have their thrust deflected for sideforce generation.

Two basic methods of energy transfer between engines and fans are modeled: (1) the gas-coupled configuration which uses the high energy heated air to drive the "tip turbine" fans, and (2) the mechanically coupled configuration which uses a shaft, clutches, and gear boxes to drive the fans. In either configuration, engine outputs are cross- and inter-connected to minimize unbalanced forces and moments due to an engine failure. The mechanically coupled configuration is used for the simulation study. Figure A.2 shows the macro flow chart of the overall mathematical model for this configuration.

In the cruise (or aerodynamic) flight, the controls are conventional (i.e., aileron, rudder and elevator control roll, yaw and pitch axes, respectively). Forward velocity is controlled by adjusting the lift/cruise

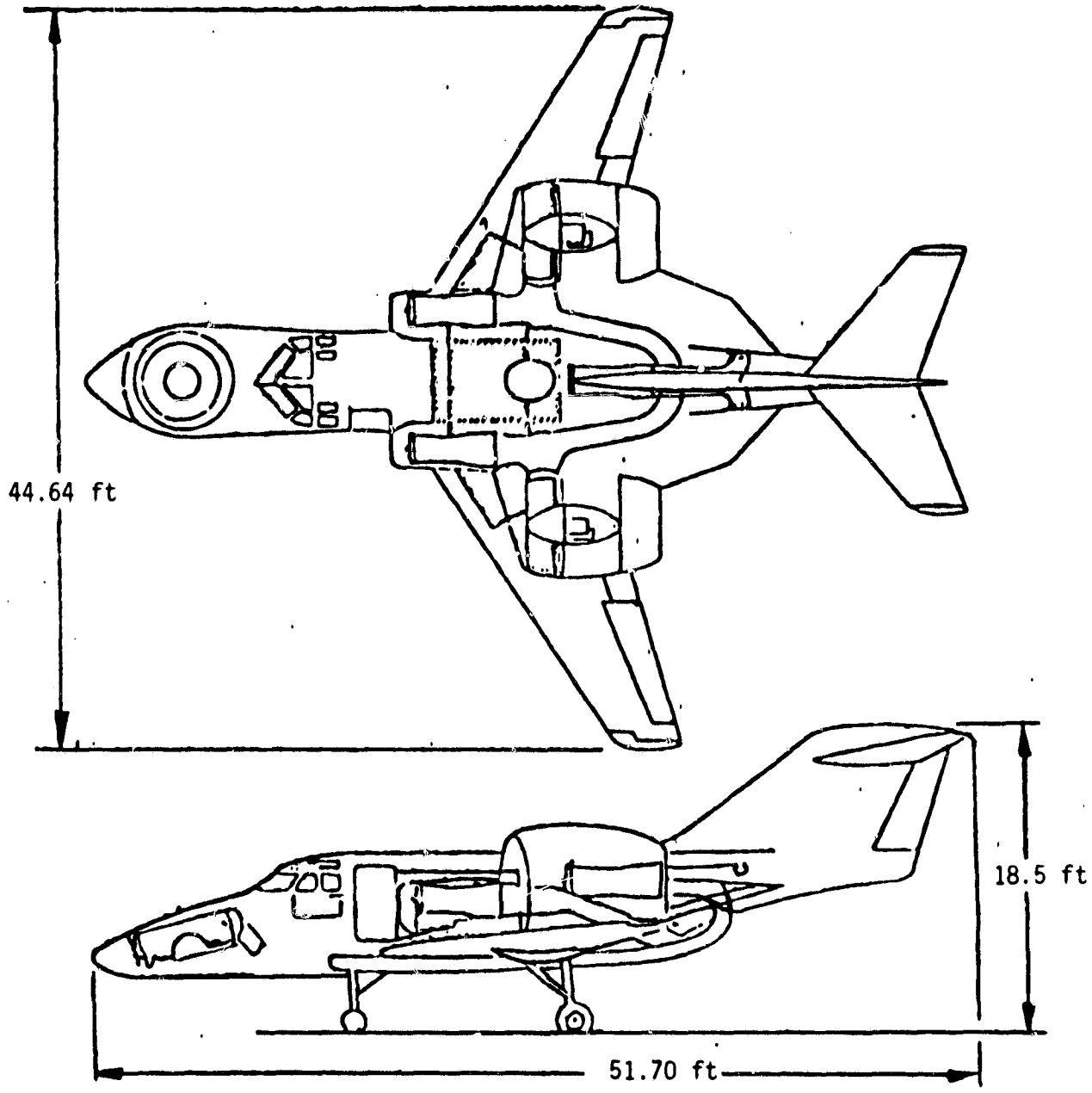

Figure A.1 Lift/Cruise Fan V/STOL Research Technology Aircraft
Modified Sabreliner (T-39)

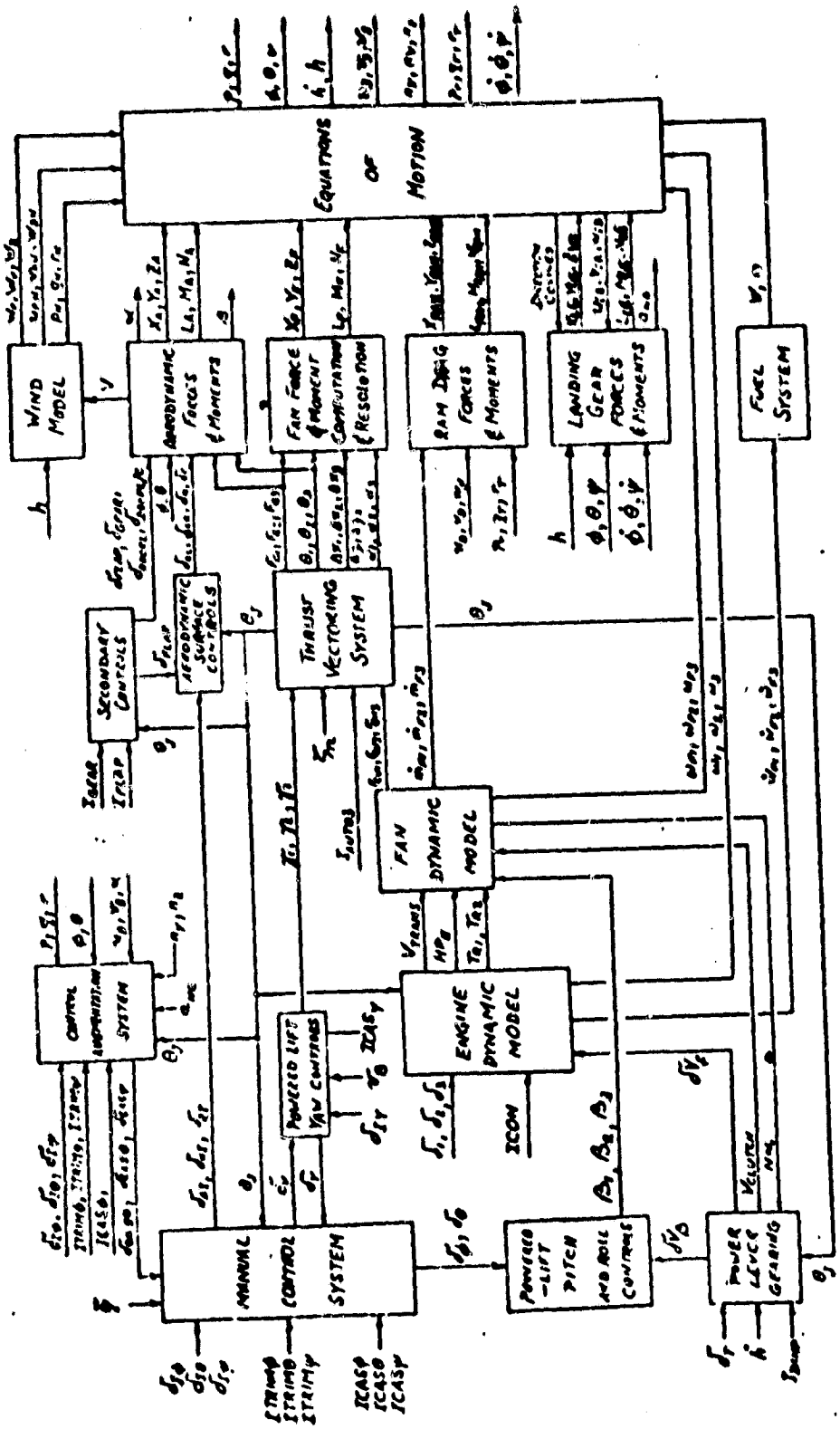

Figure A.2. Macro Flow Chart of Mathematical Model for the Mechanically Coupled Configuration.

Table A.1 - Physical Dimensions of the RTA

Symbol	Quantity	Magnitude
S_w	WING AREA	342.05 ft^2
b	WING SPAN	44.43 ft
$\bar{c}$	MEAN AERODYNAMIC CHORD	8.38 ft
S_t	HORIZONTAL TAIL AREA	75.10 ft^2
t	TAIL MOMENT ARM	21.20 ft
Z_t	TAIL MOMENT ARM	8.17 ft
W	WEIGHT	20,000 lb
I_x	MOMENTS OF INERTIA	19,400 slug ft^2
I_y		52,400 slug ft^2
I_z		67,500 slug ft^2
I_{xz}		2,575 slug ft^2

fan RPM via engine throttle. Below 120 knot IAS, the powered-lift mode is phased in. The separation of the flight regimes is shown in Fig. A.3. In the powered lift flight regime, change of forward speed, at a constant pitch angle, is achieved via thrust vectoring of three fans. Lateral translation, at a constant bank angle, is achieved via lateral deflexion of the thrust vector magnitude via fan RPM. Attitude angles (roll, pitch and yaw) are controlled via differential thrust modulation. For the guidance analysis of this study, the aircraft is in the powered-lift mode for most of the approach.

Orginially, the aircraft model used in the simulation program contained a response feed back stability and control augmentation system (SCAS) model for the flight controller. However, it was replaced by a state rate feed-back implicit model - following (SRFIMF) flight controller developed by NASA/Ames Research Center which is described in Appendix B.

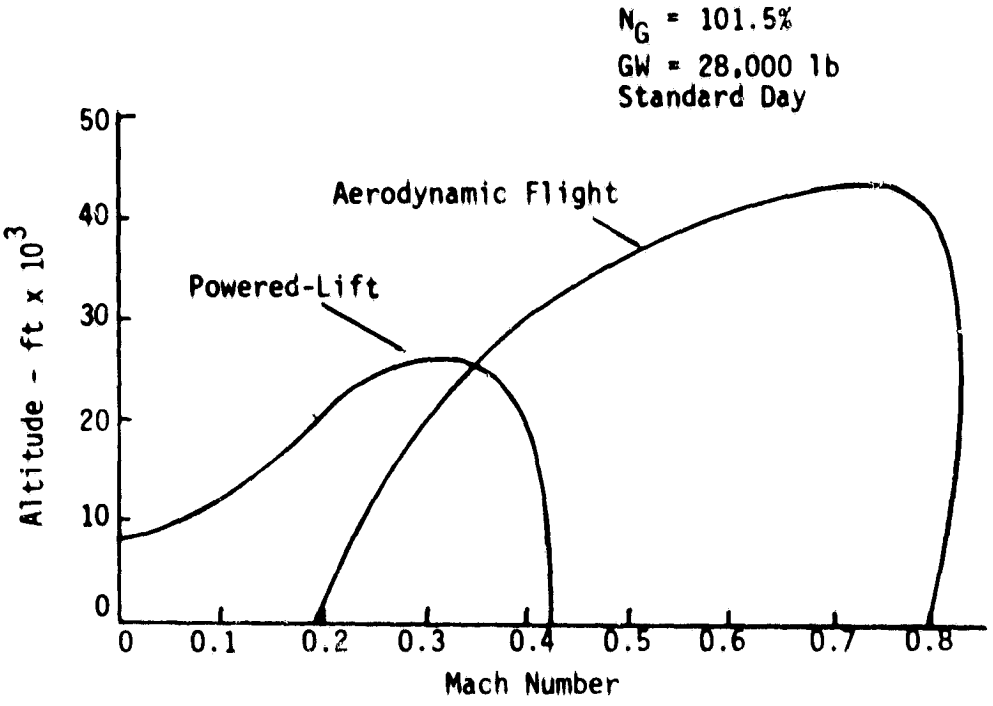

Figure A.3. Aerodynamic and Powered Lift Regimes of the RTA Aircraft

Further descriptions of the aircraft in terms of aerodynamic stability and control derivatives, engine and fan characteristics and response characteristics are contained in Reference 4. The simulation program representing the RTA aircraft used for pilot-in-the-loop experiments at the Flight Simulation for Advanced Aircraft (FSAA) facility at NASA Ames is described in Reference 11.

APPENDIX B

State Rate Feedback Implicit Model Following (SRFIMF) Controller

The purpose of any stability (and command) augmentation system is to modify the inherent dynamic response behavior of a given aircraft so as to approximate some desired input-output characteristics. This transformation is achieved by application of a controller design based on response feedback or model following concepts. Historically, response feedback controllers represent the conventional approach to aircraft stability augmentation design, where the basic idea is to use output feedback with dynamic compensation and gain scheduling algorithms to realize a desired invariant, multi-input/multi-output transfer function matrix. The principal criticism of this approach is the need for detailed apriori knowledge of the basic aircraft dynamics for a variety of flight conditions. However, the development of advanced V/STOL aircraft (having greatly expanded flight envelopes, and, therefore, variations in inherent dynamics) has led to the design of the so-called model-following controllers which are supposed to be intrinsically insensitive to aircraft parameter variations and flight conditions. The SRFIMF controller represents one such design based on the implicit model following control concept. In the following, an analysis of the SRFIMF controller structure including an interpretation of the underlying design rationale is presented. The discussion is limited to the single axis case for clarity and ease of exposition.

Ideal SRFIMF Flight Controller

Figure B.1 shows the block diagram for an ideal SRFIMF controller. G(s) represents the plant dynamics and D(s) the disturbance input transfer function. The basic idea of this controller structure is to effectively cancel the plant dynamics G(s) by introducing an equivalent inverse

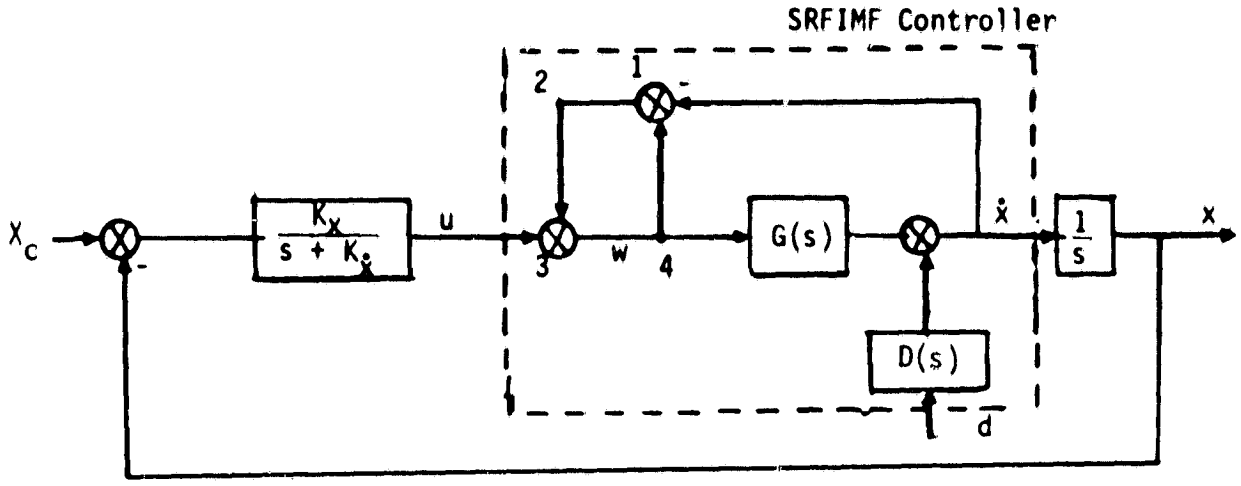

Figure B.1. Ideal SRFIMF Controller

transfer function 1/G(s) between u and w. Thus, loop 1,2,3,4 reduces to

$$w(s) = \left\{\frac{\frac{1}{G(s)}}{1 - [1 - G(s)]}\right\}[u(s) - D(s)\, d(s)]$$

$$= \frac{1}{G(s)}\,[u(s) - D(s)\, d(s)] \qquad (B.1)$$

The equivalent block diagram is shown in Figure B.2.

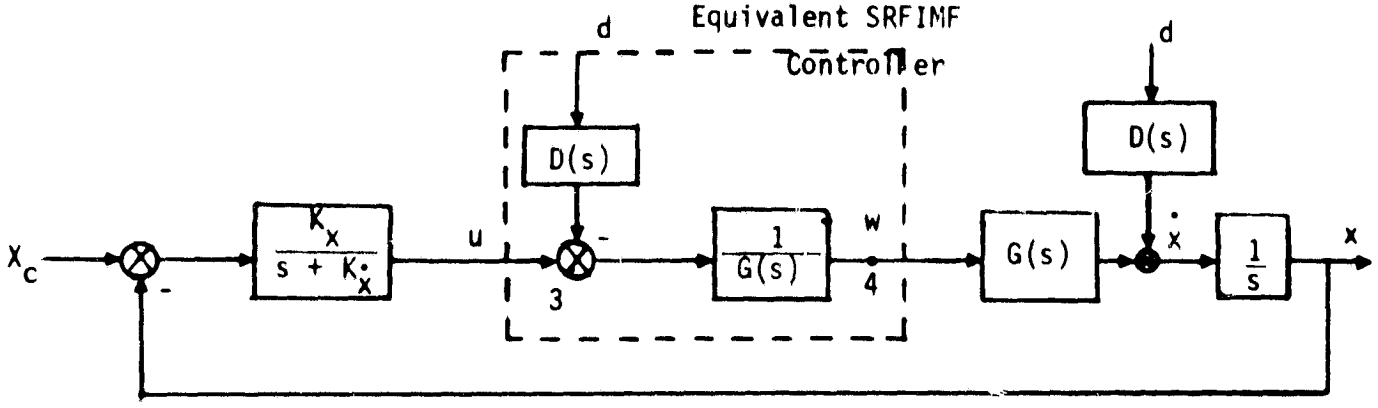

Figure B.2. Equivalent SRFIMF Controller Structure

However, this formulation of the SRFIMF controller is considered to be unrealizable for practical reasons. A practical or physically realizable version of the controller involves modification of the loop 1,2,3,4 in Figure B.1. Two types of physically realizable SRFIMF controllers corresponding to position and velocity command systems are shown in Figures B.3 and B.4, respectively.

The equivalent transfer function between w(s) and u(s), d(s) is

$$w(s) = \left[\frac{w(s)}{u(s)}\right]_{eq} u(s) + \left[\frac{w(s)}{d(s)}\right]_{eq} d(s) \tag{B.2}$$

where

$$\left.\frac{w}{u}(s)\right|_{eq} = \begin{cases} \dfrac{1}{1 - [A(s) - s^2 K\, H(s)\, G(s)]} & \text{: Position Controller} \quad (B.3) \\ \dfrac{1}{1 - [A(s) - sK\, H(s)\, G(s)]} & \text{: Velocity Controller} \quad (B.4) \end{cases}$$

and

$$\left.\frac{w}{d}(s)\right|_{eq} = -S\, D(s) \left[\left.\frac{w}{u}(s)\right|_{eq}\right] \quad \text{: Position Controller} \tag{B.5}$$

$$-s^2 D(s) \left[\left.\frac{w}{u}(s)\right|_{eq}\right] \quad \text{: Velocity Controller} \tag{B.6}$$

Transfer function A(s) is of the form

$$A(s) = 1 - s\, H(s)\, J(s) \tag{B.7}$$

where

$$H(s) = \frac{H_N(s)}{H_D(s)} = \frac{h_{No} s^k + - - + 1}{h_{Do} s^n + - - + 1} \tag{B.8}$$

and

$$J(s) = j_o \prod_{r=1}^{\ell} (s + p_r); \tag{B.9}$$

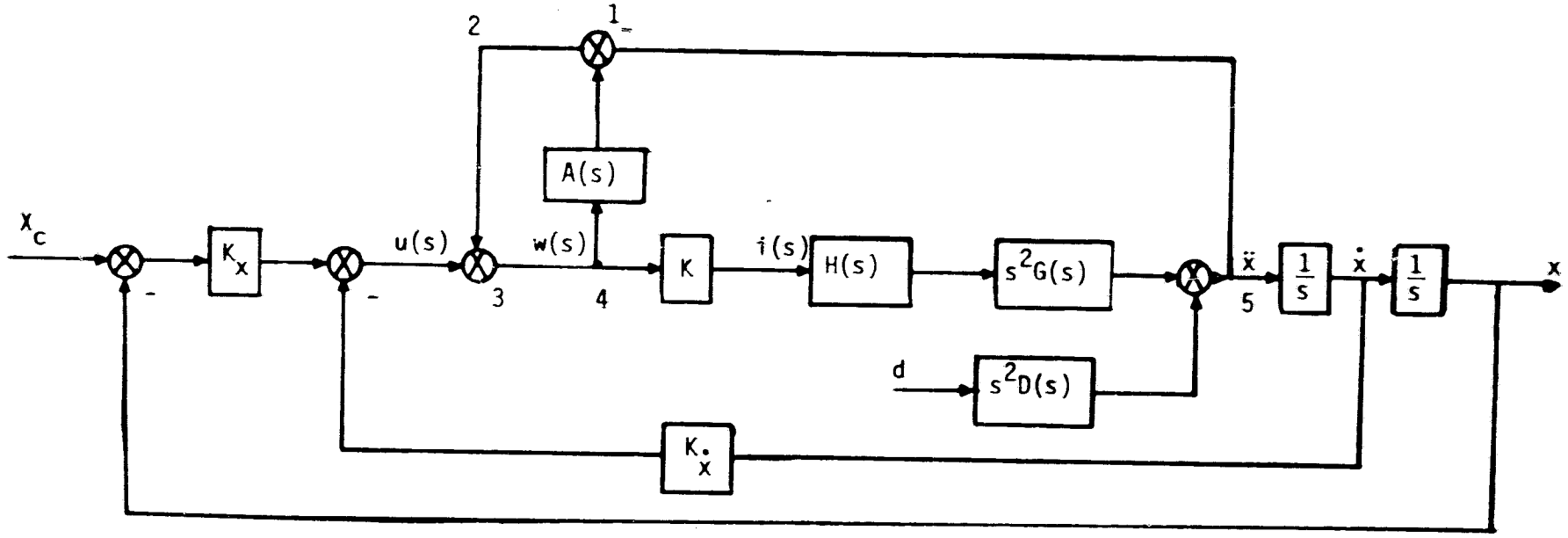

Figure B.3. SRFIMF Controller for Position Command System

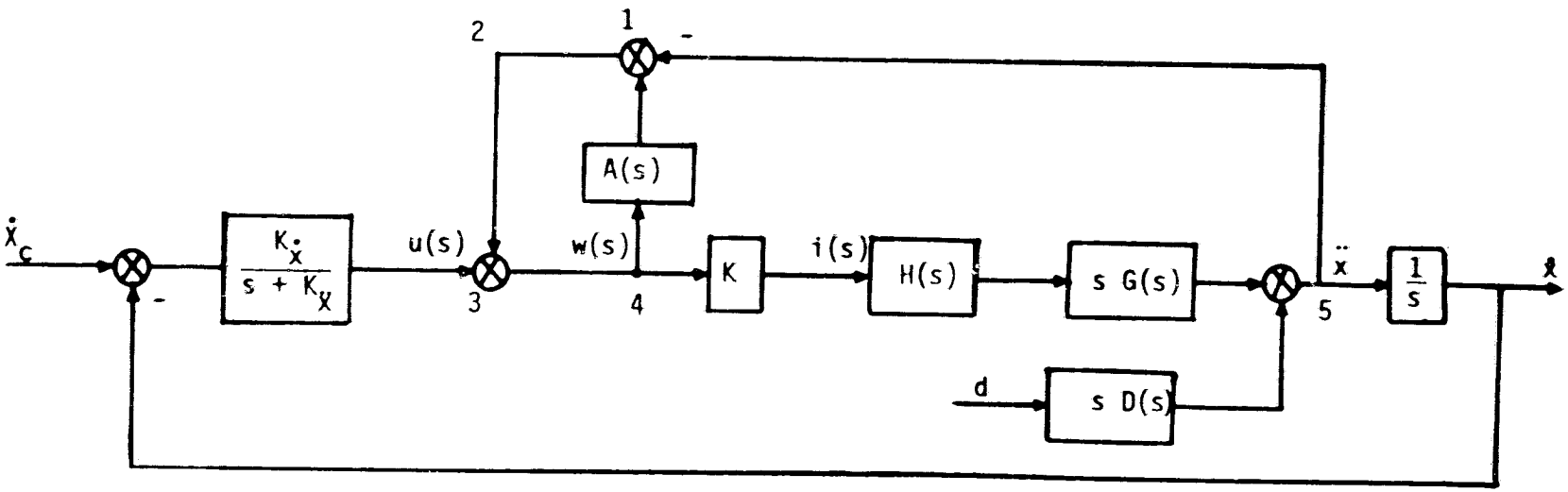

Figure B.4. SRFIMF Controller for Velocity Command System

The degree ℓ of J(s) is chosen so as to guaranteee a type 1 position (or velocity) control system and is determined by the expression

$$\ell = n - k - 1. \tag{B.10}$$

Thus, given equations (B.3) - (B.10),

$$\left.\frac{w}{u}(s)\right|_{eq} = \frac{1}{s\,H(s)[J(s) + s^q K\,G(s)]} \quad : \begin{array}{l} q = 1 \text{ Position Controller} \\ q = 0 \text{ Velocity Controller} \end{array} \tag{B.11}$$

Equivalent block diagrams for the physically realizable position and velocity controller are as shown in Figs. B.5 and B.6, respectively. In both of these controllers, the equivalent open loop transfer function between u and $\ddot{x}$ is given by

$$\frac{\ddot{x}}{u}(s) = \frac{s^q K\,G(s)}{J(s) + s^q K\,G(s)} \quad : \begin{array}{l} q = 1 \text{ Position Controller} \\ q = 0 \text{ Velocity Controller} \end{array} \tag{B.12}$$

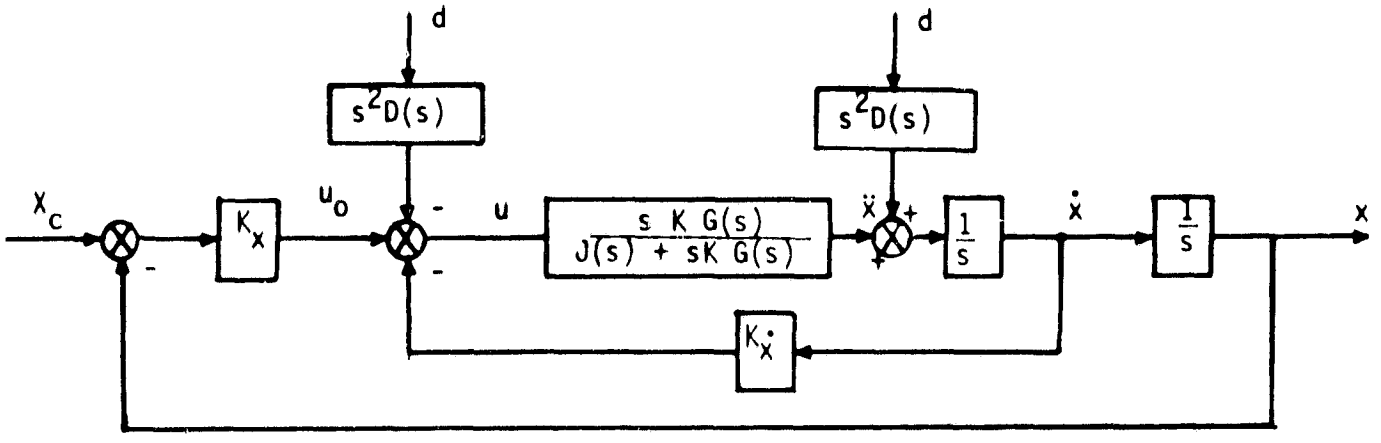

Figure B.5. Equivalent SRFIMF Position Controller Structure

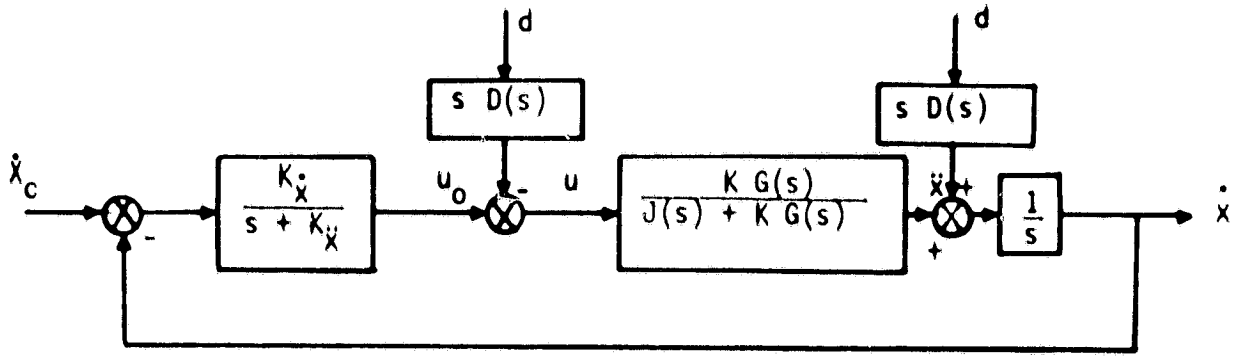

Figure B.6. Equivalent SRFIMF Velocity Controller Structure

For large values of K ($K \to \infty$), the transfer function

$$\lim_{K\to\infty} \frac{\ddot{X}}{u}(s) \cong 1. \tag{B.13}$$

This is based on assuming that all the roots of the characteristic equation

$$\Delta(s) = 1 + \frac{s^q K\, G(s)}{J(s)} \tag{B.14}$$

not converging on the zeros of $s^q K\, G(s)$ are stable for sufficiently large values of K. This is one of the fundamental assumptions made in developing the concept of the SRFIMF controller. When this assumption holds, the equivalent open loop transfer function becomes

$$\frac{\ddot{X}}{u}(s)\Big|_{k \text{ large}} \cong \begin{cases} \frac{s}{s+\eta} \; ; \; |\eta| \approx 0 & : \text{position controller} \\ 1 & : \text{Velocity controller} \end{cases} \tag{B.15}$$

Therefore, for sufficiently large value of K, the resulting closed loop transfer functions for both controllers are:

$$\frac{x}{x_c}(s) = \frac{k_x}{s^2 + k_{\dot{x}}s + k_x} \qquad \text{: Position controller} \qquad (B.16)$$

$$\frac{\dot{x}}{x_c}(s) = \frac{k_{\dot{x}}}{s^2 + k_{\dot{x}}s + k_{\dot{x}}} \qquad \text{: Velocity controller} \qquad (B.17)$$

as desired.

The SRFIMF controller design may have problems in practical implementation if for any reason the characteristic equation $\Delta(s)$ of Eq. (B.14) has roots which go unstable or lightly damped for sufficiently large values of K. This may occur for any of the following reasons:

1) The assumed actuator transfer function H(s) is not identical to the actual dynamics;
2) The function J(s) is of order 2 or higher;
3) The transfer function G(s) has higher order dynamics;
4) The digital implementation leads to system instability.

Finally, the SRFIMF controller may have additional problems in gust alleviation if the acceleration feedback (state-rate) signal is corrupted by measurement noise.

The SRFIMF controller concept was applied to all axes of the aircraft. The attitude flight controller (AFC) which used the position controller concept is shown in Fig. B.7. The flight path flight controller (FPFC) which used the velocity controller concept is shown in Fig. B.8. The command signals were obtained from the pilot inputs; AFC comes from the stick and pedal, and FPFC comes from the power management console. In the fully automatic system, it was assumed that the pilot actuators, which are essentially equivalent to the guidance commands, were driven by instantaneous

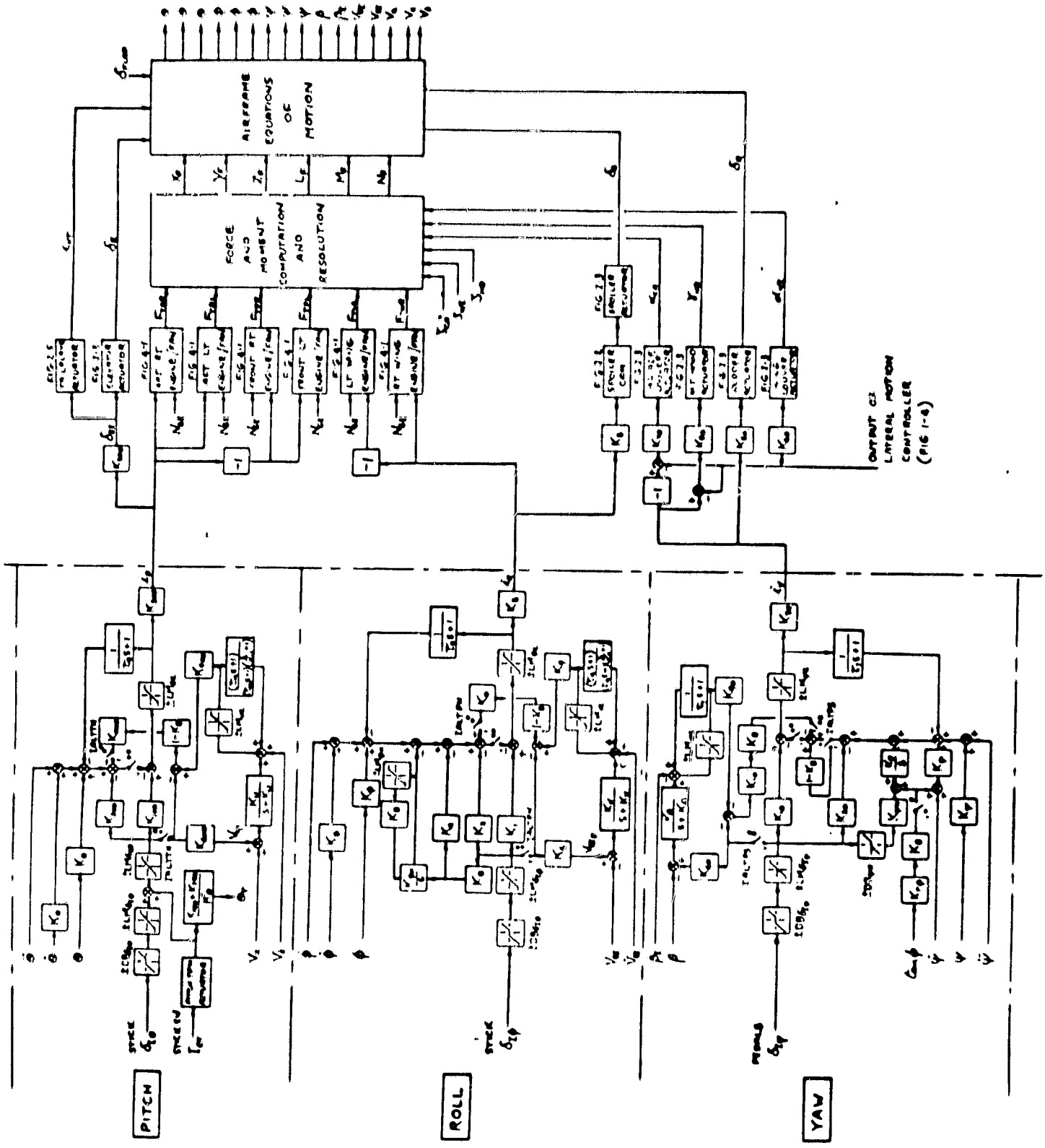

Figure B.7. SRFIMF Attitude Flight Controller.

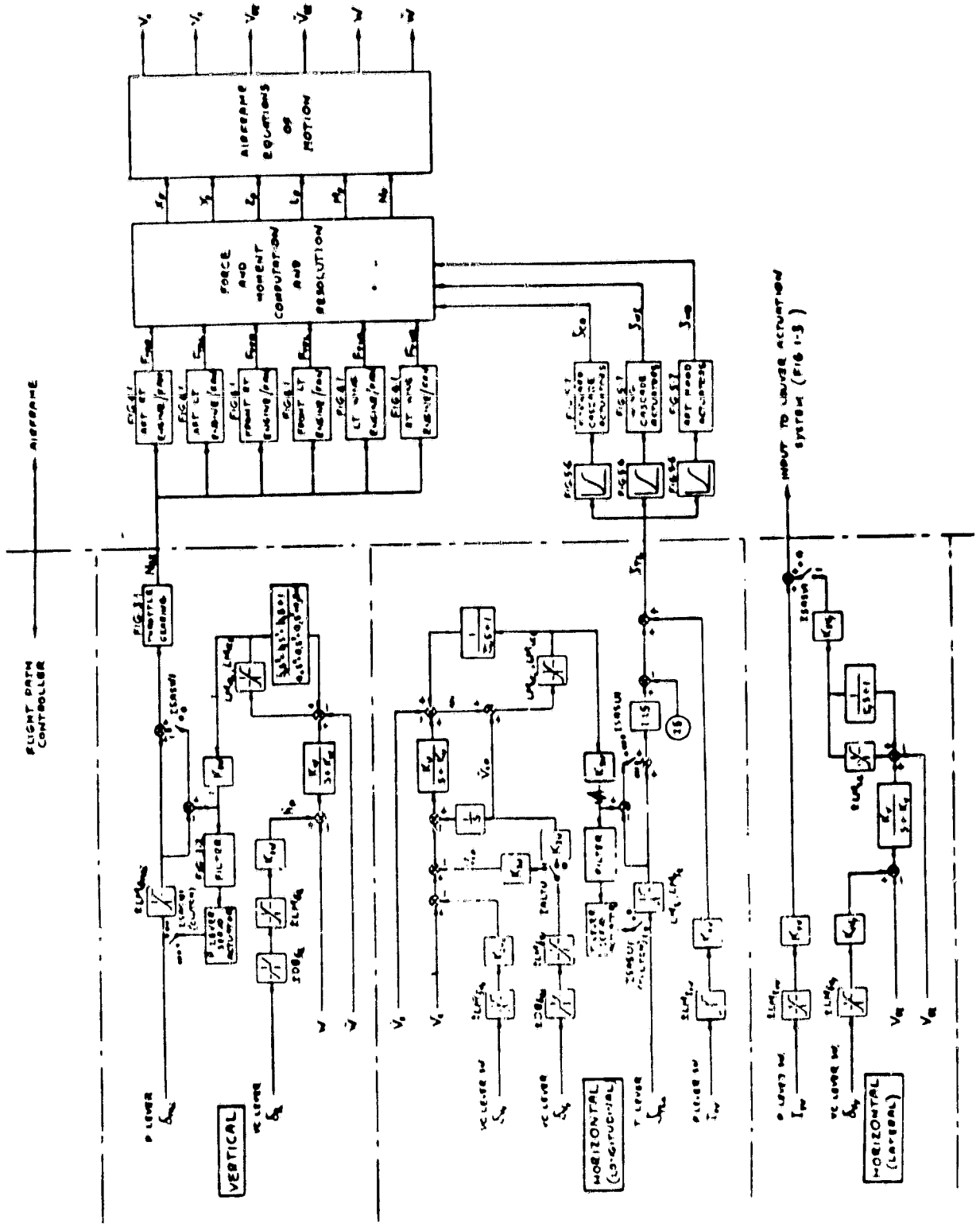

Figure B.8. SRFIMF Flight-Path Controller.

Table B.1. - Pilot Control Modes

	Attitude flight controller (stick and rudder pedals)			Flight-path flight controller (VC lever system)		
Speed range	Roll axis	Pitch axis	Yaw axis	Longitudinal x axis	Lateral y axis	Vertical z axis
0 - 20 knots	Bank-angle command* or side velocity command**	Pitch attitude command*	Yaw rate command* with heading hold	Velocity command* or acceleration command with velocity hold	Side velocity command**	Vertical velocity command*
20 - 30 knots	Blend		Blend		Phase out	
30 knots-conversion speed (≈ 120 knots)	Roll-rate command* with bank-angle hold		Yaw rate-command* with bank-angle feedback for turn coord. or sideslip angle command		- - -	

* Nominal set of pilot control modes.

** These controller modes are mutually exclusive.

and unity gain servos. Table B.1 shows the available control modes for AFC and FPFC, from which the most suitable ones are chosen for the automatic guidance.

The suitability of the SRFIMF controller design for the multiaxes application should be checked through careful analysis and simulation. As a minimum, multivariable linearized models for the given aircraft and transfer function analysis should be used in conducting the investigation.

APPENDIX C

Ship Motion Modeling

The most severe environment that the VTOL aircraft will have to land in is Sea State 5. Under these conditions, the ship motion and wind-over-deck (air wake) effects must be modeled together. The ship motion and air wake models used for this study were based on those compiled by Fortenbaugh [1,5] for previous studies. This Appendix summarizes the ship motion modeling, and Appendix D summarizes the air-wake model. Details of the model development and sources of data can be found in Reference 2.

Nine environmental parameters must be specified to quantify the airwake and ship motion models:

1. Wind over deck magnitude (V_{WOD})
2. Wind over deck direction relative to the ship (ψ_{WOD})
3. Ambient wind magnitude (V_{WIND})
4. Ambient wind direction relative to the ship (ψ_{WIND})
5. Ship speed (V_S)
6. Ship heading relative to predominant wave direction (μ_S)
7. Significant wave height (H_S)
8. Modal wave period (T_O)
9. Sea State (SS)

These parameters are related in various equations and empirical results. For example, the relationships between modal wave period (T_O), significant wave height (H_S), and ambient wind speed (V_{WIND}) are depicted in Fig. C.1.

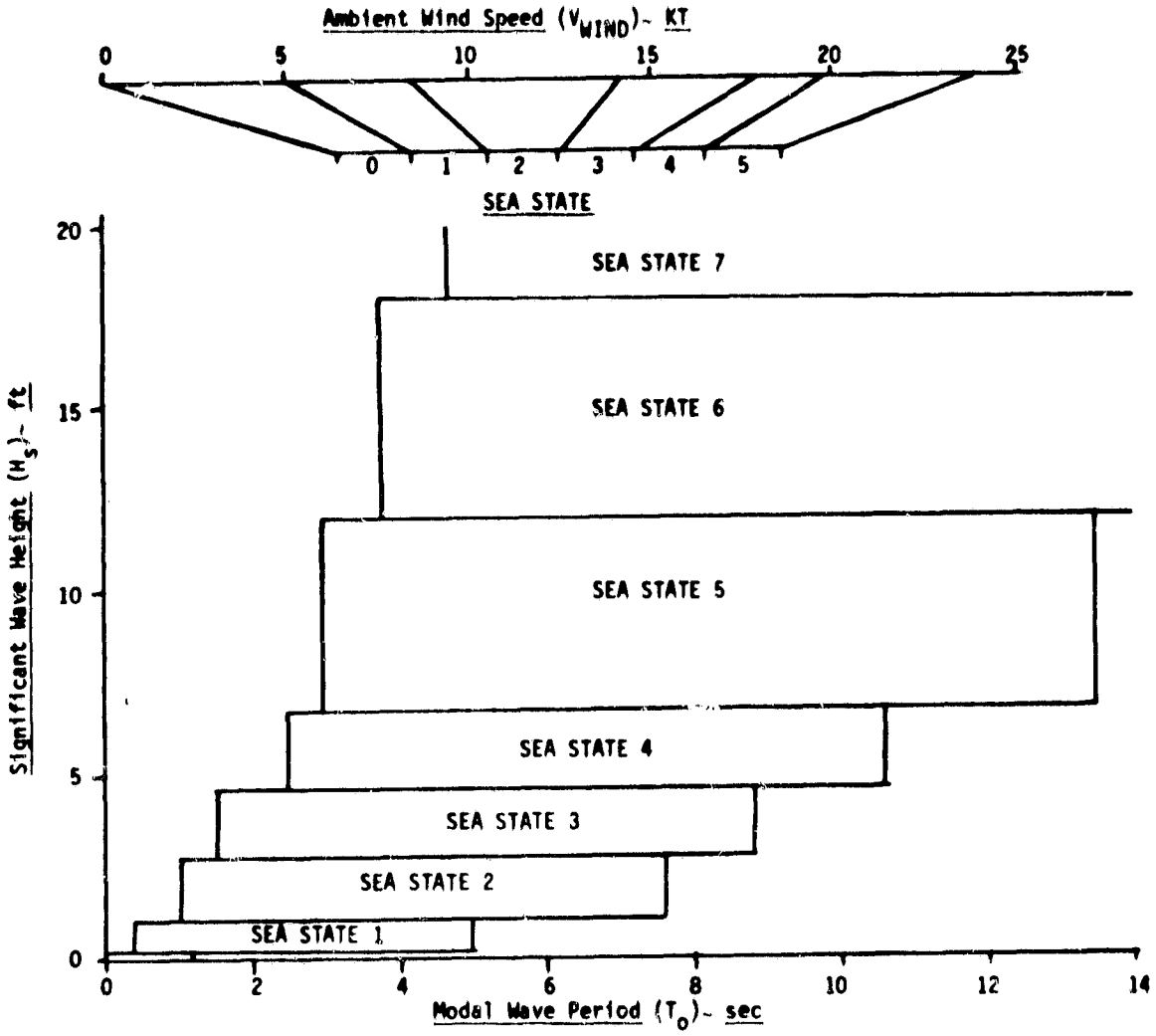

Figure C.1. Significant Wave Height, Modal Wave Period, and Ambient Wind Speed Ranges as Functions of Sea State.

Inherent in the model used by Fortenbaugh is the assumption that the seaway is long crested so that ambient winds and waves are parallel and uni-directional. This assumption is valid because ship motion in long crested seas is greater and more severe than short crested, confused seas.

To reduce the number of possible sea and wind conditions which would have to be used in a reasonable experiment and yet provide a sufficient variety of operational conditions, Fortenbaugh developed the thirteen sets of compatible environmental parameters shown in Table C.1.

Table C.1. Sets of Compatible Environmental Parameters Relating Ship Motion and Wind-Over-Deck Effects.

Condition	Sea State	V_s (kt)	μ_s (deg)	ψ_{WIND} (deg)	ψ_{WOD} (deg)	V_{WIND} (kt)	V_{WOD} (kt)	H_s (ft)	T_o (sec)
1	6	25	120	-60	-30	25.00	43.30	18	15.13
2	5	25	120	-60	-30	25.00	43.30	12	13.50
3	5	20	120	-60	-30	20.00	34.64	12	13.50
4	5	10	135	-45	-30	19.32	27.32	12	13.07
5	5	25	160	0	0	20→24	45→49	12	12.07
6	5	5	180	0	0	20→24	25→29	12	11.51
7	4	25	105	-75	-30	17.68	34.15	6.9	10.6
8	3	25	105	-75	-30	17.68	14.15	4.6	8.8
9	3	20	105	-75	-30	14.14	27.32	4.6	8.8
10	3	25	90	-90	-30	14.43	28.87	4.6	8.8
11	3	15	120	-60	-30	15.00	25.98	4.6	8.8
12	3	25	180	0	0	14→18	39→43	4.6	8.8
13	3	5	180	0	0	14→18	19→23	4.6	8.8

The most widely applied, accepted, and proven technique for modeling ship motions was introduced in the classic paper of St. Denis and Pierson. [12]. This technique has been computerized by many organizations. The NAEC version [13], was used by Fortenbaugh. Basic inputs to the computer program include RAO (Response Amplitude Operator) data for the ship being studied, H_s and T_o for the wave spectrum model, and μ_s and V_s. Program outputs include gains, phases, and frequencies of sinusoids which are summed to produce ship motion time histo[illegible].

RAO's are ship motion frequency responses, one for each degree of freedom, and are quantified as gains and phases which are functions of input frequencies. The gains are the magnitude squared of the ship motion responses at each of the input frequencies. The RAO's cannot be represented by analytic forms but must be calculated or measured at discrete frequencies. These data are produced either by measuring ship model responses in towing tanks or by analytically determining the responses with the Meyers, Sheridan, Salveson program. [14] The DD 963 data base [15] was generated by this program and covers V_s from 5 to 25 kt in 5 kt increments and μ_s from 0 (following seas) to 180 (head seas) deg in 15 deg increments. RAO's are established in the encountered frequency (ω_e) domain which is mathematically related to the natural frequency (ω) domain by the frequency mapping relation:

$$\omega_e = \omega - \frac{\omega^2 V_s \cos\mu_s}{g} \qquad (C.1)$$

where ω_e is encountered frequency (rad/sec)

ω is natural wave frequency (rad/sec)

g is acceleration due to gravity (= 32.2 ft/sec^2)

Physically, the encountered frequency is the natural wave frequency seen by a ship moving through the waves.

The two-parameter Bretschneider wave spectrum was adopted by Fortenbaugh for this application because it has been demonstrated by DTNSRDC to provide more realistic ship responses in mild and heavy seas:

$$S_W(\omega) = \frac{483.5\ H_s^2}{T_o^4\ \omega^5} e^{-1944.5/(\omega T_o)^4} \qquad (C.2)$$

Note that the wave spectrum is defined in the natural wave frequency (ω) domain. Two important features of the spectrum are as follows:

1. H_s is only a scaling parameter.
2. T_o shifts the peak of the spectrum as shown in Fig. C.2. The frequency at the peak (ω_{max}) is only a function of T_o:

   $$\omega_{max} = 6.64/T_o$$

   This feature is the basis for spectrum tuning.

A ship motion spectrum is calculated from an RAO and a wave spectrum as depicted in Fig. C.3 using the relation:

$$\Phi_{ii}(\omega_e) = S_W(\omega_e)\frac{\partial \omega}{\partial \omega_e} RAO_i(\omega_e) \qquad (C.3)$$

where $\Phi_{ii}(\omega_e)$ is the spectrum in the ω_e domain for the i degree of freedom

$S_W(\omega_e)$ is $S_W(\omega)$ transformed to the ω_e with the frequency mapping relation (Eq. C.1)

$RAO_i(\omega_e)$ is the gain of the RAO for the i degree of freedom

$\frac{\partial \omega}{\partial \omega_e}$ is required because the ω-ω_ε mapping is not a unity transformation.

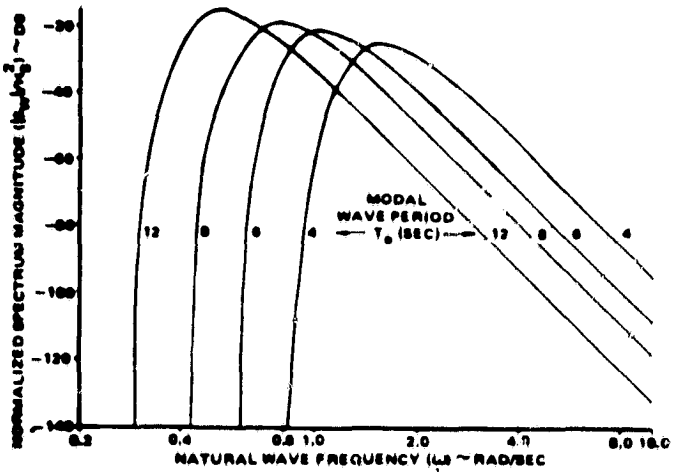

Figure C.2. Variation of Bretschneider Wave Spectrum with Modal Wave Period

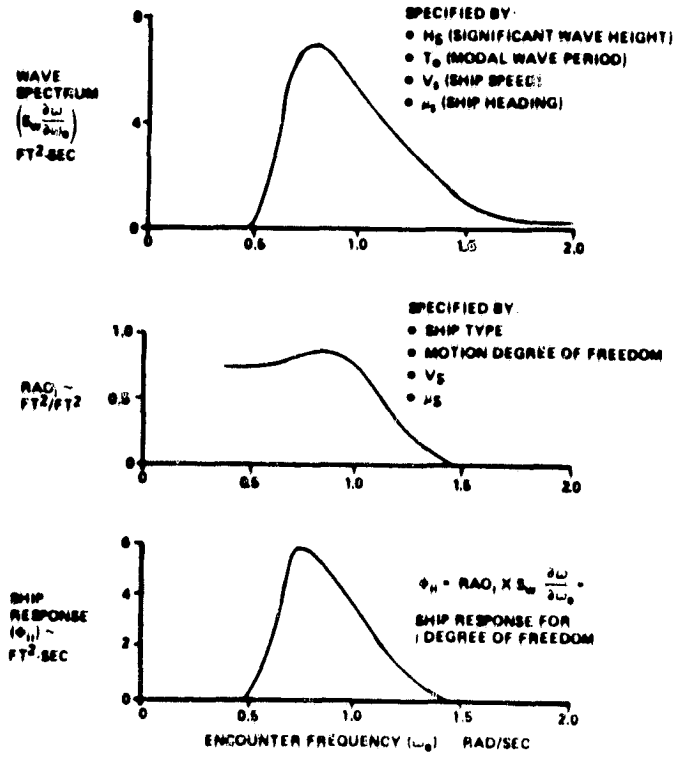

Figure C.3. Ship Motion Spectrum Development

The determination of T_o's in Table C.1 was aided by a compendium of DD 963 ship motion statistics and spectra generated by inputting a white noise spectrum to all the RAO data in the DD 963 data base. The T_o's which matched the RAO peaks were noted. If T_o was outside the T_o range of the Sea State for a Table I condition, it was set to the maximum or minimum as appropriate for that Sea State.

Spectral decomposition of the motion spectra (Φ_{ii}) results in the specification of component frequencies and associated gains and phases for the sum of sinusoids ship model form. For spectral decomposition the NAEC program approximates a motion spectrum as shown in Fig. C.4 for all frequencies where the spectrum amplitude exceeds 4% of its maximum value.

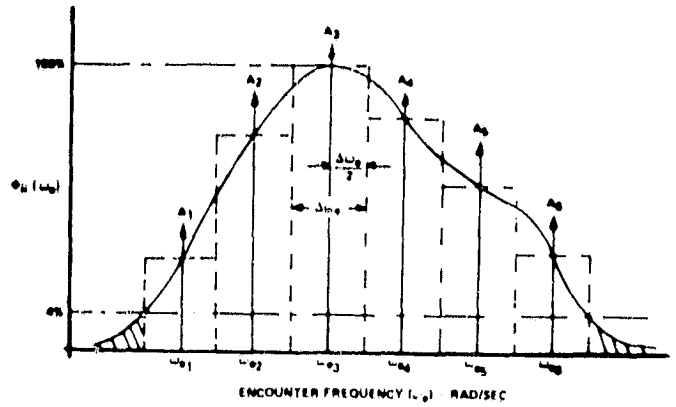

$$A_1 = \Phi_{ii}(\omega_{e_1})\Delta\omega_e$$

$$A_2 = \Phi_{ii}(\omega_{e_2})\Delta\omega_e$$

$$\vdots$$

$$A_6 = \Phi_{ii}(\omega_{e_6})\Delta\omega_e$$

with this approximation to the spectrum $\Phi_{ii}(\omega_e)$, the time history of ship motion variable is given by

$$i(t) = \sum_{n=1}^{6} \sqrt{2A_n}\cos(\omega_{e_n} t - \phi_{in} + \varepsilon_n)$$

where ϕ_{i_n} = Rao phase angle at ω_{e_n}

ε_n = random phase associated with the wave spectrum at $\omega_{e_n}(-180° < \varepsilon_n < 180°)$

Figure C.4. Decomposition of Ship Motion Spectra into Six Components

Assuming that the thirty two component approximations represent actual ship motion statistics, Ref. 5 showed that the six component approximations result in less than 5% error in most cases for RMS positions, rates, and accelerations of each degree of freedom. Since all three statistical measures were matched equally well with six components, it was concluded by Fortenbaugh that six components will give an excellent approximation for ship motions, at least for studies which involve relatively short times of exposure to the ship environment. Studies directed to the flying qualities and flight control aspects of launch and recovery on small ships would fall in this category.

Reference 5 contains tables of the seventy eight numbers required to model the ship motions of each of the conditions in Table C.1. These include the gain (A_{i_n}) and phase (Φ_{i_n}) of each of the six degrees of freedom at each of the six component frequencies (ω_{e_n}) which are common to all degrees of freedom. These data were calculated by the NAEC ship motion program [13] for the ship c.g. and are listed in Ref. 5. As an example, Table C.2 contains the data for representing the ship motions of Condition 2 of Table C.1.

Table C.2. Ship Motion Model Parameters for Environmental Condition 2

(V_s = 25 kt, μ_s = 120 deg, H_s = 12.0 ft, T_o = 13.50 sec)

Deg of Freedom	Surge		Sway		Heave		Roll		Pitch		Yaw	
ω_{e_n}	A_{X_n}	Φ_{X_n}	A_{Y_n}	Φ_{Y_n}	A_{Z_n}	Φ_{Z_n}	A_{Φ_n}	Φ_{Φ_n}	A_{Θ_n}	Φ_{Θ_n}	A_{Ψ_n}	Φ_{Ψ_n}
.3325	.04056	92.36	.1309	91.59	.1730	-.16	.03684	144.17	.01401	-65.73	.005543	-131.86
.5348	.5256	87.29	1.583	94.25	2.783	-.20	2.213	-143.11	.4348	-64.96	.2570	-159.45
.7623	.3934	84.00	1.014	91.68	2.815	1.53	1.560	-75.16	.6843	-53.93	.2398	-164.97
1.015	.1838	84.20	.4292	87.36	2.450	22.93	.8392	-80.93	.6524	-23.94	.1896	175.04
1.293	.05932	75.18	.1244	83.01	.8887	92.45	.3678	-56.88	.2838	21.47	.1203	165.53
1.596	.03103	56.83	.02075	-14.17	.1109	69.58	.1788	-71.00	.1472	50.42	.09949	153.47

NOTE: A_{X_n}, A_{Y_n}, A_{Z_n} are ft; A_{Φ_n}, A_{Θ_n}, A_{Ψ_n} are deg, all Φ_{i_n}'s are deg.

The form of the sum of sinusoids model is given on Fig. C.4. The RAO phase angles (Φi_n) enable the model to maintain correlation between the various ship motion degrees of freedom. The random phases (ε_n) associated with each of the six frequencies in the model are selected at simulation initialization and remain constant during each simulated approach or landing operation. These phases introduce seaway randomess into the problem.

As noted previously, Φ_{i_n}, ω_{e_n}, and A_{i_n} are tabulated in Reference 5 for the thirteen conditions in Table C.1. The parameters are calculated for ship c.g. motions; the motions of any other location on the ship (e.g. the touchdown point) are obtained by an Euler transformation using ship pitch, roll, and yaw angles. These tabulated data were used in the system simulation of this study to represent typical ship motion under one of the conditions chosen from Table C.1.

APPENDIX D

Environmental Wind Modelling

The environmental flight conditions in the vicinity of the moving DD 963 ship are simulated for a limited number of sea states and corresponding wind velocities as presented in Table C.1. The average "wind-over deck" is constrained to either of two directions with respect to the ship's average heading: $\psi_{WOD} = 0°$ and $\psi_{WOD} = -30°$. This angle is implied by the vector difference of the wind velocity and the ship velocity, relative to the fixed earth. The wind-over-deck model is derived from the work of Fortenbaugh [1,5]. The wind-over-deck has three orthogonal position-dependent mean values plus three orthogonal random components with standard deviations which are also position dependent. The values are obtained in what is defined as a wind-axis system centered at the ship landing pad.

The subroutine WINDEK which computes the wind components can be called by any program for which these components are needed. The required input quantities are:

1. Ship Location - coordinates of the ship e.g. (X_{SI}, Y_{SI}, Z_{SI}) relative to an inertial axis system at mean sea level, directed north, each and down.
2. Ship Attitude - These include the mean heading clockwise from north (ϕ_{SO}) and the small Euler attitude angles (ϕ_S, θ_S, ψ_S) relative to this mean heading.
3. Aircraft Location - coordinates of the aircraft c.g. (X_{AI}, Y_{AI}, Z_{AI}) relative to the inertial system which is oriented north, east, and down.
4. Aircraft Attitude - Euler angles (ϕ_A, θ_A, ψ_C) describing the aircraft attitude relative to the inertial system.

5. Wind Parameters - Wind velocity relative to earth (V_{WIND}), and direction relative to ship centerline (ϕ_{WOD}). The wind speed must exceed $V_s \sin(\phi_{WOD})$

The computations begin by calculating the earth-axis coordinates of the touchdown point (X_{TDI}, Y_{TDI}, Z_{TDI}), which depend only upon the ship c.g. location, the ship attitude, and the known coordinates in ship axes of the touchdown point relative to the c.g.

The aircraft position relative to the touchdown point is next expressed in wind axes as (X_{ASW}, Y_{ASW}, Z_{ASW}). Wind axes are centered at the landing pad and are aligned with the mean relative wind. That is, the x-axis is horizontally directed into the relative wind (0° or 30° left of the ship longitudinal axis), the y-axis is directed horizontally to the right, and the z-axis is directed down. These coordinates are then multiplied by the factor .85 (the ratio of beam widths of the FF1052 and the DD963 ships), to correspond to the aircraft location relative to a FF1052 ship. This is done because the wind data have been numerically determined with respect to the smaller FF1052 ship, and the relative position coordinates (X_{1052}, Y_{1052}, Z_{1052}) are scaled for this reason. Brief computations also yield values for the position-dependent break frequencies of the white-noise filters which generate random airwake -omponents for the FF1052, at a reference wind-over-deck airspeed of 45 kts (76 fps). These frequencies are then scaled to equivalent values for the DD963 ship; for an arbitrary value of wind-over-deck airspeed.

The wind-axis aircraft coordinates (X_{1052}, etc.) and the wind direction (ϕ_{WOD}) relative to the ship centerline are next input to subroutine SHAPE, which determines the shaping function logic for data-base extrapolation to free-stream conditions, to the side of or far behind the ship. The logic yields a geometrically-dependent numerical factor F1, which falls between 0 and 1, and which is used to modulate the magnitude of the airwake velocities in the volume of airspace immediately adjacent to the landing pad. That is, if F1 = 1, the aircraft is located inside the 3-dimensional data base wnere the wind velocity components (and their

standard deviations) are specified numerically on a point-by-point basis. In this case, linear interpolation gives the value of velocity as a linear combination of the eight corner-values specified by the data.

If the aircraft is outside of this data base region but is inside the larger volume to the side or rear of the ship, the perturbed airspeed components, to which the aircraft is subject, are extrapolated toward zero. An idealized one-dimensional version of this data-variation is shown in Fig. D.1.

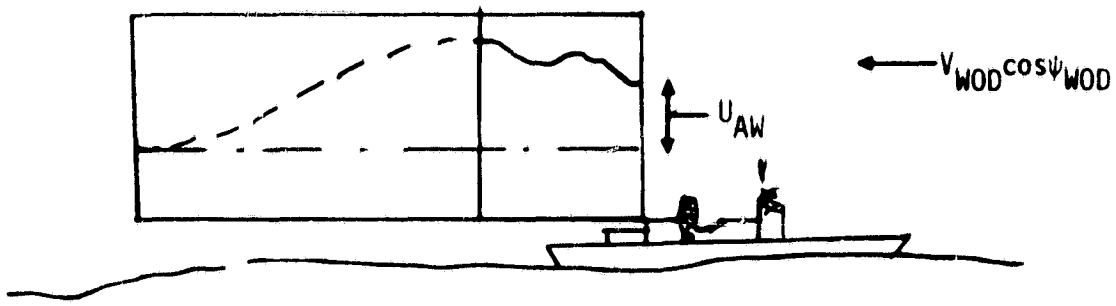

Figure D.1. Representation of Perturbed Airflow Near Ship

The sketch (Fig. D.1) shows the variation, with distance aft of the landing pad, of the mean vertical wind velocity along a locus which is 25 ft above the landing pad. A similar sketch could indicate the variation with x of the standard deviation of the vertical wind velocity. Sharp spatial veriations of both of these parameters are found in the data, as tabulated in subroutine INTPOL. For example, the mean and standard deviation of the perturbed wind velocity can change from 20 $\pm$ 4 fps to 4 $\pm$ 12 fps between two adjacent geometric points.

The total wind velocity at a given point relative to the landing pad is then the sum of the mean value (V_{XAWB}, etc.) and a random component of specified standard deviation (V_{XR}, etc). Both of these components are measured in the fixed-earth axis system. The total wind velocities are summed in the ship wind axes, and these are converted first to earth axes (V_{XAW}, etc.) and then to aircraft body axes (U_{AW}, V_{AW}, W_{AW}), in terms of heading and orientation angles.

A representative trajectory for a 30° relative wind angle is shown on the ship-fixed wind-axis system in Fig. D.2. The wind velocity relative to earth is equal to the ship velocity of 20 kts (33.8 f/s). The figure shows the relatively small volume behind the landing pad in which wind velocity perturbations are given tabularly. The indicated trajectory of the aircraft is nominally a constant-heading path, which is aligned with the landing pad, at 27° to the ship centerline. The aircraft trajectory enters the perturbed wind volume when the range-to-go is about 300 m (1000 ft). The "wind decay zone" is a volume inside of which the wind velocities vary smoothly from the steady wind value to the values at the edge of the zone labelled "wind specified". This smooth variation has the form of a cosine wave in both x and y directions, and the wind outside this zone is unaffected by the pressence of the ship.

A representative trajectory entering the dashed volume aft of the ship leads to modifications in the aerodynamic forces, engine thrust, and to subsequent changes in the aircraft path relative to the no-wind path.

APPENDIX E

The Ship Approach and Landing Navigation System

The ship approach and landing navigation system provides the relative aircraft position and velocity estimates to be used by the guidance system. While there are many navigation configurations and schemes possible, one based on shipboard MLS/DME (microwave landing system and distance measurement equipment) has been used in this study. It is based on previous work described in more detail in Ref. 2 . Basic elements for this configuration are shipboard MLS/DME, airborne MLS receiver/DME transmitter, ship attitude and acceleration sensors, aircraft attitude and acceleration sensors, an uplink channel from ship to aircraft, and both airborne and shipboard digital computers. Figure E.1 depicts the interconnections among the various components of this system.

The MLS/DME antenna is fixed to the ship and located forward of the landing pad. The antenna is not pitch, roll or yaw stabilized. This system provides azimuth and elevation angles and range measurements of the aircraft relative to the ship. The MLS/DME signals are corrupted by random and bias errors. The measurement equations are given by

$$\begin{aligned} &\text{(range)} && r = [x_r^2(1) + x_r^2(2) + x_r^2(3)]^{1/2} + \tilde{r}, \\ &\text{(azimuth)} && A_z = \tan^{-1}\left(x_r(2)/x_r(1)\right) + \tilde{A}_z, \\ &\text{(elevation)} && E\ell = \tan^{-1}\left(-x_r(3)/|x_r(1)|\right) + \tilde{E}\ell, \end{aligned} \qquad \text{(E.1)}$$

where $x_r(1)$, $x_r(2)$, $x_r(3)$ are the Cartesian coordinates of the aircraft position with respect to the MLS/DME antenna location. The term $\tilde{r}$, $\tilde{A}_z$, and $\tilde{E}\ell$ represent the measurement errors (see Appendix G).

The ship attitude and acceleration sensors (vertical and direction gyros; linear accelerometers) are used to track the MLS/DME antenna position

C-3

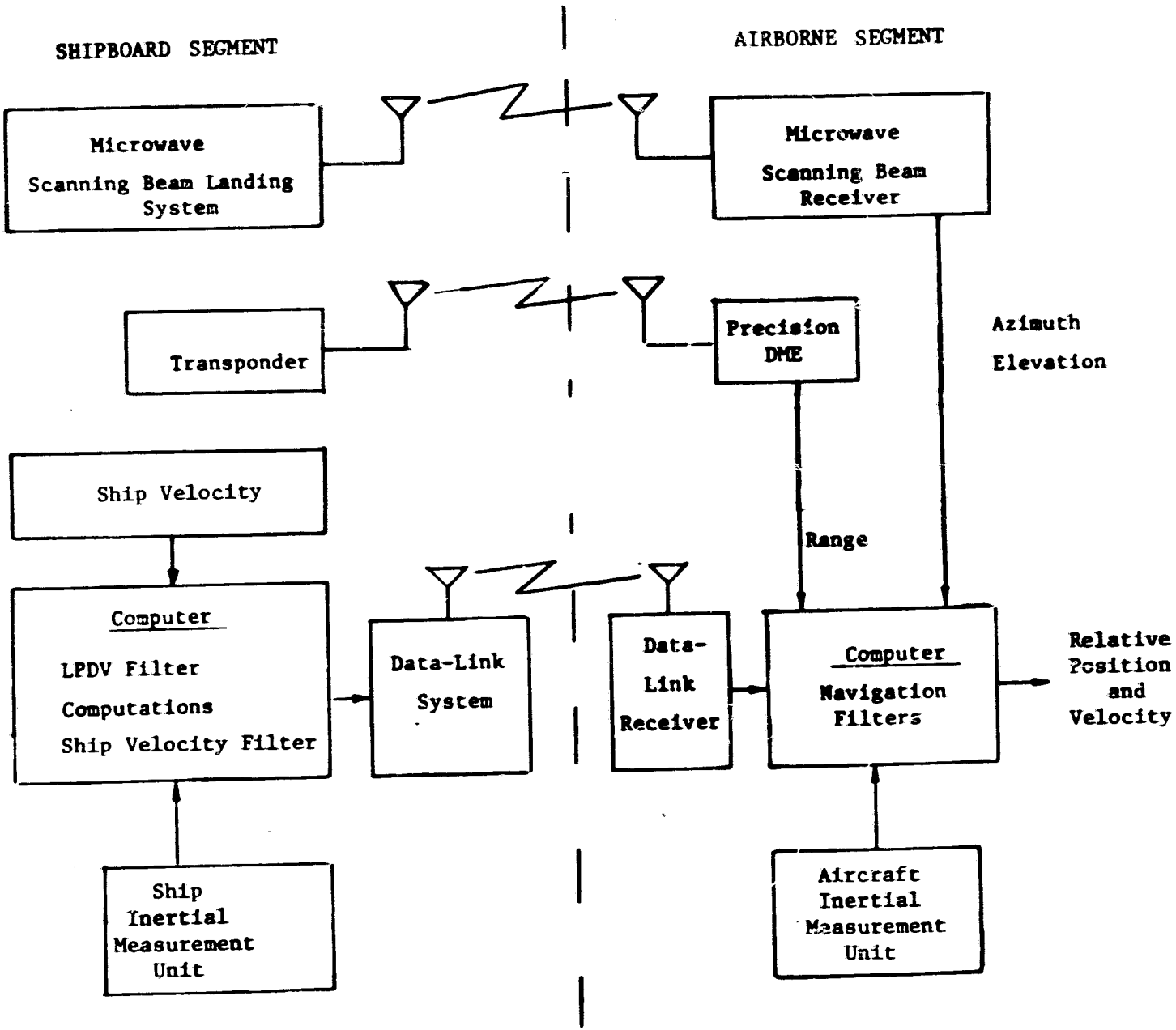

Figure E.1. Macro Flowchart of the Ship Approach and Landing Navigation System

and ship attitude with respect to some "average" antenna position and ship attitude. A ship in a high sea state undergoes considerable motion due to wave action. Because the MLS/DME antenna is fixed to the ship, the signals contain the ship motion component, as well as the aircraft motion which, if uncompensated, would induce undesirable aircraft steering activity. Ship motion effects on the MLS signal are reduced by use of the landing pad deviation vector. The landing pad deviation vector (LPDV) is an estimate of the landing pad position from some "average" position; it is defined by

$$x_f = \begin{bmatrix} z_\ell \sin \phi_s \sin \psi_s \\ z_\ell \sin \phi_s \cos \psi_s \\ G(s)\, \ddot{z}_s \end{bmatrix} \qquad \text{(E.2)}$$

where

z_ℓ = landing pad height above the ship center of gravity,

ϕ_s = ship roll attitude measurement,

ψ_s = ship yaw attitude (heading) measurement,

$\ddot{z}_s$ = ship vertical acceleration measurement,

$$G(s) = \frac{s}{(s + 0.05)(s^2 + 0.3535s + 0.0025)} \qquad \text{(E.3)}$$

= vertical filter transfer function.

Note that this last term is in the form of a complementary filter for the vertical direction. The position measurement is set to an average constant value above sea level, and the complementary filter estimates the landing pad vertical motion about this average.

The ship speed can be obtained by blending longitudinal acceleration with measurements from the ship speed log. Ship heading is obtained from the directional gyro. The average ship speed and heading can also be entered manually into the shipboard part of the navigation system. The LPDV and ship's velocity vector estimates are uplinked to the aircraft. The LPDV is used for navigation, and ship velocity is used for pursuit guidance.

The ship attitude measurements are corrupted by colored noise with nominal standard deviations of 0.1 deg. The ship accelerometer errors consist of colored noise with nominal standard deviation of 1 ft/sec^2 and misalignment of the accelometers with respect to the ship body axes. The aircraft attitude and acceleration sensors are modeled similarly to the ship sensor models.

Figure E.2 shows the overall block diagram of the simulated navigation system. Starting in the upper lefthand corner, the MLS/DME measures of relative aircraft position are converted to the ship landing pad Cartesian reference frame. The transformation matrix representing ship attitude (computed from ship gyro measurements) is used to transform relative aircraft position to the N-E-D (north-east-down) reference frame. The landing pad deviation vector is added to these transformed measurements. The result is the raw position of the aircraft in the N-E-D reference frame origined at the "average" landing pad position.

The aircraft attitude sensor (directional and vertical gyros or IMU) signals are used to transform the aircraft accelerations (body-mounted accelerometers) into the N-E-D frame, and the gravity effect is removed. The resulting acceleration measurements are compatible with the raw position measurements. These measurements are combined by the airborne complementary filter to generate the relative position and velocity estimates of the aircraft relative to the landing pad.

A three-state complementary filter algorithm is used to obtain the position and velocity estimates for each axis. First, the estimates are initialized by a linear regression technique with a 5 second span of data. The filter gains are obtained depending on the aircraft geometry relative to the ship to minimize the signal to noise ratio. The filter residual is passed through a data rejection algorithm to protect the filter from "bad" data. When a bad data is detected, the filter operates in the dead reckoning mode by integrating the acceleration signals. A more detailed description of the navigation system can be found in Ref. 2.

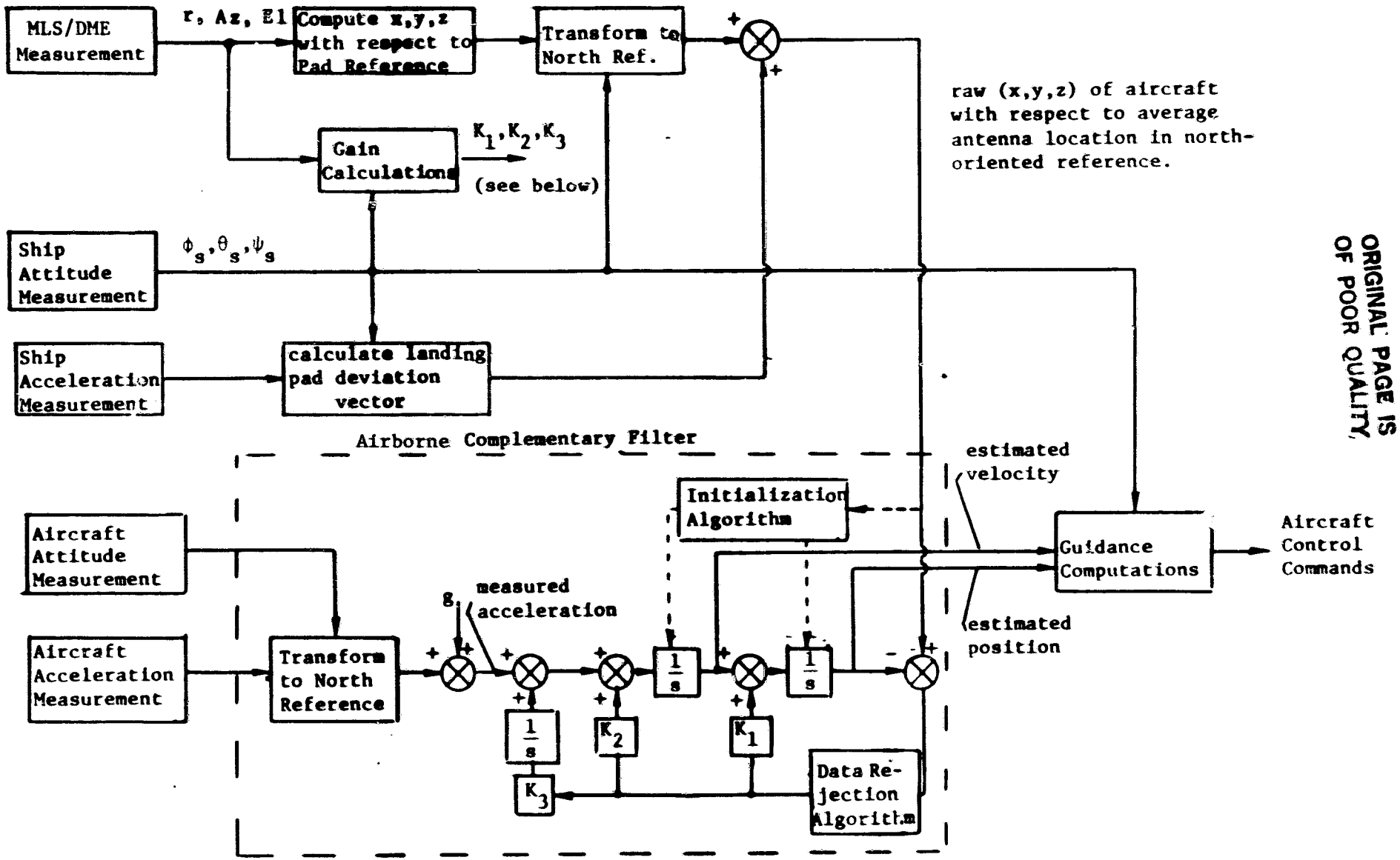

Figure E.2. Block Diagram of Navigation System Computations

APPENDIX F

AUTOMATIC APPROACH GUIDANCE TECHNIQUES

The purpose of the approach guidance system is to steer the aircraft to null out position and velocity errors and to approach the ship along some desirable path. The position and velocity errors are determined (by the MLS-based navigation system described in Appendix E) by comparing the measured aircraft relative state to that of the desired approach trajectory. This desired path may be either pre-determined or it may be computed in real time.

The approach guidance commands are decoupled into lateral, vertical, and longitudinal components. In this study, four lateral, five vertical, and two longitudinal steering concepts were examined. The results of this examination are the subject of Chapter III. In the following, the mathematical formulations of the different guidance concepts are first presented. These are followed by specific implementation details of the two sets of guidance concepts studied in more detail. Other descriptions of guidance schemes are found in Refs. 17 and 18.

Mathematical Formulation of Guidance Concepts

Define the following vectors:

$\vec{X}$ = position of the aircraft with respect to the ship hover point,
$\vec{V}$ = velocity of the aircraft with respect to the ship,
$\vec{V}_s$ = commanded ship velocity telemetered to the aircraft, and
$\vec{V}_a = \vec{V} + \vec{V}_s$ = computed inertial velocity of the aircraft.

With these quantities, four different lateral guidance laws can be commanded.

Pursuit Guidance This is also called homing guidance or "tail chase" guidance. The idea is to orient the inertial velocity vector of the aircraft to point at the stern of the ship (or at an offset hover point). The law can be implemented in the horizontal, and vertical, or both planes.

The pursuit law comes from forming the vector normal to $\bar{V}_a$ and $\bar{X}$,

$$\vec{V}_n = \vec{V}_a \times \frac{(-\vec{X})}{|\vec{X}|} = |\vec{V}_a| \sin\alpha \, \vec{U}_n \, , \tag{F.1}$$

Here, $\vec{U}_n$ is the normal unit vector, and $|\vec{V}_a| \sin\alpha$ is the velocity to be gained normal to $\vec{V}_a$ to turn $\vec{V}_a$ into $\vec{X}$. Then, define

$$\vec{V}_1 = \vec{V}_n \times \frac{\vec{V}_a}{|\vec{V}_a|} \tag{F.2}$$

in the direction of the acceleration to accomplish this change. The guidance law is then

$$\ddot{\vec{X}} = K_v \vec{V}_n \times \frac{\vec{V}_a}{|\vec{V}_a|} \, , \tag{F.3}$$

$$= K_v \left[\left(\vec{V}_a \times \frac{-\vec{X}}{|\vec{X}|} \right) \times \frac{\vec{V}_a}{|\vec{V}_a|} \right] ,$$

where K_v is the desired acceleration per unit error. Note that implementation of this law requires that the nominal ship velocity $\vec{V}_s$ be transmitted to the aircraft.

Constant Heading Guidance This type of guidance would be used to fly the aircraft along a fixed inertial path that intercepts the ship at a future point in time. It is dependent upon the ability of the aircraft system to predict the future position of the ship. It also must consider the longitudinal deceleration used to bring the aircraft to ship's speed.

Again, assume that V_s is transmitted to the aircraft and that a standard approach consists of (a) flying with fixed airspeed V_a for a period t_1, (b) decelerating at a fixed rate a_t for a period t_2, and (c) following a linear flare law to drive the airspeed and position errors to zero with respect to the hover point. Assume that the third phase (c) begins with distance and speed (r_f, V_f) with respect to the hover point.

The distance and speed (r_1, V_1) at the beginning of the second phase (b) can be computed from

$$V_f = V_1 - a_t t_2 \tag{F.4}$$

$$r_f = r_1 + V_1 t_2 - a_t t_2^2/2$$

Thus,

$$t_2 = (V_1 - V_f)/a_t, \tag{F.5}$$

$$r_1 - r_f = -V_1(V_1 - V_f)/a_t + (V_1 - V_f)^2/2a_t , \tag{F.6}$$

and V_1 is set equal to the approach speed V_a.

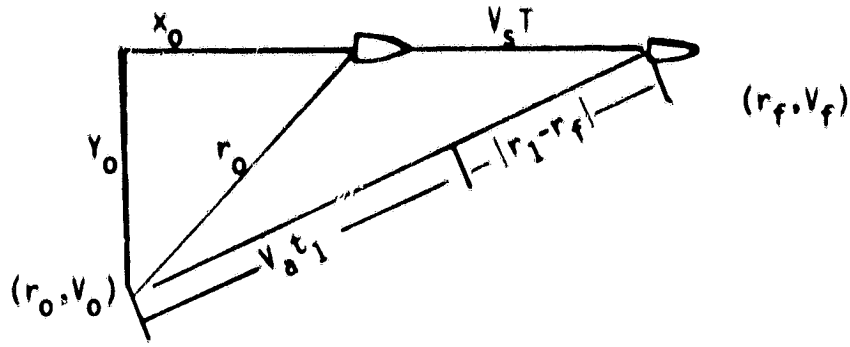

Figure F.1. Approximate Geometry of Constant Heading Guidance

From the above figure, we can work with the three legs of the triangle (r_o, V_sT, and $V_at_1 + |r_1-r_f|$). Define,

$$T = t_1 + t_2 . \tag{F.7}$$

Let

$$r_2 = r_1 - r_f . \tag{F.8}$$

Then,

$$y_o^2 + (x_o + V_sT)^2 = (V_at_1 + r_2)^2.$$

or

$$y_o^2 + [x_o + v_s(t_1 + t_2)]^2 = (V_at_1 + r_2)^2 .$$

From this,

$$(V_a^2-V_s^2)t_1^2 + (2V_ar_2-2V_s(x_o+V_st_2))t_1 + (r_2^2-y_o^2-(x_o+V_st_2)^2). = 0. \tag{F.9}$$

This quadratic equation is solved for t_1. Then, T is computed from Eq. (F.7) so that the approximate future intercept point ($\vec{r}_o + \vec{V}_sT$) is known.

Let

$$\vec{X}_f = \vec{r}_o + \vec{V}_sT \tag{F.10}$$

Then, $\vec{X}_f$ is substituted for $-\vec{X}$ in Eq. (F.3) to obtain the constant heading guidance law. If the aircraft is perturbed laterally or updated ship velocity is obtained, Eq. (F.10) must be recomputed to produce a new intercept. One mathod of compensating for longitudinal perturbations is to recompute the deceleration constant a_T (Eq. F.4.) in real time to maintain the same intercept point.

Variable and Constant Bearing A variable bearing guidance law would cause the aircraft to tend to fly along the constant bearing direction to the ship from wherever the aircraft happens to be. This could also be referred to as zero bearing rate guidance. In this case, V is substituted for $\vec{V}_a$ in Eq. (F.3), and

$$\ddot{\vec{X}} = \ddot{\vec{K}}_V \left[\left(\vec{V} \times \frac{-\vec{X}}{|\vec{X}|} \right) \times \frac{\vec{V}}{|\vec{V}|} \right] . \tag{F.11}$$

This law will null out any initial bearing rate. However, if the wind perturbs the aircraft off a given path, a new bearing will be eventually followed.

For the constant bearing guidance law, both position and velocity errors are computed with respect to a vertical plane fixed with a constant bearing passing through the hover point. If $\hat{U}_x$ is a horizontal unit vector in the constant bearing plane, then the lateral position error is

$$\vec{X}_e = (-\vec{X} \times \hat{U}_x) \times \hat{U}_x , \tag{F.12}$$

and the lateral velocity error is

$$\vec{V}_e = (-\vec{V} \times \hat{U}_x) \times \hat{U}_x . \tag{F.13}$$

These can be removed by the guidance law

$$\ddot{\vec{X}} = K_x \vec{X}_e + K_v \vec{V}_e \tag{F.14}$$

Vertical Guidance The previous four mentioned guidance concepts were mainly discussed in the context of nulling out lateral errors. They each have their counterparts in the vertical direction. Pursuit guidance, expressed by Eq. (F.3), also is valid for vertical steering. Constant heading guidance, expressed by Eq. (F.10), also represents constant inertial glideslope in the vertical plane. Variable bearing angle (zero bearing rate) guidance, expressed by Eq. (F.11), can also be used for variable elevation angle (with respect to the hover point) guidance. Constant bearing angle guidance (Eq. (F.14)) is equivalent to constant elevation angle guidance.

Guidance in the vertical plane can be broken into segments based on the distance-to-go to the hover point. For example, the aircraft can be commanded to fly at constant altitude by

$$\ddot{z} = K_z(z - h_c) + K_v \dot{z} , \qquad (F.15)$$

where h_c is the desired altitude, and z and $\dot{z}$ are the actual altitude and its rate. This command can be maintained until the aircraft reaches the point where it intersects the constant elevation angle or glideslope. Also, the aircraft can be commanded to reach the hover point altitude before it gets there along the longitudinal axis. Again, Eq. (F.15) is used to maintain the hover altitude.

The vertical guidance path can be broken into a number of steps where the aircraft alternately holds constant altitude and constant glideslope. This is often how the pilot likes to fly where deceleration takes place during the constant altitude portions of the approach.

An alternative to flying along a constant angle in the vertical plane is to hold a constant sink rate to change altitudes. Here, the guidance command is simply

$$\ddot{z} = K_v (\dot{z} - \dot{z}_c) , \qquad (F.16)$$

where $\dot{z}_c$ is the desired sink rate. This option was combined with lateral pursuit guidance for detailed investigation, as reported in Chapter V.

Longitudinal Guidance Two types of longitudinal guidance were studied up to the point of linear flare (about 30 ft before the hover point is reached). These were:

a) Constant speed/constant deceleration - In this case, the aircraft holds constant speed (e.g., 120 kt) until it reaches the point where by constant deceleration (e.g., 0.1g), it reaches the linear flare point at the appropriate forward speed relative to the ship.

b) Step guidance - This is a combination of constant longitudinal deceleration/constant speed at fixed altitudes alternating with constant descent glideslope/constant speed segments. An example is shown in Fig. F.2.

For both of these types of guidance, the nominal trajectory is found by integrating simple equations, such as Eq. (F.4), backwards in time and by matching appropriate boundary conditions.

Various deceleration schedules could be used in place of constant values. However, no particular advantage is derived (in an automatic sense) from other than constant values, so non-constant values were not examined in this study.

The longitudinal flare transition is going to the hover situation uses a separate control law which is explained later.

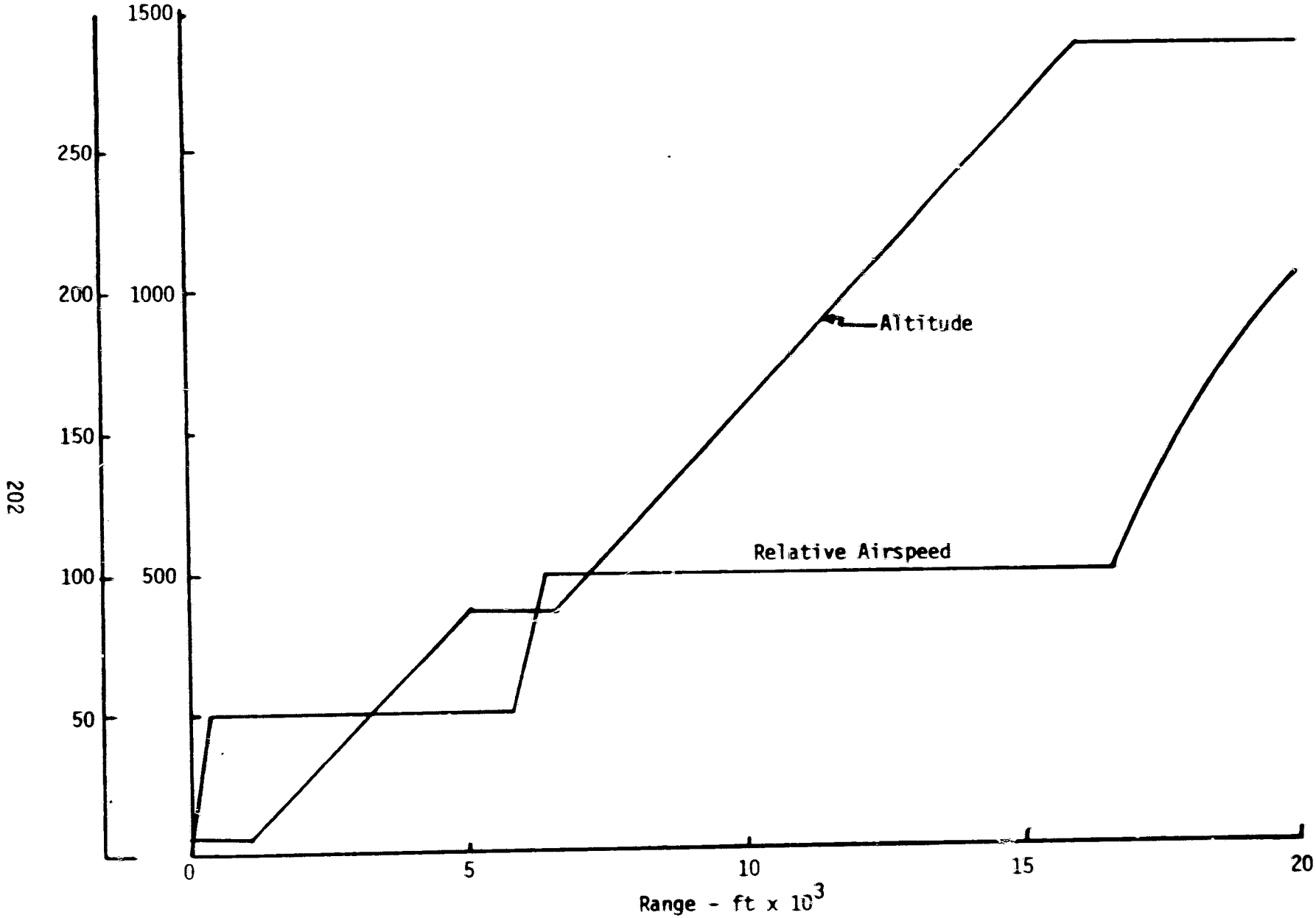

Figure F.2. An Example of Longitudinal Vertical Step Guidance

Guidance Law Development and Mechanization

The guidance laws are now developed for the corresponding concepts discussed previously. The guidance laws and their mechanization were made realistic so that the software developed here may be transferred directly to an airborne computer for an actual man-in-the-loop simulation. This section gives additional details concerning development and implementation of the guidance laws for the three main control axes.

The SRFIMF flight controller (inner loop) has capability of accepting lateral velocity commands ($\dot{y}^c$) at the lower relative speed of less than 30 knots as well as roll (ϕ^c), longitudinal velocity (V_x^c) and vertical velocity ($\dot{h}^c$) commands for lateral, longitudinal and vertical axes. Table F.1 summarizes the appropriate command modes over the speed range. The speed range of the table corresponds roughly to the powered lift flight regime for the RTA aircraft.

Step responses of the aircraft closed with the SRFIMF controller are given in Figure 11 through 13. They show the performance and limitations of the flight controller which must be kept in mind when designing and implementing the guidance (or outer-loop) laws. Thus, the guidance law must interface with the flight controller in such a manner that compatible and stable commands are generated to steer the aircraft along the desired trajectory, given the aircraft position and velocity estimates.

Guidance Mode Flags, Logic, and Guidance Laws

The guidance modes implemented for this simulation are directed by several mode flags, called autopilot directors. They are irreversible and point to the desired mode for each axis. Table F.2 summarizes the autopilot director functions. In an actual airborne implementation, they will service the flight sequencing light to keep the pilot updated. The autopilot switching logic and the associated guidance laws are now explained in detail for each axis.

Table F.1. SRFIMF Flight Control Command Modes at Various Relative Speeds.

Relative Speed Range (knots)	Attitude Flight Controller			Translational Flight Controller		
	Roll axis	Pitch axis	Yaw axis	Longitudinal axis	Lateral axis	Vertical axis
0	Roll-to-zero	Zero Pitch HOLD	Heading Hold/ Align-ment	Velocity command	Side velocity command	Vertical velocity command
30	Roll Com-mand		Blend		Phase Out	
120			Turn coordina-tion			

Longitudinal Axis - Referring to Figure F.3, if IVG = 1, then a check is made to see whether it is time to initiate the constant deceler ion maneuver. This test is performed by computing the reference velocity at that range,

$$V_{ref} = [a \cdot (2\hat{R} - R_o)]^{\frac{1}{2}} \qquad (F.17)$$

with

a = desired deceleration nominally 0.1g,

$\hat{R}$ = estimated range, and

R_o = the range of the hover point.

The value is compared with the current estimated speed, $\hat{V}_x$. If $\hat{V}_x$ is less than the reference, then it is not time to switch; therefore, the ground speed hold mode remains in force. In this case, the velocity command, V_x^c, is given by

$$V_x^c = \int K (\hat{V}_x - V_{ref}(0))dt, \qquad (F.18)$$

Table F.2. Autopilot Directors and Their Definitions

Longitudinal Autopilot Director (IVG)	Longitudinal Autopilot Modes
1	Ground Speed Hold (used as initial mode)
2	Constant deceleration
3	Exponential Flare
4	Longitudinal hover
Lateral Autopilot Director (ILOC)	**Lateral Autopilot Mode**
1	Heading hold or level flight (used as initial mode)
2	Localizer (constant bearing) mode, and Lateral pursuit mode
3	Heading alignment, Transition to lateral velocity mode Roll-to-zero Reference bearing slew
Vertical Autopilot Directors (IGS)	**Vertical Autopilot Mode**
1	Altitude hold (used as initial mode)
2	"Glide Slope" capture mode (not applicable for constant sink rate mode)
3	"Glide Slope" track mode, or Constant sink rate
4	Exponential flare
5	Vertical hover
6	Let down

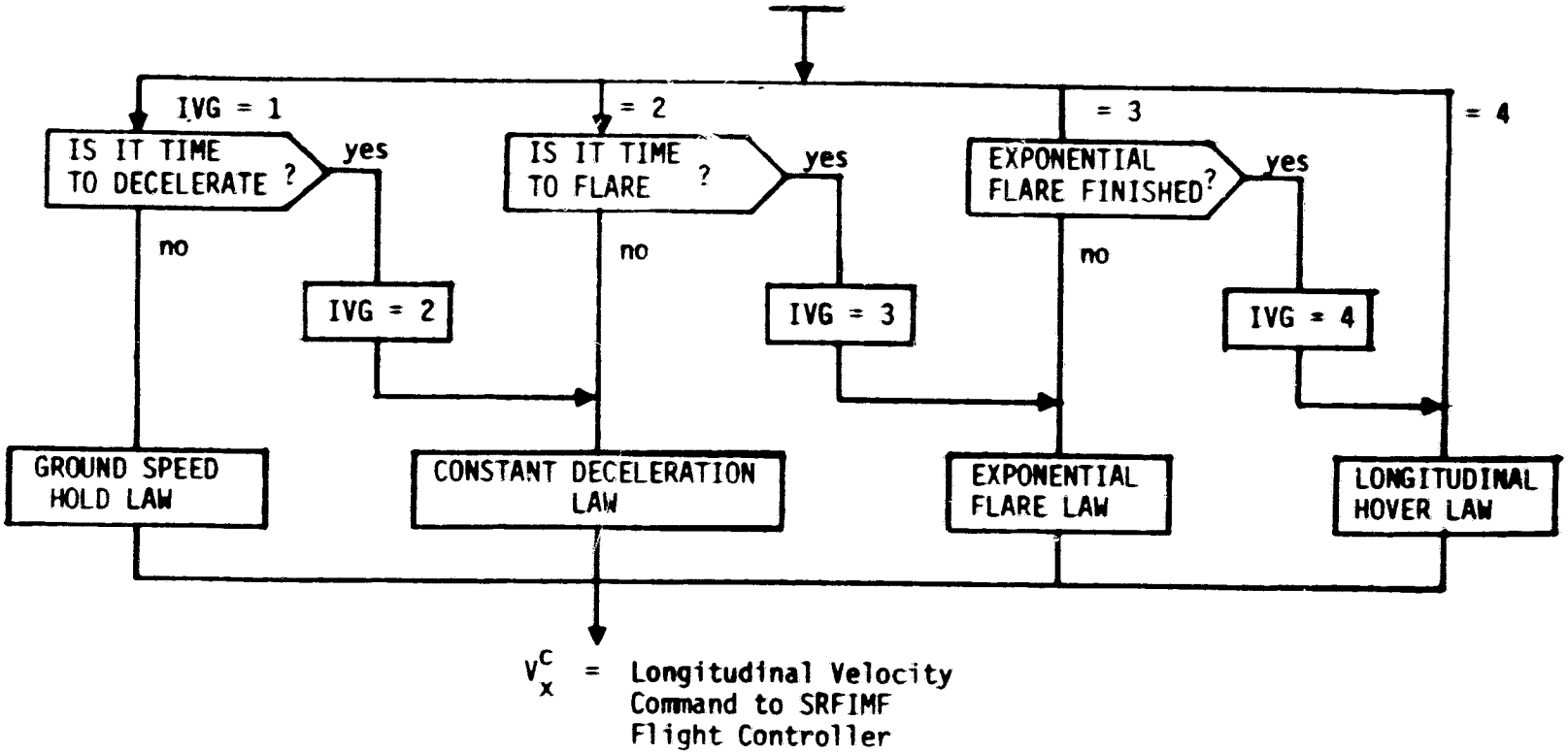

Figure F.3. Longitudinal Axis Guidance Logic

where $V_{ref}(0)$ is the ground speed at the engagement, and K is the control gain.

If $\hat{V}_x$ becomes less than the reference, V_{ref}, then it is time to initiate the constant deceleration mode. This is done by setting IVG = 2. When IVG = 2, it is checked to see whether it is time to initiate a flare maneuver to hover. This test is performed by computing the quantity,

$$XTST = \hat{R} [\hat{R} + \tau_x \hat{V}_x] , \tag{F.19}$$

where τ_x (= 5 sec) is the flare initiation time constant. When XTST becomes less then zero, then the aircraft has less than 5 seconds to hover at the current range and speed; therefore, the flare-to-hover is initiated by setting IVG = 3. If XTST remains positive, then the constant deceleration mode is in effect, and the corresponding command, V_x^c is given by (see Figure F.4(a))

$$V_x^c = \int \{a + k [\hat{V}_x - V_{ref}]\} dt \tag{F.20}$$

During the flare maneuver, the command is generated by

$$V_x^c = \int [k_1(t) \hat{R} + k_2(t) \hat{V}_x + k_3(t) V_x^c] dt , \tag{F.21}$$

where $k_i(t)$ are time varying gains to facilitate a smooth flare maneuver (see Fig. F.4 (b)). The hover state (IVG = 4) is declared when the above gains become the steady state regulator values. The time varying flare law is discussed in more detail later.

Lateral Axis Referring to Fig. F.5, first, the navigation status flag is checked; if it is initialized, then the constant bearing (localizer) or pursuit guidance mode is initiated by setting the director, ILOC, to 2. Otherwise, the wing level mode is commanded by $\phi^c = 0$.

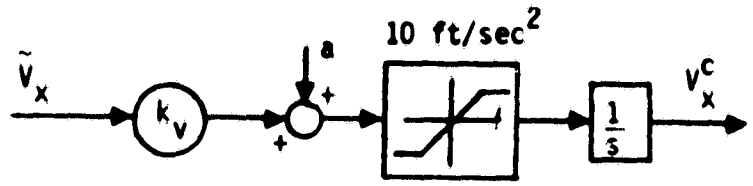

$\tilde{V}_x$ = longitudinal speed error

a = nominal deceleration command (= 0 for speed hold mode)

V_x^c = longitudinal speed command to flight controller

a). Ground speed hold or constant deceleration mode.

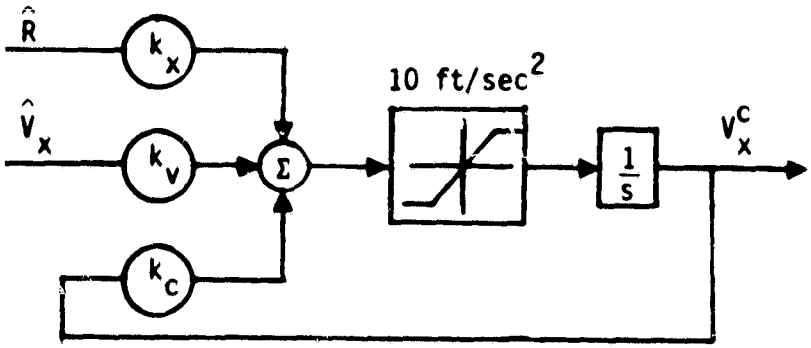

$\hat{R}$ = longitudinal distance-to-go

$\hat{V}_x$ = longitudinal speed

k_x, k_v, k_c = time varying gain for flare and track

b). Exponential flare and hover mode.

Figure F.4. Longitudinal Guidance Law

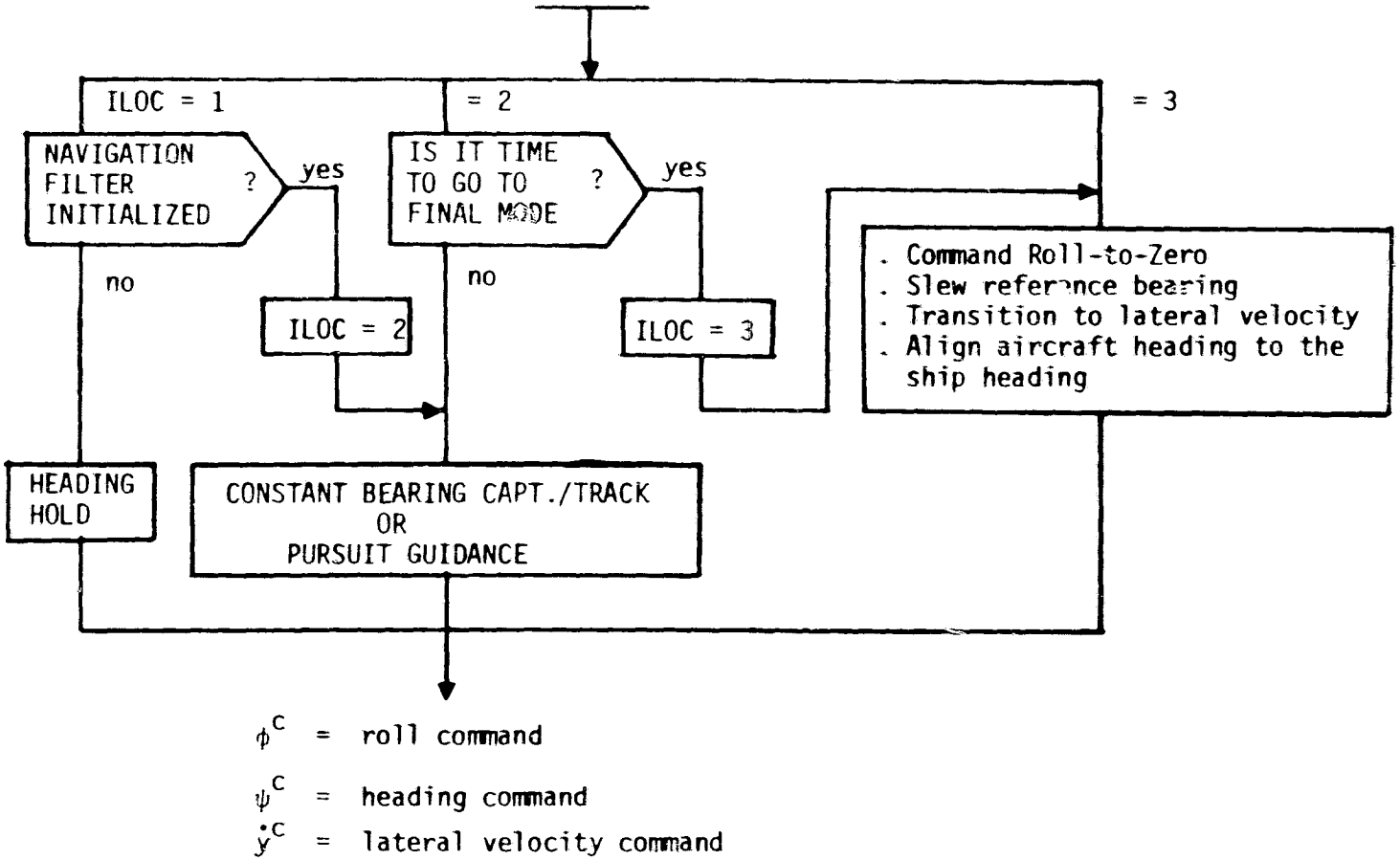

Figure F.5. Lateral Guidance Logic

When ILOC = 2, it is checked to see whether it is time to initiate the final mode for the lateral axis. Currently, this test consists of checking to see if the longitudinal speed, $\hat{v}_x$, is less than 50 ft/sec. If it is, the final mode is initiated by setting ILOC = 3. Otherwise, the constant bearing or pursuit mode is in effect. The corresponding roll command, ϕ^c, is given by (see Fig. F.6)

$$\phi^c = \tan^{-1}\left|\frac{k_y\Delta y + k_{\dot{y}}\Delta\dot{y}}{g}\right| \quad \text{- constant bearing}$$

$$\phi^c = \tan^{-1}\left|\frac{k'_{\dot{y}}\ddot{y}^c}{g}\right| \quad \text{- pursuit,} \qquad \text{(F.22)}$$

where k_y, $k_{\dot{y}}$, $k'_{\dot{y}}$ are the guidance law gains, Δy and $\Delta\dot{y}$ are the cross-track error and its rate, $\ddot{y}^c$ is the pursuit command given by Eq. (F.3), and g is the gravity constant.

When in the final mode (ILOC = 3), several maneuvers take place simulteneously. These are:

(i) The reference bearing is slewed to zero (from the nominal 27 deg) at 0.65 deg/sec for the constant bearing guidance and set to zero for pursuit;

(ii) Roll-to-zero is commanded at 2 deg/sec;

(iii) The lateral velocity command mode is initiated; and

(iv) The aircraft heading is aligned with that of the ship at 2 deg/sec.

Figure F.7 shows the mechanization of these maneuvers. It is noted that prior to the final mode, the yaw axis is slaved to the roll axis; the yaw axis is used to coordinate the turn. In the final mode, the yaw axis flight controller picks up ILOC = 3 and goes into the commanded heading mode. Also, for the pursuit guidance, the roll command, ϕ^c, essentially nulls out the lateral velocity error. Therefore, in order to null out both the lateral position and velocity errors, pursuit guidance is switched to the constant bearing guidance with the reference angle of 0°.

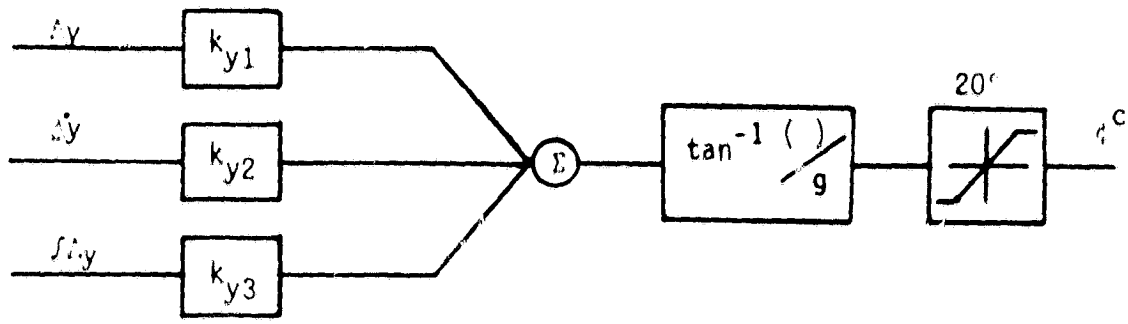

Δy = lateral error

$\dot{\Delta y}$ = lateral error rate

$\int \Delta y$ = integral of lateral error

g = 32.2 ft/sec^2

k_{y1} = proportional gain (= 0 for pursuit)

k_{y2} = derivative gain

k_{y3} = integral gain

Figure F.6. Lateral Guidance Law for the Roll Mode.

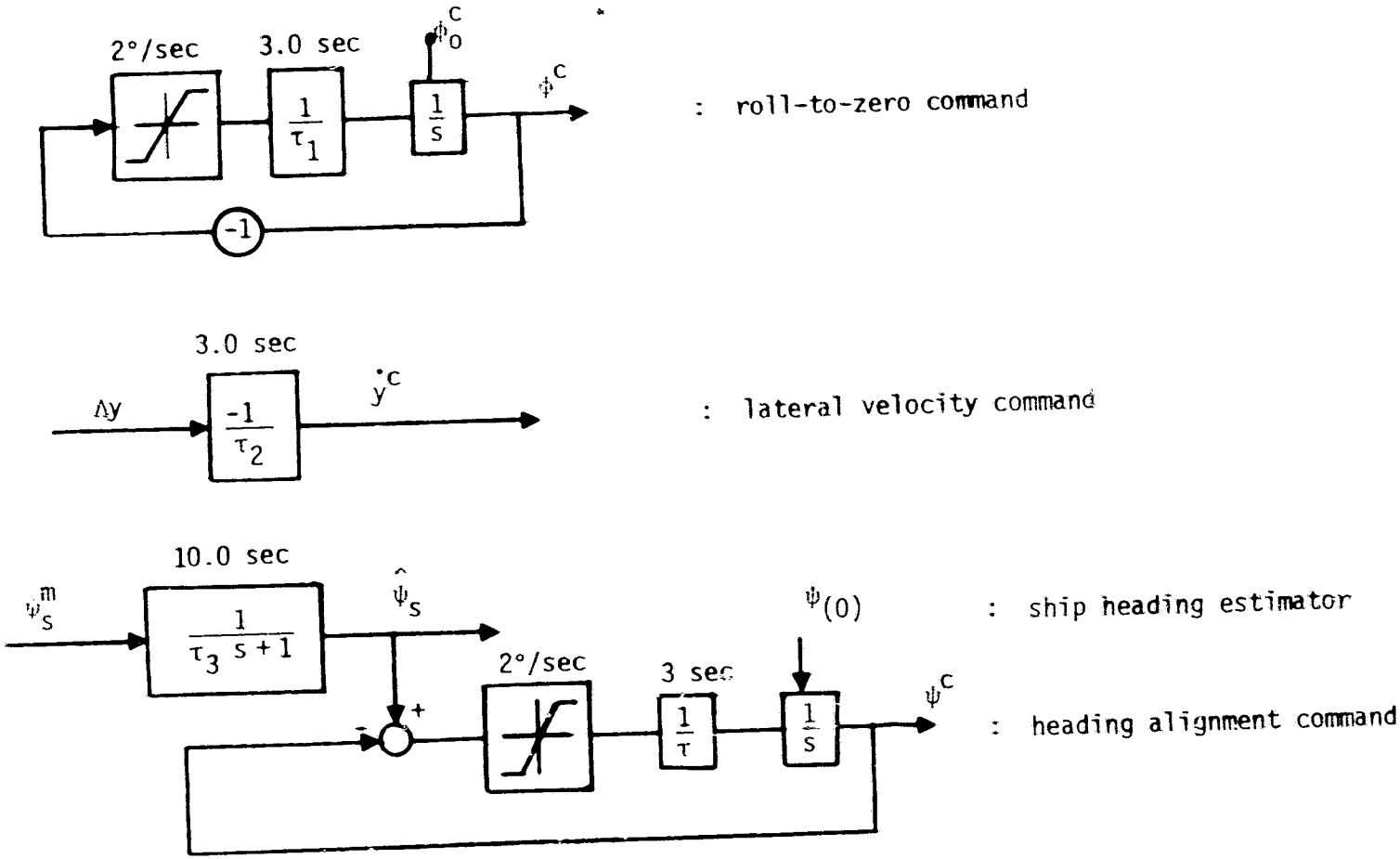

Figure F.7. Lateral Guidance Law for the Near-Hover Condition.

Vertical Axis First, constant elevation (or glideslope) guidance is explained. Referring to Fig. F.8, when IGS = 1, a check is made to see whether it is time to capture the glideslope. For this test, the quantity, VTST, is computed as follows

$$VTST = \Delta\hat{h}\,(\Delta\hat{h} + \tau_h \Delta\dot{\hat{h}}), \tag{F.23}$$

where $\Delta\hat{h}$, $\Delta\dot{\hat{h}}$ are the vertical error and its rate from the glideslope (nominally 3 deg with respect to the landing pad). Also, τ_h is the glideslope capture time constant of 5 seconds. When VTST becomes negative, then there is less than 5 seconds to the glideslope at the current closing rate. Therefore, the glideslope mode is initiated by setting IGS = 2. Otherwise, the altitude at the time of engagement is held by the guidance law,

$$\dot{z}^c = \int [k_1 (\hat{z} - z_{ref}) + k_2 \dot{\hat{z}} + k_3 \dot{z}^c]\, dt \tag{F.24}$$

where k_i's are the regulator gains.

When in the glideslope mode (IGS = 2), the following guidance law is used:

$$\dot{z}^c = \int [k_1(t)\, \Delta\hat{h} + k_2(t)\, \Delta\dot{\hat{h}} + k_3(t)(\dot{z}^c - \dot{z}_{ref})]\, dt \tag{F.25}$$

where $k_i(t)$ are time varying gains and $\dot{z}_{ref}$ is the nominal vertical speed on the glideslope. It is given by

$$\dot{z}_{ref} = V_{ref} \tan 3°. \tag{F.26}$$

This mechanization is shown in Fig. F.9.

For the constant sink rate guidance, the associated logic differs a little. Now referring to Fig. F.8(b), when IGS = 1, then the altitude hold command is given by Eq. (F.24). The test to initiate the constant sink rate command is as follows. First, time-to-go to the hover altitude, TTGV is computed by

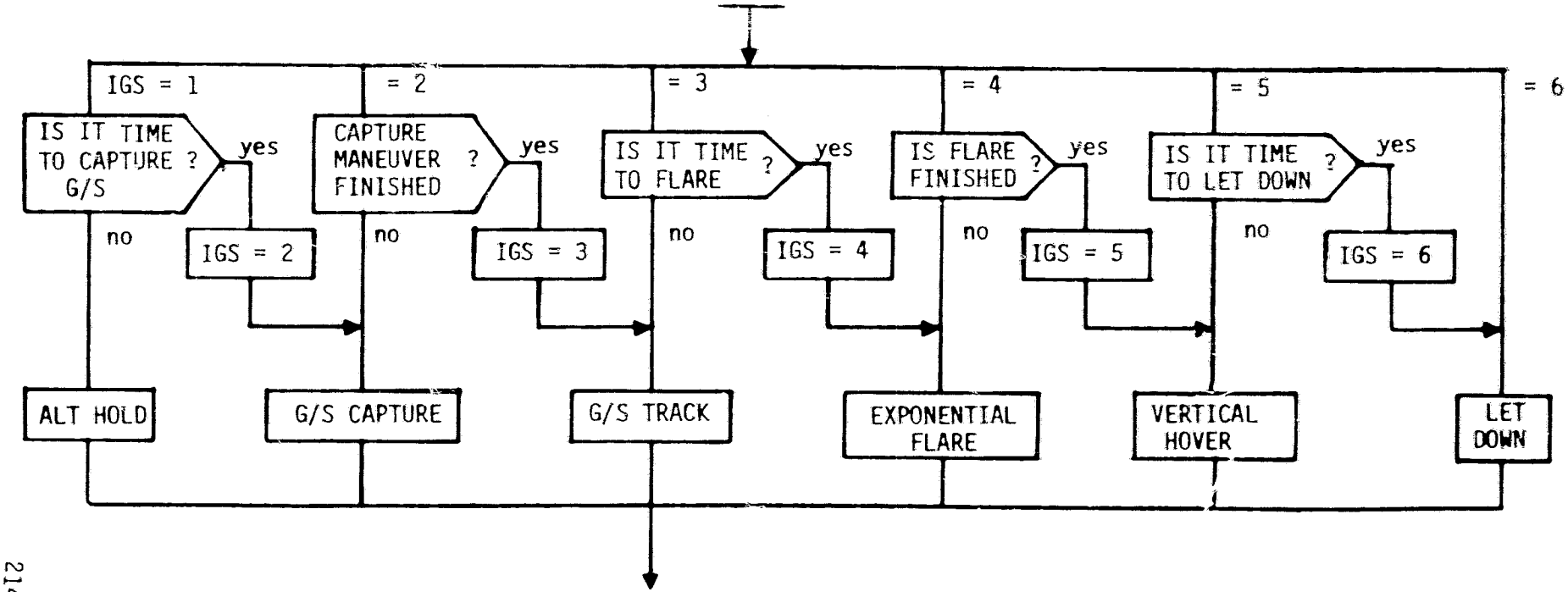

h^c = Vertical velocity command to SRFIMF flight path controller.

Figure F.8(a). Vertical Guidance Logic for Constant Elevation.

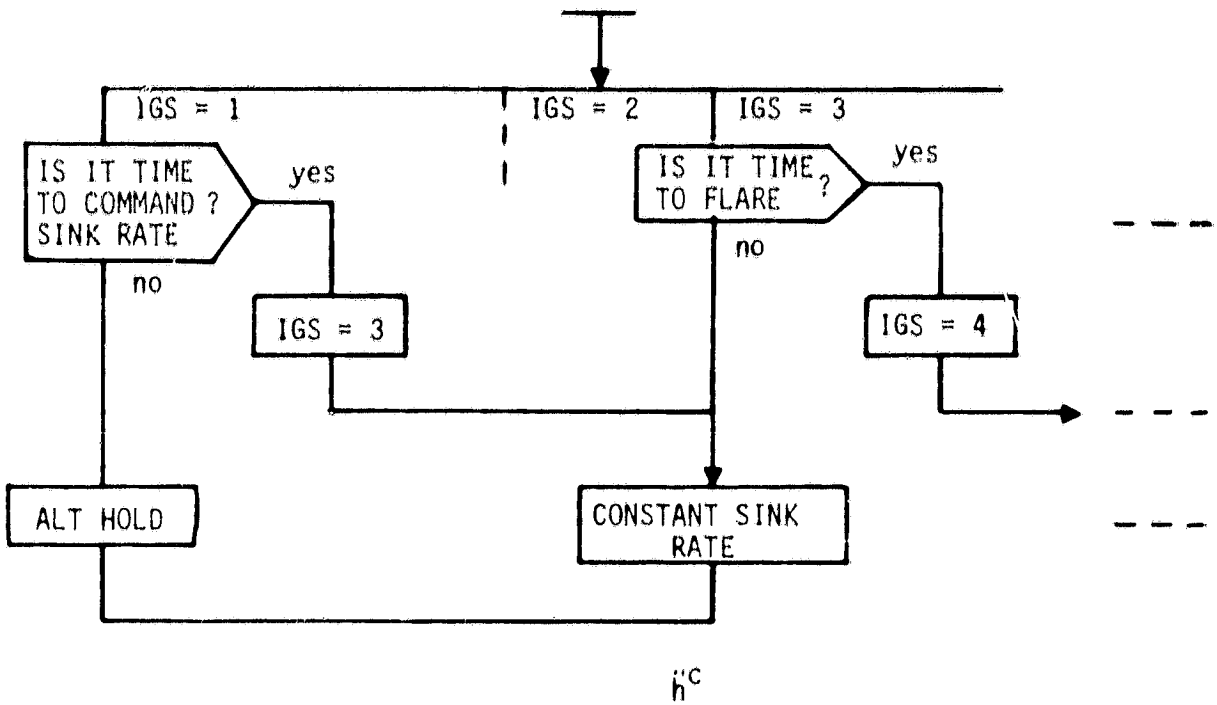

Figure F.8(b). Vertical Guidance Logic for Constant Sink Rate

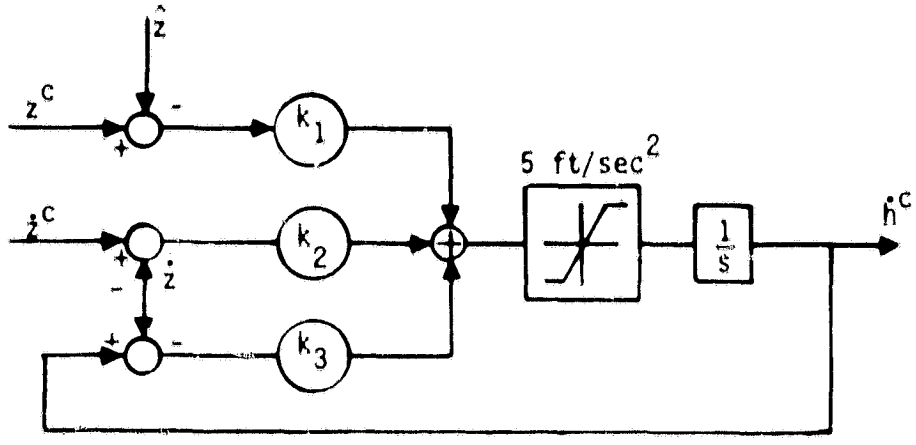

z^c = commanded altitude, ($z^c = z$ for constant sink rate)

$\dot{z}^c$ = commanded altitude rate,

$\hat{z}, \hat{\dot{z}}$ = estimated altitude and rate,

$\dot{h}^c$ = sink rate command to flight controller

k_1, k_2, k_3 = control gains whose values depends on the vertical mode.

Figure F.9 Vertical Guidance Law

$$TTGV = \hat{z}/\dot{z}^c \quad , \tag{F.27}$$

where $\dot{z}^c$ is the nominal commanded sink rate of 10 ft/sec. Next, time-to-go to the longitudinal hover point, TTGL, is computed by

$$TTGL = (\hat{V}_o - \hat{V}_F)/a + (\hat{R} - \hat{R}_o)/\hat{V}_x \quad , \tag{F.28}$$

where

$\hat{V}_o$ = speed at the deceleration maneuver initiation,

$\hat{V}_F$ = speed at the desired range of 600 ft,

a = nominal deceleration,

$\hat{R}$ = current estimated range,

$\hat{R}_o$ = range at deceleration maneuver initiation, and

$\hat{V}_x$ = current estimated speed.

The test consists of comparing TTGV and TTGL. If TTGV becomes less than or equal to TTGL, then the constant sink rate mode is initiated by setting IGS = 3. The commanded sink rate is given by

$$\dot{z}^c = \dot{z}_{ref} + k(\hat{\dot{z}} - \dot{z}_{ref}) \quad . \tag{F.29}$$

The constant sink rate command initiation logic was implemented in order to prevent the situation where the aircraft reaches the hover altitude prematurely. When this occurs, then the aircraft will experiance a long period of level flight at the hover altitude (nominally 50 feet above the MLS) before it catches up to the ship horizontally. With the above logic, the aircraft will come down to the hover altitude when it is in the immediate vicinity (200 ~ 300 feet) of the landing pad longitudinally.

Now going back to Fig. F.8 (a), when IGS = 3, it is checked to see whether it is time to initiate the vertical flare to the hover altitude. This check is done as in Eq. (F.23) except that it uses the altitude and its rate with respect to the landing pad, or

$$VTST = \hat{h}(\hat{h} + \tau_h \hat{\dot{h}}) \quad . \tag{F.30}$$

If VTST is negative, then there is less then 5 seconds to go to the hover altitude (h = 0); therefore the vertical flare maneuver is initiated by setting IGS = 4.

The vertical flare guidance law is exactly the same as the glide-slope capture and track law of Eq. (F.25) except that the deviations are based on the average landing pad position. The hover mode is declared by setting IGS = 5, when the time varying gains become the regulator gains for the vertical guidance.

When IGS = 5, then a check is made to see whether it is time to initiate the let-down maneuver. Currently this test is purely time dependent. The let-down mode (IGS = 6) is initiated 15 seconds into the vertical hover mode (IGS = 5) stricitly on an open loop basis. When this happens, the let-down maneuver is initiated at .9 m/s (3 ft/s) using the constant sink rate mode.

In the future, more elaborate and realistic logic and guidance law will be designed which incorporates ship motion or landing pad motion predictors, a "lull" predictor, or the feed forward command to overcome the dynamic lag.

Exponential Flare Law Design

A transition (or a flare) maneuver is needed to smoothly transfer the aircraft state from one reference to another. A typical example of such a maneuver is transitioning from constant sink rate to the hover mode. In this case, the vertical speed must be reduced from the nominal 3 m/s to zero without inducing undue acceleration. A typical guidance law is the exponential flare law given by

$$\dot{h}^c = -\frac{1}{\tau} h \quad , \tag{F.31}$$

where $\dot{h}^c$ is the commanded velocity, h is the current altitude, and τ is the flare time constant. If the dynamic delay is neglected, then the solution is given by

$$h(t) = h(0)\exp(-\frac{t}{\tau}) \ . \qquad \text{(F.32)}$$

Therefore, the altitude is reduced to zero from the initial altitude very smoothly. However, a few of the shortcomings of Eq. (F.31) are;

(i) The initial acceleration is too large,

(ii) The maneuver is sensitive to the initial altitude error, and

(iii) The dynamic lag is not explicitly taken into account.

It is noted that the ideal exponential flare law traces a straight line through the origin in the $(h,\dot{h})$ phase plane as depicted in Fig. F.10.

A modified exponential flare law was designed for this simulation. The dynamic delay due to the inner control loop is assumed to be a first order lag, even though the step response is more like a second order system. With this assumption, the dynamic equation is given by

$$\begin{aligned} \frac{d}{dt} h &= \dot{h} \\ \frac{d}{dt} \dot{h} &= -\frac{1}{\tau_D} \dot{h} + \frac{1}{\tau_D} \dot{h}^c \ , \end{aligned} \qquad \text{(F.33)}$$

where τ_D represents the dynamic delay time constant. A suitable acceleration command for a regulator is given by

$$\ddot{h}^c = \frac{d}{dt} \dot{h}^c = k_1 h + k_2 \dot{h} + k_3 \dot{h}^c \qquad \text{(F.34)}$$

By concatenating Eqs. (F.33) and (F.34), the following matrix equation is obtained,

$$\frac{d}{dt} \begin{bmatrix} h \\ \dot{h} \\ \dot{h}^c \end{bmatrix} = \begin{bmatrix} 0 & 1 & 0 \\ 0 & -\frac{1}{\tau_D} & \frac{1}{\tau_D} \\ k_1 & k_2 & k_3 \end{bmatrix} \begin{bmatrix} h \\ \dot{h} \\ \dot{h}^c \end{bmatrix} \ . \qquad \text{(F.35)}$$

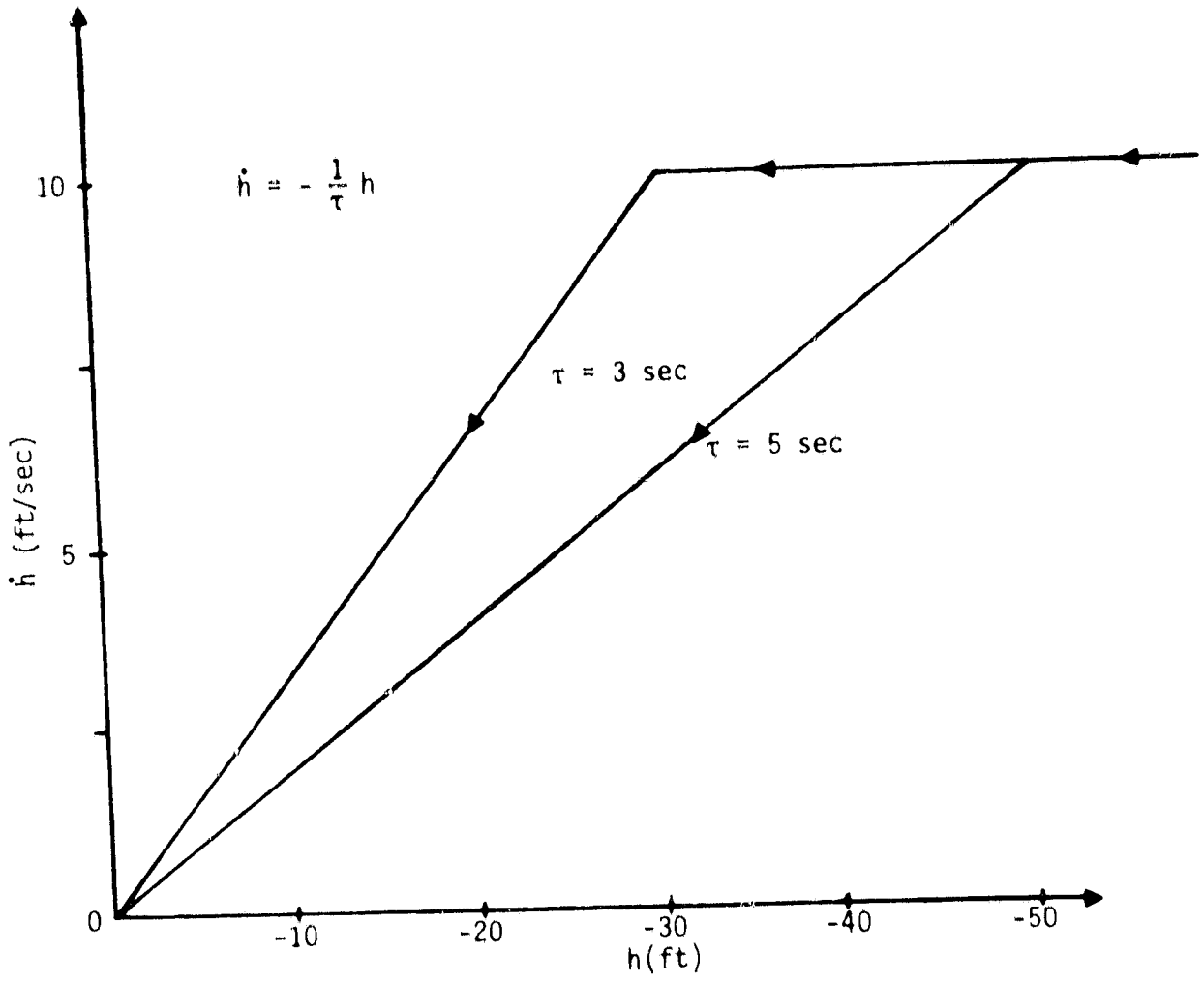

Figure F.10. Ideal Exponential Flare Law

The gains k_1, k_2 and k_3 are chosen so that the closed loop characteristic function is given by

$$f(s) = (s + \alpha)^2 (s + \alpha + \frac{1}{\tau_D}) \qquad \text{(F.36)}$$

The quantity α of 0.5 approximately produces desired effect for a time constant τ_D of 1.5 sec.

The main idea of the modified exponential law is to make the gains time scheduled ($k_i(t)$) so that the initial acceleration command is zero. After a sufficient period of time, the gains become those of the regulator. This is done as linear functions of time as follows:

$$\begin{aligned}
k_1'(t) &= [G_1 \cdot (T-t) + k_1 \cdot t]/T \,, && 0 < t \leq T \\
&= k_1 \,, && t > T \\
k_2'(t) &= [G_2 \cdot (T-t) + k_2 \cdot t]/T \,, && 0 < t \leq T \\
&= k_2 \,, && t > T \\
k_3'(t) &= k_3 \cdot t/T \,, && 0 < t \leq T \\
&= k_3 \,, && t > T
\end{aligned} \qquad \text{(F.37)}$$

where G_1 and T are the parameters to be adjusted by experiment, and G_2 is given by

$$G_1 h(0) + G_2 \dot{h}(0) = 0. \qquad \text{(F.38)}$$

For the approximate time constant of 1.5 sec, G_1 is $0.5k_1$, and T is 2.5 τ_D. These values were chosen for the example flare which initiates the maneuver at 5 seconds to go,

$$\hat{h}(\hat{h} + 5\dot{\hat{h}}) \leq 0 \,. \qquad \text{(F.39)}$$

Figure F.11 compares the modified and the classical exponential flare law in the $(h,\dot{h})$ phase plane. Peak accelerations were 2.5 ft/sec^2 at t of 2 sec for the modified and 2.5 at t of 0 sec for the classical flare law.

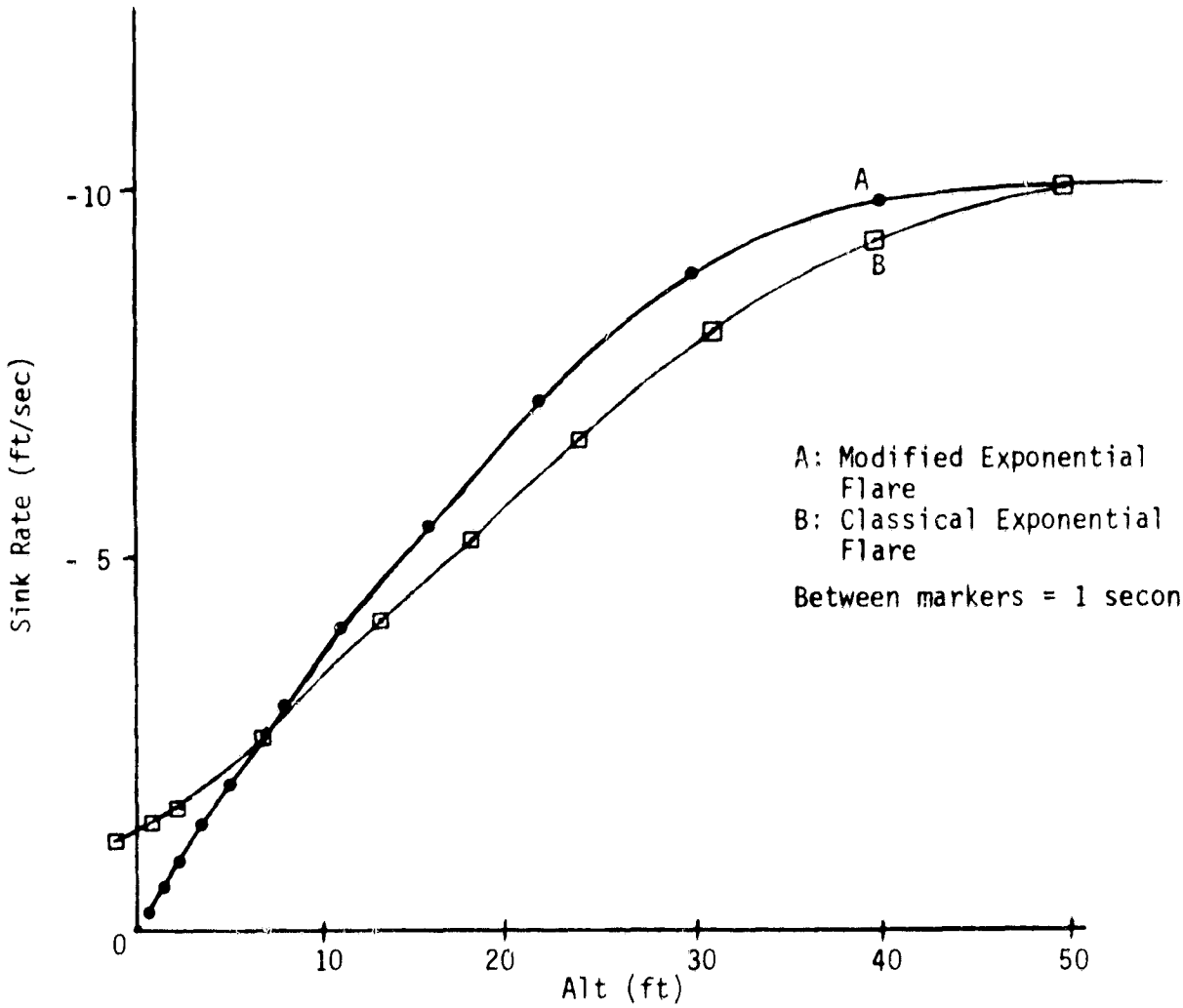

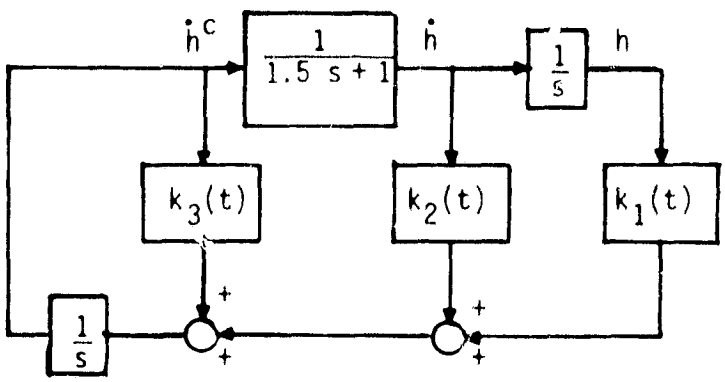

System A. Modified

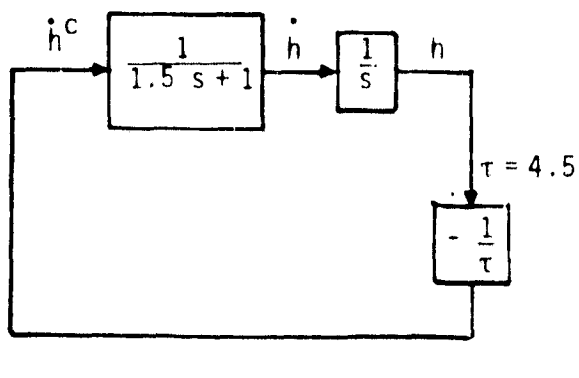

System B. Classical

Figure F.11. Comparison of Modified Exponential Flare and Classical Exponential Flare Laws for Simplified Dynamics.

Advantages of the modified exponential flare law are

(i) the acceleration command at the initiation time is small,

(ii) it is the position/velocity feedback law,

(iii) there is no need to "switch" gains for the regulator (or hover) mode,

(iv) it is very simple to implement, and

(v) the law is robust in the sense that a simple dynamic model is needed.

The modified flare law was used in two axes. For the longitudinal axis, it was used to transition from the constant deceleration to the hover mode. For the vertical axis, it was used to transition from the altitude hold to glideslope capture and track and from the glideslope or the constant sink rate to vertical hover mode. From the results of the six-degree-of-freedom nonlinear model, the performance of the modified law is as expected. This indicates that (a) the modified transition (or flare) guidance law is a reasonable alternative, and (b) for the guidance law design, the first order lag model used for the simplified inner loop and aircraft is sufficiently accurate. Point (b) is a useful fact when the more elaborate let-down law is synthesized.

APPENDIX G

Sensor Error Models

The sensor data used for VTOL aircraft navigation, guidance, and flight control are modified by several types of errors. These errors change each measured variable's magnitude from its true time history. Nonlinear, stochastic, and time-varying effects are all present. This appendix reduces these effects to parameters contained in simple linear error equations suitable for analysis. In the analysis and simulations used for this study, these errors are simulated by these model equations and the error effects are evaluated.

The instrumentation system is mathematically represented by a set of equations describing each data channel. (See Refs. 2, 19 for more details.) Figure G.1 is a block diagram which illustrates major sources of error which affect the data. The exact form of the submodels contained within each block of the figure may change somewhat from channel to channel, as is explained shortly. Figure G.1 shows the typical sequence of error effects which modify a variable y_1 starting from its assumed true value y_{1i} and ending with the recorded value y_{1o} used in the airborne computer.

The assumed true value of the variable (y_{1i}) is first subjected to the dynamic response of the sensor which is indicated in Fig. G.1 by the second-order term. Such a model approximately characterizes the response of a rate gyro, for example. For some instruments, such as the airspeed measurements and rate integrating gyros, this term is more appropriately modeled as a first-order term.

The measurement is next subjected to a scale factor error indicated by ε_{11}. This term is assumed to be constant; however, it encompasses the effects of non-linear scaling and time-varying scaling such as scale factor errors caused by temperature and power supply variations.

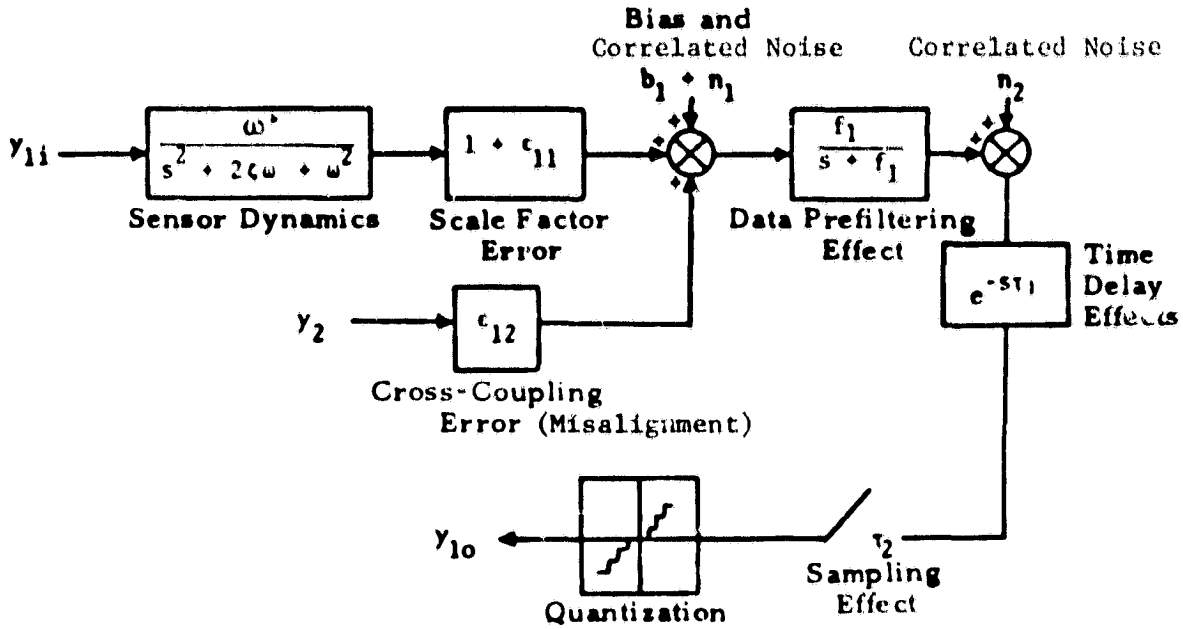

FIGURE G.1 - BLOCK DIAGRAM OF BASIC MEASUREMENT ERROR MODEL

Another error term is the cross-coupling between the measurements. This is indicated by the term ε_{12} which multiplies the variable y_2 before it is added to y_1. Such terms exist when the measurements of one variable are affected by changes in mignitude of other variables. Sources of cross-coupling error are instrument misalignment, center of gravity (c.g.) and instrument location uncertainty, and linear acceleration dependent terms of the gyro and angular accelerometer readings.

Other error terms which affect data accuracy are instrument bias b_1 and noise n_1. The noise is due to vibration, electrical sources, unsteady aerodynamics and various other sources. The noise can be modeled as white noise passed through a shaping filter, and as sinusoidal terms. However, this noise can be encompassed into the bias term; also, prefilters may be used to remove the noise and sinusoidal terms adequately so that n_1 can be neglected.

Next, the measurement is subjected to another dynamic term shown in Fig. G.1 as a first-order lag. This represents the prefilter. The phase error from this filter has usually higher than first-order characteristics. But the model constant f_1 can be adjusted so that phase lag is approximately correct for frequencies in the region of the prefilter break frequency.

The filter terms in each data channel usually produce lower cutoff frequencies than the basic sensor response dynamics, so the effect of the instrument dynamics can usually be ignored. This isn't true for pressure-dependent measurements however.

After passing through the prefiltering, other white noise due to various electrical sources or from transmission affects the data. This is modeled by the addition of the term n_2.

Up to this point, the data which exist in each channel are considered to be in continuous analog form. However, for data transmission the data are usually sampled and digitized. The data are sampled at regular intervals and converted to a digital number at each sample point. The data from several channels are typically sequentially sampled so that the data points taken from each channel are not taken simultaneously. This effect can be modeled as a variable time delay in each channel represented by $e^{-s\tau_1}$, where τ_1 is the delay time. Error here is also due to the difference in the delay times τ_1. If sampling is done rapidly enough (e.g., ten times highest system frequency which is to be measured), this error is insignificant.

The data is sampled once every τ_2 seconds and passed through a quantizer. For most flight instrumentation systems, the standard deviation (σ) of the signal noise is much larger than the quantization level Q. Thus, it can be assumed that the distribution of the noise error on the final digitized output y_{1o} is the same as that for the noise n_2.

To summarize, for the example of the variable y_1 just discussed, the following random error sources are assumed to be predominant:

ε_{11} : scale factor error

ε_{12} : cross coupling error

b_1 : bias

n_2 : white noise

All these random terms can be assumed to have Gaussian distribution. Any of them may have nonzero mean values. Installation errors, such as ground loops, are ignored because they are assumed to be removed during calibration.

There are several sources of phase lag due to dynamic effects (sensor response, high order prefilters) in each channel. However, these effects can be lumped into one first-order lag represented by the inverse time constant f_1. This represents the overall dynamics of the specific channel. In this study, these dynamic effects are ignored.

The noise n_1 is assumed to be removed by filtering. Also, it is assumed that the time delay $e^{-s\tau_1}$ due to sequential sampling is removed in data processing, and quantization effects (Q) are negligible. The scale factor errors and biases are set large enough to encompass the effect of nonlinear type errors (e.g., threshold, hysteresis) and time-varying errors (e.g., power supply fluctuation).

The scale factor errors and cross-coupling terms (such as ε_{11} and ε_{12}) are included in a matrix T. In T, the diagonal terms represent scale factor errors, and off-diagonal terms represent cross-coupling errors. Also,

the bias terms and the noise (such as b_1 and n_2) are represented by vectors B and n, respectively. Then, the final indicated output vector y_o is described by the vector equation

$$y_o = T_{y_i} + B + n \qquad (G.1)$$

These simple models of the error sources are used in the analysis of error effects on guidance system performance. They contain most of the elements required to determine the effect of different kinds of errors. The Monte Carlo analysis computer program developed for this study is flexible such that if increased complexity of the models is desired, the programs can readily be changed.

In order to study the quantitative effects of instrument errors, numerical values of the parameters in the error models must be known. Ranges of values of typical instrumentation errors are presented in Table G.1. These numbers represent statistical variations; they are based on summarizing absolute values given in Refs. 2 and 19 and conversations with several individuals. Manufacturers' absolute accuracy ranges were assumed to be $\pm$ 2σ values which provides a conservative estimate of the instrument quality available. The random numbers are assumed to have Gaussian distribution unless otherwise stated.

The values for the range of errors given in Table G.1 represent the authors' best judgements of the state of typical flight test instrumentation accuracy based on available information. There exist considerable manufacturers' data on available accuracies of rate gyros, rate integrating gyros, and linear accelerometers. Thus, the numerical values for the first three rows of Table G.1 have sufficient supporting verification. Generally, test center laboratory calibration of gyros and accelerometers confirm manufacturers' claims; thus, manufacturers' specifications have a high probability of being correct.

The error magnitudes used for the DME and MLS angular measurements are based on projected accuracies which can be expected from a ship-board system. The shipboard system will be developed based on experience obtained with various permanent and portible MLS system now being used for flight tests.

The instrument whose accuracy is least known is the angular accelerometer. Angular accelerometers are seldom used and only limited manufacturers data exists on them. The results in row 4 of Table G.1 are based on conservative generalization of the values presented in Ref. 19.

The numbers presented in Table G.1 are the range of the instruments' outputs, noise, bias, scale factor, and typical cross coupling terms. From these values, a set of numbers can be selected to model a typical instrument set. Table G.1 was used to select typical error magnitudes for the error analysis which was conducted in this study. The results are presented in the fifth chapter along with a discussion of the relative importance of each of the error sources.

TABLE G.1 - FLIGHT SYSTEM INSTRUMENTS AND THEIR RANGE OF ERROR MAGNITUDES

	Instrument/Device	Units	Full Scale Deflection	Random Noise (1σ)	Random Bias (1σ)	Random Scale Factor (1σ)	Cross Coupling Errors Other Errors (1σ)
1	Rate Gyros - p,q,r	^{o}/sec	30-60	0.001-0.3	0.001-0.3	0.01-2.0	Mass Unbalance (^{o}/sec-g): 0.01-0.1 Misalignment (^{o}): 0.1-1.0
2	Rate Integrating Gyros - ϕ,ϑ,ψ	o	30-360	0.01-0.2	0.01-0.2	0.01-1.5	Misalignment (^{o}): 0.1-1.0
3	Linear Accelerometer - $n_{x,y,z}$	g	0.5-3	0.001-0.7	0.001-0.003	0.025-1.0	Misalignments (^{o}): 0.0-1.0 c.g. Uncertainty (ft): 0.25-1.0 Cross Axis Sensitivity (g/g): 0.001-0.005
4	Angular Accelerometer - $\dot{p},\dot{q},\dot{r}$	^{o}/sec^2	60	0.05=0.1	0.05-0.1	0.1-0 2	Misalignment (^{o}): 1.0 g. Sensitivity (%/g): 0.2-1.0 Cross Axis Sensitivity (-): 0.01
5	Distance Measuring Equipment - r	m	20,000	1-10	1-10	.01	Occasional spikes and data dropouts in transmission
6	MLS Angular Measurements	o	$\pm$ 90^o	0.1-1.0	0.1-1.0	.01	Can have multipath effects

APPENDIX H

Simulation Program Description - MAALS

The purpose of this appendix is to give a brief functional description of the digital simulation program developed for this study. It is referred to as MAALS - for Marine/Aircraft Approach and Landing Simulation. The program includes all the simulation model elements which were previously discussed. It is resident on a CDC 7600 computer at NASA Ames Research Center

Figure H.1 shows the macro flowchart for the ship motion and navigation and guidance blocks. Table H.1 gives a brief description of the corresponding subroutines.

Figure H.2 shows the macro flowchart for the flight controller, engine, aerodynamics, wind model and integration subroutines. Table H.2 gives a brief description of the corresponding subroutines. This part of the program is organized similar to the Ames BASIC standard real time aircraft simulation configuration.

The whole program, including the aerodynamic and engine static and dynamic data tables, occupies some 62 K bites of core. The CPU-to-real-time ratio is approximately 1 to 7 (it takes 14.5 CPU seconds for 107 seconds of simulated flight time) at an integration cycle time of 50 msec.

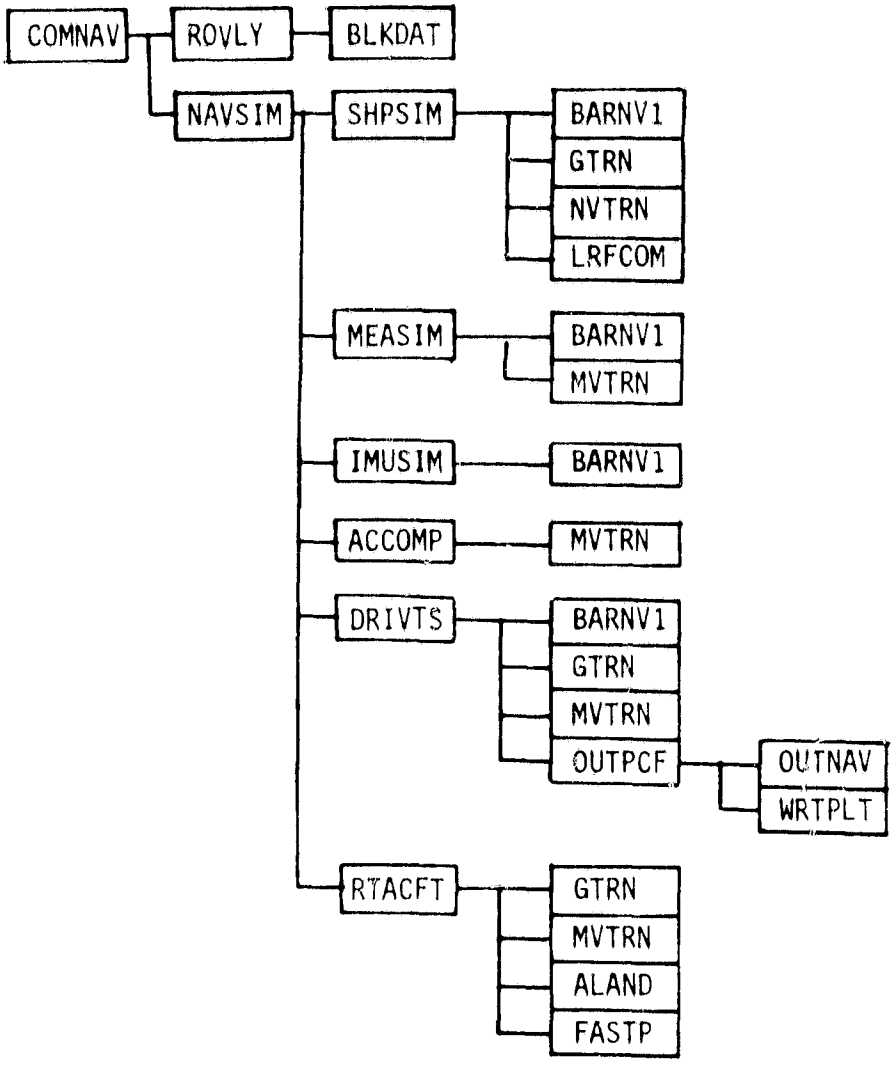

Figure H.1 Macro Flow Chart for Navigation, Guidance and Ship Simulation

COMNAV	-	Driver (Main) program.
NAVSIM	-	Navaid, sensor and filter driver routine.
SHPSIM	-	Computes ship position, velocity, attitude and its rate and linear acceleration and also antenna dynamics.
MEASIM	-	Computes navigation aid signals received by the aircraft.
IMUSIM	-	Aircraft inertial measurements
ACCOMP	-	Computes aircraft acceleration in north reference from gyro and accelerometer data on-board aircraft.
DRIVTS	-	Computes landing pad deviation vector, transform navaid signals, and estimates positions and velocities of the aircraft with respect to the ship reference coordinate.
RTACFT	-	Computes the guidance references, guidance deviations and flight controller commands.
ALAND	-	Computes open loop letdown command.
FASTP	-	Aircraft flight controller, actuator, engine, aerodynamics and kinematics. (see Fig. H.2 and Table H.2)
ROVLY BLKDAT	-	Loads input commons with simulation parameters.
LRFCOM	-	Initialize the aircraft dynamic variables.
OUTPCF OUTNAV WRTPLT	-	Output routines for line printer and tape units for printing and plotting of the results.
BARNV1	-	Random number (uniform or normal) generator.
GTRN	-	Transformation matrix from one reference frame to another.
MVTRN	-	Matrix vector multiplication.

Table H.1. Brief Functional Descriptions of Navigation, Guidance and Ship Simulation Subroutines.

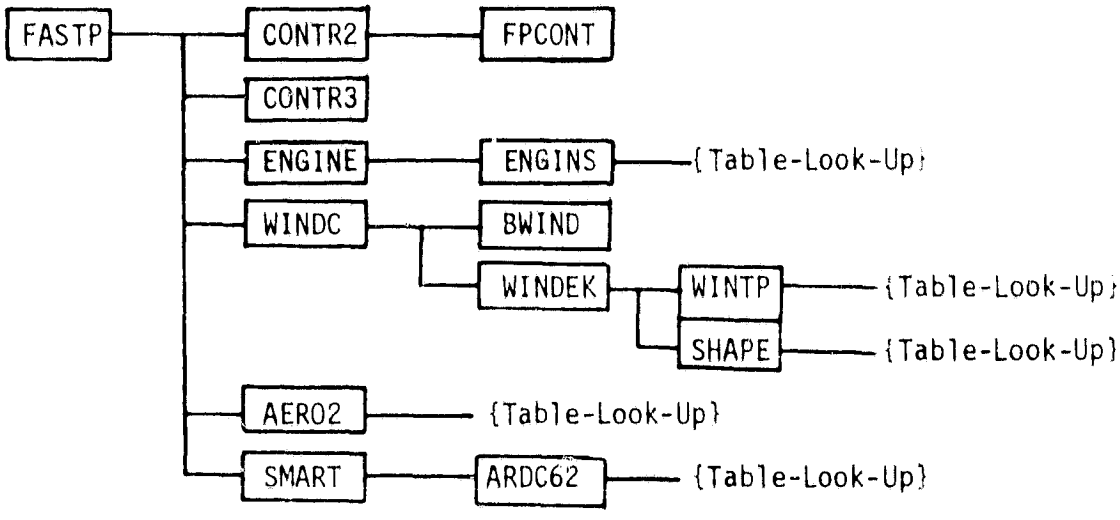

Figure H.2. Macro Flow Chart for Inner Loop, Engine Dynamics, Actuators, Wind, Aerodynamics and Integration.

FASTP	-	Driver routine for aircraft simulation.
CONTR2	-	SRFIMF attitude flight controller.
FPCONT	-	SRFIMF translational flight controller.
CONTR3	-	Control actuators.
ENGINE	-	Throttle, fan, nozzle and vane actuators
ENGINS	-	Engine statics and dynamics
WINDC	-	Wind generator
BWIND	-	Constant and Dreyden turbulence model
WINDEK WINTP SHAPE	-	Wind-over-deck turbulence with interpolation and shaping filters.
AERO2	-	Aerodynamic forces and moments.
SMART	-	Total forces and moments, accelerations, attitude and kinematic integrations.
ARDC62	-	Air density and ambient temperature table.

Table H.2. Brief Functional Descriptions of Flight Controller and RTA Subroutines.

REFERENCES

1. Fortenbaugh, R.L., " Progress in Mathematical Modeling of the Aircraft Operational Environment of DD963 Class Ships," AIAA Atmospheric Flight Mechanics Conference, Boulder, CO, August 1979.

2. Schmidt, S.F., and Merz, A.W., "Shipboard Landing Guidance Systems for VTOL Aircraft," Analytical Mechanics Assoc. Report No. 79-7, June 1979.

3. Merrick, V.K., "Study of the Application of an Implicit Model - Following Flight Controller to Lift-Fan VTOL Aircraft," NASA Technical Paper 1040, 1977.

4. Bland, M.P., and Konsewicz, R.K., "Mathematical Model for Lift/Cruise Fan V/STOL Aircraft," NASA CR 151916, December 1976.

5. Fortenbaugh, R.L., "Mathematical Models of the Aircraft Operational Environment of DD963 Class Ships," Vought Report 2-55800/8R-3500, September 1978.

6. Garnett, T.S., Jr., "Investigation to Study the Aerodynamic Ship Wake Turbulence Generated by an FF 1052 Frigate," Boeing Vertol Report D210-11140-1, December 1970.

7. Paulk, C.H., Jr., Private Communication, NASA Ames Research Center, Moffett Field, CA, September 1979.

8. Merrick, V.K., Private Communication, NASA Ames Research Center, Moffett Field, CA, September 1979.

9. McMuldrock, C.G., "VTOL Controls for Shipboard Landing," LIDS-TH-928, Massachusetts Institude of Technology, August 1979.

10. Box, G.E.P., and Jenkins, G.M., Time Series Analysis, Forecasting and Control, Holden-Day, San Francisco, 1970.

11. Bland, M.P., and Konsewicz, R.K., "Simulation Test Results for Lift/Cruise Fan Research and Technology Aircraft," Mc Donnell Douglas Corp. Report No. MDCA 4439, December 1976.

12. St. Denis, M. and Pierson, W.J., "On the Motions of Ships in Confused Seas," Transactions of the Society of Naval Architects and Marine Engineers, Vol. 61, pp 280-357, 1953.

13. Brown, R.G., and Camaratta, F.A., "NAVAIRENGCEN Ship Motion Computer Program," NAEC Report MISC-903-8, 1978.

14. Meyers, W.G., Sheridan, D.J., and Salveson, N., "NSRDC Ship Motion and Sea Load Computer Program," NSRDC Report 3376, February 1975.

15. Baitis, A.E., Meyers, W.G., and Applebee, T.R., "A Non-Aviation Ship Motion Data Base for the DD 963, CG 26, FF 1052, FFG 7, and the FF 1040 Ship Classes," DTNSRDC Report STD-738-01, December 1976.

16. Anonymous, "Destroyer Motion Simulation Study," Bell Helicopter Report 299-099-399, October 1974.

17. Ringland, R.F., "Approach Trajectory Considerations for Terminal Operations of Navy V/STOL Aircraft," AIAA Guidance and Control Conference, Palo Alto, CA, August 1978.

18. Wolkovitch, J., and Brassell, B.B., "System Requirements for V/STOL Automatic Approach and Vertical Landing," Vought Corp. Report No. NADC-78084-60, August 1979.

19. Sorensen, J.A., Mohr, R.L., and Cline, T.B., "Instrumentation Requirements for Aircraft Parameter Identification with Application to the Helicopter," NASA CR-132675, June 1975.

20. Wolkovitch, J., and Brassell, B.B., "VOLAR: A Digital Computer Program for Simulating VSTOL Aircraft Launch and Recovery from Small Ships," NADC Report No. 77123-30, December 1978.

21. Sidar, M. and Doolin, B.F., "On the Feasibility of Real-Time Prediction of Aircraft Carrier Motion at Sea," NASA Ames TM-X-62454, June 1975 (18 pp).

22. McGee, L.A., et al, "Evaluation of the Navigation Preformance of Shipboard - VTOL - Landing Guidance Systems," AIAA Guidance and Control Conference, Boulder, CO, August 1979.

23. Stapleford, R.L., Clement, W.F., and R.K. Heffley, "Flight Control/Flying Qualities Investigation for Lift/Cruise Fan V/STOL, Volume II, Piloted Simulation," Report No. NADC-77143-30, Naval Air Development Center, Warminster, PA, August 1979.